University of Huddersfield

University of Huddersfield Repository

Moon, Ryan N.

Allosteric control of supramolecular systems

Original Citation

Moon, Ryan N. (2006) Allosteric control of supramolecular systems. Doctoral thesis, University of Huddersfield.

This version is available at http://eprints.hud.ac.uk/id/eprint/5970/

The University Repository is a digital collection of the research output of the University, available on Open Access. Copyright and Moral Rights for the items on this site are retained by the individual author and/or other copyright owners. Users may access full items free of charge; copies of full text items generally can be reproduced, displayed or performed and given to third parties in any format or medium for personal research or study, educational or not-for-profit purposes without prior permission or charge, provided:

- The authors, title and full bibliographic details is credited in any copy;
- A hyperlink and/or URL is included for the original metadata page; and
- The content is not changed in any way.

For more information, including our policy and submission procedure, please contact the Repository Team at: E.mailbox@hud.ac.uk.

http://eprints.hud.ac.uk/

Allosteric Control of Supramolecular Systems

RYAN N. MOON B.Sc. (Hons)

University of
HUDDERSFIELD

Thesis submitted in partial fulfilment of the requirements for the Degree of Doctor of Philosophy

Department of Chemical and Biological Sciences,
The University of Huddersfield,

December 2006

Contents

Contents i
List of Figures vi
List of Schemes xiii
List of Tables xiii
List of Abbreviations xiv
Acknowledgements xvi
Abstract xvii

Chapter 1 1
1. Introduction 2
1.0 Supramolecular Chemistry 2
1.1 The Origins of Supramolecular Chemistry 2
1.2 Supramolecular Interactions 4
1.2.1 Ion-dipole Interactions 4
1.2.2 Dipole-dipole interactions 4
1.2.3 Hydrogen Bonding 5
1.2.4 π-π stacking 5
1.3 Host-guest Chemistry 5
1.3.1 Crown Ethers 6
1.4 Metallosupramolecular Chemistry 8
1.4.1 Grids 8
1.4.2 Cages 9
1.4.3 Ladders 11
1.4.4 Racks 12
1.4.5 Formation of a Library of Complexes 13
1.5 Helicates 15
1.5.1 Helicate Nomenclature 16
1.5.2 Homoleptic Helicates 17
1.5.3 Heteroleptic Helicates 18
1.5.4 Unsaturated Helicates 19
1.5.5 Head-To-Tail (Directional) Helicates 20

1.5.6 Heteronuclear Helicates 21
1.5.7 Enantioselective and Diastereoselective Helicates 22
1.5.8 Mesocates 26
1.5.9 Ligand Recognition 27
1.5.10 Ligand Programming 29
1.6 Ditopic Ligands 33
1.7 Allosteric Interactions 45

Chapter 2 52
2. Allosteric-Controlled Metal Specificity of a Ditopic Ligand 53
2.1 Ligand Synthesis 53
2.1.1 Synthesis of $\mathbf{L_1}$ 54
2.1.2 Synthesis of $\mathbf{L_2}$ 55
2.2 Coordination Chemistry 57
2.2.1 Complexes of $\mathbf{L_1}$ with Copper(I) 57
2.2.2 Complexes of $\mathbf{L_1}$ with Zinc(II) 60
2.2.3 Complexes of $\mathbf{L_2}$ with Copper(I) 62
2.2.4 Complexes of $\mathbf{L_2}$ with Zinc(II) 64
2.3 ^{1}H NMR Studies 64
2.3.1 Complexes with $\mathbf{L_1}$ 64
2.3.2 Complexes with $\mathbf{L_2}$ 65
2.3.3 Addition of $Ba(ClO_4)_2$ to Complexes with $\mathbf{L_1}$ 67
2.3.4 Addition of $Ba(ClO_4)_2$ to Complexes with $\mathbf{L_2}$ 68
2.3.5 Reaction of $\mathbf{L_1}$ with a Mixture of Copper(I) and Zinc(II) 70
2.3.6 Reaction of $\mathbf{L_2}$ with a Mixture of Copper(I) and Zinc(II) 71
2.3.7 Addition of s-block Metal Cations to the $\mathbf{L_1}$ Mixed Metal System 72
2.3.8 Addition of s-block Metal Cations to the $\mathbf{L_2}$ Mixed Metal System 73
2.4 Discussion 75
2.4.1 Discussion of the Ditopic Ligand $\mathbf{L_1}$ 75
2.4.2 Discussion of the Ditopic Ligand $\mathbf{L_2}$ 77

Chapter 3 80
3. Electrostatic Control of the Formation of Heteroleptic Helicates 81
3.1 Ligand Synthesis 82

3.1.1 Synthesis of $\mathbf{L_3}$ 82
3.2 Coordination Chemistry 83
3.2.1 Complexes of $\mathbf{L_3}$ with Zinc(II) 83
3.2.2 Addition of $Ba(ClO_4)_2$ to Complexes with $\mathbf{L_3}$ 86
3.3 ^{1}H NMR Studies 89
3.3.1 Complexes with $\mathbf{L_3}$ 89
3.3.2 Formation of Heteroleptic Complexes 89
3.3.3 Addition of $Ba(ClO_4)_2$ to the Mixed Ligand System 90
3.4 Discussion 91

Chapter 4 94
4. Deprogrammable Heterometallic Helicates 95
4.1 Ligand Synthesis 96
4.1.1 Synthesis of $\mathbf{L_4}$ 96
4.1.2 Synthesis of $\mathbf{L_5}$ 100
4.1.3 Synthesis of $\mathbf{L_6}$ 101
4.2 Coordination Chemistry 104
4.2.1 Complexes of $\mathbf{L_4}$ with Copper(I) and Zinc(II) 104
4.2.2 Complexes of $\mathbf{L_5}$ with Copper(I) and Zinc(II) 108
4.2.3 Complexes of $\mathbf{L_6}$ with Copper(I) and Zinc(II) 108
4.3 ^{1}H NMR Studies 112
4.3.1 Complexes with $\mathbf{L_4}$ 112
4.3.1.1 Addition of $Ba(ClO_4)_2$ to $[CuZn_2(\mathbf{L_4})_2]^{5+}$ 114
4.3.2 Complexes with $\mathbf{L_5}$ 116
4.3.2.1 Addition of $Ba(ClO_4)_2$ to $[CuZn_2(\mathbf{L_5})_2]^{5+}$ 117
4.3.3 Complexes with $\mathbf{L_6}$ 118
4.3.3.1 Addition of $Ba(ClO_4)_2$ to $[Cu_2Zn_2(\mathbf{L_6})_2]^{6+}$ 119
4.4 Conclusion 121

Chapter 5 123
5. Conclusion 124

Chapter 6 127
6. Experimental 128
6.1 Synthesis of 2,2'-bipyridine-3,3'-dicarboxylic acid, (**2**) 128
6.2 Synthesis of 3,3'-dicarbomethoxy-2,2'-bipyridine, (**3**) 129
6.3 Synthesis of 2,2'-bipyridine-3,3'-dimethanol, (**4**) 130
6.4 Synthesis of 2,2'-bipyridine-crown ether, (**5**) 131
6.5 Synthesis of bis-N,N'-oxide, (**6**) 132
6.6 Synthesis of 2,2'-bipyridine-crown ether-6,6'-dicarbonitrile, (**7**) 133
6.7 Synthesis of 2,2'-bipyridine-crown ether 6,6'-dithioamide, (**8**) 134
6.8 Synthesis of (**L_1**) 135
6.9 Synthesis of 3-hydroxy-2-iodopyridine, (**11**) 136
6.10 Synthesis of 3,3-dihydroxy-2,2-bipyridine, (**12**) 137
6.11 Synthesis of 2,2'-bipyridine-crown ether, (**13**) 138
6.12 Synthesis of bis-N,N'-oxide, (**14**) 139
6.13 Synthesis of 2,2'-bipyridine-crown ether-6,6'-dicarbonitrile, (**15**) 140
6.14 Synthesis of 2,2'-bipyridine-crown ether-6,6'- dithioamide, (**16**) 141
6.15 Synthesis of (**L_2**) 142
6.16 Synthesis of (**L_3**) 143
6.17 Synthesis of bipyridine 1- N-oxide, (**20**) 144
6.18 Synthesis of 2,2'-bipyridine-6-carbonitrile, (**21**) 144
6.19 Synthesis of 2,2'-bipyridine thioamide, (**22**) 145
6.20 Synthesis of tridentate ester, (**23**) 145
6.21 Synthesis of tridentate alcohol, (**24**) 146
6.22 Synthesis of 5-hydroxy-6-iodo-2-methylpyridine, (**26**) 147
6.23 Synthesis of 6,6'-dimethyl-2,2'-bipyridine-3,3'-diol, (**27**) 148
6.24 Synthesis of 2,2'-bipyridine-crown ether, (**28**) 149
6.25 Synthesis of bis-N,N'-oxide, (**29**) 150
6.26 Synthesis of the acetylated 2,2'-bipyridine, (**30**) 151
6.27 Synthesis of 2,2'-bipyridine-6,6'-dimethanol-crown ether, (**31**) 152
6.28 Synthesis of 2,2'-bipyridine-6,6'-dimethylchloride-crown ether, (**32**) 153
6.29 Synthesis of (**L_4**) 154
6.30 Synthesis of (**L_5**) 155
6.31 Synthesis of compound (**36**) 157
6.32 Synthesis of compound (**37**) 158

6.33 Synthesis of compound (**38**) 159
6.34 Synthesis of ($\mathbf{L_6}$) 160
6.35 Synthesis of the Complex $[Cu_2(\mathbf{L_1})_2Ba_2](ClO_4)_6$ 162
6.36 Synthesis of the Complex $[Zn(\mathbf{L_1})Ba](ClO_4)_4$ 162
6.37 Synthesis of the Complex $[Cu_2(\mathbf{L_2})_2Ba_2](ClO_4)_6$ 162
6.38 Synthesis of the Complex $[Zn_2(\mathbf{L_3})_2](ClO_4)_4$ 163
6.39 Synthesis of the Complex $[Zn_2(\mathbf{L_3})_2Ba_2](ClO_4)_8$ 163
6.40 Synthesis of the Complex $[CuZn_2(\mathbf{L_4})_2](ClO_4)_5$ 163
6.41 Synthesis of the Complex $[Cu_2Zn_2(\mathbf{L_6})_2](ClO_4)_6$ 163

References 164

Appendix I:- Crystal Data Tables xix
Appendix II:- Publications xxvii

List of Figures

Figure 1.1. The three macrocyclic ligands:-

(a) Pedersen's *corand*..... 2

(b) Lehn's *cryptand*..... 2

(c) Cram's *spherand*..... 2

Figure 1.2. Ion-dipole interaction between the oxygen lone pairs and the positive cation..... 3

Figure 1.3. Dipole-dipole interaction.....3

Figure 1.4. The formation of a hydrogen bond.....4

Figure 1.5. π-π stacking interactions. 4

Figure 1.6. Examples of useful macrocycles within modern technology:-

(a) Ruthenium based luminescent sensor for divergent cations.. 6

(b) Crown ether based dye of spectrophotometric detectio.....6

Figure 1.7. Square [2 × 2] grid structure formed upon reaction of various metal cations with $\mathbf{L_a}$. Where M^{II} could be Co^{II}, Ni^{II}, Cu^{II} or Zn^{II} ions.....9

Figure 1.8. Representation of $[Co_{12}(\mathbf{L_b})_{18}][BF_4]_{24}$ showing the dodecanuclear cage of Co^{II} ions and the encapsulated tetrafluoroborate anions.... 10

Figure 1.9. (a) Representation of Funjita's cage structure.....10

(b) Cartoon representation of the stacking of the mononuclear acac complexes within the cavity. M = Pt^{II}, Pd^{II} or Cu^{II}..... 10

Figure 1.10. Ladder type complex $[Cu_4(\mathbf{L_c})_2(\mathbf{L_d})_2]^{4+}$..... 11

Figure 1.11. Rack type complex $[Ru^{II}{}_2(\mathbf{L_a})(tpy)_2]^{4+}$..... 12

Figure 1.12. Structure of the chameleonic ligand $\mathbf{L_e}$.....13

Figure 1.13. The structural motifs of V. Patroniak's formed by reaction of a chameleonic ligand with various metal ions..... 14

Figure 1.14. Formation of the homoleptic helicate $[Cu_2(\mathbf{L_f})_2]^{2+}$ upon reaction of $\mathbf{L_f}$ with Cu^{I} ions..... 17

Figure 1.15. Representation of the mononuclear complex $[Cu^{II}\mathbf{L_f}]^{2+}$..... 17

Figure 1.16. Cartoon representation of the formation of both homoleptic and heteroleptic helicates upon reaction of $\mathbf{L_g}$ and $\mathbf{L_h}$ with copper(I) ions..... 18

Figure 1.17. Cartoon representation of the formation of the unsaturated helicate $[Cu_2(\mathbf{L_i})_2(OAc)_2]^{2+}$ 19

Figure 1.18. Cartoon representation of the formation of both HT and HH isomers with $\mathbf{L_j}$ and only the HT isomer with $\mathbf{L_k}$ 20

Figure 1.19. Schematic representation of the formation of the heteronuclear double helicate $[CoAg(\mathbf{L_l})_2]^{3+}$ 21

Figure 1.20. Diagram showing both the right handed (plus, P) and the left handed (minus, M) rotations of a helicate. *l* is the pitch and z is the helical axis 22

Figure 1.21. Absolute configuration of both Δ and Λ stereoisomers of a tetrahedral and an octahedral metal centre 23

Figure 1.22. The simple *ortho*-linked quaterpyridine $\mathbf{L_m}$ and sexipyridine $\mathbf{L_n}$ polydentate ligands 23

Figure 1.23. The two (P) and (M) enantiomeric representations of the dinuclear double helicates:-

(a) $[Cu_2(\mathbf{L_m})_2]^{2+}$ 24

(b) $[Cd_2(\mathbf{L_n})_2]^{4+}$ 24

Figure 1.24. Structures of E. C. Constable's ligand $\mathbf{L_o}$ and Von Zelewsky's ligand $\mathbf{L_p}$ 25

Figure 1.25. Cartoon representation showing the formation of the heteroleptic mesocate $[Zn_2(\mathbf{L_q})(\mathbf{L_r})]^{4+}$ 26

Figure 1.26. Self-recognition in the self-assembly of only homoleptic helicates from a mixture of ligand strands $\mathbf{L_s}$ – $\mathbf{L_v}$ 27

Figure 1.27. Cartoon representation showing ligand recognition between two tri-bidentate ligands $\mathbf{L_t}$ and $\mathbf{L_w}$ 28

Figure 1.28. Schematic representation showing the various complexes exhibited by $\mathbf{L_n}$ 29

Figure 1.29. The two pyridyl-thiazole ligands $\mathbf{L_x}$ and $\mathbf{L_y}$ 31

Figure 1.30. The two pyridyl-thiazole ligands $\mathbf{L_z}$ and $\mathbf{L_{aa}}$ 32

Figure 1.31. Ditopic ligand $\mathbf{L_{bb}}$, containing a phenanthroline N-donor domain attached to an adjacent [18]crown-6 ether fragment 33

Figure 1.32. (a) The conformation adopted by $\mathbf{L_{cc}}$ upon reaction with the diquat dication.....34
(b) The conformation adopted upon reaction with $[Ru^{II}(bipy)_2](PF_6)$ and Na^+ ions..... 34
Figure 1.33. The biphenyl [20]crown-6 ether zinc(II) porphyrin ligand $\mathbf{L_{dd}}$..... 35
Figure 1.34. The ditopic macrobicyclic receptor $\mathbf{L_{ee}}$, indicating the position of the anion and cation binding sites..... 36
Figure 1.35. The heteroditopic receptor, $\mathbf{L_{ff}}$..... 37
Figure 1.36. The formation of the anion receptor upon reaction of $\mathbf{L_{gg}}$ with $RuCl_3$.....38
Figure 1.37. The 1,2-alternate conformation adopted by $\mathbf{L_{hh}}$ in the presence of a PF_6^- counter ion.....39
Figure 1.38. The urea functionalised isoquinoline ligand $\mathbf{L_{ii}}$..... 40
Figure 1.39. Representation of:-
(a) The 1,2-alternate conformation formed upon addition of Cl^-, Br^- or I^- anions.....41
(b) The cone conformation formed upon addition of $H_2PO_4^-$ or SO_4^{2-} anions.....41
Figure 1.40. The potentially tetradentate ligand $\mathbf{L_{jj}}$, comprising of amide substituents.....42
Figure 1.41. Cartoon representation showing ligand recognition between $\mathbf{L_x}$ and $\mathbf{L_{jj}}$ upon addition of nitrate anions.....43
Figure 1.42. The asymmetric ligand $\mathbf{L_{kk}}$.....44
Figure 1.43. Cartoon representation showing ligand recognition upon addition of nitrate anions to the asymmetric ligand $\mathbf{L_{kk}}$.....45
Figure 1.44. 2,2-bipyridine crown ether ligand, $\mathbf{L_{ll}}$.....46
Figure 1.45. The various conformations adopted by $\mathbf{L_{ll}}$ upon coordination via the crown ether unit and the bipyridyl unit..... 46
Figure 1.46. The potentially tetra-dentate ligand $\mathbf{L_{mm}}$..... 47
Figure 1.47. Allosteric reprogramming of the ditopic ligand, $\mathbf{L_{mm}}$..... 49
Figure 1.48. The potentially tetradentate ligand $\mathbf{L_{nn}}$..... 50
Figure 1.49. The conversion of the HT $\mathbf{L_{nn}}$ helicate species to a side-by-side species upon addition of Ba^{2+} or Na^+ ions..... 51
Figure 2.1. The potentially tetradentate ligands $\mathbf{L_1}$ and $\mathbf{L_2}$.....53

Figure 2.2. X-ray crystal structure of the complex cation $[Cu_2(\mathbf{L_1})_2Ba_2]^{6+}$ showing:-

(a) The structural framework..... 57

(b) The space filling representation..... 58

Figure 2.3. Structure of $\mathbf{L_1}$ showing the partitioning of the ligand into two bis-bidentate binding domains..... 59

Figure 2.4. X-ray crystal structure of the complex cation $[Zn(\mathbf{L_1})Ba]^{4+}$ showing:-

(a) The structural framework..... 60

(b) The space filling representation..... 61

Figure 2.5. X-ray crystal structure of the complex cation $[Cu_2(\mathbf{L_2})_2Ba_2]^{6+}$ showing:-

(a) The structural framework..... 62

(b) The space filling representation..... 63

Figure 2.6. Selected regions of the ^{1}H NMR spectra (CD_3CN) of:-

(a) $[Cu_2(\mathbf{L_1})_2]^{2+}$..... 65

(b) $[Zn(\mathbf{L_1})]^{2+}$..... 65

Figure 2.7. Selected regions of the ^{1}H NMR spectra (CD_3CN) of:-

(a) $[Cu_2(\mathbf{L_2})_2]^{2+}$..... 66

(b) $[Zn(\mathbf{L_2})]^{2+}$..... 66

Figure 2.8. Selected regions of the ^{1}H NMR spectra (CD_3CN) of:-

(a) $[Cu_2(\mathbf{L_1})_2]^{2+}$..... 68

(b) $[Cu_2(\mathbf{L_1})_2Ba_2]^{6+}$..... 68

(c) $[Zn(\mathbf{L_1})]^{2+}$..... 68

(c) $[Zn(\mathbf{L_1})Ba]^{4+}$..... 68

Figure 2.9. Selected regions of the ^{1}H NMR spectra (CD_3CN) of:-

(a) $[Cu_2(\mathbf{L_2})_2]^{2+}$..... 69

(b) $[Cu_2(\mathbf{L_2})_2Ba_2]^{6+}$..... 69

(c) $[Zn(\mathbf{L_2})]^{2+}$..... 69

(d) $[Zn(\mathbf{L_2})Ba]^{4+}$..... 69

Figure 2.10. Selected regions of the ^{1}H NMR spectra (CD_3CN) of:-

(a) $[Cu_2(\mathbf{L_1})_2]^{2+}$..... 70

(b) $[Zn(\mathbf{L_1})]^{2+}$..... 70

(c) $\mathbf{L_1}$ + Cu^+ and Zn^{2+} ions..... 70

Figure 2.11. Selected regions of the ^{1}H NMR spectra (CD_3CN) of:-
(a) $[Cu_2(\mathbf{L_2})_2]^{2+}$ 72
(b) $[Zn(\mathbf{L_2})]^{2+}$ 72
(c) $\mathbf{L_2}$ + Cu^+ and Zn^{2+} ions 72
Figure 2.12. Selected regions of the ^{1}H NMR spectra (CD_3CN) of:-
(a) $\mathbf{L_1}$ + Cu^+ and Zn^{2+} ions 73
(b) $\mathbf{L_1}$ + Cu^+ and Zn^{2+} plus excess Ba^{2+} ions 73
(c) $\mathbf{L_1}$ + Cu^+ and Zn^{2+} plus excess St^{2+} ions 73
Figure 2.13. Selected regions of the ^{1}H NMR spectra (CD_3CN) of:-
(a) $\mathbf{L_2}$ + Cu^+ and Zn^{2+} ions 74
(b) $\mathbf{L_2}$ + Cu^+ and Zn^{2+} plus excess Ba^{2+} ions 74
(c) $\mathbf{L_2}$ + Cu^+ and Zn^{2+} plus excess St^{2+} ions 74
Figure 2.14. Cartoon representation of the distribution of products following the addition of various s-block metal cations to $\mathbf{L_1}$ 76
Figure 2.15. Cartoon representation of the distribution of products following the addition of various s-block metal cations to $\mathbf{L_2}$ 79
Figure 3.1. The potentially hexadentate ligands $\mathbf{L_3}$ 81
Figure 3.2. X-ray crystal structure of the complex cation $[Zn_2(\mathbf{L_3})_2]^{4+}$ showing:-
(a) The structural framework 83
(b) The space filling representation 84
Figure 3.3. Structure of $\mathbf{L_3}$ showing the partitioning of the ligand into two bis-tridentate binding domains 85
Figure 3.4. X-ray crystal structure of the complex cation $[Zn_2(\mathbf{L_3})_2Ba_2]^{8+}$ showing:-
(a) The structural framework 86
(b) The space filling representation 87
Figure 3.5. Selected regions of the ^{1}H NMR spectrum of $[Zn_2(\mathbf{L_3})_2]^{4+}$ 89
Figure 3.6. Selected regions of the ^{1}H NMR spectrum (CD_3CN) of a mixture of $[Zn_2(\mathbf{L_3})_2]^{4+}$, $[Zn_2(\mathbf{L_z})_2]^{4+}$ and $[Zn_2(\mathbf{L_3})(\mathbf{L_z})]^{4+}$ 90

Figure 3.7. Selected regions of the ^{1}H NMR spectrum of a mixture of ($[Zn_2(\mathbf{L_3})_2]^{4+}$, $[Zn_2(\mathbf{L_z})_2]^{4+}$ and $[Zn_2(\mathbf{L_3})(\mathbf{L_z})]^{4+}$ following the addition of:-

(a) 0 equivalents of $Ba(ClO_4)_2$ 91

(b) 20 equivalents of $Ba(ClO_4)_2$ 91

(c) 40 equivalents of $Ba(ClO_4)_2$ 91

Figure 3.8. Cartoon representation showing the change in the ligand recognition properties between $\mathbf{L_3}$ and $\mathbf{L_z}$ following the addition of excess barium ions 93

Figure 4.1. Structures of ligands $\mathbf{L_4}$, $\mathbf{L_5}$ and $\mathbf{L_6}$ 95

Figure 4.2. X-ray crystal structure of the complex cation $[CuZn_2(\mathbf{L_4})_2]^{5+}$ showing:-

(a) The structural framework 104

(b) The space filling representation 105

Figure 4.3. Structure of $\mathbf{L_4}$ showing the partitioning of the ligand into two bis-tridentate and one central bidentate binding domains 106

Figure 4.4. The central bipyridyl unit from the crystal structure of $\mathbf{L_4}$ 106

Figure 4.5. Part of the crystal structure of $\mathbf{L_4}$ showing:-

(a) The distorted tetrahedral 107

(b) The octahedral metal centres 107

Figure 4.6. X-ray crystal structure of the complex cation $[Cu_2Zn_2(\mathbf{L_6})_2]^{6+}$ showing:-

(a) The structural framework 109

(b) The space filling representation 109

Figure 4.7. Structure of $\mathbf{L_6}$ showing the partitioning of the ligand into two bis-tridentate and two bis-bidentate binding domains 110

Figure 4.8. The central bipyridyl unit from the crystal structure of $\mathbf{L_6}$ showing the NCCN torsion angle of 58.62° 111

Figure 4.9. Selected regions of the ^{1}H NMR spectrum of $[CuZn_2(\mathbf{L_4})_2]^{5+}$ 113

Figure 4.10. Aromatic region from the ^{1}H/^{1}H COSY spectrum of $[CuZn_2(\mathbf{L_4})_2]^{5+}$ recorded in CD_3CN 113

Figure 4.11. Selected aromatic and aliphatic regions of the ^{1}H NMR spectrum, recorded in CD_3CN, of:-

(a) $[CuZn_2(\mathbf{L_4})_2]^{5+}$ 114

(b) $[CuZn_2(\mathbf{L_4})_2]^{5+}$ + 4 equivalents $Ba(ClO_4)_2$ 114

(c) $[CuZn_2(\mathbf{L_4})_2]^{5+}$ + 10 equivalents $Ba(ClO_4)_2$ 114

(d) $[CuZn_2(\mathbf{L_4})_2]^{5+}$ + 20 equivalents $Ba(ClO_4)_2$ 114

Figure 4.12. Cartoon representation of the deprogramming of the $\mathbf{L_4}$ helicate species upon addition of Ba^{2+} ions, which leads to the formation of a series of coordination polymers 116

Figure 4.13. Selected aromatic and aliphatic regions of the ^{1}H NMR spectra recorded in CD_3CN of:-

(a) $[CuZn_2(\mathbf{L_5})_2]^{5+}$ 117

(b) $[CuZn_2(\mathbf{L_5})_2]^{5+}$ + 20 equivalents of $Ba(ClO_4)_2$ 117

Figure 4.14. Selected aromatic regions of the ^{1}H NMR spectrum of $[Cu_2Zn_2(\mathbf{L_6})_2]^{6+}$ 118

Figure 4.15. Selected aromatic and aliphatic regions of the ^{1}H NMR spectra recorded in CD_3CN of:-

(a) $[Cu_2Zn_2(\mathbf{L_6})_2]^{6+}$ 120

(b) $[Cu_2Zn_2(\mathbf{L_6})_2]^{6+}$ + 20 equivalents of Ba^{2+} ions 120

Figure 4.16. Aromatic region from the ^{1}H/^{1}H COSY spectrum of $[Cu_2Zn_2(\mathbf{L_6})_2]^{6+}$ + 20 equivalents of Ba^{2+} ions, recorded in CD_3CN 120

List of Schemes

Scheme 1. Synthesis of $\mathbf{L_1}$ from 1,10-phenanthroline (**1**).....55
Scheme 2. Synthesis of $\mathbf{L_2}$ from 3-hydroxypyridine (**10**)..... 56
Scheme 3. Synthesis of $\mathbf{L_3}$ from 6,6'-dithioamide (**16**)..... 82
Scheme 4. Synthesis of compound (**24**) from 2,2'-bipyridine (**19**).....97
Scheme 5. Synthesis of compound (**32**) from 5-hydroxy-2-methylpyridine (**25**)..98
Scheme 6. Synthesis of the ligand $\mathbf{L_4}$ by means of a coupling reaction between py-py-tz-OH (**24**) and the dichloride (**32**)..... 99
Scheme 7. Synthesis of $\mathbf{L_5}$ by means of a coupling reaction between py-py-tz-OH (**24**) and the dichloride (**34**).....100
Scheme 8. Synthesis of compound (**38**) from 3-hydroxypyridine (**10**).....102
Scheme 9. Synthesis of the ligand $\mathbf{L_6}$ by means of a coupling reaction between the alcohol (**24**) and the dichloride (**38**)..... 103

List of Tables

Table 1. Selected crown ether cavity diameters and compatible cation diameters.....7
Table 2. Selected bond lengths (Å) for the complex cation$[Cu_2(\mathbf{L_1})_2Ba_2]^{6+}$.....58
Table 3. Selected bond lengths (Å) for the complex cation $[Zn(\mathbf{L_1})Ba]^{4+}$.....61
Table 4. Selected bond lengths (Å) for the complex cation $[Cu_2(\mathbf{L_2})_2Ba_2]^{6+}$.... 63
Table 5. Selected bond lengths (Å) for the complex cation $[Zn_2(\mathbf{L_3})_2]^{4+}$.....84
Table 6. Selected bond lengths (Å) for the complex cation $[Zn_2(\mathbf{L_3})_2Ba_2]^{8+}$.....87
Table 7. Selected bond lengths (Å) for the complex cation $[CuZn_2(\mathbf{L_4})_2]^{5+}$.....105
Table 8. Selected bond lengths (Å) for the complex cation $[Cu_2Zn_2(\mathbf{L_6})_2]^{6+}$.....110
Table A1. Crystallographic data of the $\mathbf{L_1}$ complex $[Cu_2(\mathbf{L_1})_2Ba_2]^{6+}$.....xx
Table A2. Crystallographic data of the $\mathbf{L_1}$ complex $[Zn(\mathbf{L_1})Ba]^{4+}$..... xxi
Table A3. Crystallographic data of the $\mathbf{L_2}$ complex $[Cu_2(\mathbf{L_2})_2Ba_2]^{6+}$.....xxii
Table A4. Crystallographic data of the $\mathbf{L_3}$ complex $[Zn_2(\mathbf{L_3})_2]^{4+}$.....xxiii
Table A5. Crystallographic data of the $\mathbf{L_3}$ complex $[Zn_2(\mathbf{L_3})_2Ba_2]^{8+}$.....xxiv
Table A6. Crystallographic data of the $\mathbf{L_4}$ complex $[CuZn_2(\mathbf{L_4})_2]^{5+}$..... xxv
Table A7. Crystallographic data of the $\mathbf{L_6}$ complex $[Cu_2Zn_2(\mathbf{L_6})_2]^{6+}$.....xxvi

List of Abbreviations

Å	Angstroms
py	pyridyl
tz	thiazole
tpy	terpyridine
bipy	bipyridine
V	Volts
vs.	versus
K_1	Rate constant
K_2	Rate constant
d^6DMSO	deuterated dimethylsulphoxide
MS	mass spectrometry
DCM	dichloromethane
ppm	parts per million, δ (delta), chemical shift
NMR	nuclear magnetic resonance
UV/vis	Ultraviolet / visible spectrophotometry
TBA	tetrabutyl ammonium
THF	tetrahydrofuran
DMF	dimethylformamide
*m*CPBA	*meta*-chloroperoxybenzoic acid
RT	room temperature
TMSCN	trimethylsilyl cyanide
ESI-MS	electrospray ionization mass spectrometry
m/z	mass/charge
MHz	megahertz
Hz	hertz
α	alpha
β	beta
γ	gamma
δ	delta (chemical shift)
COSY	correlation spectroscopy
g	gram
l	length

ml	millilitre
mol	moles
mmol	millimoles
M	molar
s	singlet
dd	doublet of doublets
t	triplet
dt	doublet of triplets
ddd	doublet of doublet of doublets
m	multiplet
(g)	gas
(aq)	aqueous
J	coupling constant
TLC	thin layer chromatography

Acknowledgements

I would like to thank my supervisors Dr. Craig Rice and Dr. Gary Midgley for their excellent supervision and guidance throughout my three year PhD programme. I would also like to thank the University of Huddersfield for the funding that has made this PhD possible.

I would also like to thank Dr. Lindsay Harding and Dr. Neil McLay for providing Mass Spec. and NMR facilities and also Dr. Riis-Johannessen and Dr. J. Jeffery for the determination of my crystal structures and the pain staking job of refining many hundreds of atoms.

The biggest thank you of all goes to my parents Ray and Mary, for all their support they have provided both financially and emotionally since I started school. Without their support none of my recent achievements would have been possible.

Finally I would like to thank my fiancee Dr. Sarah Churchman and the rest of my family and friends for their support over recent years.

Abstract

The ability of ligands to partition into distinct binding domains is instrumental in the formation of self-assembling transition metal supramolecular architectures. In order to control such self-assembling processes, ligands are designed and synthesised with a specific number of binding sites of various natures. Thus reaction of such ligands with specific transition metal cations results in the formation of a desired supramolecular assembly. Following the successful synthesis of a given ligand the information within it is said to be permanently stored, and at this point the ligand is effectively "preprogrammed". Described herein, is the synthesis and coordination chemistry of six ligands $\mathbf{L_1}$ – $\mathbf{L_6}$, of which five are ditopic (shown below), whose binding modes can be effectively "reprogrammed" through either allosteric and/or electrostatic effects associated with the coordination of various s-block metal cations to a crown ether moiety.

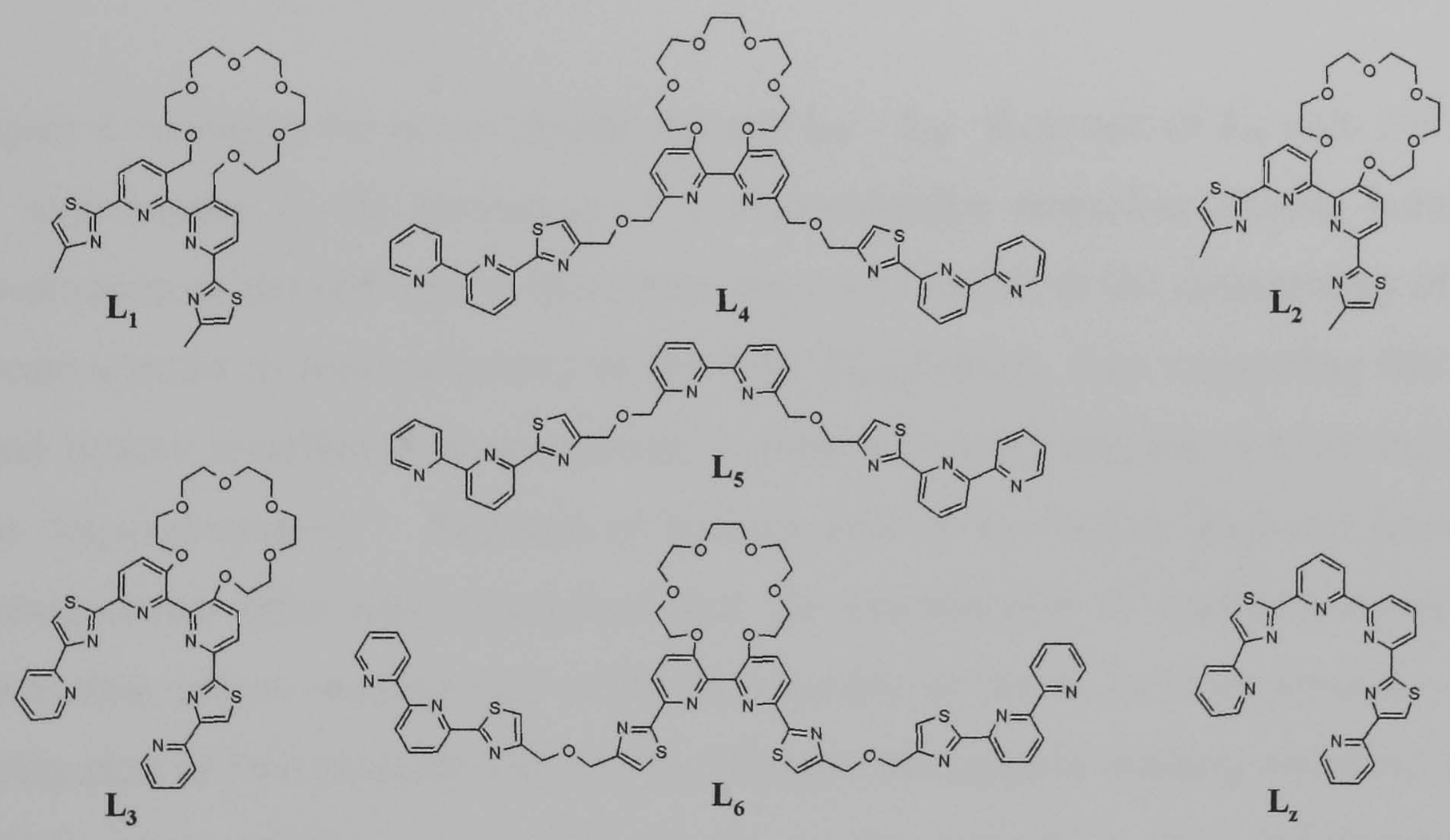

Described within Chapter 1 are a number of elegant examples of recent supramolecular assemblies, covering most aspects of supramolecular chemistry required to give a thorough understanding of the topics covered in the later chapters. Chapter 2 considers the ditopic ligands $\mathbf{L_1}$ and $\mathbf{L_2}$, which both contain a potentially tetradentate pyridyl-thiazole N-donor unit and an additional external crown ether binding site. Reaction of $\mathbf{L_1}$ with either Cu^{I} or Zn^{II} ions results in the formation of either the dinuclear double helicate $[Cu_2(\mathbf{L_1})_2]^{2+}$ or the mononuclear Zn^{II} species $[Zn(\mathbf{L_1})]^{2+}$. In a competitive environment both of these species are formed, with the copper species being slightly favoured. Coordination of s-block metal cations to the

crown ether moiety effectively reprograms the ligands selectivity in such a manner that only the zinc containing species is formed. Reaction of $\mathbf{L_2}$ with Cu^I or Zn^{II} ions results in the formation of three $\mathbf{L_2}$ containing species, $[Cu_2(\mathbf{L_2})_2]^{2+}$, $[CuZn(\mathbf{L_2})_2]^{3+}$ and $[Zn(\mathbf{L_2})]^{2+}$. In a competitive environment the zinc mononuclear species is slightly favoured, however, addition of s-block metal cations to the crown ether moiety effectively reprograms the ligands selectivity so that the distribution of products strongly favours the zinc mononuclear species.

Chapter 3 considers the potentially hexadentate ditopic ligand $\mathbf{L_3}$. Reaction of this ligand with the parent ligand $\mathbf{L_z}$ in the presence of zinc(II) results in the formation of both the homoleptic and heteroleptic helicates ($[Zn_2(\mathbf{L_3})_2]^{4+}$, $[Zn_2(\mathbf{L_z})_2]^{4+}$ and $[Zn_2(\mathbf{L_3})(\mathbf{L_z})]^{4+}$), although very little of the heteroleptic species is observed. Addition of excess barium ions to the mixed ligand system results in all ligand recognition being lost, and the three helicate species present in a statistical ratio.

Chapter 4 considers the novel ditopic ligands $\mathbf{L_4}$ – $\mathbf{L_6}$. Reaction of $\mathbf{L_4}$ with Cu^I and Zn^{II} ions results in the formation of a heterometallic trinuclear double helicate. Coordination of barium ions to the crown ether unit results in the disassembly of the helicate species to form polymers of the type $[(\mathbf{L_4})ZnBa]_n$, thus suggesting that the ligand is now insufficient programming to form a helicate and has correspondingly been "*deprogrammed*". Addition of barium ions to $\mathbf{L_5}$ (which does not have an external crown ether unit) confirmed that the coordination of barium ions to the crown ether unit is instrumental in the disassembly of the $\mathbf{L_4}$ helicate species. The introduction of two thiazole units in $\mathbf{L_6}$ changes the ligands binding domains, thus reaction of $\mathbf{L_6}$ with Cu^I and Zn^{II} results in the formation of a heterometallic tetranuclear double helicate $[Zn_2Cu_2(\mathbf{L_6})_2]^{6+}$. Coordination of Ba^{2+} ions to the crown ether unit of $\mathbf{L_6}$ has no effect on the stability of the helicate species as the ligand is still sufficiently programmed to act as a helicating ligand in the presence of Ba^{2+} ions.

With the exception of one crystal structure all the crystals required for the determination of the structures are novel and have been produced by myself, however, the structures were obtained by Dr's Jeffery and Riis-Johannessen (School of Chemistry University of Bristol).

Chapter 1

1. Introduction

1.0 Supramolecular Chemistry

Supramolecular chemistry has been defined by many chemists over recent years; one definition by J.-M. Lehn, described supramolecular chemistry as "chemistry of molecular assemblies and of the intermolecular bond".[1] This definition has been further defined as "chemistry beyond the molecule"[1] and is concerned with the assembly and control of increasingly complex systems, held together by non covalent bonds. Supramolecular chemistry can also be regarded as a highly interdisciplinary field, bringing together chemists, biologists, biochemists and a whole host of other researchers.[2]

Although some concepts within supramolecular chemistry can be dated back to the beginning of modern chemistry itself, it is still a relatively new field of chemistry dating back to the discovery of various macrocyclic ligands in the late 1960's. This pioneering research was carried out by the groups of C. J. Pedersen, J.-M. Lehn and more recently D. J. Cram. It is these researchers who are largely responsible for the existence of supramolecular chemistry we have come to know over recent years.

1.1 The Origins of Supramolecular Chemistry

The groups of C. J. Pedersen,[3, 4] J.-M. Lehn[5] and D. J. Cram,[6] received the Nobel Prize in 1987 for their contributions within supramolecular chemistry. They investigated the host-guest chemistry of three novel macrocyclic ligands for coordination with metal cations (Figure 1.1).

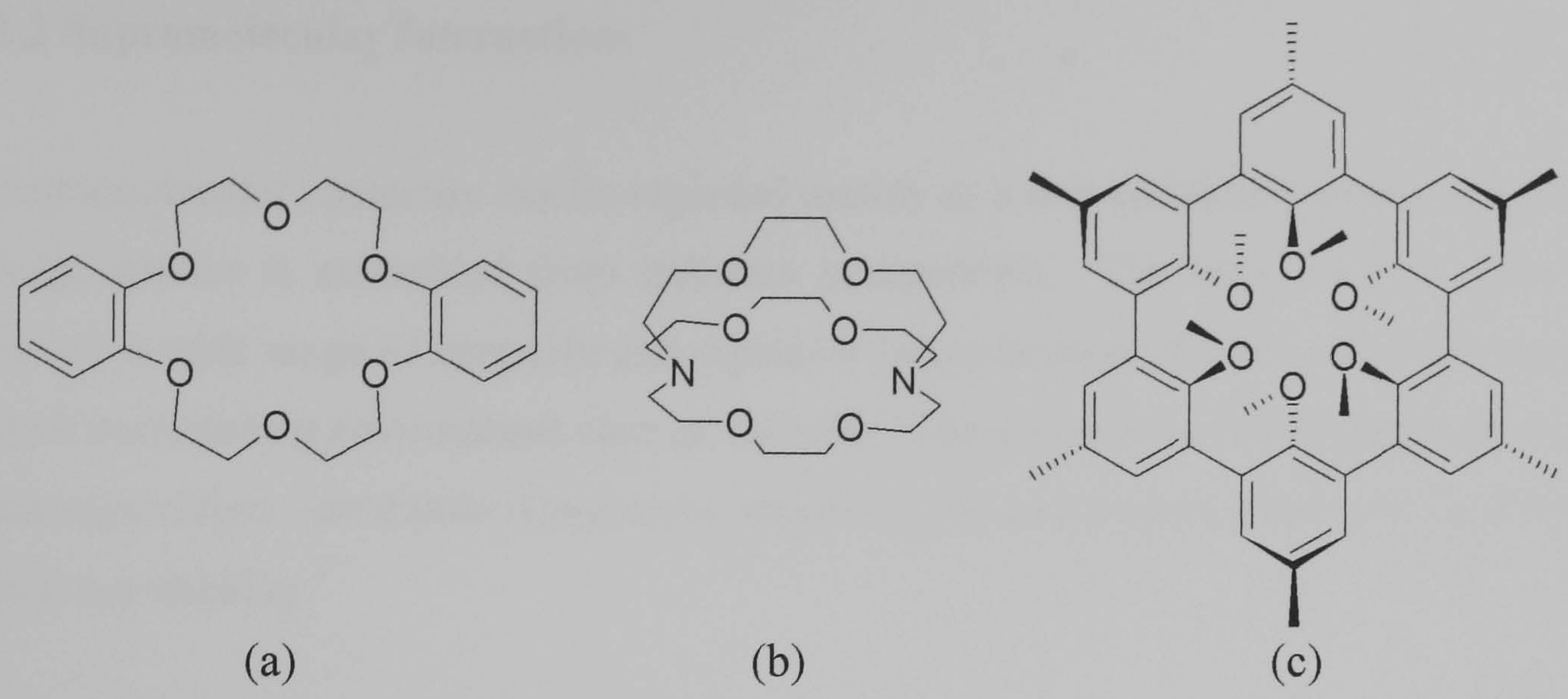

Figure 1.1. The three macrocyclic ligands (a) Pedersen's *corand*, (b) Lehn's *cryptand* and (c) Cram's *spherand*.

Following these early examples of macrocyclic ligands, supramolecular chemistry has received considerable interest over recent years with further studies into simple host-guest chemistry. Initial studies focused on the design and synthesis of simple macrocyclic ligands based on those in Figure 1, for coordination with various guest species.[2] Since these early discoveries, supramolecular chemistry has become one of fastest growing areas of modern day experimental chemistry, with the design and synthesis of increasingly complex systems. A majority of these systems still include host units like those first discovered in the late 1960's, where binding of one or more guest species occurs at well defined binding sites within the host. However, the design and synthesis of modern day supermolecules has changed dramatically as factors such as ligand recognition, self-assembly and allosteric interactions have to be taken into account. The modern supermolecules have featured in many different applications but much of the current research focuses on the development of cancer drugs[7] and chemical sensors.[8, 9]

1.2 Supramolecular Interactions

Supramolecular chemistry can be regarded mainly as a non-covalent process where a large species is assembled from different components. The term "non-covalent" covers a wide range of attractive and repulsive forces between the host, the guest and their surrounding environment such as solvents. These attractive forces may include, amongst others; ion-dipole interactions, dipole-dipole interactions, hydrogen bonding and π-π stacking.[2]

1.2.1 Ion-dipole Interactions

Ion-dipole interactions involve the bonding of an ion such as K^+, with a polar molecule. A good example is the coordination of a potassium cation within a crown ether unit, where the electron-rich oxygen atoms play the role as a polar molecule (Figure 1.2).

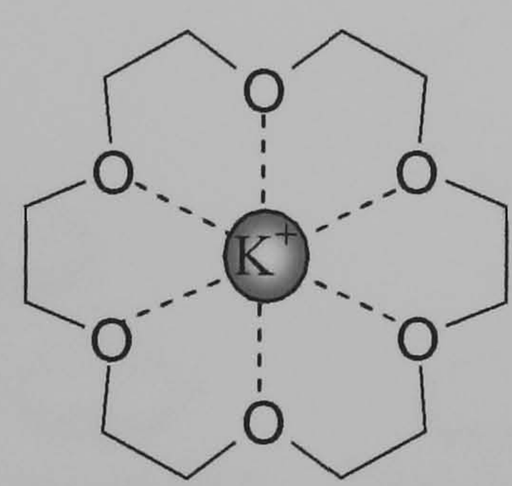

Figure 1.2. Ion-dipole interaction between the oxygen lone pairs and the positive cation.

1.2.2 Dipole-dipole interactions

Dipole-dipole interactions occur when two dipoles align resulting in a significant attraction between a pair of poles with opposite charges on adjacent molecules (Figure 1.3).

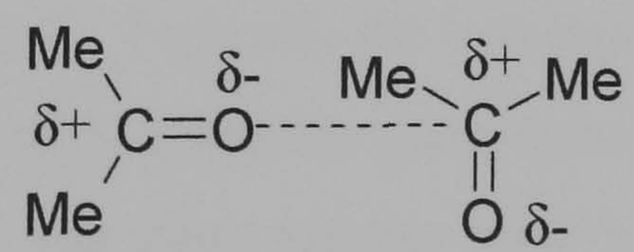

Figure 1.3. Dipole-dipole interaction.

1.2.3 Hydrogen Bonding

Hydrogen bonds may be regarded as very strong dipole-dipole attractions which occur between a hydrogen atom bound to a highly electronegative atom (usually O, N, or F) and an electron pair on another electronegative atom (Figure 1.4).

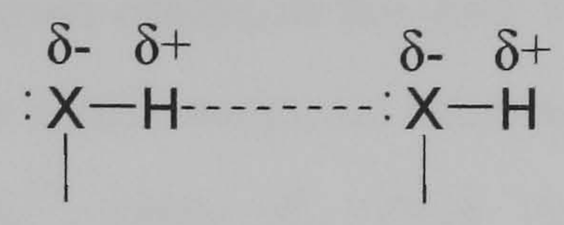

Figure 1.4. The formation of a hydrogen bond.

1.2.4 π-π stacking

A weak electrostatic interaction such as π-π stacking occurs between aromatic rings, one that is electron rich and one that is electron poor. Two types of such interactions exist one being face-to-face and the other being edge-to-face (Figure 1.5).[2]

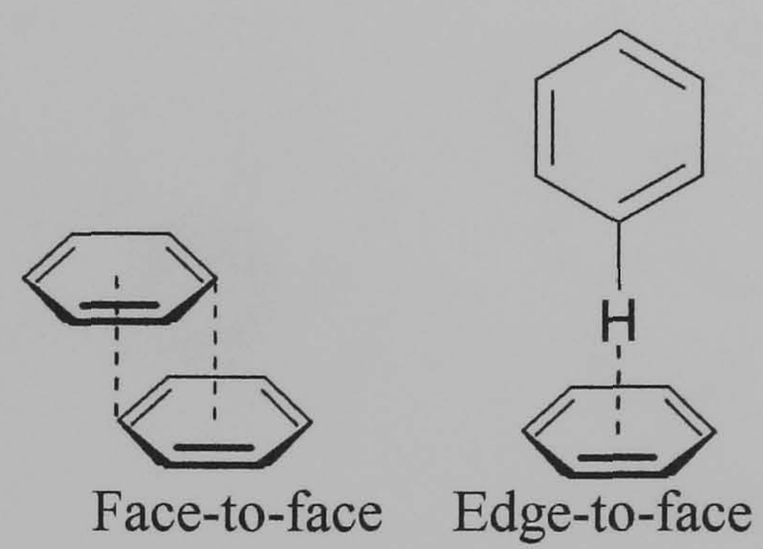

Figure 1.5. π-π stacking interactions.

1.3 Host-guest Chemistry

Supramolecular chemistry in its simplest form involves the non-covalent intermolecular interaction between two different species. These two species are defined as the host and the guest. Typically the host possesses a cavity which has the capability to recognise and bind to a specific guest species; often simple monoatomic cations or inorganic anions. The guest species must also complement the receptor site of the host in terms of its geometric size and shape. Only when the correct guest species has bound to the host will the host species function as it is designed to do so.

A suitable example would be the non-covalent interaction between a cation and the receptor site of a crown ether (macrocycle).

1.3.1 Crown Ethers

Following the discovery of crown ethers in the late 1960's by Pedersen and related systems by Lehn and Cram, a whole range of macrocyclic ligands now exists with many thousands of examples,[10] many of which contain different types of ring systems. These ring systems include *corands*, *podands*, *cryptands*, and *spherands* all of which can be regarded as well developed systems with varying structures while still containing the typical oxygen atoms linked by dimethylene groups. Many of the macrocycles developed over recent years (Figure 1.6) have important roles within modern technology, some of which include; molecular switches,[11] chromatography,[12] sensors[13] and dyes for spectrophotometric detection.[14]

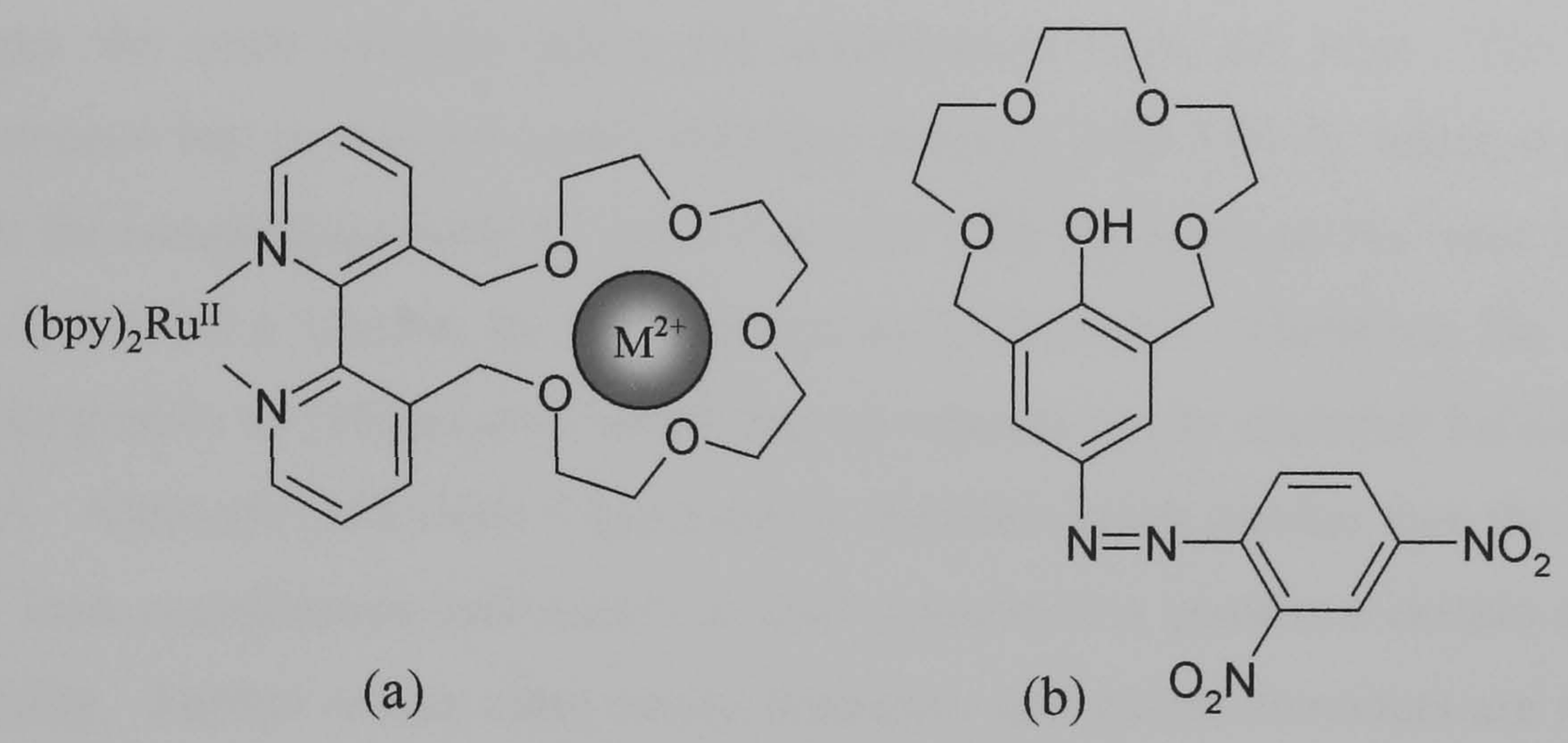

Figure 1.6. Examples of useful macrocycles within modern technology (a) Ruthenium based luminescent sensor for divergent cations,[13] (b) Crown ether based dye of spectrophotometric detection.[14]

Crown ethers are members of the *corand* family and in their simplest form are comprised of a cyclic array of ethylene glycol units –O–CH_2CH_2-O–, the most well known crown ether being [18]crown-6. Crown ethers can also contain three dimensional analogues of the original crown ethers known as *cryptands*, side arms otherwise known as *lariat ethers* and *podands* which consist of ethylene glycol chains which wrap around suitable metal cations. Each of these types can exist with varying ring sizes. All variations of crown ethers have a series of O-donors generating a cavity suitable for coordination with guest species, usually s-block

metal cations. The reason crown ethers have received considerable interest within supramolecular chemistry over recent years is as a result of two major properties. Firstly the *chelate* effect, which relates to the observation that multidentate ligands are significantly more stable than monodentate ligands when bound to a suitable metal cation, and is observed in the binding of metal cations by *podands*. Secondly the *macrocyclic* effect, whereby closed ring systems such as [18]crown-6 have a significantly higher binding affinity towards s-block cations relative to an open chain *podand* system as the closed ring systems are said to be pre-organised.[2]

The selective binding of a particular guest is the basis of molecular recognition and is easily rationalised by the size match between the cation and the host cavity. A particular crown ether will bind most strongly to a cation which is complementary to the host cavity. The size of the cavity can easily be changed by varying the number of O-donors or alkyl spacers within the macrocycle, changing the cavity size thus changes the most suitable cation for coordination with the host. For instance [18]crown-6 has an internal cavity diameter between 2.60-3.20 Å, which is a perfect match for coordination with K^+ ions (diameter 2.66 Å), whereas Na^+ ions (diameter 1.90 Å) are not a suitable for coordination to [18]crown-6. However, Na^+ ions are complementary to [15]crown-5 which has an internal cavity diameter between 1.70-2.20 Å. Although [15]crown-5 has a cavity diameter much smaller than the diameter of K^+ ions, coordination still occurs as such macrocycles possess a certain degree of flexibility. Further crown ether cavity diameters and cation diameters are shown in Table 1.[2]

Crown Ether	Cavity Diameter/Å	Cation	Cation Diameter/Å
[12]crown-4	1.20-1.50	Li^+	1.36
[15]crown-5	1.70-2.20	Na^+	1.90
[18]crown-6	2.60-3.20	K^+	2.66
[21]crown-7	3.40-4.30	Cs^+	3.38
		Mg^{2+}	1.44
		Ca^{2+}	2.20
		Sr^{2+}	2.26
		Ba^{2+}	2.68

Table 1. Selected crown ether cavity diameters and compatible cation diameters.

1.4 Metallosupramolecular Chemistry

Metallosupramolecular chemistry can be described as the interaction between ligands and metal ions. Such ligands have to be synthetically designed to have complimentary structures so that the disposition of binding sites within the ligand enables multiple ligands to bind a single metal ion. Ligands can also have specific recognition features (in terms of size, shape, symmetry and the electronic properties of the binding sites) which can lead to selective self-assembly of a supramolecular complex. Self-assembly has been described by many chemists over recent years. G. M. Whitesides defined it as "the spontaneous assembly of molecules into structured, stable, non-covalent joined aggregates".[15] The self-assembly of supermolecules is also present in nature, the most common being the self-assembling double helical structure of DNA.

Many examples of self-assembling supramolecular systems are known,[16] including, amongst others: grids,[17, 18] cages,[19] ladders,[20] racks[21] and helicates. Helicates, of which there are many examples[22, 23] are the main topic of this thesis.

1.4.1 Grids

Many grid type structures have been prepared from various ligands over recent years.[24-27] One elegant example of a grid structure has been reported by G. S. Hannon and co-workers,[28] who prepared a potentially hexadentate ligand $\mathbf{L_a}$, comprising of two bipyridine units, one either side of a central pyrimidine ring. The pyrimidine unit allows the ligand to partition into bis-tridentate binding domains, which, upon reaction with metal ions favouring octahedral coordination geometry, results in the formation of a square [2 × 2] grid type complex (Figure 1.7). Each metal centre occupies a distorted octahedral coordination geometry formed by two tridentate domains, one from each ligand, with the two ligands at 90° to each other.

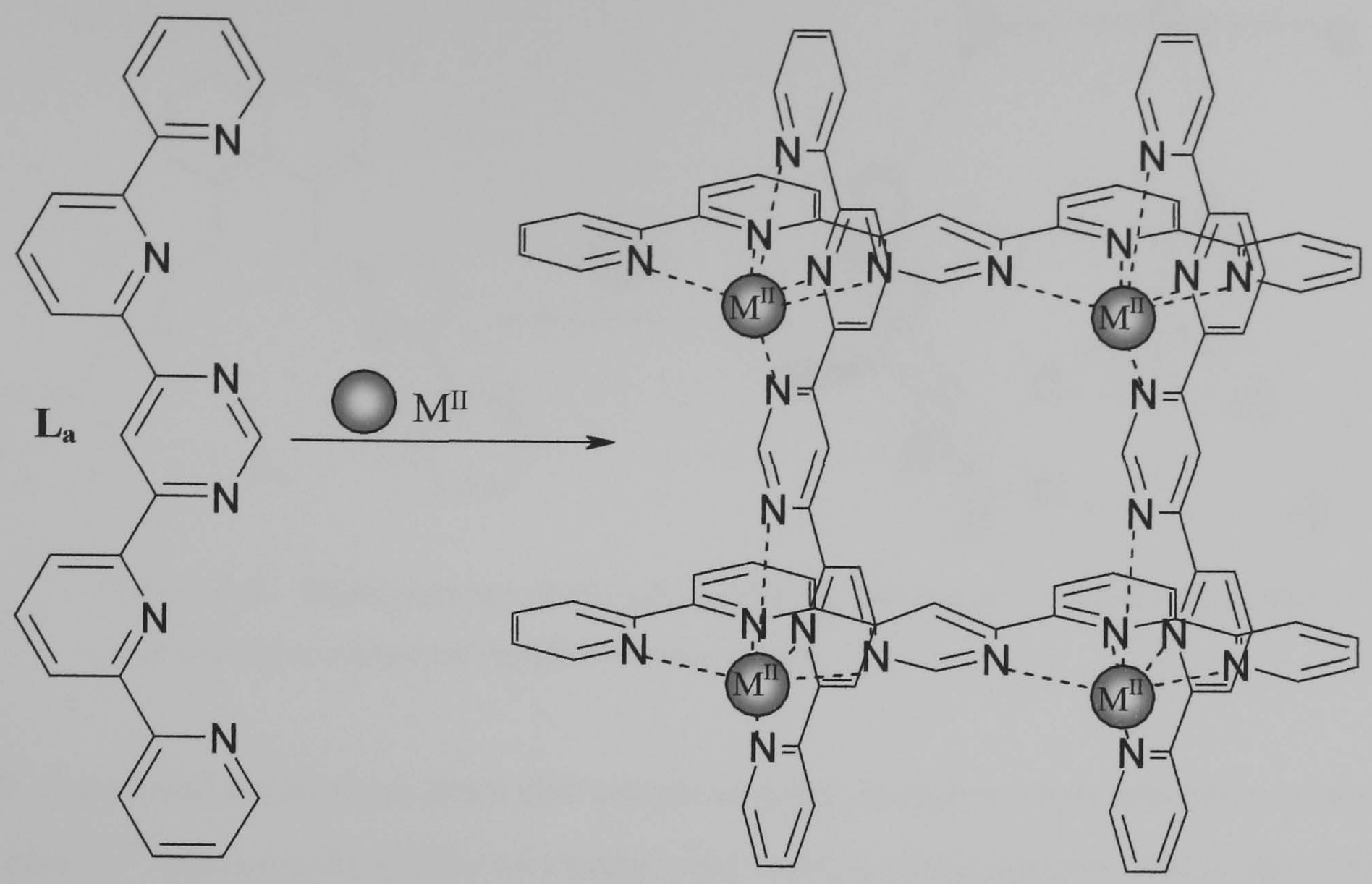

Figure 1.7. Square [2 × 2] grid structure formed upon reaction of various metal cations with $\mathbf{L_a}$. Where M^{II} could be Co^{II}, Ni^{II}, Cu^{II} or Zn^{II} ions.

1.4.2 Cages

Cages are slightly more complex than grid type structures and have received much interest over recent years due to their ability to form central cavities, suitable for coordination with a variety of guest species, of which many examples have been reported over recent years.[29-32] One particular example has been demonstrated by M. D. Ward *et al.*,[33] who synthesised a pyrazolylpyridine type ligand $\mathbf{L_b}$, comprising of two bidentate pyrazolylpyridine units either side of an aromatic core (acting as a simple spacer group). Reaction of this ligand with cobalt(II) ions resulted in the formation of the dodecanuclear cage $[Co_{12}(\mathbf{L_b})_{18}][BF_4]_{24}$, encapsulating four tetrafluoroborate anions within the central cavity (Figure 1.8). Each cobalt(II) ion is coordinated by meridional arrangement of three bidentate pyrazolylpyridine donors in a distorted octahedral coordination geometry.

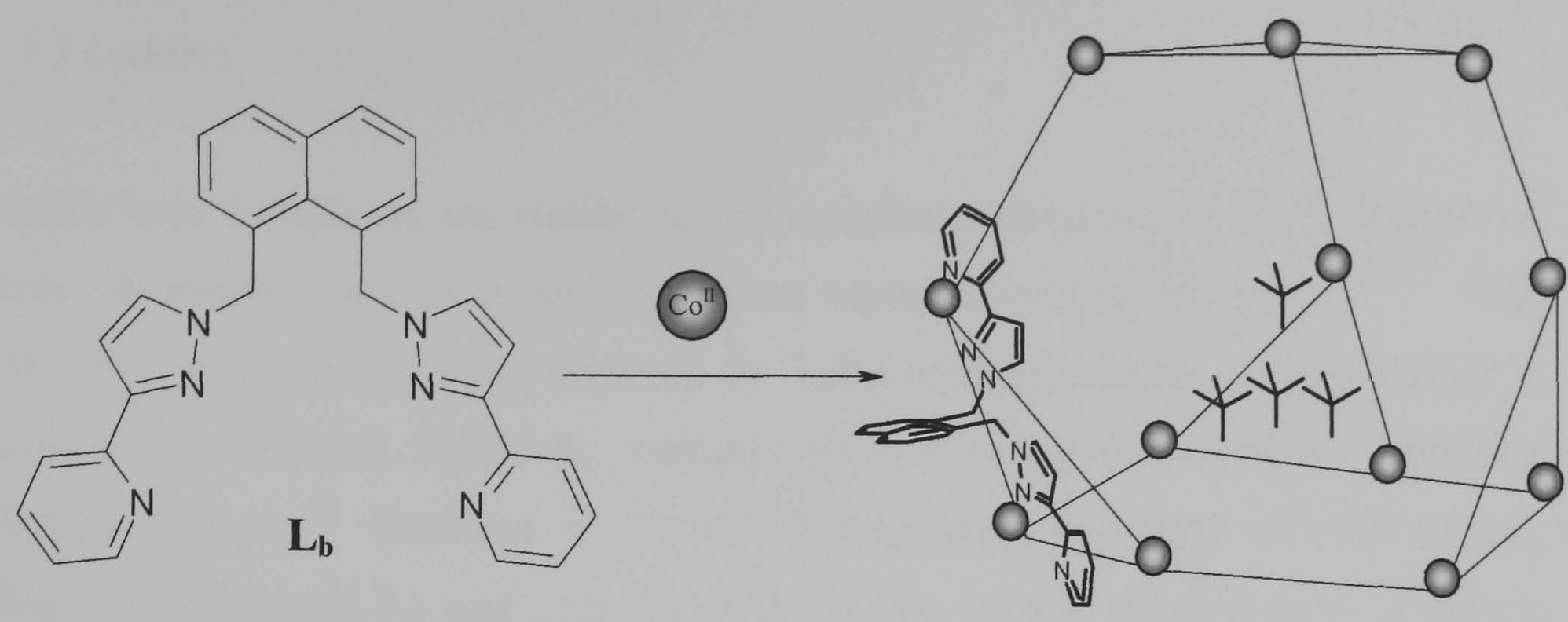

Figure 1.8. Representation of $[Co_{12}(\mathbf{L_b})_{18}][BF_4]_{24}$ showing the dodecanuclear cage of Co^{II} ions and the encapsulated tetrafluoroborate anions.

M. Fujita and co-workers have also prepared many complex cage structures in recent years,[34-36] utilising the ability to encapsulate various guest species within the central cavity of the cage complexes. One particular example demonstrates characteristic metal-metal interactions through accommodation within a coordination cage.[37] The cage structure consists of an organic-pillared framework with a large box shaped hydrophobic cavity, ideal for binding two planar molecules. Thus, upon formation of the cage structure comprising of palladium corner units connected by tritopic organic linkers, the two planar metal acac complexes may then be inserted into the cavity within the cage (Figure 1.9), the structure of which has been confirmed by X-ray crystallography. Due to the close proximity of the metal complexes within the cavity, metal-metal d-d interactions occur between the two metal centres leading to possibilities of unique optical, electroconductive and magnetic properties.

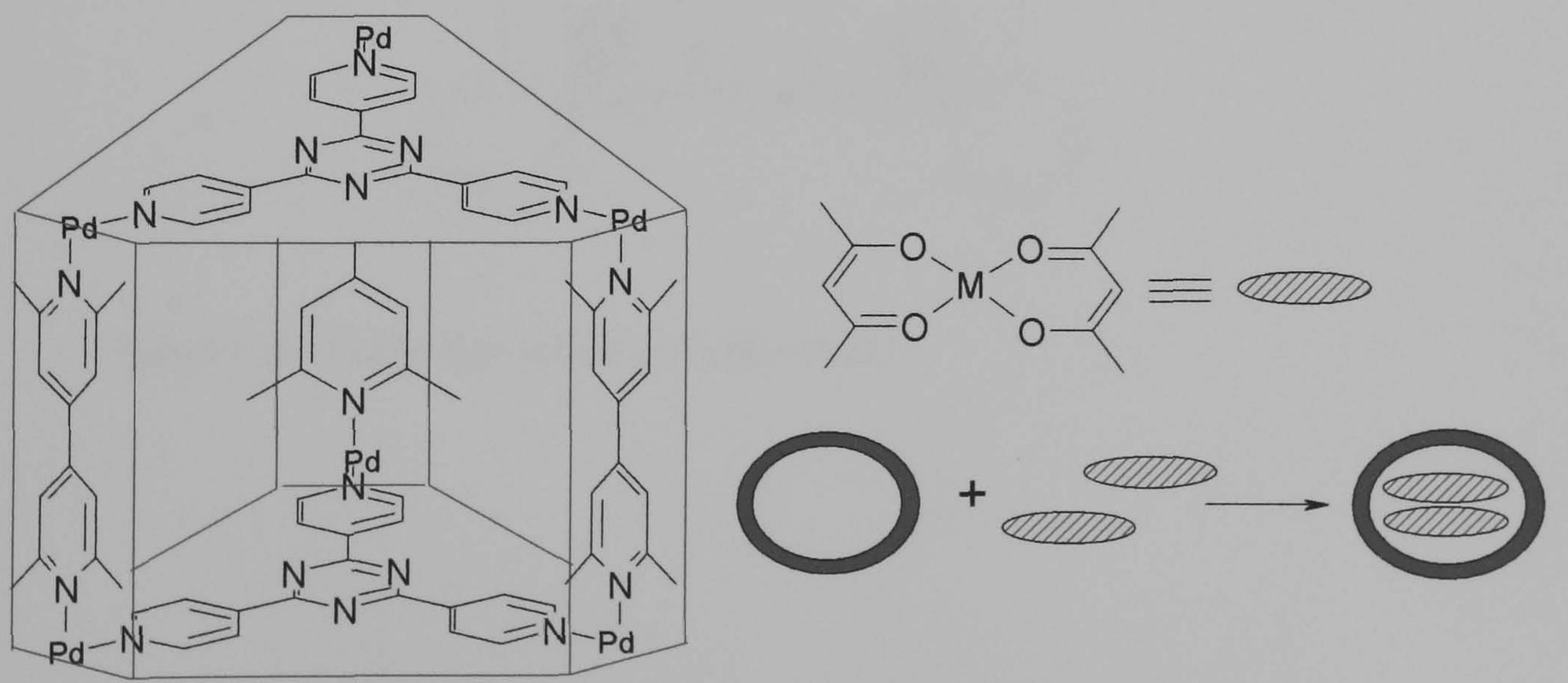

Figure 1.9. (a) Representation of Fujita's cage structure. (b) Cartoon representation of the stacking of the mononuclear acac complexes within the cavity. M = Pt^{II}, Pd^{II} or Cu^{II}.

1.4.3 Ladders

Ladder type complexes are similar to the complexes observed in the formation of grids, of which many examples have been reported over recent years.[38, 39] One particular example has been reported by Lehn and co-workers, who prepared a multidentate bridging ligand $\mathbf{L_c}$, comprising of a series of bidentate bipyridine binding domains.[40] Reaction of this multidentate bridging ligand with the ditopic bipyridinium ligand $\mathbf{L_d}$ and copper(I) ions in the correct stoichiometric amounts results in the formation of a ladder type complex (Figure 1.10). Each copper(I) centre occupies a distorted tetrahedral coordination geometry formed by two bidentate binding domains, one from the multidentate bridging ligand and the second from the bipyridinium ligand. The bipyridinium ligand is then coordinated in the same manner to a second multidentate bridging ligand, producing a structure resembling a ladder.

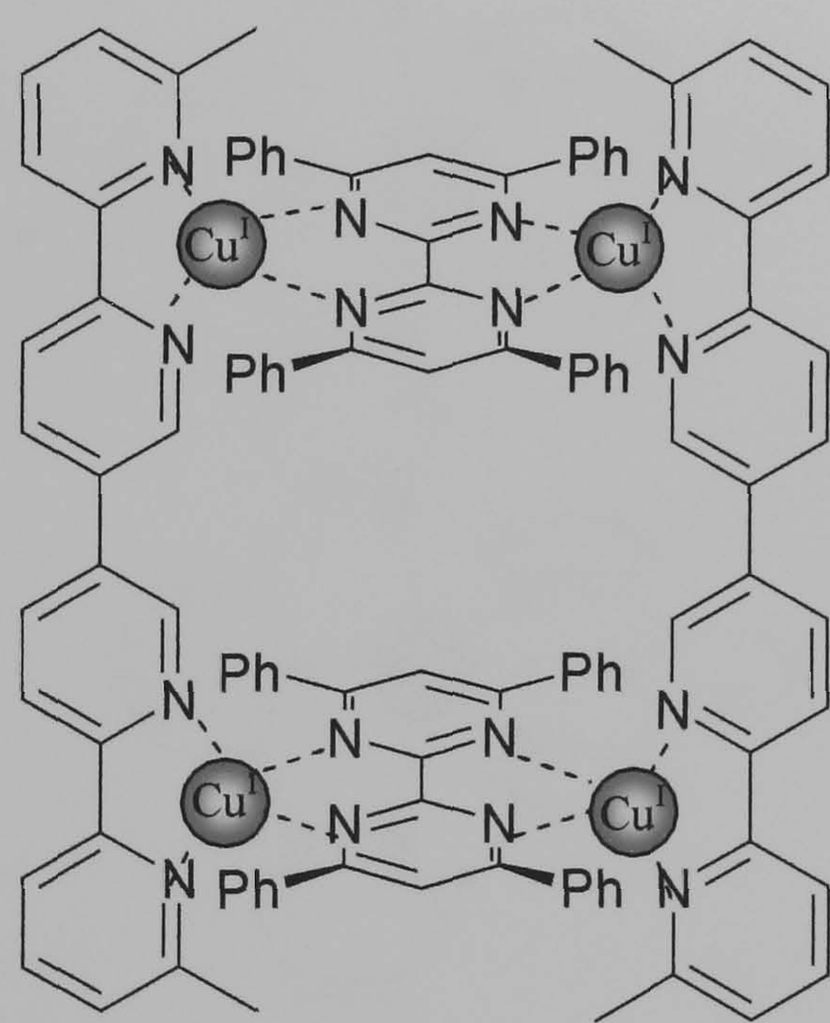

Figure 1.10. Ladder type complex $[Cu_4(\mathbf{L_c})_2(\mathbf{L_d})_2]^{4+}$.

1.4.4 Racks

Rack type complexes are similar to the complexes observed in the formation of ladders. One particular example has been reported by Lehn and co-workers, who prepared a potentially hexadentate ligand $\mathbf{L_a}$, comprising of two bipyridine units, one either side of a central pyrimidine ring.[21] The pyrimidine unit allows the ligand to partition into bis-tridentate binding domains, which upon reaction with $[Ru^{II}(tpy)Cl_3]$ results in the formation of the rack type complex (Figure 1.11). Each metal centre occupies a distorted octahedral coordination geometry formed by two tridentate domains, one from the multidentate bridging ligand and the second from the terpyridine ligand. The terpyridine ligand is oriented at approximately 90° to $\mathbf{L_a}$, thus producing a structure resembling a rack.

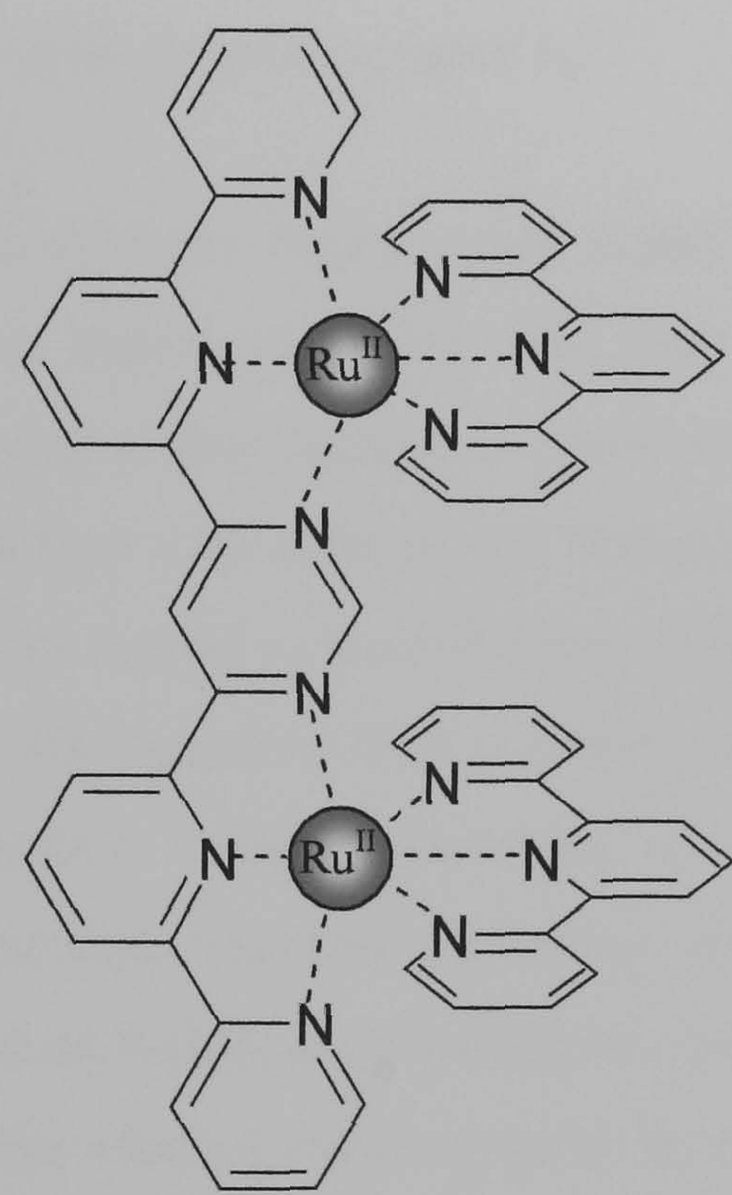

Figure 1.11. Rack type complex $[Ru^{II}_2(\mathbf{L_a})(tpy)_2]^{4+}$.

1.4.5 Formation of a Library of Complexes

The ability of a single ligand to self-assemble into a library of coordination complexes has received considerable interest over recent years.[41] One elegant example have been demonstrated by V. Patroniak *et al.*,[42-44] where a chameleonic ligand $\mathbf{L_e}$, (Figure 1.12) comprising of NNO donor units forms different structural motifs upon reaction with various metal ions.

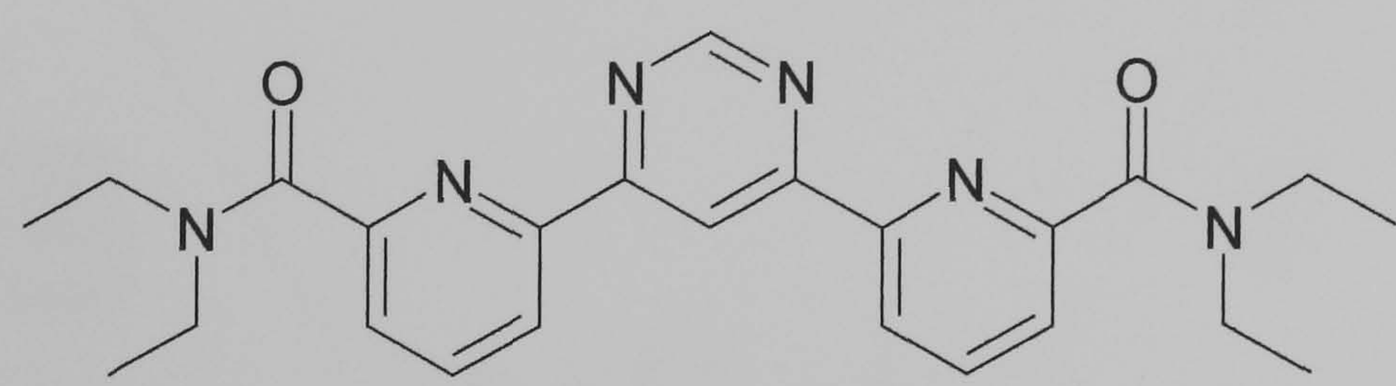

Figure 1.12. Structure of the chameleonic ligand $\mathbf{L_e}$.

Upon reaction of the chameleonic ligand with metal ions favouring octahedral coordination geometry the ligand partitions into two tridentate (NNO) binding domains. However, the ligand is also capable or partitioning into two bidentate (NN) binding domains upon reaction with a metal ion favouring tetrahedral coordination geometry. The ability of this ligand to partition into different binding domains with various metal ions allows the ligand to form a variety of polynuclear coordination architectures and coordination modes, consisting of octahedral [2 × 2] grids, tetrahedral [2 × 2] grids, intricate dinuclear complexes and a zigzag polymeric chain (Figure 1.13). The type of architecture generated is a consequence of the preferred coordination geometry of the selected metal ion used for coordination.

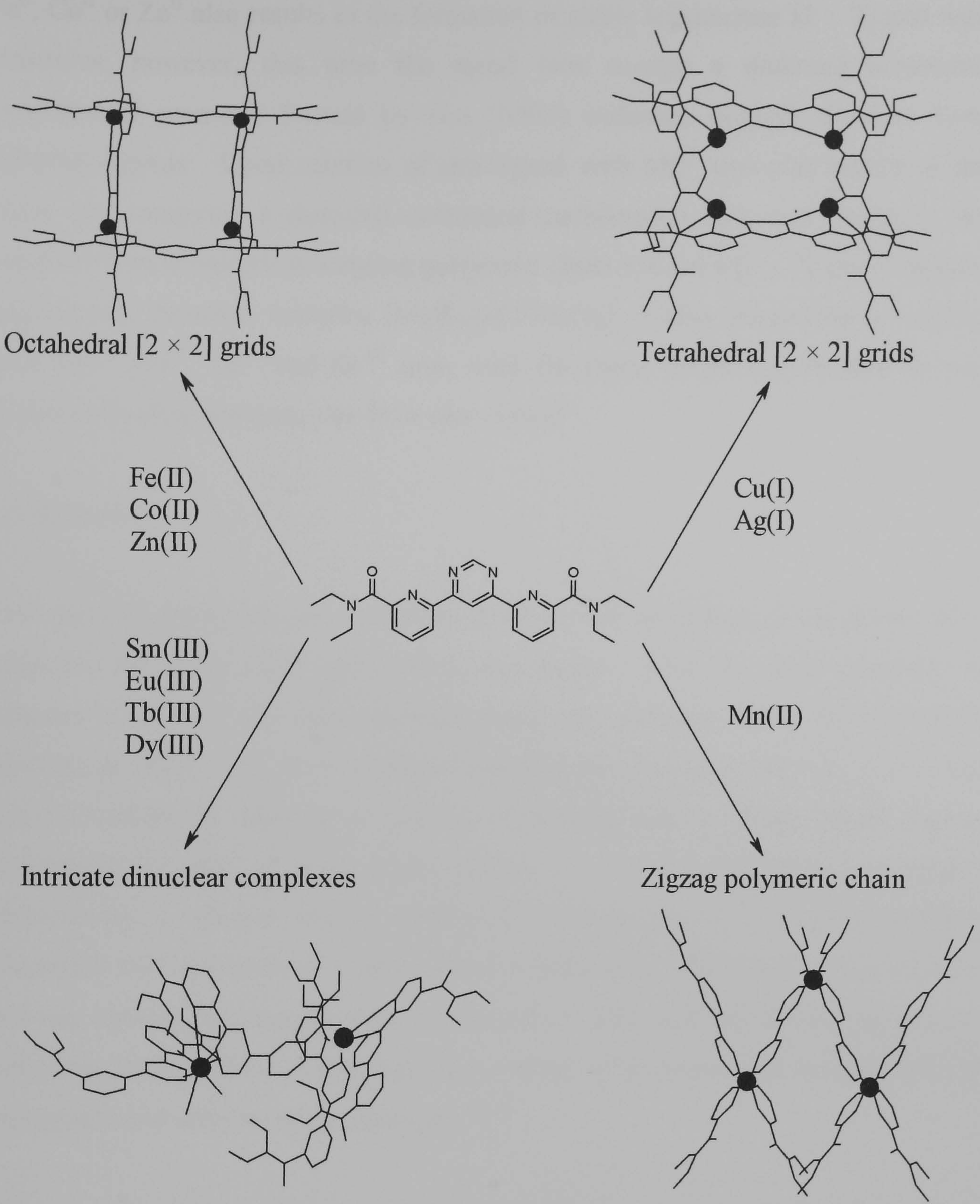

Figure 1.13. The structural motifs of V. Patroniak's formed by reaction of a chameleonic ligand with various metal ions.

The results obtained demonstrate how the binding domains of this particular ligand can be flexible and versatile enough to form stable complexes with metal ions of varying coordination geometries. For instance upon reaction with Cu^{I} or Ag^{I} results in the formation of a tetranuclear [2 × 2] grid structure, with the metal ions coordinated in a distorted tetrahedral coordination geometry formed by two (NN) bidentate binding domains from different ligands. In contrast, upon reaction with

Fe^{II}, Co^{II} or Zn^{II} also results in the formation of stable tetranuclear [2 × 2] grid type structures; however, this time the metal ions occupy a distorted octahedral coordination geometry formed by two (NNO) tridentate binding domains from different ligands. Upon reaction of this ligand with Mn^{II} ions also results in the metal ion occupying a distorted octahedral coordination geometry, however the complex formed represents a zigzag polymeric chain and not a [2 × 2] grid structure. An intricate dinuclear complex $[M_2(\mathbf{L_e})_4(CF_3SO_3)_6]$ is also formed upon reaction with Sm^{III}, Eu^{III}, Tb^{III} and Dy^{III} ions, with the metal centre coordinated by two tridentate binding domains, one from each ligand.

1.5 Helicates

One area of supramolecular chemistry involves the formation of transition metal helicates, and is the main topic area of this thesis. There are many examples of helicates in nature, the most common being the self-assembling double helical structure of DNA. The term "helicate" was first introduced in 1987 by J.-M. Lehn and co-workers to describe a complex containing two or more ligand strands coordinated by two or more metal centres in a double helical arrangement.[45] Alternatively a helicate may be defined as a compound that possesses chirality associated with the sense of a screw about a fixed axis. The pitch of this screw is then the distance between the turns of the helix.[2] Since the introduction of helicate chemistry, considerable research has been carried out to understand the principles of recognition and self-assembly processes.[22, 23]

Helicate complexes consist of multidentate bridging ligands containing more than one set of donor atoms that are capable of chelating different metal centres. The formation of helicate species depends on both the metal ion used and the design of the ligand. For instance the metal ion may, amongst others; (i) have a preferred coordination geometry, (ii) vary in size, and (iii) vary in binding strength and stability. The ligand may; (i) vary in number and disposition of the binding sites, and thus (ii) be capable of coordinating a metal ion with a given coordination geometry, (iii) be flexible enough to form various supramolecular architectures and (iv) be capable of self-recognition and self-assembly processes.[23]

1.5.1 Helicate Nomenclature

With so many different types of helicate species, the nomenclature can become quite complicated as many different aspects of helicates need to be taken into account, such as, amongst others; (a) number of ligands, (b) number of metal centres and (c) number of binding sites. A simple helicate will be named in terms of the number of metal centres and the number of ligand strands involved, for instance *mononuclear, dinuclear, trinuclear, tetranuclear* and so on, refer to; one, two, three and four metal centres respectively. The helicate may then be made up from two ligand strands thus *double helicate* or three ligand strands thus *triple helicate*, so a *trinuclear triple helicate* refers to a helicate species consisting of three metal centres and three identical ligand strands. Helicate species may also be assembled from different ligand strands, thus introducing the terms *homostranded* (identical) and *heterostranded* (different) and the resulting helicates are termed *homoleptic and heteroleptic* helicates. Asymmetric ligands and heterostranded systems can form helicates that can exist in two different isomeric forms according to the orientations of the coordinated ligand strands; these isomeric forms are thus termed *HH (head-to-head)* and *HT (head-to-tail)*. The terms *homo* and *hetero* are also introduced when helicates consist of different metal centres; for example a helicate consisting of two identical ligand strands coordinated by both a copper(I) and a copper(II) ion would be termed a *heterometallic dinuclear double helicate.* When the stereochemical requirements or the metal centre are completely fulfilled by the ligand strands, the metal centre is referred to as being *saturated* or the term *unsaturated* is used when the stereochemical requirements or the metal centre are completed by a combination of ligands strands and supplementary anions or solvent molecules. Helicates may also be termed *meso-helicates (non-chiral)* or *mesocates (chiral)* when the ligand's strands coordinate the metal centres in a side-by-side fashion and not a helicating fashion.

1.5.2 Homoleptic Helicates

As already established, homoleptic helicates[45, 46] are assembled from identical helicands; for example the *ortho*-linked quarterpyridine ligand $\mathbf{L_f}$, (Figure 1.14), developed by E. C. Constable and co-workers.[47] They demonstrated that upon reaction of the potentially tetradentate ligand $\mathbf{L_f}$, with equimolar amounts of copper(I) ions results in the formation of the homoleptic dinuclear double helicate $[Cu_2(\mathbf{L_f})_2]^{2+}$. The copper(I) centres occupy a distorted tetrahedral coordination geometry formed by two bidentate binding domains, one from each ligand in a double helical arrangement.

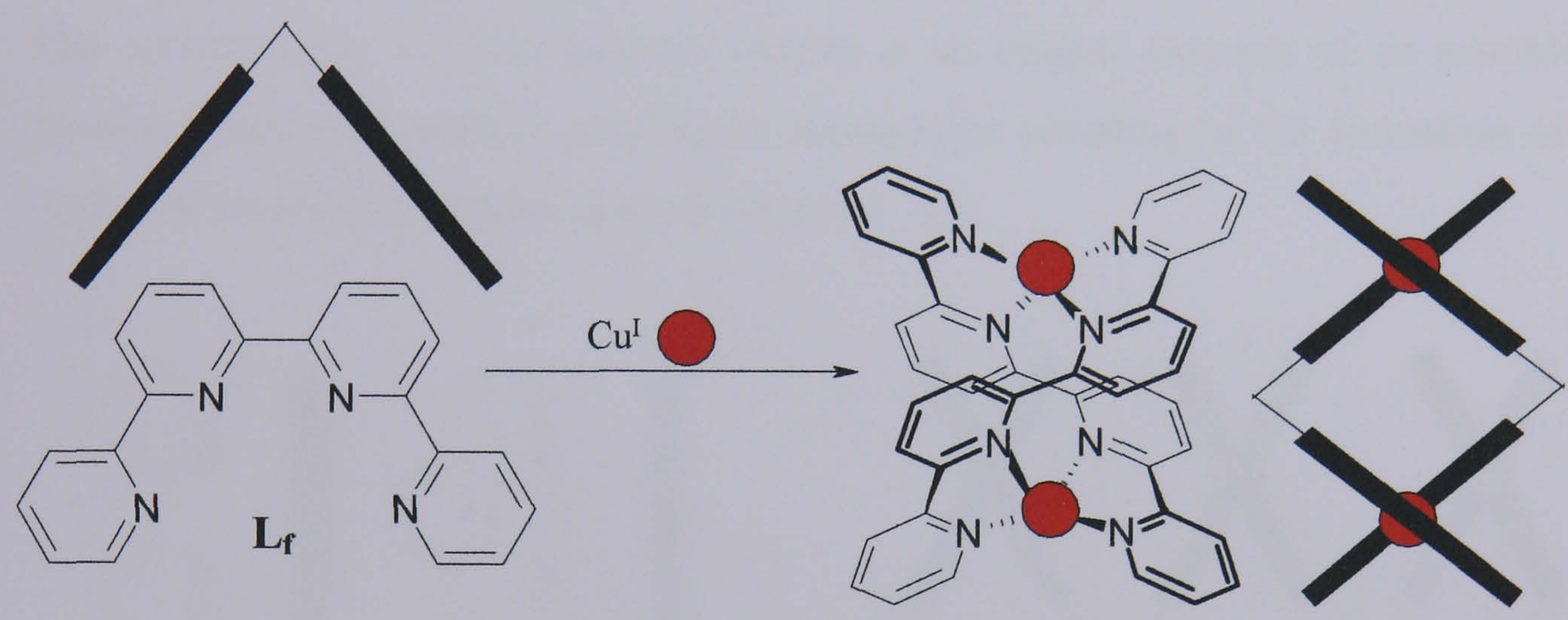

Figure 1.14. Formation of the homoleptic helicate $[Cu_2(\mathbf{L_f})_2]^{2+}$ upon reaction of $\mathbf{L_f}$ with Cu^I ions.

However, upon reaction of $\mathbf{L_f}$ with a metal ion favouring octahedral coordination geometry such as Cu^{II}, results in the formation of a mononuclear complex with the four N-donors coordinating the equatorial plane of the Cu^{II} ion (Figure 1.15).

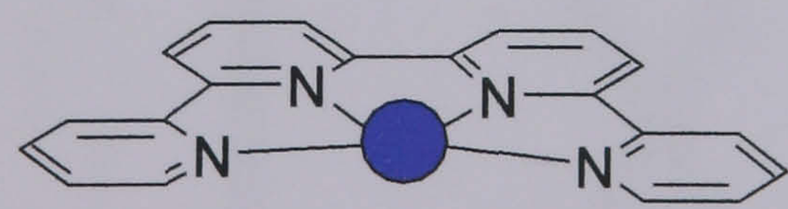

Figure 1.15. Representation of the mononuclear complex $[Cu^{II}\mathbf{L_f}]^{2+}$.

1.5.3 Heteroleptic Helicates

Heteroleptic helicates[48] are assembled from two different ligand strands, an elegant example of which has been demonstrated by Y. Cohen *et al.*,[49] who prepared two similar ligands $\mathbf{L_g}$ and $\mathbf{L_h}$, consisting of alternating 2,2'-bipyridine and 1,10-phenanthroline units linked by methylene spacers. The distribution of the N-donor units partitions the ligands into a series of bidentate binding domains. Thus, upon reaction of a mixture of these ligands with Cu^I ions resulted in the formation of both homoleptic and heteroleptic helicates. In both cases the copper centres occupy a distorted tetrahedral coordination geometry formed by two bidentate binding domains, one from each ligand strand, in a trinuclear double helical arrangement. The self-assembly of these helicate species is an elegant example of an assembly process proceeding without any ligand recognition resulting in the formation of a statistical mixture of helicate species (Figure 1.16).

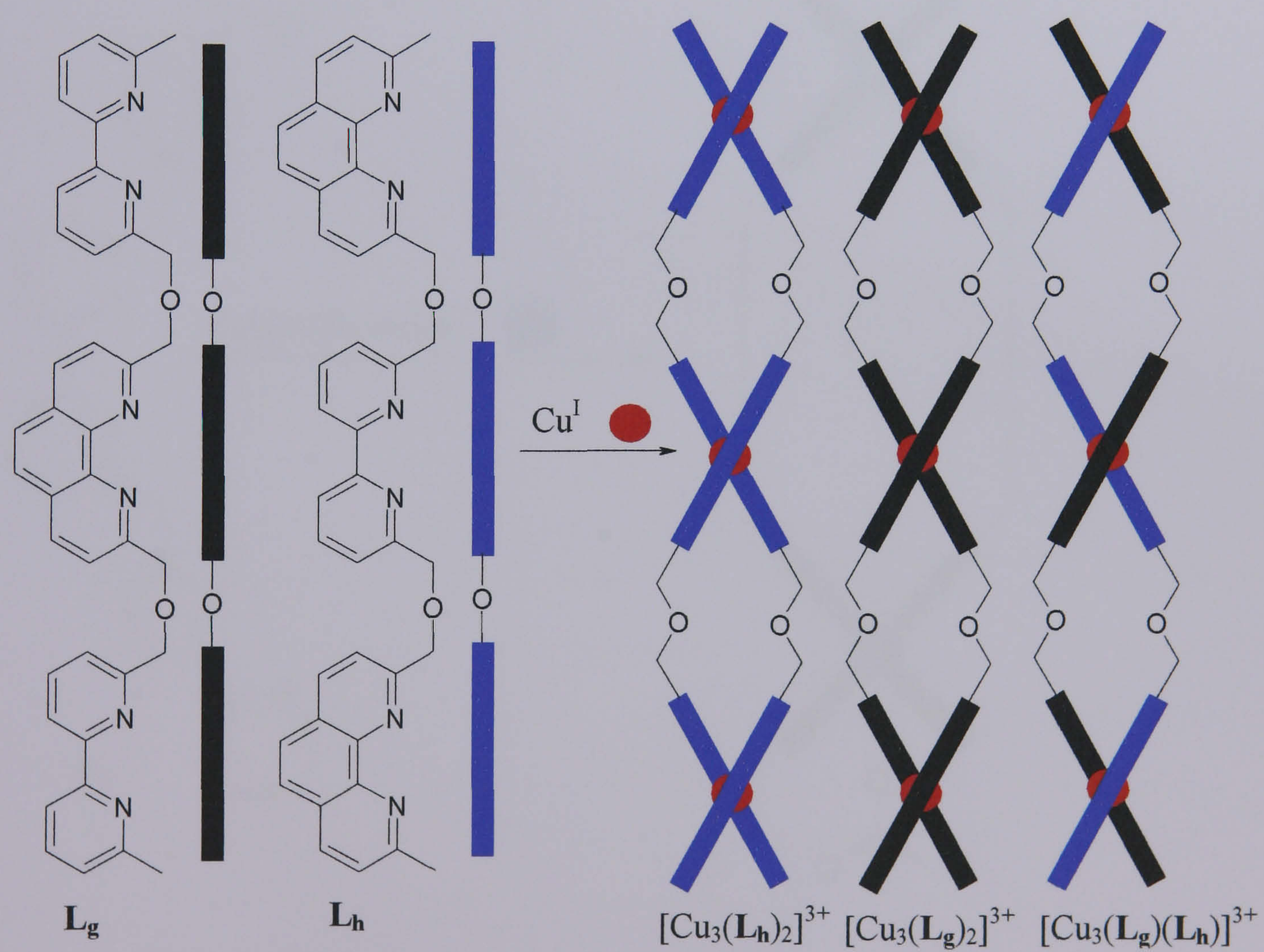

Figure 1.16. Cartoon representation of the formation of both homoleptic and heteroleptic helicates upon reaction of $\mathbf{L_g}$ and $\mathbf{L_h}$ with copper(I) ions.

1.5.4 Unsaturated Helicates

Unsaturated helicates arise when the coordination sphere of one or more of the transition metal cations is incomplete following coordination with a particular ligand. The metal cation then completes its coordination sphere by coordinating to anions or solvent molecules.[50-52] One such example has been demonstrated by the group of M. D. Ward[53] where a bis-bidentate bridging ligand $\mathbf{L_i}$, comprising of pyrazolyl-pyridine N-donor units forms the unsaturated dinuclear double helicate $[Cu_2(\mathbf{L_i})_2(OAc)_2]^{2+}$ upon reaction with copper(II) acetate hydrate (Figure 1.17). The copper(II) centre occupies a square pyramidal coordination geometry (five coordinate), arising from two pyrazolyl/pyridine groups (one from each ligand) and a monodentate acetate unit.

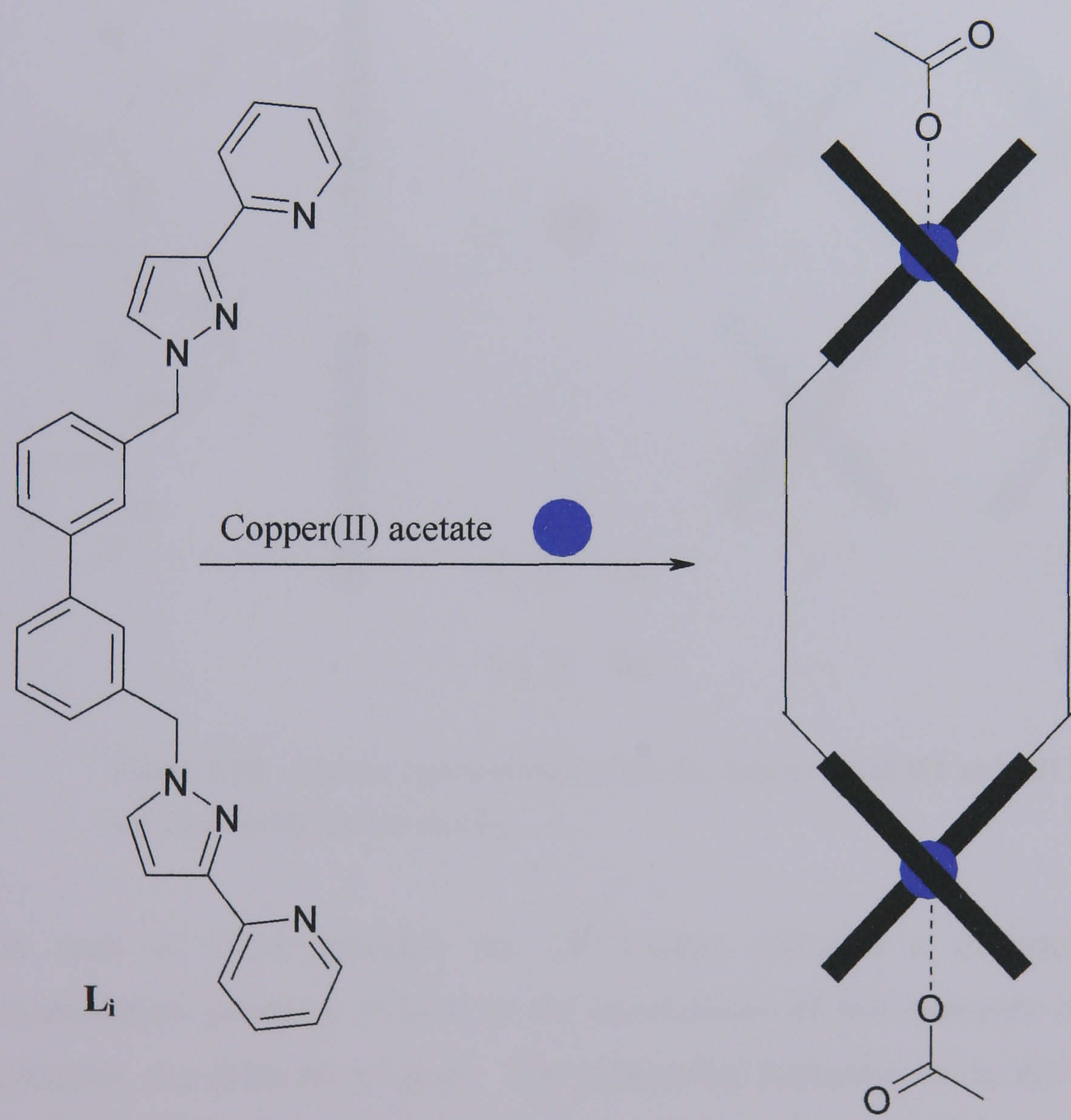

Figure 1.17. Cartoon representation of the formation of the unsaturated helicate $[Cu_2(\mathbf{L_i})_2(OAc)_2]^{2+}$.

1.5.5 Head-To-Tail (Directional) Helicates

Upon reaction of an asymmetrical ligand with a given metal cation can result in the formation two possible conformational helicate isomers, the HH (head-to-head) and the HT (head-to-tail).[54, 55] An elegant example of which has been demonstrated by E. C. Constable *et al.*,[56] who prepared two asymmetric ligands $\mathbf{L_j}$ and $\mathbf{L_k}$, comprising of a methyl unit and *tert*-butyl substituent, respectively, attached to one end of an *ortho*-linked quaterpyridine ligand. Upon reaction of $\mathbf{L_j}$ with Cu^I ions results in the formation of both conformational helicate isomers, and reaction of $\mathbf{L_k}$ with Cu^I results in the formation of only the HH isomer (Figure 1.18).

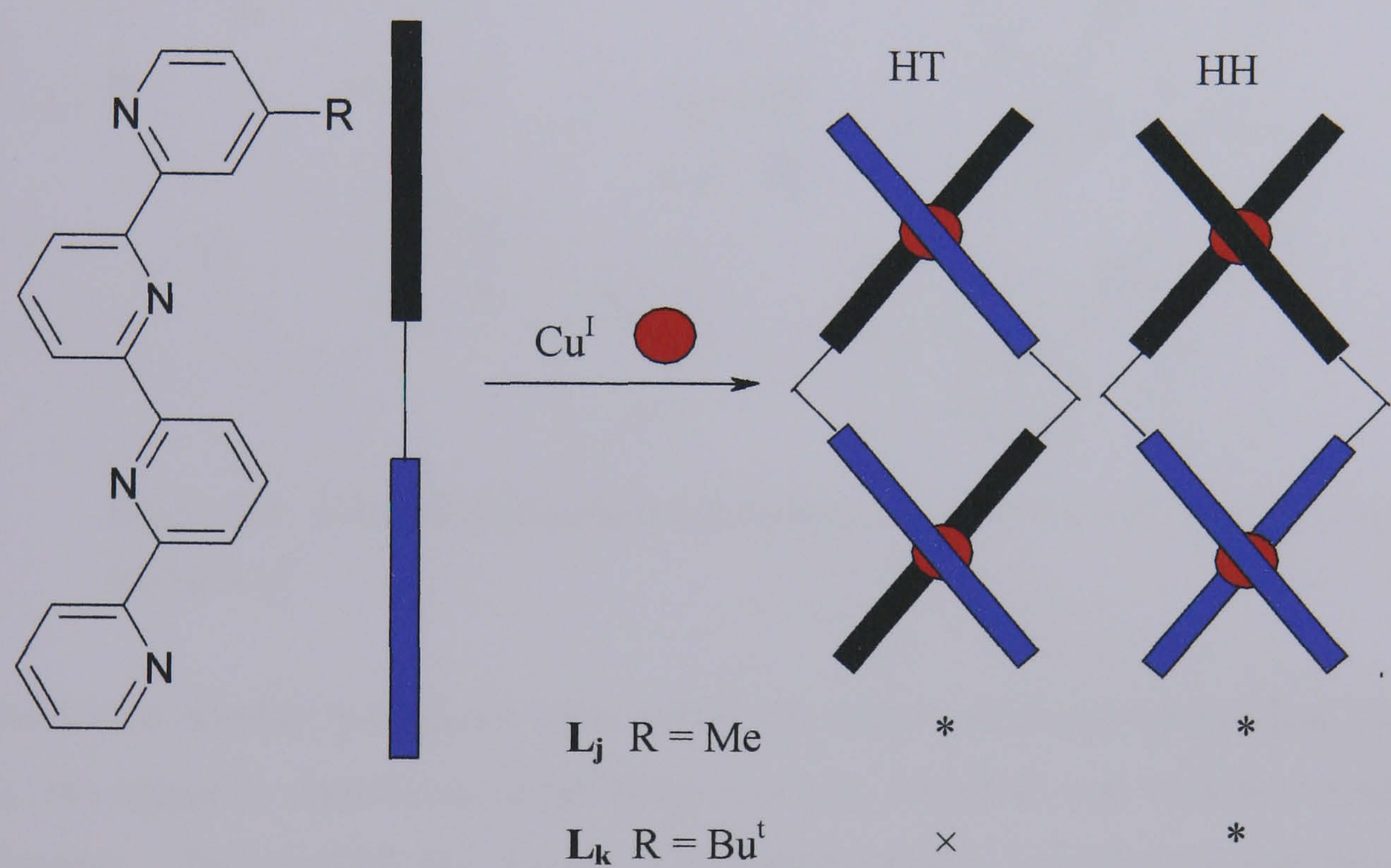

Figure 1.18. Cartoon representation of the formation of both HT and HH isomers with $\mathbf{L_j}$ and only the HT isomer with $\mathbf{L_k}$.

In each of these helicates the Cu^I centres occupies a distorted tetrahedral coordination geometry formed by the coordination of two bidentate py-py binding domains, one from each ligand. The preferential formation of the HH isomer upon reaction of $\mathbf{L_k}$ with Cu^I ions is a consequence of short contacts between the *tert*-butyl substituents in the HT isomer.

1.5.6 Heteronuclear Helicates

It is also possible for helicate species to undergo self-assembly processes with metal ions of various coordination geometry preferences, thus forming heteronuclear helicates.[57, 58] Such a helicate species has also been demonstrated by the *ortho*-linked polypyridines of E. C. Constable.[47, 59] Whereupon reaction of the *ortho*-linked quinquepyridine ligand $\mathbf{L_I}$, with equimolar amounts of cobalt(II) and silver(I) results in the formation of the heteronuclear double helicate $[CoAg(\mathbf{L_I})_2]^{3+}$ (Figure 1.19).

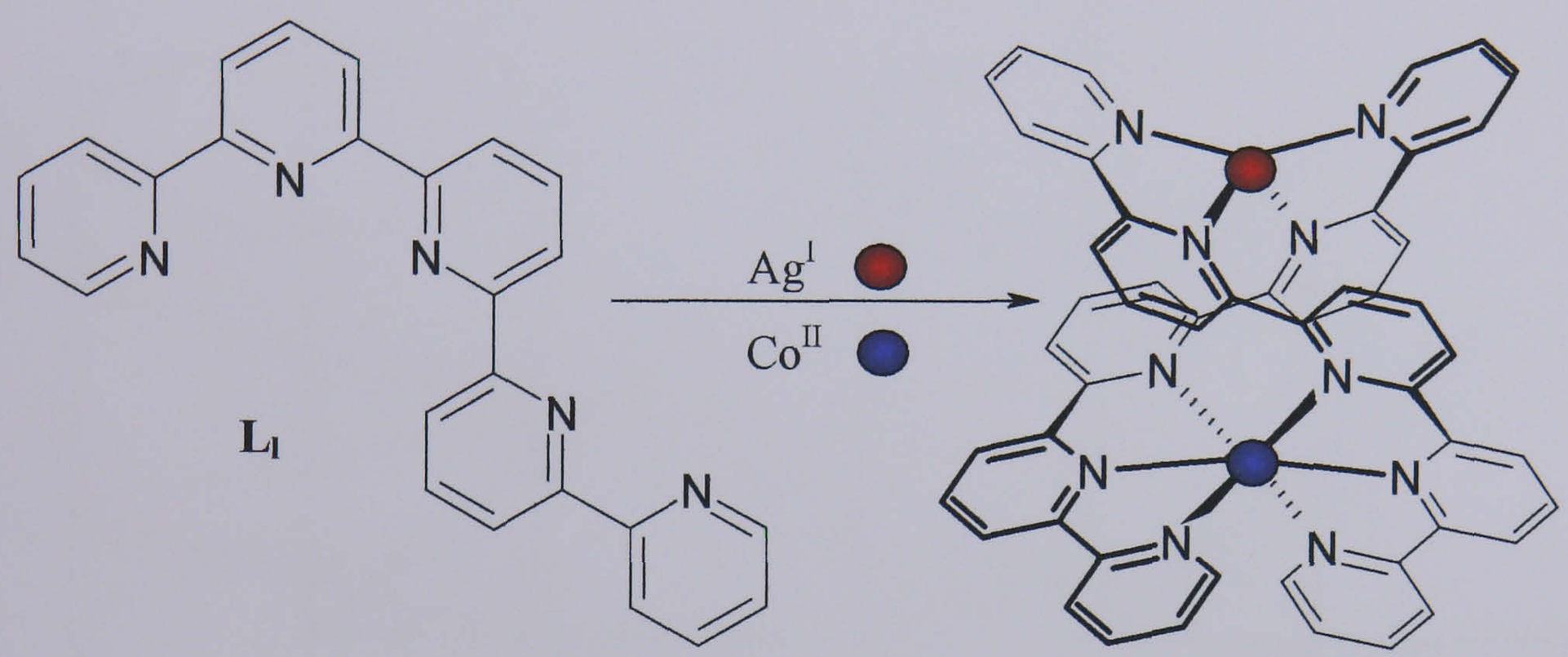

Figure 1.19. Schematic representation of the formation of the heteronuclear double helicate $[CoAg(\mathbf{L_I})_2]^{3+}$.

Due to the number or N-donor units within the *ortho*-linked quinquepyridine ligand $\mathbf{L_I}$, the ligand is capable of partitioning into both bidentate and tridentate binding domains. This enables the ligand to coordinate metals of different coordination geometries in a double helical arrangement. Thus the Co^{II} centre occupies a distorted octahedral coordination geometry formed by the coordination of one tridentate binding domain from each ligand. While the Ag^{I} ion occupies a distorted tetrahedral coordination geometry formed by coordination with the remaining bidentate binding domains from each ligand.

1.5.7 Enantioselective and Diastereoselective Helicates

Before looking at examples of enantioselective and diastereoselective helicates, it is necessary to consider at how such helicates arise. As previously described a helicate may be defined as a compound that possesses chirality associated with the sense of a screw about a fixed axis (z). The pitch (l) of this screw is then the distance between the turns of the helix[2] (Figure 1.20). The screw may travel in two directions, clockwise (plus, P) or anti-clockwise (minus, M).[23]

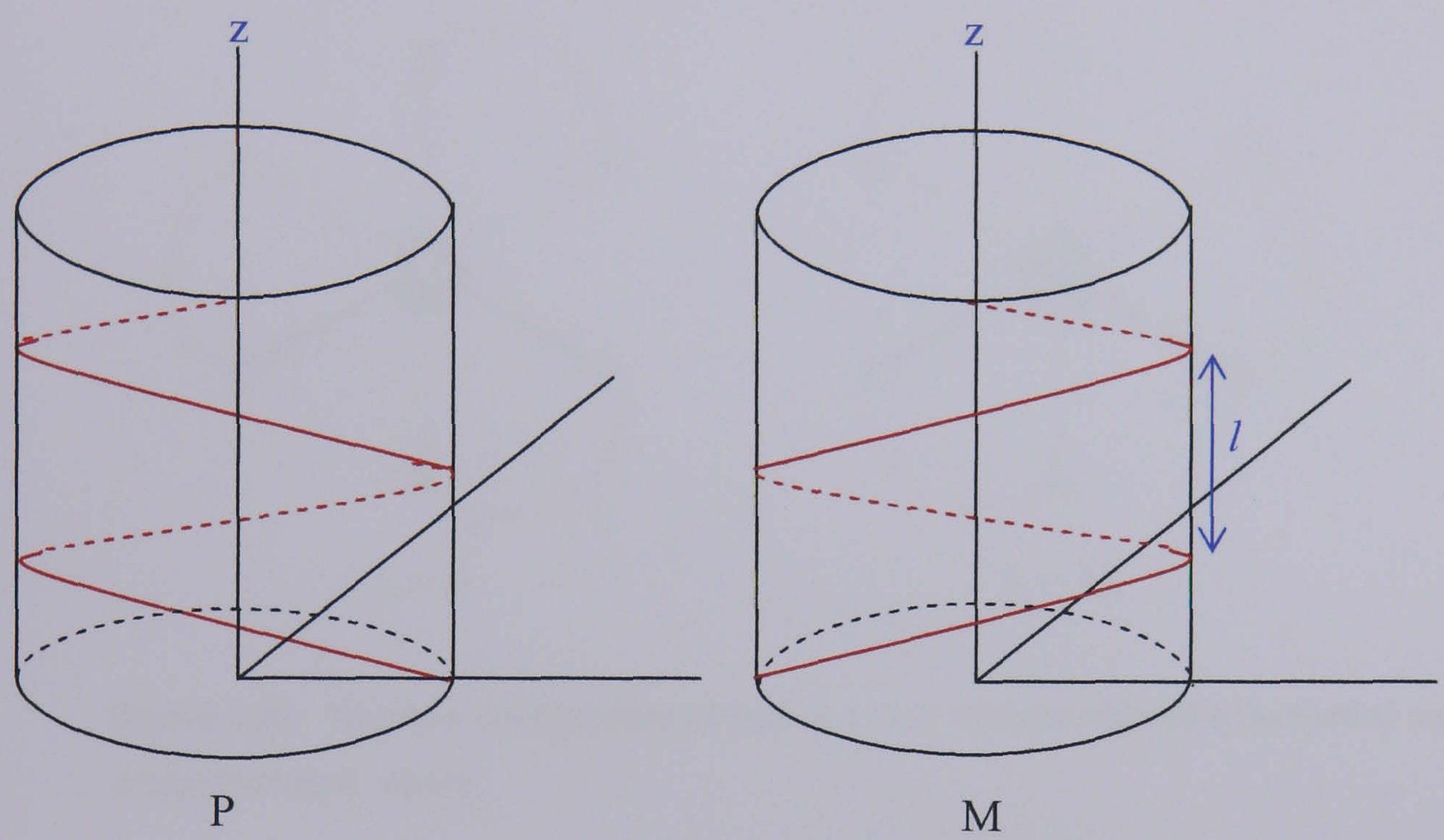

Figure 1.20. Diagram showing both the right handed (plus, P) and the left handed (minus, M) rotations of a helicate. *l* is the pitch and z is the helical axis.

The stereochemistry of the metal centres within P and M helicates are also different (Figure 1.21). The formation of P helicates requires all the metal centres to be (Δ = right-handed) and for M helicates all the metal centres to be (Λ = left-handed). If, however, the stereochemistry of the metal centres is different then side-by-side helicates (meso-helicates) are formed.[23]

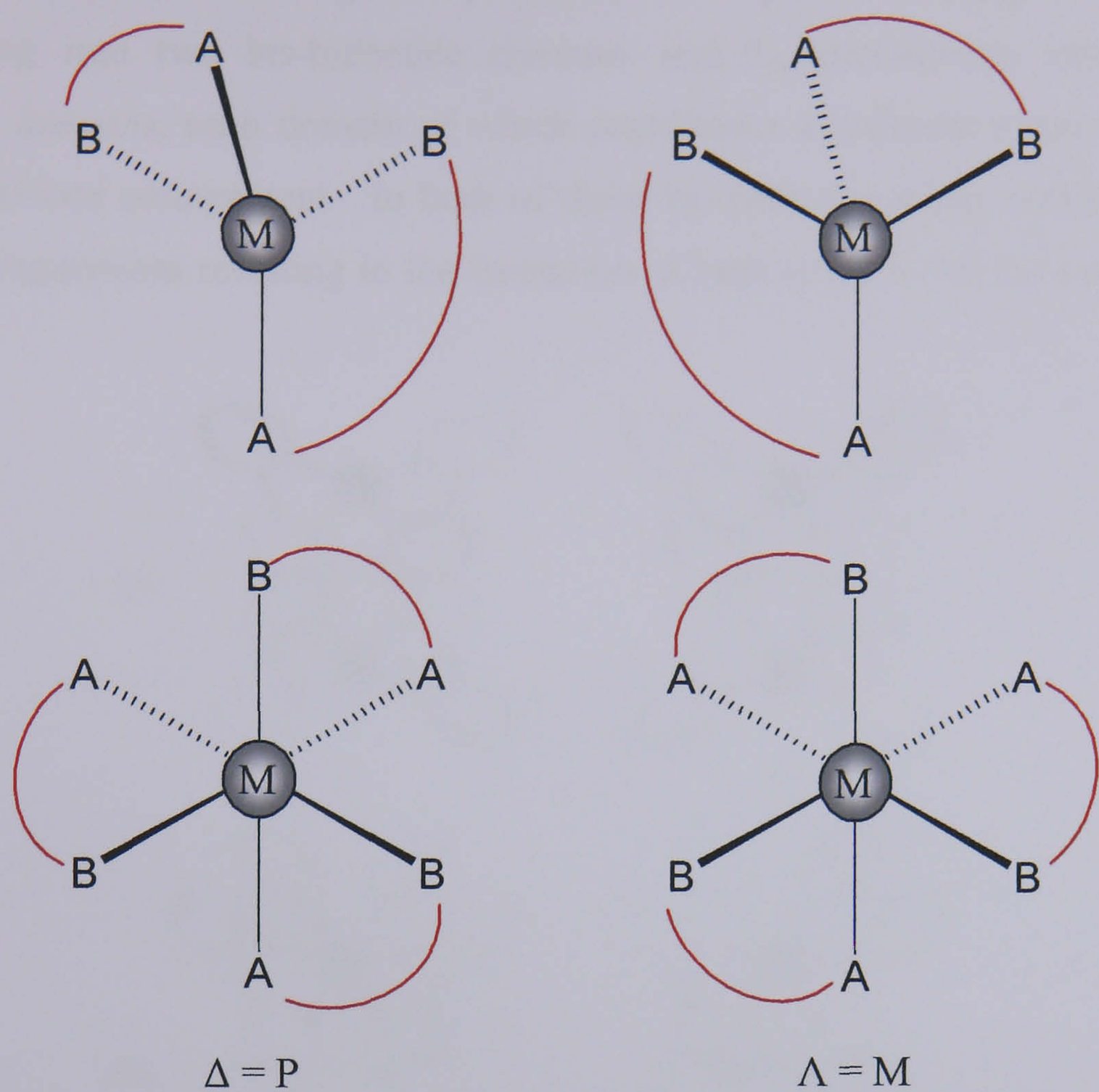

Figure 1.21. Absolute configuration of both Δ and Λ stereoisomers of a tetrahedral and an octahedral metal centre.

The *ortho*-linked quaterpyridine $\mathbf{L_m}$ and sexipyridine $\mathbf{L_n}$ polydentate ligands of Constable[47, 60, 61] (Figure 1.22) provide an elegant example of both left-handed (M) and right-handed (P) helicates.

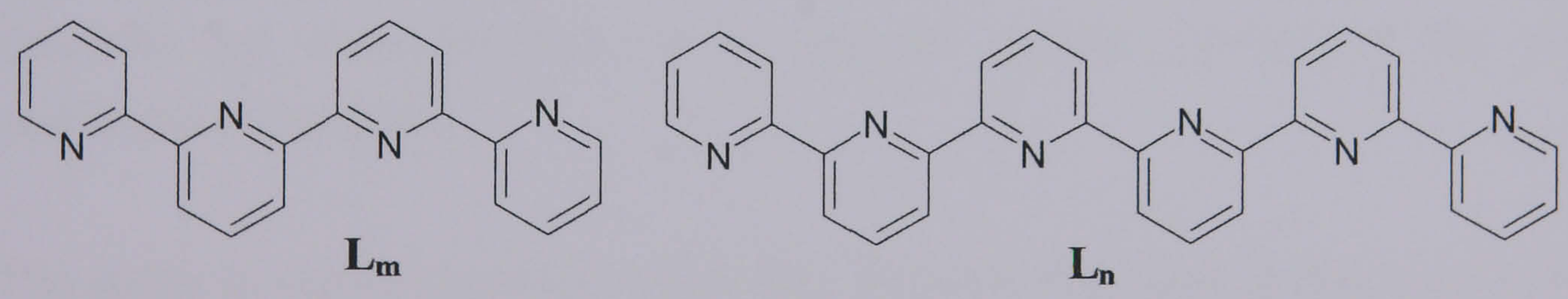

Figure 1.22. The simple *ortho*-linked quaterpyridine $\mathbf{L_m}$ and sexipyridine $\mathbf{L_n}$ polydentate ligands.

Reaction of $\mathbf{L_m}$ and $\mathbf{L_n}$ with equimolar amounts of Cu^{I} and Cd^{II}, respectively, resulted in the self-assembly of the dinuclear double stranded helicates $[Cu_2(L_m)_2]^{2+}$ and $[Cd_2(L_n)_2]^{4+}$, both of which were confirmed through X-ray crystallographic

studies. Each of these ligands partitions into distinct binding domains, $\mathbf{L_m}$ partitioning into two bis-bidentate domains and $\mathbf{L_n}$ partitioning into two bis-tridentate domains, each domain of which coordinates a different metal centre in a double helicate arrangement. In both of these helicates the metal centres have the same configurations resulting in the formation of both (P) and (M) helicates (Figure 1.23).

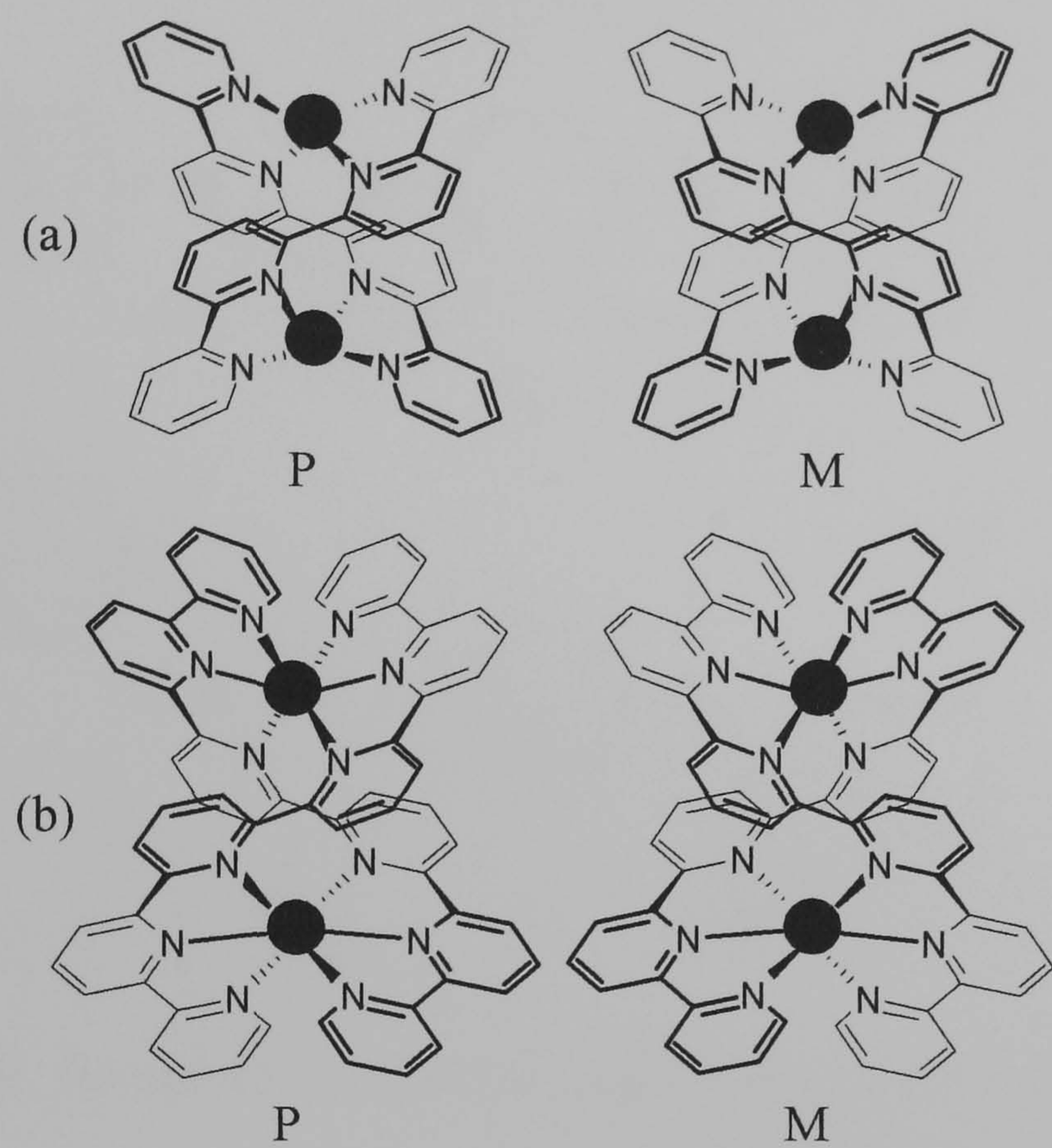

Figure 1.23. The two (P) and (M) enantiomeric representations of the dinuclear double helicates (a) $[Cu_2(\mathbf{L_m})_2]^{2+}$ and (b) $[Cd_2(\mathbf{L_n})_2]^{4+}$.

The self-assembly of helicate species such as those depicted in Figure 1.23, are generally not enantioselective, so a statistical racemic mixture of the two enantiomers is observed.

The ability to control enantioselectivity has, however, seen considerable success by many research groups over recent years. The groups of Constable[62] and Von Zelewsky[63] have both produced ligands incorporating resolved chiral pinene substituents (Figure 1.24). The introduction of such groups could lead to the formation of a number of possible diastereomeric species; however the steric environments of the chiral substituent means that the formation of one helicate species may be more favourable than another. Both of these ligands consist of two

bipyridine units, separated by a methylene spacer in $\mathbf{L_o}$ and a phenyl spacer in $\mathbf{L_p}$, thus partitioning the two bipyridine units into bis-bidentate binding domains. The partitioning of $\mathbf{L_o}$ in to bis-bidentate binding domains favours the formation of dinuclear double helicates with metal ions that prefer tetrahedral coordination geometry, such as copper(I) in this case, while $\mathbf{L_p}$ favours the formation of dinuclear triple helicates with metal ions favouring octahedral coordination geometry.

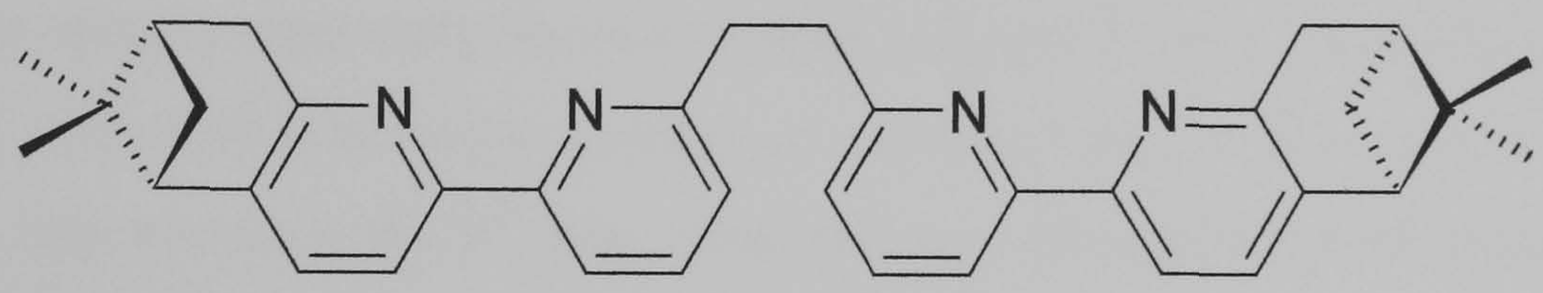

$\mathbf{L_o}$

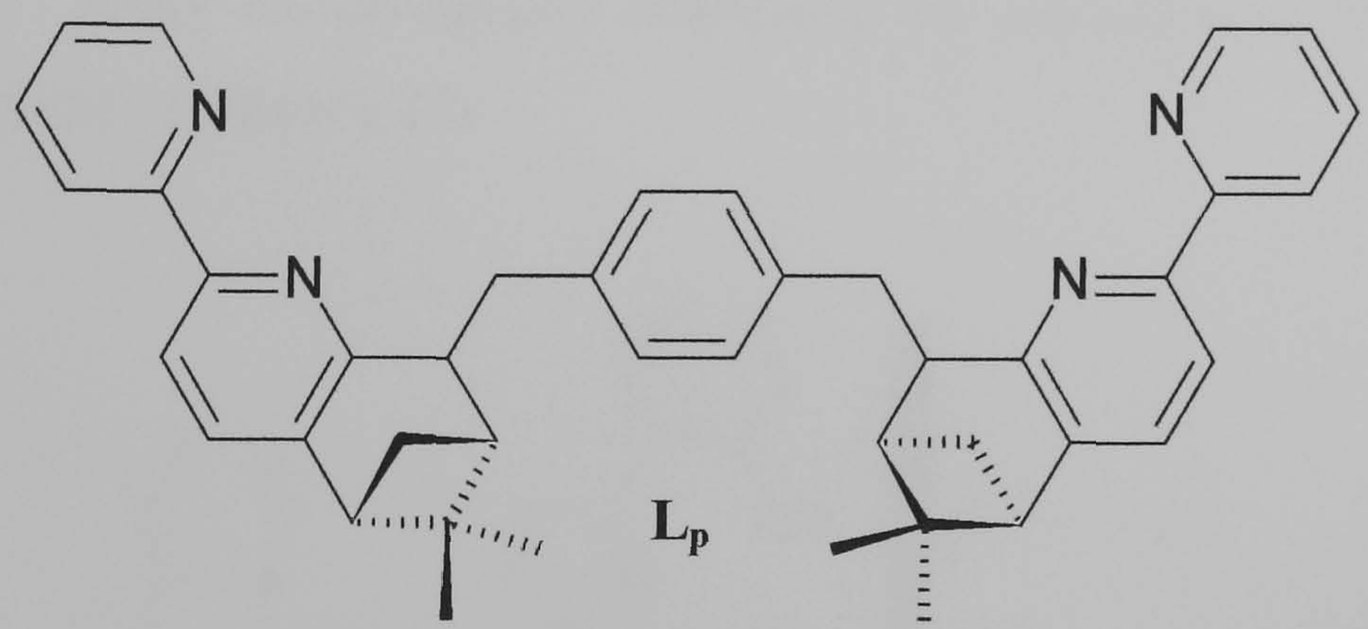

$\mathbf{L_p}$

Figure 1.24. Structures of E. C. Constable's ligand $\mathbf{L_o}$ and Von Zelewsky's ligand $\mathbf{L_p}$.

E. C. Constable demonstrated that upon reaction of either the (S,S) or (R,R) $\mathbf{L_o}$ enantiomers with an equimolar amount of Ag^I ions resulted in the (S,S) ligand forming only the P helicate and the (R,R) ligand forming the M helicate. However, reaction of either of the two ligands with Cu^I ions in methanol, showed modest diastereoselective formation of the P and M helicates in the ratio 10 : 7 with preference for the P helicate. Crystallisation of the resulting solution gave two different types of crystals, structural determination of these crystals revealed that the crystals were a *quasi*-racemate containing equal quantities of both diastereomeric P and M helicates. Thus no diastereoselectivity was observed in the solid state. The ligand system developed by Von Zelewsky also showed similar results to that observed by Constable, whereupon reaction of either the (+)- and (-)- $\mathbf{L_p}$ enantiomer with a metal:ligand stoichiometry of 2 : 3 with either Cd^{II}, Zn^{II} and Fe^{II} ions resulted in the formation of a dinuclear triple helicate species showing preferential formation of one stereoisomer.

1.5.8 Mesocates

As already established, in a true helicate all the metal centres must have the same stereochemistry. However, it is possible for the metal centres to have different stereochemistry thus forming a 'side-by-side' species or mesocate. A recent example has been by M. D. Ward and co-workers who prepared two bis-bidentate N,O-donor ligands $\mathbf{L_q}$ and $\mathbf{L_r}$, comprising of pyrazolyl-phenolate binding domains but with different spacers separating the two binding domains.[64] A 1 : 1 mixture of the two ligands, with a stoichiometric amount of triethylamine, to deprotonate the phenol donors, was reacted with Zn^{II} ions. This reaction afforded the preferential formation of the heteroleptic mesocate $[Zn_2(\mathbf{L_q})(\mathbf{L_r})]^{4+}$, with a 'side by side' arrangement of the two ligands. X-ray crystallography confirmed the formation of the heteroleptic mesocate complex (Figure 1.25).

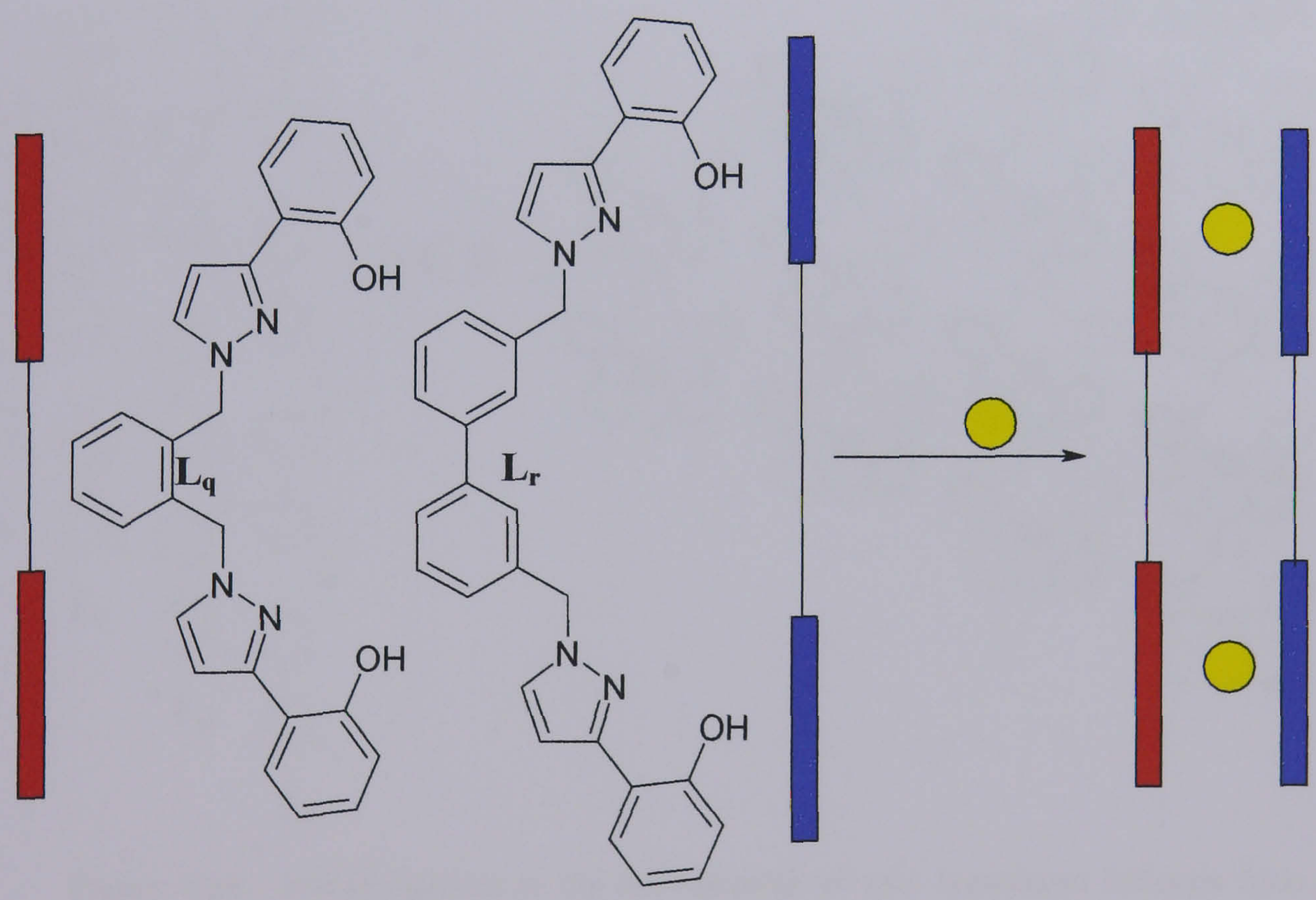

Figure 1.25. Cartoon representation showing the formation of the heteroleptic mesocate $[Zn_2(\mathbf{L_q})(\mathbf{L_r})]^{4+}$.

1.5.9 Ligand Recognition

In a previous example by Y. Cohen *et al.*,[49] mixtures of ligands can form statistical mixtures of both homoleptic and heteroleptic helicates when the self-assembly processes occur without any ligand recognition. However, it is also possible for a mixture of various ligands to form only the homoleptic helicate species. One elegant example of such an observation has been demonstrated by J.-M. Lehn *et al.*,[65] whereby upon reaction of four different oligo(2,2')-bipyridine strands $\mathbf{L_s}$ – $\mathbf{L_v}$ with copper(I) ions resulted in the spontaneous formation of only homoleptic helicates (Figure 1.26).

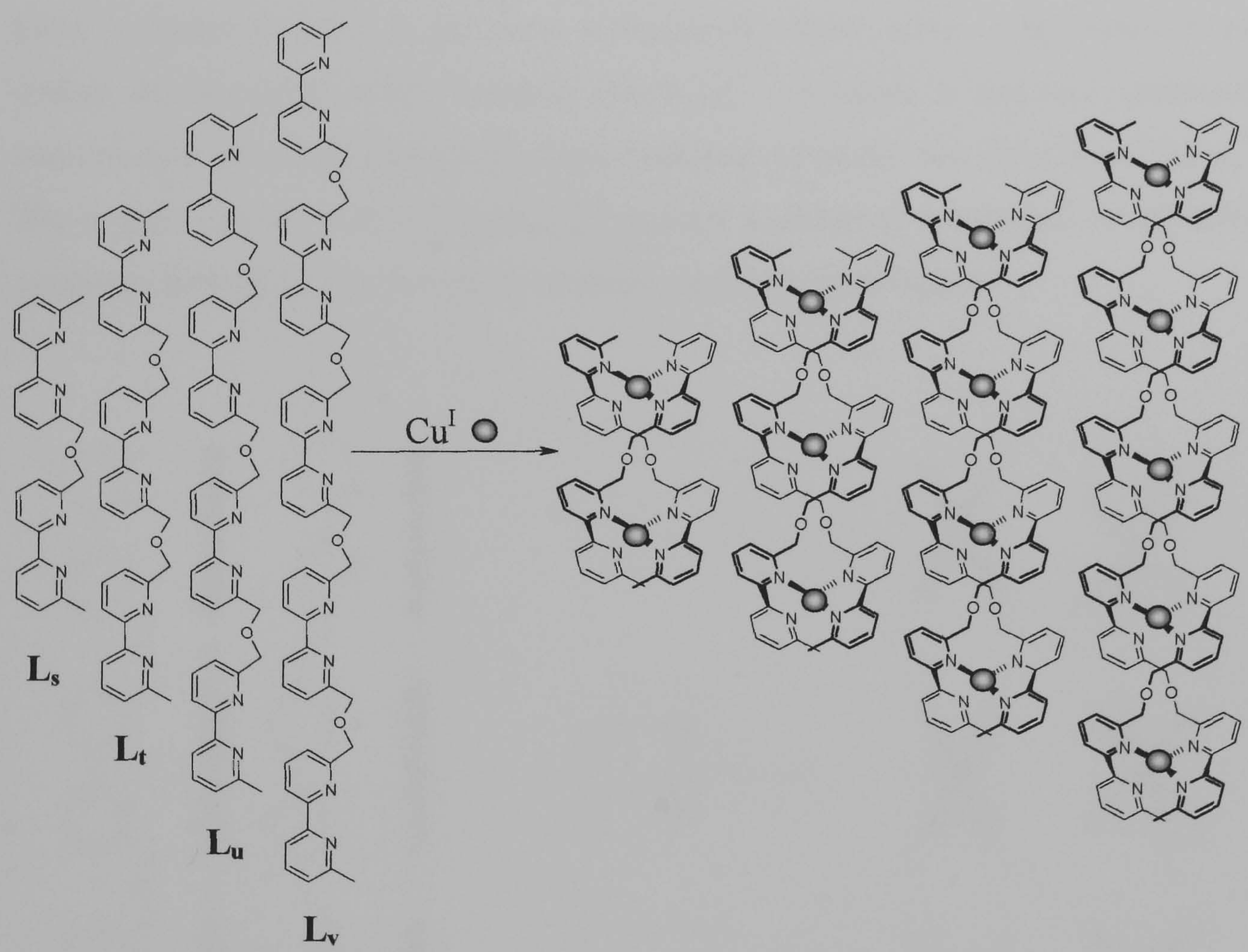

Figure 1.26. Self-recognition in the self-assembly of only homoleptic helicates from a mixture of ligand strands $\mathbf{L_s}$ – $\mathbf{L_v}$.

Each of the ligands $\mathbf{L_s}$ – $\mathbf{L_v}$ consist of bipyridine units separated my methylene spacers, thus partitioning the ligand strands into bidentate binding domains which upon reaction with copper(I) results in the formation of homoleptic helicates where each Cu^I centre occupies a distorted tetrahedral coordination geometry. This demonstrates how ligands containing a different number of binding sites can self-

recognise as the formation of a heteroleptic species would be highly unfavourable as uncoordinated bidentate binding domains would exist.

Lehn and co-workers then further demonstrated ligand recognition occurring between two ligands strands $\mathbf{L_t}$ and $\mathbf{L_w}$, both of which contain the same number of tri-bidentate binding domains and only differing in the substitution of the spacer units (Figure 1.27). Reaction of the mixture $\mathbf{L_t}$, $\mathbf{L_w}$, Cu^{I} and Ni^{II} ions in the correct stoichiometric amounts yielded only the homoleptic species $[Cu_3(\mathbf{L_w})_2]^{3+}$ and $[Ni_3(\mathbf{L_t})_3]^{6+}$. This result was expected as the formation of a trinuclear triple helicate with $\mathbf{L_w}$ would be unfavourable due to the steric requirements associated with the connection of the oligobipyridines via the 5 positions, so the ligand would prefer to form a double helicate as no steric interactions would occur. The nickel centre within the trinuclear triple helicate $[Ni_3(\mathbf{L_t})_3]^{6+}$, occupies a distorted octahedral coordination geometry formed by three bidentate domains, one from each ligand.[66] The copper centres within $[Cu_3(\mathbf{L_w})_2]^{3+}$ occupy a distorted tetrahedral coordination geometry formed by two bidentate domains, one from each ligand.

Figure 1.27. Cartoon representation showing ligand recognition between two tri-bidentate ligands $\mathbf{L_t}$ and $\mathbf{L_w}$.

1.5.10 Ligand Programming

Ligands can be specifically designed to contain binding domains for coordination with various metal ions of a preferred geometry. Thus, reaction with a given metal ion results in the formation of a supramolecular assembly as a result of the disposition of the binding sites. Following the successful synthesis of a particular ligand, the information within the ligand in terms of the disposition of the binding sites is permanently stored within it and at this point the ligand is said to be *programmed.*

The *ortho*-linked sexipyridine ligand $\mathbf{L_n}$, demonstrates how the ability of ligands to partition into different binding domains is instrumental in the formation of various supramolecular architectures. As *ortho*-linked ligands of this type are capable of rotating about the interannular py-py bonds, $\mathbf{L_n}$ is able to partition into various sets of discrete binding domains upon reaction with various metal cations.[67] Thus, this ligand could potentially partition into tri-bidentate, bis-tridentate or hexadentate binding domains (Figure 1.28).

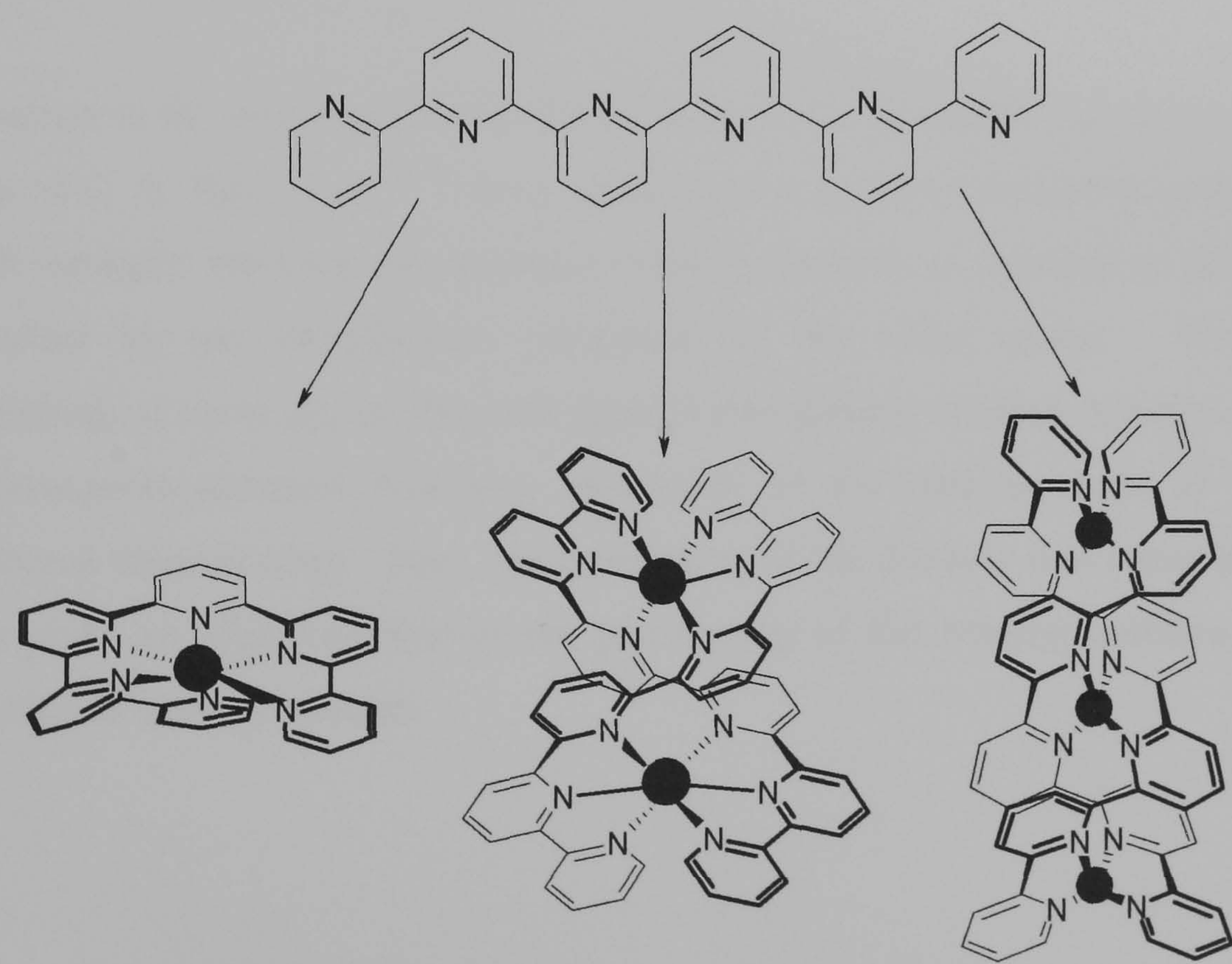

Figure 1.28. Schematic representation showing the various complexes exhibited by $\mathbf{L_n}$.

Reaction of $\mathbf{L_n}$ with copper(I) ions results in the formation of a trinuclear double helicate system, with each ligand partitioning into tri-bidentate (py-py) binding domains and each of the Cu^I centres acquiring stabilisation from the distorted tetrahedral arrangement of the N-donor units.[47, 60] When a metal cation with a preference for octahedral coordination geometry is used, such as cadmium(II), this also results in the formation of a helicate species. However, in this case the ligand partitions into bis-tridentate (py-py-py) binding domains with each Cd^{II} centre coordinated in a distorted octahedral manner.[68] Finally, reaction with europium(III) ions results in the formation of a hexadentate mononuclear system, where all six N-donors coordinate a single metal centre.[69] These examples studied by E. C. Constable and co-workers, elegantly demonstrate the ability of ligands to form various supramolecular architectures. The various structures adopted by this particular ligand are mainly due to the preferred coordination geometry of the metal ion used and is not a consequence of ligand programming. The ability of the ligand to twist about the interannular py-py bonds allows the ligand to accommodate the required coordination environment. These helicate species are further stabilised by the extensive π-π stacking interactions between the overlapping aromatic rings of adjacent ligand strands.

In contrast to the well studied oligopyridines by E. C. Constable and co-workers, the group of C. R. Rice *et al.*,[70-72] have synthesised a series of pyridyl-thiazole ligands which naturally partition into separate binding domains as opposed to partitioning controlled by the coordination preference of the metal cation. The natural partitioning of these pyridyl-thiazole ligands into distinct binding domains is due to the divergence between N-donors, introduced by the shallow angle of the five-membered thiazole rings. Thus, the positioning of the thiazole unit along the ligand chain plays an important role in the partitioning of the binding domains and the formation of helicate species.

Consider the two pyridyl-thiazole ligands $\mathbf{L_x}$ and $\mathbf{L_y}$, both of which contain py-tz units however an extra pyridine unit has been introduced in between the two thiazole rings in $\mathbf{L_y}$ (Figure 1.29).

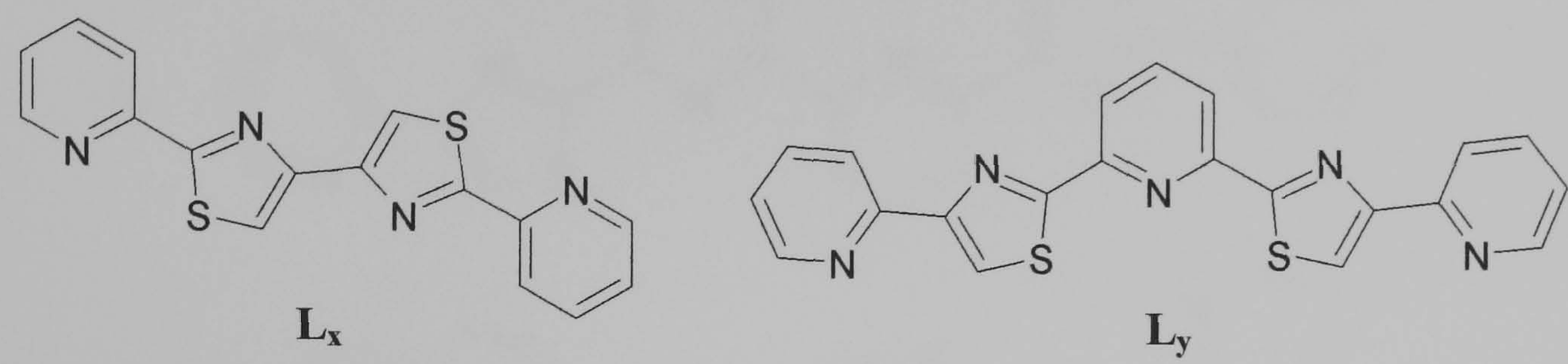

Figure 1.29. The two pyridyl-thiazole ligands $\mathbf{L_x}$ and $\mathbf{L_y}$.

The natural partitioning of the pyridyl-thiazole units is exemplified by the potentially tetradentate ligand $\mathbf{L_x}$.[70] Six-coordinate first row transition metal cations Co^{II}, Cu^{II} and Zn^{II} react to form dinuclear triple helicates of the type $[M^{II}_2(\mathbf{L_x})_3]^{4+}$. Each ligand partitions into bis-bidentate binding domains with each metal centre coordinated by three bridging ligands in a triple helical arrangement and each of the metal centres occupies a distorted octahedral coordination geometry. The formation of such helicates species demonstrates the ability of the py-tz units to partition into different binding domains, as the related *ortho*-linked quaterpyridine ligand forms mononuclear complexes with the first row metal cations.[73, 74] The potentially pentadentate ligand $\mathbf{L_y}$ forms the dinuclear double helicate $[Cu_2(\mathbf{L_y})_2]^{4+}$ upon reaction with Cu^{II} ions.[75] Each of the Cu^{II} centres is four coordinate, with each Cu^{II} ion coordinated by two bidentate py-tz units in a double helical arrangement. The partitioning of the ligand in this manner results in the central pyridine unit being uncoordinated and thus acting as a simple spacer group separating the two py-tz bidentate binding domains.

The group of C. R. Rice and co-workers has also studied the ability of two similar pyridyl-thiazole ligands $\mathbf{L_z}$ and $\mathbf{L_{aa}}$ (Figure 1.30) to form heteroleptic helicates with Ni^{II}, Cu^{II} and Zn^{II} ions.[71]

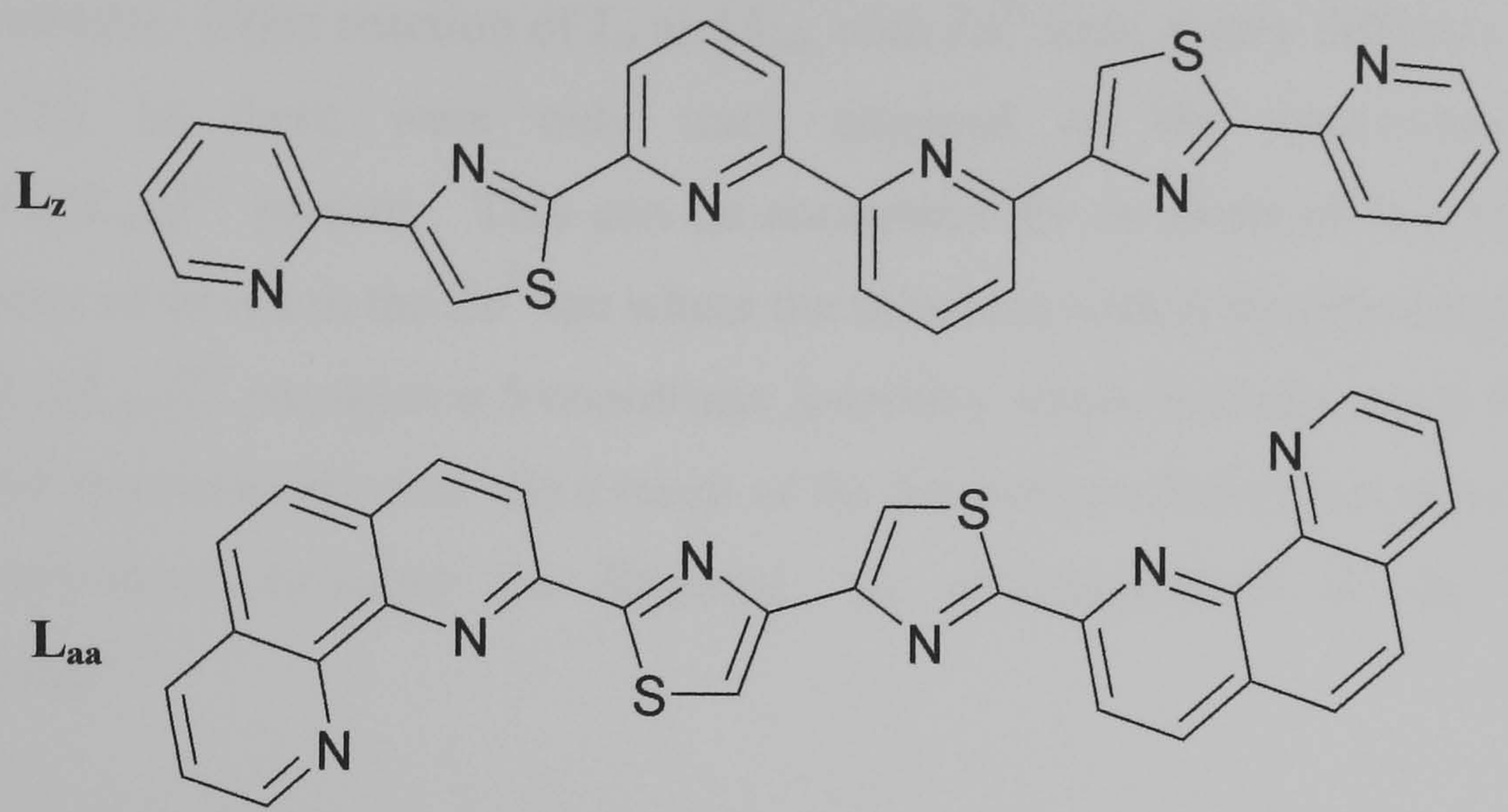

Figure 1.30. The two pyridyl-thiazole ligands $\mathbf{L_z}$ and $\mathbf{L_{aa}}$.

Both $\mathbf{L_z}$ and $\mathbf{L_{aa}}$ react with Ni^{II} ions to form the dinuclear double helicates $[Ni_2(\mathbf{L_z})_2]^{4+}$ and $[Ni_2(\mathbf{L_{aa}})_2]^{4+}$ respectively. In both cases each metal centre occupies a distorted octahedral coordination geometry formed by two tridentate binding domains, one from each ligand strand. A similar type of arrangement is observed in the complex $[Cu_2(\mathbf{L_{aa}})_2]^{4+}$. However, in the case of $[Cu_2(\mathbf{L_z})_2]^{4+}$ the copper(II) centre occupies a distorted tetrahedral coordination geometry formed by two py-tz bidentate binding domains, one from each ligand, with the central bipyridine unit uncoordinated and effectively acting as a spacer unit.[75] A similar tetrahedral / octahedral coordination geometry is observed in the Zn^{II} analogues, $[Zn_2(\mathbf{L_z})_2]^{4+}$ and $[Zn_2(\mathbf{L_{aa}})_2]^{4+}$. This ability of $\mathbf{L_z}$ to act as either a bis-tridentate or a bis-bidentate donor has implications in the formation of the heteroleptic helicates. Reaction of $\mathbf{L_z}$ and $\mathbf{L_{aa}}$, with Ni^{II} ions results in the formation of a statistical mixture of species (i.e. $[Ni_2(\mathbf{L_z})_2]^{4+}$, $[Ni_2(\mathbf{L_z})(\mathbf{L_{aa}})]^{4+}$ and $[Ni_2(\mathbf{L_{aa}})_2]^{4+}$ in a ratio 1 : 2 : 1). This was unsurprising, as in both ligands the metal centre is coordinated in an octahedral fashion. Thus in the heteroleptic complex, the coordination is similar with the metal centre coordinated via two tridentate binding domains, one from each ligand strand. A similar arrangement is seen when both $\mathbf{L_z}$ and $\mathbf{L_{aa}}$ react with Cu^{II} ions, where a statistical mixture of species is also observed (i.e. $[Cu_2(\mathbf{L_z})_2]^{4+}$, $[Cu_2(\mathbf{L_z})(\mathbf{L_{aa}})]^{4+}$ and $[Cu_2(\mathbf{L_{aa}})_2]^{4+}$ in a ratio 1 : 2 : 1). This observation was initially surprising given the

structures of $[Cu_2(\mathbf{L_z})_2]^{4+}$ (4-coordinate) and $[Cu_2(\mathbf{L_{aa}})_2]^{4+}$ (6-coordinate) are quite different and that the metal centre within the heteroleptic complex $[Cu_2(\mathbf{L_z})(\mathbf{L_{aa}})]^{4+}$ is 5-coordinate. This, however, Cu^{II} transition metal cation is stable in a 5-coordinate environment. Upon reaction of $\mathbf{L_z}$ and $\mathbf{L_{aa}}$ with Zn^{II} ions, a very different result was observed, as there were only trace amounts of the heteroleptic helicate $[Zn_2(\mathbf{L_z})(\mathbf{L_{aa}})]^{4+}$ present. This can be accounted for in terms of the coordination geometry observed in the Zn^{II} ion where the metal ion within the heteroleptic helicate $[Zn_2(\mathbf{L_z})(\mathbf{L_{aa}})]^{4+}$ occupies a 5-coordinate geometry which is disfavoured for the Zn^{II} ions for electronic reasons. As a result of the heteroleptic helicate being disfavoured the homoleptic helicates are favoured, i.e. self-recognition of the ligands is occurring.[71]

1.6 Ditopic Ligands

A ditopic ligand is one that possesses two guest binding sites capable of coordinating various or specific guest species. The synthesis and characterisation of ditopic receptors has received considerable attention over recent years with many examples reported.[76, 77] The simplest ditopic ligands generally contain N-donor domains capable of coordinating transition metal cations, and O-donor domains capable of coordinating anions. The ligands may simply be organic frameworks capable of coordinating two guest species, or more complicated systems whereby the ligand must form a transition metal ion complex before binding at a second site may occur.

A simple yet elegant example of a ditopic ligand has been demonstrated by M. D. Ward and co-workers, who prepared a series of ligands containing a phenanthroline binding site attached to an adjacent crown ether unit of various sizes (Figure 1.31).[78]

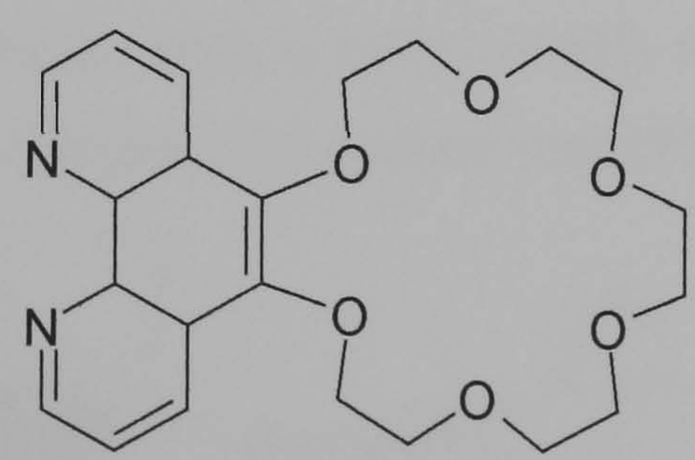

Figure 1.31. Ditopic ligand $\mathbf{L_{bb}}$, containing a phenanthroline N-donor domain attached to an adjacent [18]crown-6 ether fragment.

These ligands contain two binding domains, an N-donor domain (capable of coordination transition metal cations) comprising of a bidentate phenanthroline unit and an O-donor domain (capable of coordinating group I and II metal ions) formed from the attached crown ether fragment. Reaction of this ditopic ligand with $[Ru^{II}(bipy)_2Cl_2].2H_2O$ afforded a range of complexes of the type $[Ru^{II}(bipy)_2(\mathbf{L_{bb}})][PF_6]_2$. Upon formation of the ruthenium complex the redox properties of $[Ru^{II}(bipy)_2(\mathbf{L_{bb}})]^{2+}$ were investigated upon addition of barium ions. The redox properties observed for $[Ru^{II}(bipy)_2(\mathbf{L_{bb}})][PF_6]_2$ were typical for a $[Ru^{II}(bipy)_3]^{2+}$ derivative, with a Ru(II)/Ru(III) couple at -0.89 V *vs.* ferrocene/ferrocenium (Fc/Fc^+), and three ligand centred couples at -1.74, -1.93 and -2.17 *vs.* (Fc/Fc^+) in acetonitrile. Upon addition of barium ions to this solution resulted in the ligand centred reductions becoming broader, while a positive shift to +0.94 was observed for the Ru(II)/Ru(III) couple. This clearly demonstrates that barium ions are coordinated by the crown ether moiety, causing slight electrostatic destabilisation of the Ru(III) state.

Beer and co-workers have also incorporated two crown ether arms into a bipyridyl unit to produce an elegant example of a ditopic receptor, $\mathbf{L_{cc}}$, comprising of both N-donor and O-donor domains.[79] When the N-donor units are uncoordinated the ligand possesses a degree of conformational freedom, which upon reaction with the diquat dication allows the ligand to adopt a conformation where the planar dicationic guest intercalates between the two benzo-crown ether units (Figure 1.32a). Coordination of the N-donor units with a $[Ru^{II}(bipy)_2](PF_6)_2$ unit restricts the conformational freedom of the crown ether groups and causes the bipyridyl unit to approach planarity, in doing so the coordination of the dication in-between the two benzo-crown ether units is unfavourable. However, the rigid conformation adopted by the ligand following coordination with a ruthenium(II) ion, is capable of forming an intramolecular sandwich complex with sodium ions (Figure 1.32b).

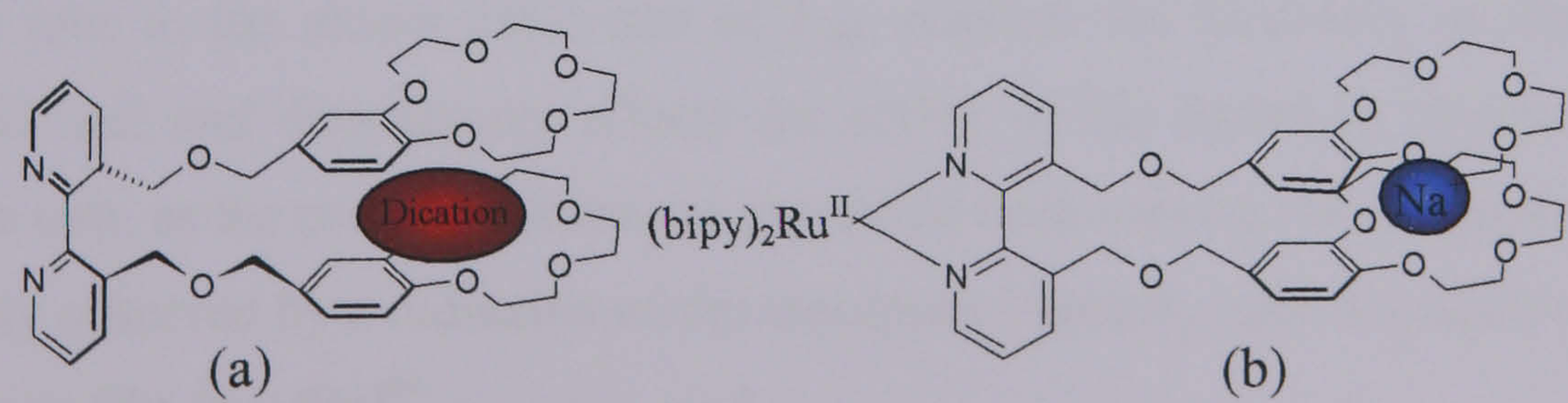

Figure 1.32. (a) The conformation adopted by $\mathbf{L_{cc}}$ upon reaction with the diquat dication, (b) The conformation adopted upon reaction with $[Ru^{II}(bipy)_2](PF_6)_2$ and Na^+ ions.

The bis-porphyrinic ditopic ligand system ($\mathbf{L_{dd}}$) incorporating a crown ether moiety developed by Kubo and co-workers also demonstrates how such ditopic ligands can undergo conformational changes.[80] This ditopic ligand comprises of two porphyrin units which coordinate zinc(II) ions, linked together by a biphenyl [20]crown-6 ether spacer (Figure 1.33).

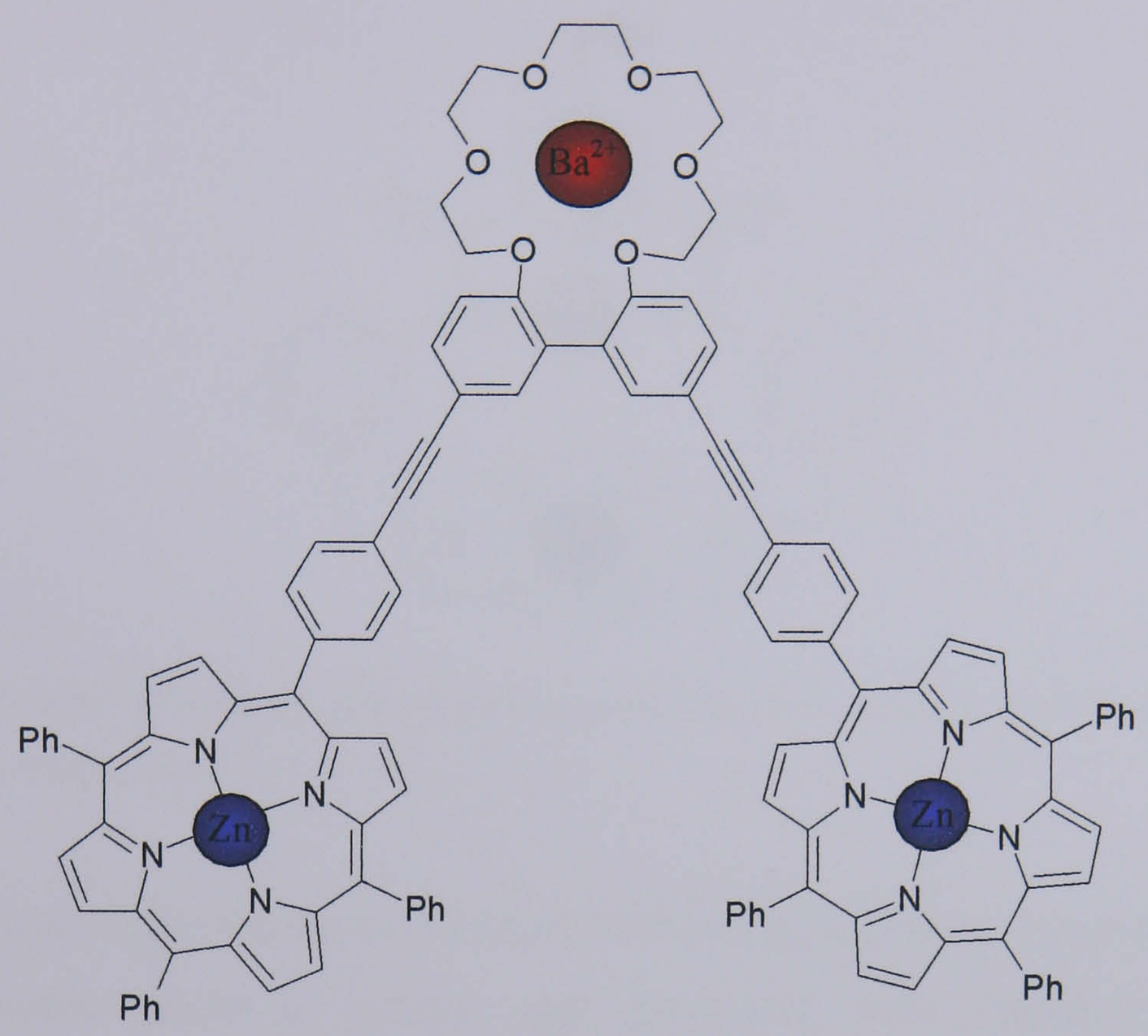

Figure 1.33. The biphenyl [20]crown-6 ether zinc(II) porphyrin ligand $\mathbf{L_{dd}}$.

When the crown ether binding site is uncoordinated, the ligand possesses a degree of flexibility about the central biphenyl spacer unit. This flexibility allows the two porphyrin arms to move closer together in the presence of the diamine, 1,4-bis(3-aminopropyl)piperazine, so that the diamine can coordinate to the two zinc(II) centres. As a consequence of this conformational change the dihedral angle between the two central phenyl rings becomes smaller. The incorporation of the diamine unit within the porphyrin ligand is very easily followed by the changes in the UV/vis spectrum of the strong porphyrin optical absorbance. However, coordination of barium ions to the crown ether unit of $\mathbf{L_{dd}}$, restricts the flexibility of the central biphenyl unit and dramatically effects the ability of the ligand to incorporate the diamine unit, as the prophyrin arms are prevented from moving closer together. This is clearly observed by a reduction of the absorption intensity upon the addition of the diamine to $[Zn_2(\mathbf{L_{dd}})Ba]^{6+}$.

The group of B. D. Smith and co-workers developed an elegant example of a ditopic macrobicyclic receptor with an adjacent anion and cation binding site (Figure 1.34).[81] The macrobicyclic receptor $\mathbf{L_{ee}}$, consists of a cation binding domain contained within the diaza-crown cavity and an anion binding domain formed by the two amide residues along the aromatic spacers.

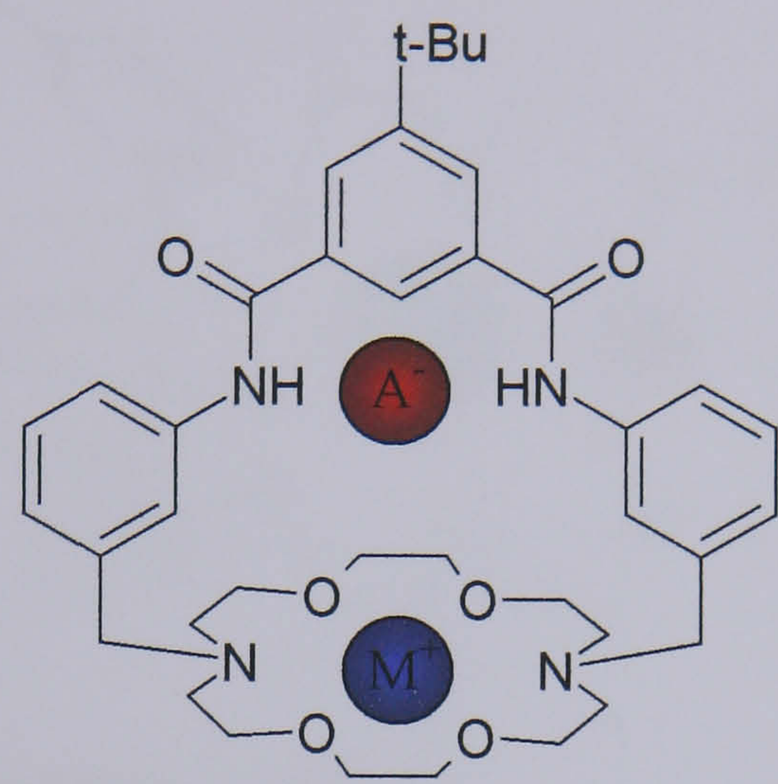

Figure 1.34. The ditopic macrobicyclic receptor $\mathbf{L_{ee}}$, indicating the position of the anion and cation binding sites.

The positioning of the two binding domains allows the ligand to simultaneously bind contact ion-pairs such as sodium and potassium salts ($NaNO_3$ and KNO_3 respectively), with the metal cation located within the cavity of the diaza-crown and the trigonal oxyanion hydrogen bonded to amide receptor residues. The orientation of the anion within the cavity is controlled by a complex interplay of steric factors, coordination bonding of the metal cation, and the hydrogen bonding of the anion to the amide receptors. This example by Smith and co-workers is an elegant example of how a relatively simple organic framework can act as a ditopic ligand.

The group of Beer and co-workers, has also carried out extensive research into the development of ligands capable of simultaneously binding both anions and cations, and have recently reported a heteroditopic receptor, $\mathbf{L_{ff}}$ (Figure 1.35), which binds contact ion pairs in a cooperative manner and shows recognition capabilities.[82]

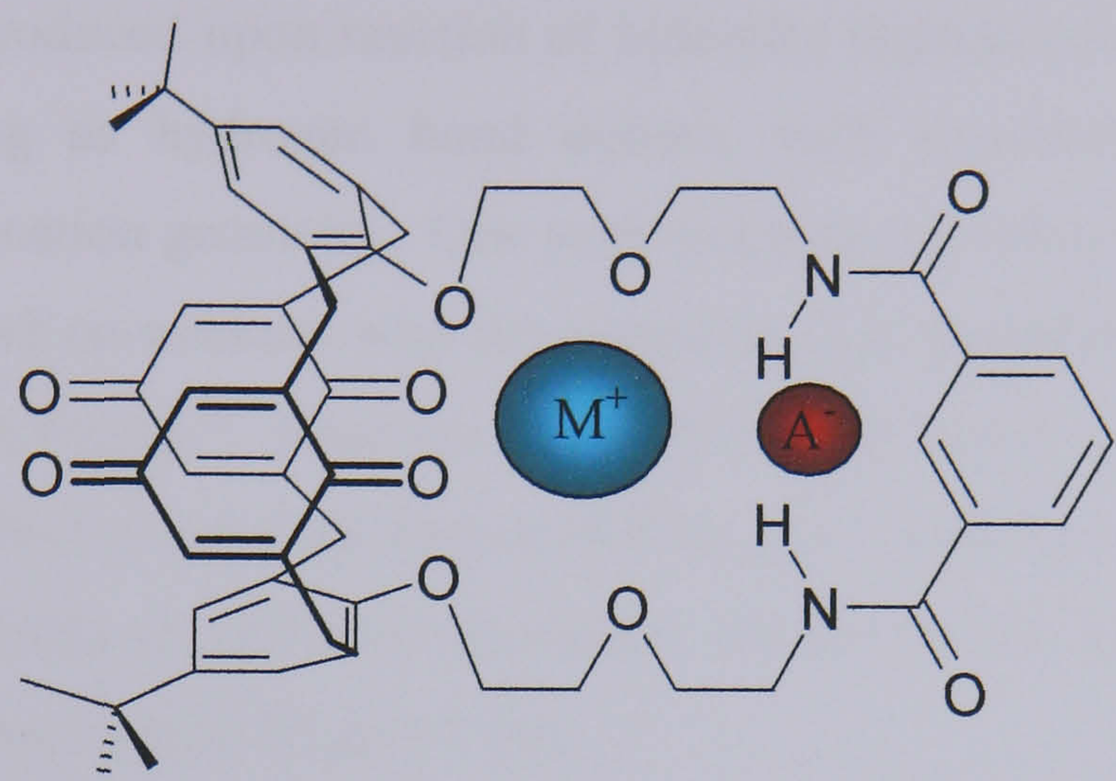

Figure 1.35. The heteroditopic receptor, $\mathbf{L_{ff}}$.

This heteroditopic receptor comprises of calix[4]diquinone and an isophthalamide moieties connected by two diethylene glycol units, the series of oxygen donors within the glycol cavity form the cation binding site and the attached amide residues forms the anion binding site. The resulting compound is capable of simultaneously binding s-block cation halide salts as contact ion pairs.[83] Upon extensive studies into the binding of various cation halide salts, it was found that the receptor would only bind halide anions in the presence of a suitable co-bound cationic guest species. Therefore the recognition of Cl^-, Br^- and I^- anions by the amide units within the isophthalamide moiety is effectively 'switched on' in the presence of a suitable co-bound cation such as K^+ ions. It was also noticed that receptor units exhibit affinity for particular ion-pairs and no affinity for the relative free ions. The binding properties demonstrated by $\mathbf{L_{ff}}$ are consistent with cooperative AND recognition of ion-pairs.

Although many examples of ligands capable of binding both anions and cations have been reported, there are however, a number of examples of ditopic ligands which upon coordination with a transition metal cation forms an anion binding site or cavity.[84-87] One such example is this formation of a C_3 or quasi-C_3 symmetric anion binding cavity, produced upon reaction of bidentate ligands possessing substituents capable of acting as hydrogen bond donors, with transition metals favouring octahedral coordination geometry. One such example has been demonstrated by the group of Beer and co-workers who developed by 2,2'-bipyridine ligand $\mathbf{L_{gg}}$, with attached amide receptors.[88] Reaction of this bidentate ligand with $RuCl_3$ results in the formation of the mononuclear system $[Ru^{II}(\mathbf{L_{gg}})_3]^{2+}$, with the metal ion occupying a distorted octahedral coordination geometry, formed by the coordination to three bidentate bipyridine ligands (Figure 1.36).

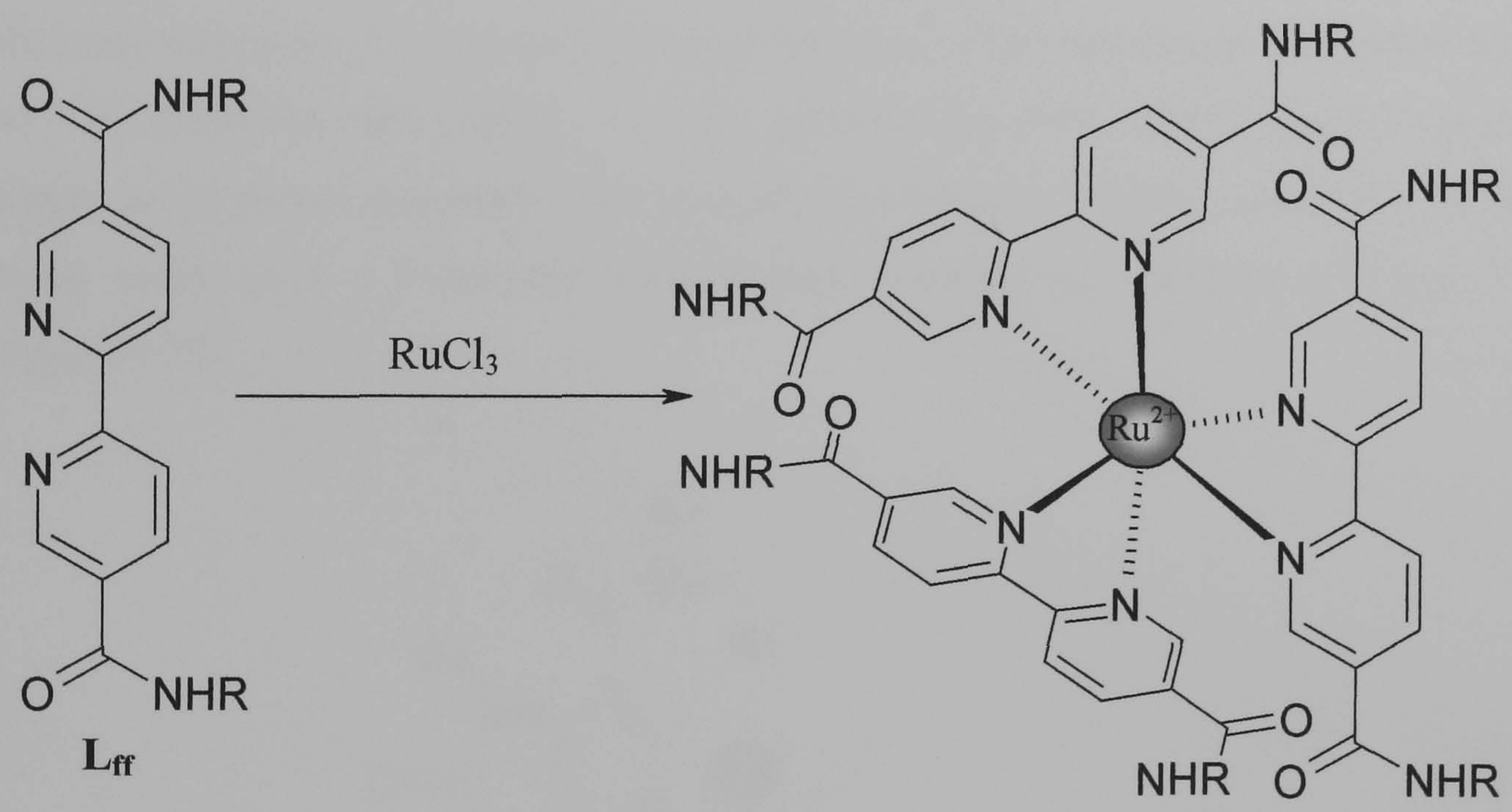

Figure 1.36. The formation of the anion receptor upon reaction of $\mathbf{L_{gg}}$ with $RuCl_3$.

Interestingly the amide substituents in the 5,5'-positions of the bipyridine unit produce three C_3-symmetric cavities capable of hydrogen bonding to anions. The selectivity of the assembled cavity to anions depends on the solvent system and the substituents attached to the amide receptor.

Mono-dentate ligands containing substituents capable of acting as hydrogen bond donors, may react with a transition metal cation favouring square planar coordination geometry. In such an example the ligand is derived form a simple 3-substituted pyridine, which upon reaction with a suitable metal cation forms a mononuclear complex with four ligands coordinating the metal ion in a square planar geometry. Such a complex may exist in four distinct conformations; (a) a cone, when all substituents in the 3-position point in the same direction (b) a partial cone when three of the substituents point in one direction and the fourth in another direction (c) the 1,2-alternate where *cis* pairs are pointing in the same direction and (d) 2,3-alternate where *trans* pairs are pointing in the same direction.

An example by P. A. Gale *et al.*,[89] elegantly demonstrates the formation of a 1,2-alternate formation, by reaction of a monodentate *n*-butylnicotinamide ligand $\mathbf{L_{hh}}$, with $PtCl_2(EtCN)_2$ and $AgPF_6$. As the platinum(II) metal centre prefers square planar coordination geometry, four *n*-butylnicotinamide ligands coordinate to the metal centre in a 1,2-alternate conformation forming the complex $[Pt^{II}(\mathbf{L_{hh}})_4]^{2+}$ (Figure 1.37).

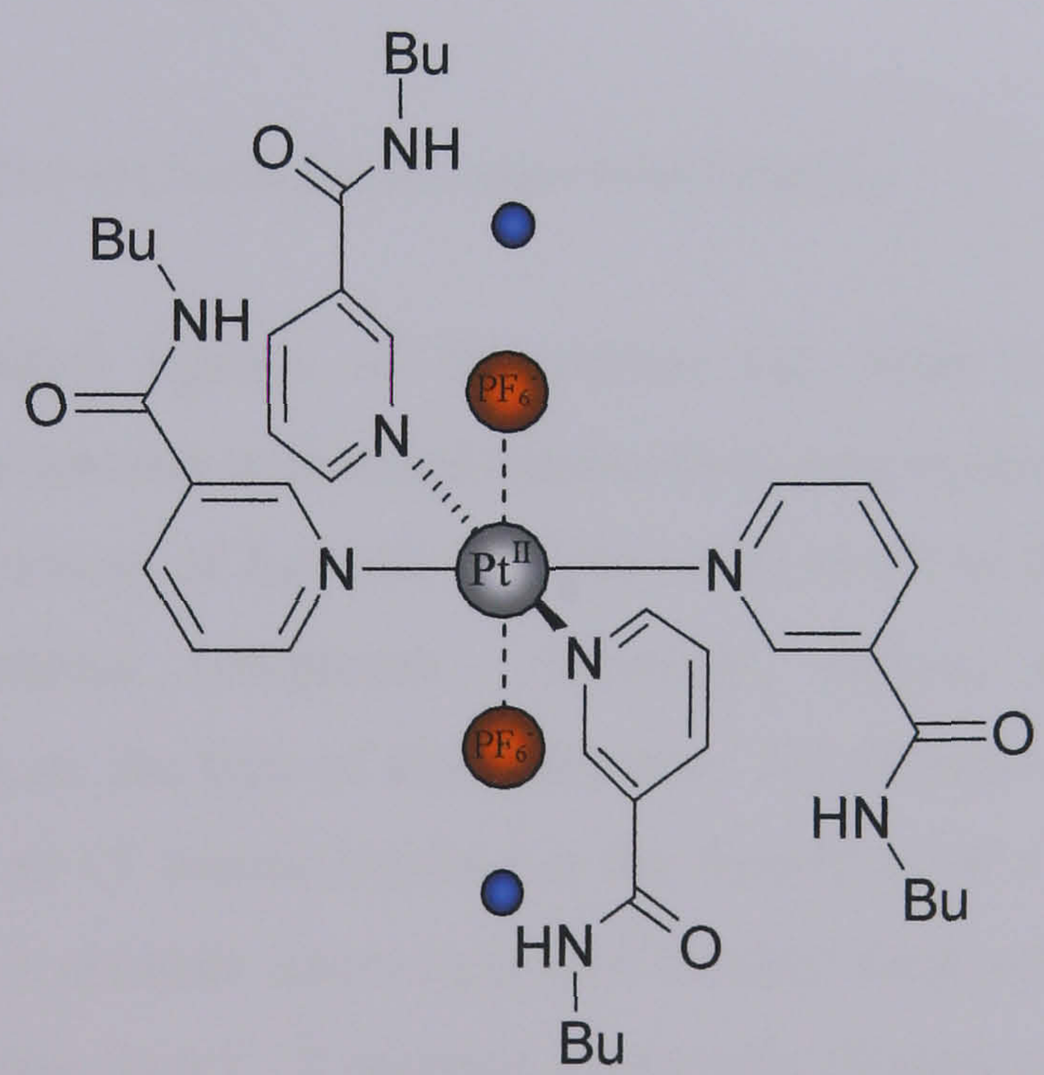

Figure 1.37. The 1,2-alternate conformation adopted by $\mathbf{L_{hh}}$ in the presence of a PF_6^- counter ion.

In the 1,2-alternate conformation *cis* pairs of amide substituents point above and below the plane of the Pt^{II} ion, resulting in the formation of two amide cavities

capable of forming hydrogen bonds to various tetrahedral or distorted tetrahedral anions. The amide cavity is capable of binding a variety of anions, in particular planar bidentate anions such as NO_3^- and $CH_3CO_2^-$ are bound in a receptor:anion ratio of 2 : 1, thus demonstrating how the shape of the amide receptor cavity can be selective to certain anions. One very notable result was observed for the binding of acetate anions in a solvent mixture of CD_3CN and DMSO (1 : 9) where K_2 is more than twice observed for K_1. This result suggests that the binding of the first acetate anion has a positive allosteric effect that favours the binding of the second acetate anion.

Another example has also been demonstrated by the group of P. A. Gale, who have prepared a urea functionalised isoquinoline ligand $\mathbf{L_{ii}}$ (Figure 1.38) capable of forming an anion binding cavities upon reaction with Pt^{II} ions.[90]

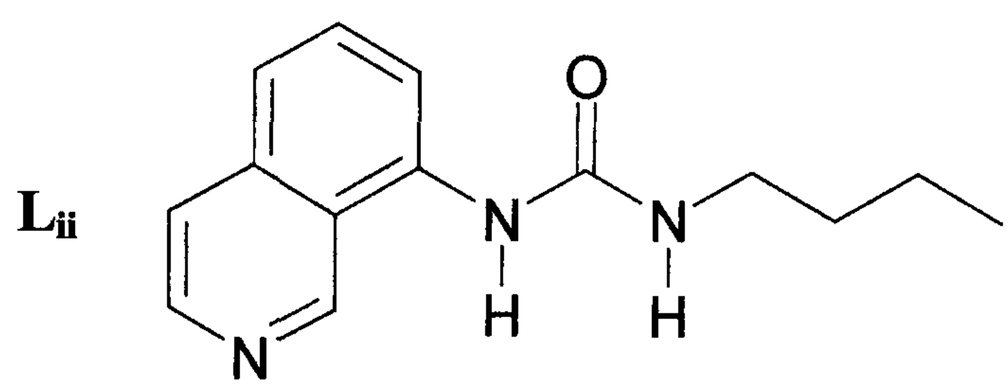

Figure 1.38. The urea functionalised isoquinoline ligand $\mathbf{L_{ii}}$.

As already established ligands of this nature can form a variety of distinct conformations upon reaction with metal cations favouring square planar coordination geometry. Thus, reaction of $\mathbf{L_{ii}}$ with Pt^{II} ions could result in the formation of four different conformational complexes. However, various conformations were observed depending on the type of anion present. For instance reaction of $\mathbf{L_{ii}}$ with Pt^{II} in the presence of Cl^- anions resulted in the formation of a 1,2- or 1,3-alternate conformation, with a chloride anion hydrogen bonded deep within each of the two urea containing cavities in a 1 : 2 receptor:anion ratio (Figure 1.39a). Each chloride anion is situated deep within the cavity and is hydrogen bonded by two pairs of adjacent urea N-H donors, a further C-H$\cdots$$Cl^-$ hydrogen bond is formed between the ligand framework and the chloride anion. Similar observations were also seen upon addition of Br^- and I^- anions, and all K_1 values were much greater than the K_2 values,

suggesting a reduction of electrostatic interactions following the binding of the first anion. Addition of $H_2PO_4^-$ or SO_4^{2-} however, results in the formation of a cone conformation with a 1 : 1 receptor:anion ratio (Figure 1.39b). The X-ray crystal structure of the sulphate derivative shows all eight NH·····O interaction from all four urea groups to three of the four sulphate oxygen atoms, thus securing the anion deep within the cavity.

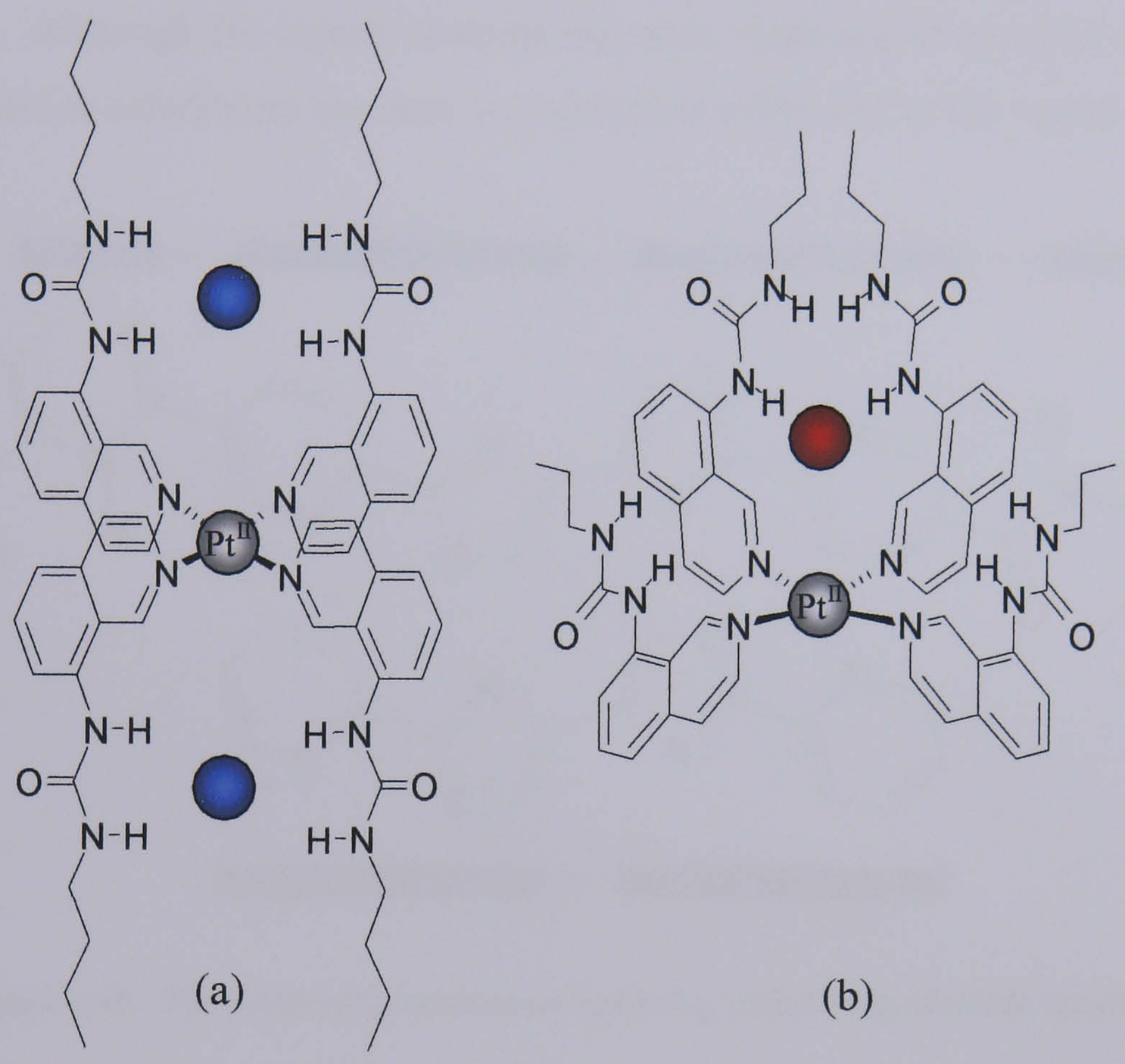

Figure 1.39. Representation of:- (a) The 1,2-alternate conformation formed upon addition of Cl^-, Br^- or I^- anions (b) The cone conformation formed upon addition of $H_2PO_4^-$ or SO_4^{2-} anions.

Although most ditopic anion receptors are based on simple organic frameworks or mononuclear systems, there are however, a few examples of ditopic transition metal helicate systems. One such example has been demonstrated by the pyridyl-thiazole ligand $\mathbf{L_{jj}}$, (Figure 1.40) developed by the group of Rice *et al.*,[91] which contains the same bis-bidentate binding domains as the previously discussed pyridyl-thiazole ligand $\mathbf{L_x}$. Although the ligand contains the same sequence of pyridine and thiazole rings, an amide substituent has been introduced at either end of the ligand.

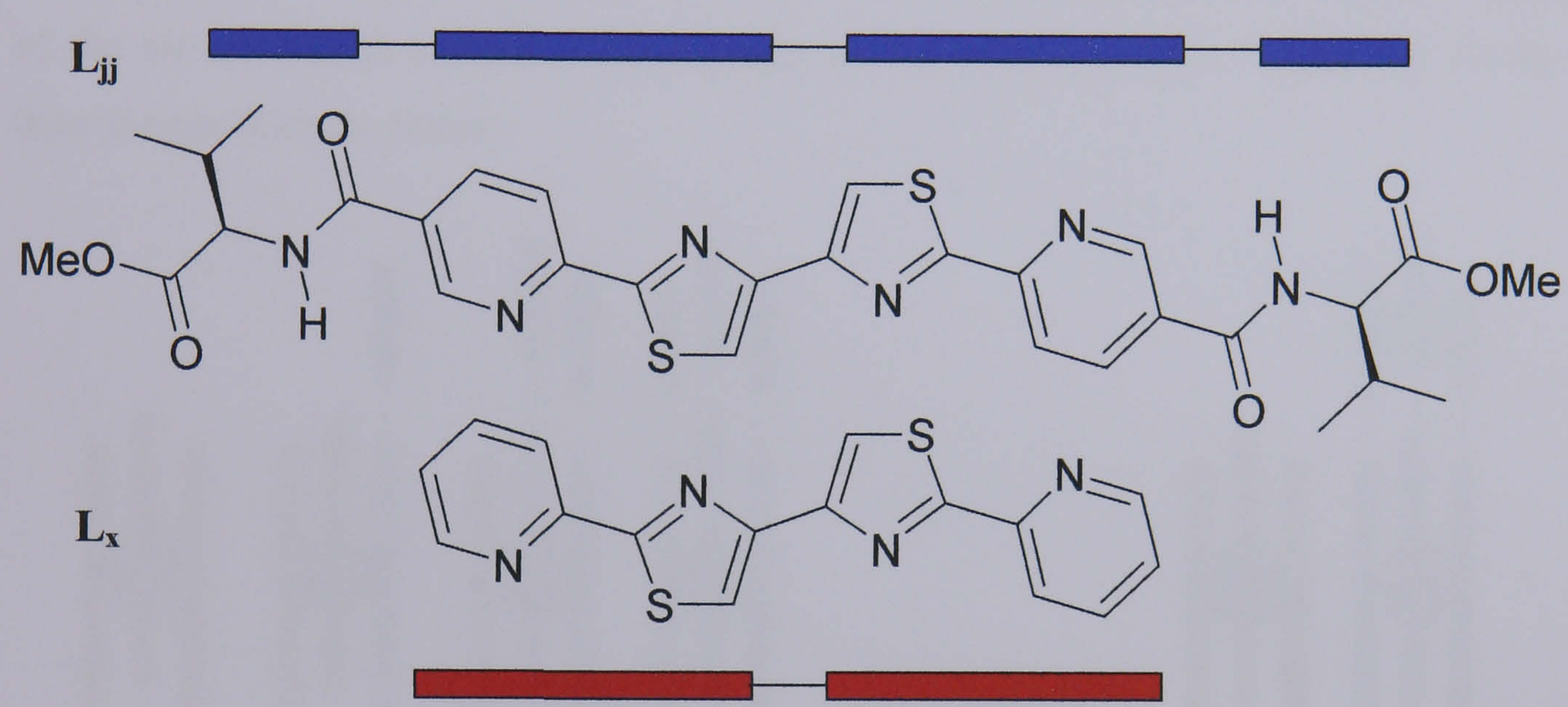

Figure 1.40. The potentially tetradentate ligand $\mathbf{L_{jj}}$, comprising of amide substituents.

Reaction of this ligand with Co^{II} ions in the correct stoichiometric amounts results in the formation of a dinuclear triple helicate, with each cobalt(II) centre occupying a distorted octahedral coordination geometry formed by three bidentate py-tz domains, one from each ligand. The introduction of the amide substituent at either end of the ligand chain results in the formation of C_3-symmetric cavity upon formation of the helicate $[Co_2(\mathbf{L_{jj}})_3]^{4+}$, comprising of three amide hydrogen bond donors. In the solid state the perchlorate anions are encapsulated within the cavity via two hydrogen bonding interaction between the oxygen atoms of the perchlorate anion and the –NH donors of the amides. However, addition of NO_3^- ions to this species results in the NO_3^- ions replacing the perchlorate anions within the cavity with all three oxygen atoms forming hydrogen bonds to all three –NH donors of the amides. Most interestingly the nitrate anion is sited much deeper within the cavity than the

perchlorate anion, indicating the binding of the nitrate anion is much stronger than the perchlorate anion. The ability of nitrate anions to bind strongly to the amide donors within the cavity, introduces ligand recognition capabilities. Reaction of $\mathbf{L_{ii}}$ with the unsubstituted ligand $\mathbf{L_x}$ and Co^{II} ions in the correct stoichiometric amounts resulted in the formation of a statistical mixture of both the homoleptic and heteroleptic helicate species $[Co_2(\mathbf{L_{jj}})_3]^{4+}$, $[Co_2(\mathbf{L_x})_3]^{4+}$, $[Co_2(\mathbf{L_{jj}})(\mathbf{L_x})_2]^{4+}$ and $[Co_2(\mathbf{L_{jj}})_2(\mathbf{L_x})]^{4+}$ in the ratio 1 : 1 : 3 : 3. This observation did not come as a surprise as both ligands contain identical coordination domains. However, addition of NO_3^- ions resulted in the formation of only the homoleptic helicate species $[Co_2(\mathbf{L_{jj}})_3]^{4+}$ and $[Co_2(\mathbf{L_x})_3]^{4+}$ (Figure 1.41). This observation can be accounted for by the ability of the nitrate anions to bind more strongly to the amide receptor within the cavity than the perchlorate anions.

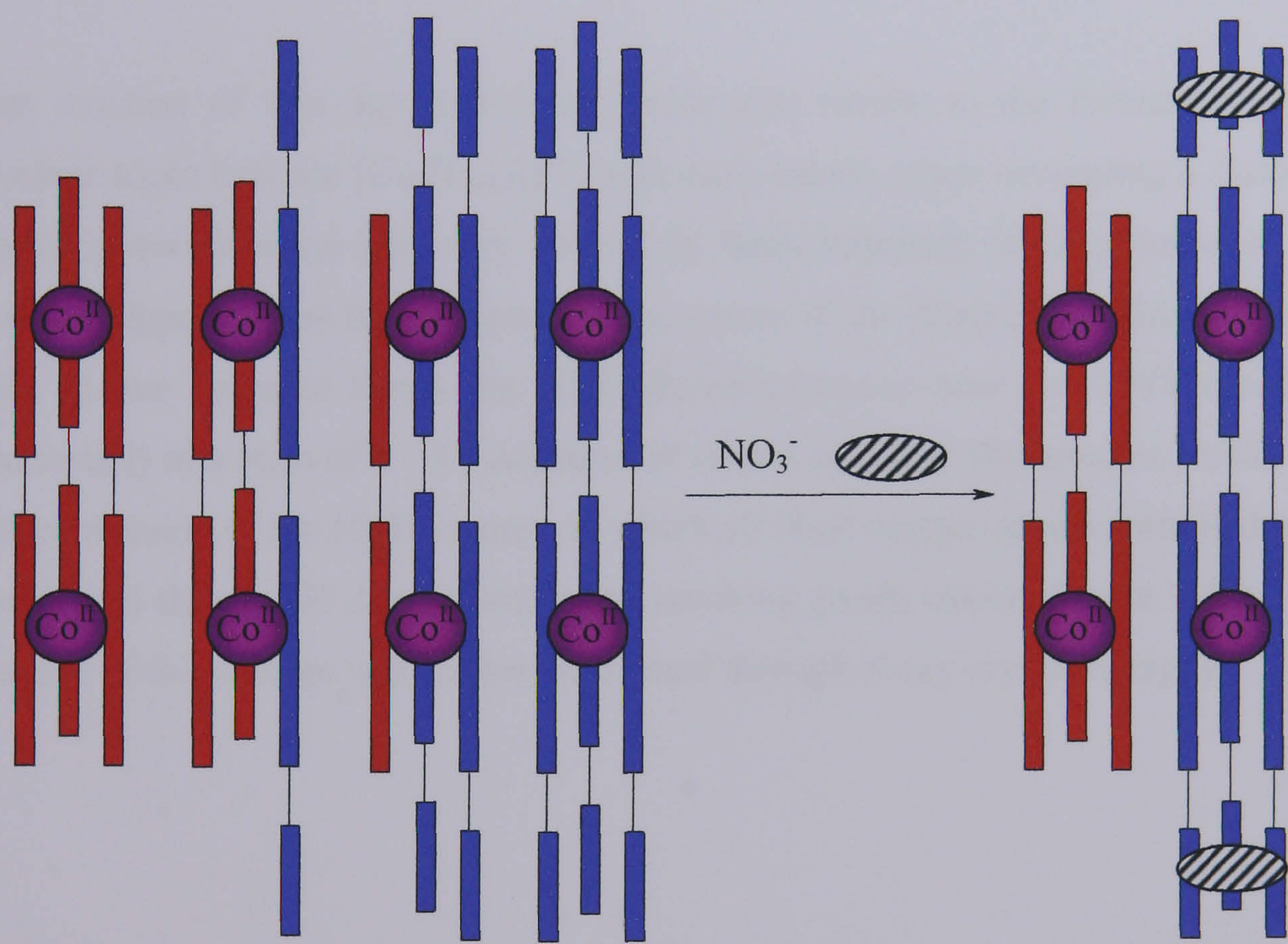

Figure 1.41. Cartoon representation showing ligand recognition between $\mathbf{L_x}$ and $\mathbf{L_{jj}}$ upon addition of nitrate anions.

Ligand recognition capabilities were also observed in a similar pyridyl-thiazole ligand, $\mathbf{L_{kk}}$, which contains the same N-donor binding domains but only contains one amide substituent at one end of the ligand, as apposed to both ends of the ligand in the previous example (Figure 1.42).[92]

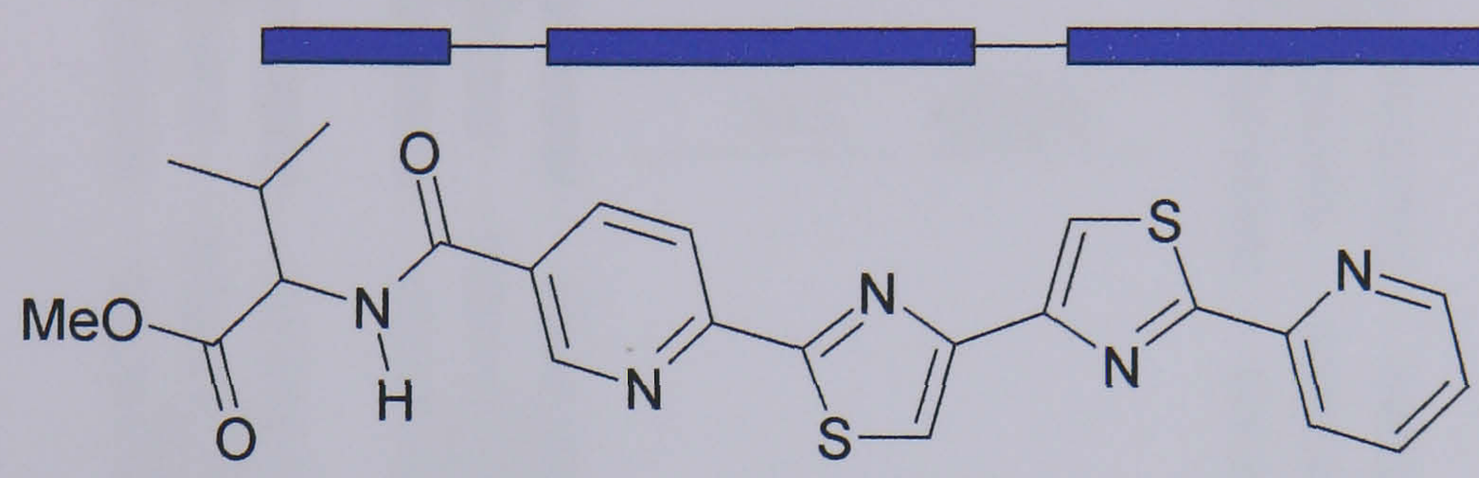

Figure 1.42. The asymmetric ligand $\mathbf{L_{kk}}$.

Upon reaction of this ligand with Co^{II} ions also results in the formation of the dinuclear triple helicate $[Co_2(\mathbf{L_{kk}})_3]^{4+}$, with each cobalt centre occupying a distorted octahedral coordination geometry formed by three bidentate binding domains, one from each ligand. Due to the asymmetrical nature of the ligand, the helicate species exists in two isometic forms the HHH (head-to-head-to-head) an HHT (head-to-head-to-tail) in a ratio of 1 : 3. Addition of nitrate anions to this species results in a 95% conversion to the HHH isomer, in which all three oxygen atoms form hydrogen bonds to all three –NH donors within the resulting amide cavity (Figure 1.43). The structure of this species was further confirmed through X-ray crystallography.

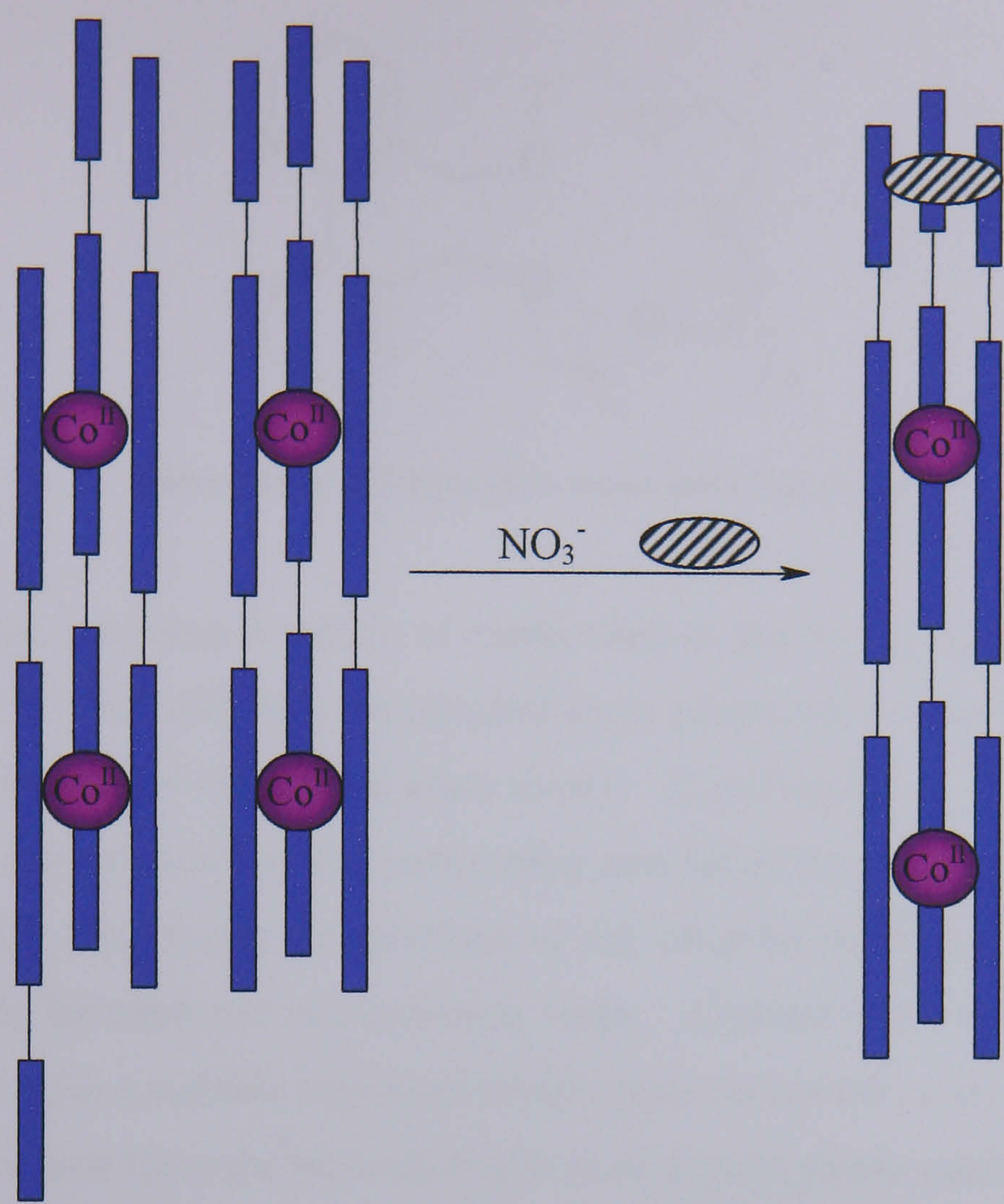

Figure 1.43. Cartoon representation showing ligand recognition upon addition of nitrate anions to the asymmetric ligand $\mathbf{L_{kk}}$.

1.7 Allosteric Interactions

For an allosteric effect to occur within a ligand (or any other system capable of experiencing an allosteric effect) there must be at least two different binding domains. In an allosteric system, binding at one domain produces a conformational change that influences the binding (switches on or off) ability at another domain within the ligand.[2] There are many examples within the literature of allosteric systems,[93] the first example of a supramolecular allosteric system was described by Rebek *et al.*, who synthesised a 2,2-bipyridine crown ether ligand, $\mathbf{L_{ll}}$ (Figure 1.44), consisting of two binding domains.[94-96] One domain comprises of an O-donor region within the crown ether moiety, which is capable of coordinating various alkali or ammonium ions, a second domain comprises of N-donor units formed by the 2,2'-bipyridine unit, which are capable of coordinating various transition metal cations.

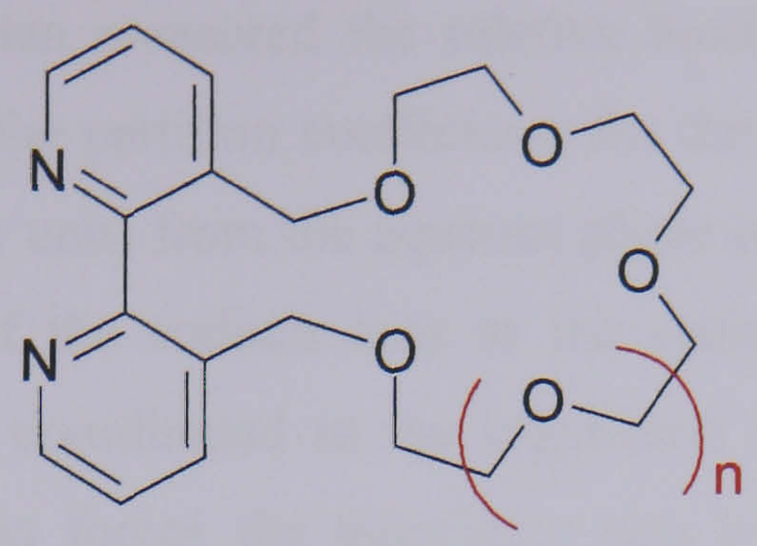

Figure 1.44. 2,2-bipyridine crown ether ligand, $\mathbf{L_{II}}$.

The free ligand can adopt a variety of conformations due to the flexibility about the central bipyridyl unit, although the dihedral angle adopted between the two aromatic rings alters the size of the crown ether cavity. Coordination of an s-block metal cation to the oxygen atoms of the crown ether unit brings the benzylic oxygen atoms closer together, thus fixing the position of the benzylic hydrogen atoms and the dihedral angle between the two aromatic rings. Alternatively coordination to the bipyridyl unit with a suitable transition metal cation forces the $-CH_2-$ units to move closer together and fixes the bipyridine unit in an almost planar conformation. As a consequence the benzylic oxygen atoms move further apart and effectively reduces the size of the crown ether binding site (Figure 1.45).

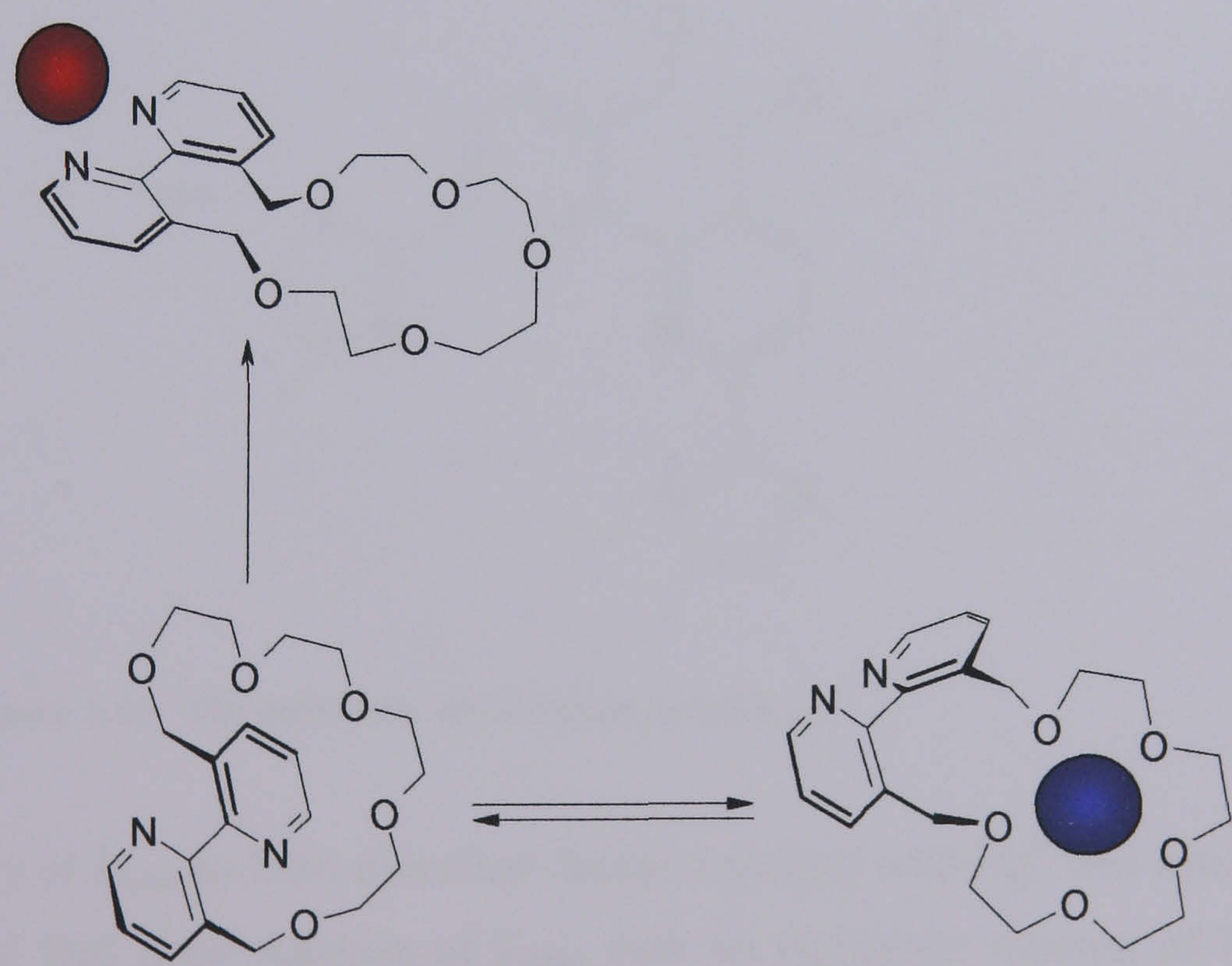

Figure 1.45. The various conformations adopted by $\mathbf{L_{II}}$ upon coordination via the crown ether unit and the bipyridyl unit.

Rebek and co-workers then measured the relative binding constants which were obtained by determining the partition coefficients for the extraction of sodium ions (bound to the crown ether unit) from the aqueous phase to the organic phase. They found that the affinity of the sodium ions to the crown ether was dramatically reduced as $W(CO_4)$ was coordinated to the bipyridine unit. Coordination at the bipyridine binding domain forces the bipyridine unit to approach planarity, thus producing a conformational change. This conformational change, known as an allosteric effect, affects the reactivity of the crown ether unit so that it lowers the affinity for coordination with sodium ions.

The group of Rice *et al.*, further developed this allosteric effect by introducing two thiazole rings in the 6-positions of the 2,2'-bipyridine unit.[97] Thus, the ligand, $\mathbf{L_{mm}}$, is now potentially tetra-dentate and could in theory accommodate transition metal cations favouring either tetrahedral or octahedral coordination geometry (Figure 1.46).

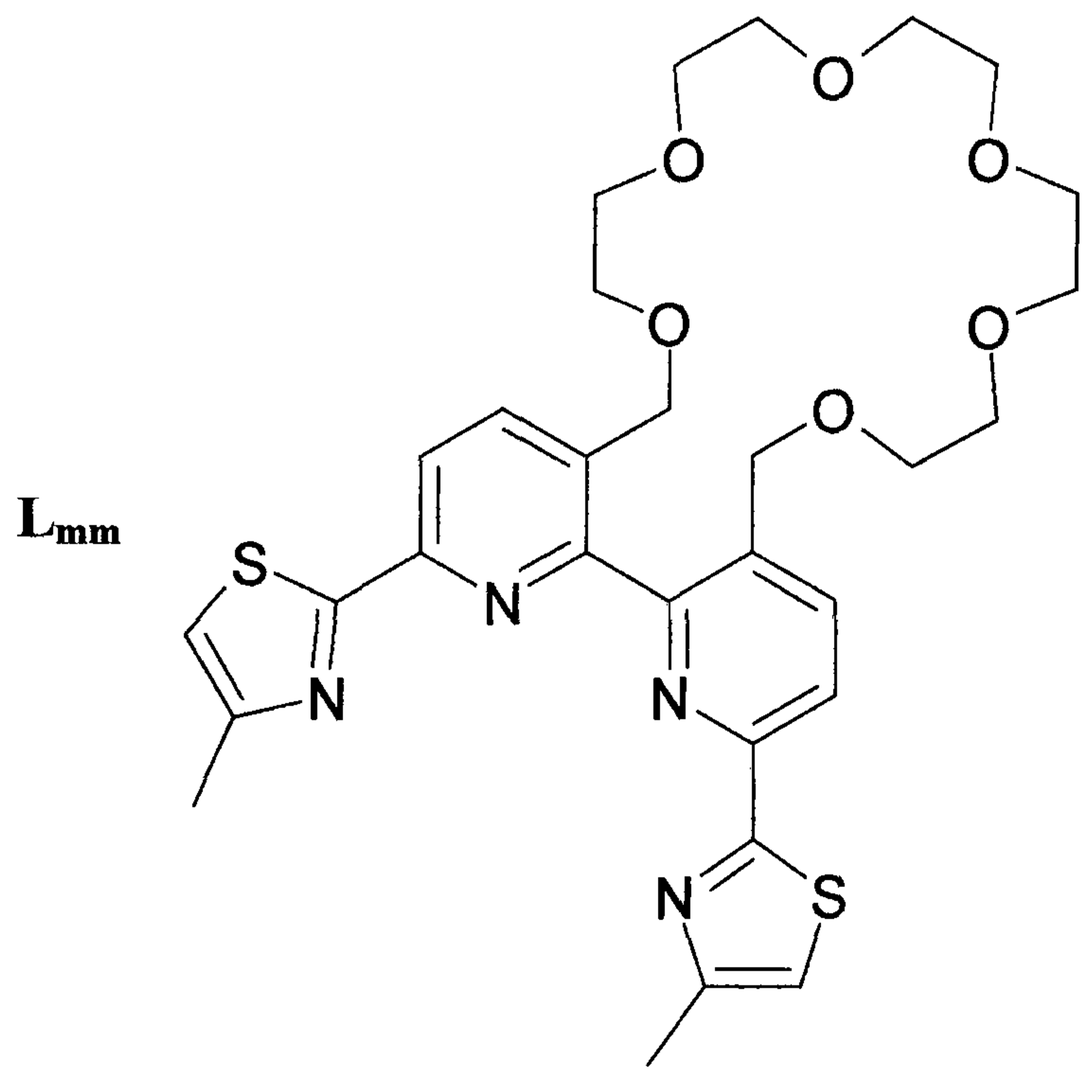

Figure 1.46. The potentially tetra-dentate ligand $\mathbf{L_{mm}}$.

The ability of $\mathbf{L_{mm}}$ to form dinuclear double helicates with Hg^{II} was investigated. It was found that upon reaction of $\mathbf{L_{mm}}$ with an equimolar amount of Hg^{II} ions, a dinuclear double helicate $[Hg_2(\mathbf{L_{mm}})_2]^{4+}$ was formed. Addition of excess Na^+ ions to this helicate species resulted in the formation of the complex $[Hg_2(\mathbf{L_{mm}})_2Na_2]^{6+}$. Single crystal X-ray diffraction studies confirmed the formation of the helicate

species, with each ligand partitioning into two bis-bidentate (tz-py) binding domains with two Hg^{II} ions coordinated by two bridging ligands in a double helical arrangement. Each of the two metal centres occupies a distorted tetrahedral coordination geometry formed by two bidentate (tz-py) binding domains, one from each ligand. In both ligands the crown ethers have at least one benzylic oxygen atom uncoordinated, this would be expected as the Na^+ cation is relatively small in comparison to the [16]crown-6 ether fragment, thus coordination by all six O-donors does not occur. As a consequence of at least one benzylic oxygen atom being uncoordinated, the 2,2'-bipyridine unit possesses some flexibility, thus allowing the ligand to partition into two bidentate binding domains allowing the formation of a dinuclear double helicate.

However, addition of excess Ba^{2+} ions to the helicate $[Hg_2(\mathbf{L_{mm}})_2]^{4+}$ gave a very different result, as the formation of the mononuclear complex $[Hg(\mathbf{L_{mm}})Ba]^{4+}$ was observed. With the Ba^{2+} ions coordinating all of the oxygen atoms within the [16]crown-6 ether fragment the benzylic oxygen atoms attached to the central 2,2'-bipyridine unit becomes more rigid, thus restricting the ligand from partitioning into separate binding domains, so the ligand now acts as a simple tetradentate donor (Figure 1.47). However, the coordination of barium ions to the crown ether has also increased the charge of the overall complex, so disassembly to a mononuclear complex may occur to lower the electrostatic repulsion associated with the high charge. X-ray crystallography studies confirmed the presence of this mononuclear complex, with the mercury metal centre occupying a distorted octahedral coordination geometry. The ligand acts as a simple tetradentate donor, coordinating the metal centre in the equatorial plane, with two perchlorate anions acting as bidentate axial ligands.

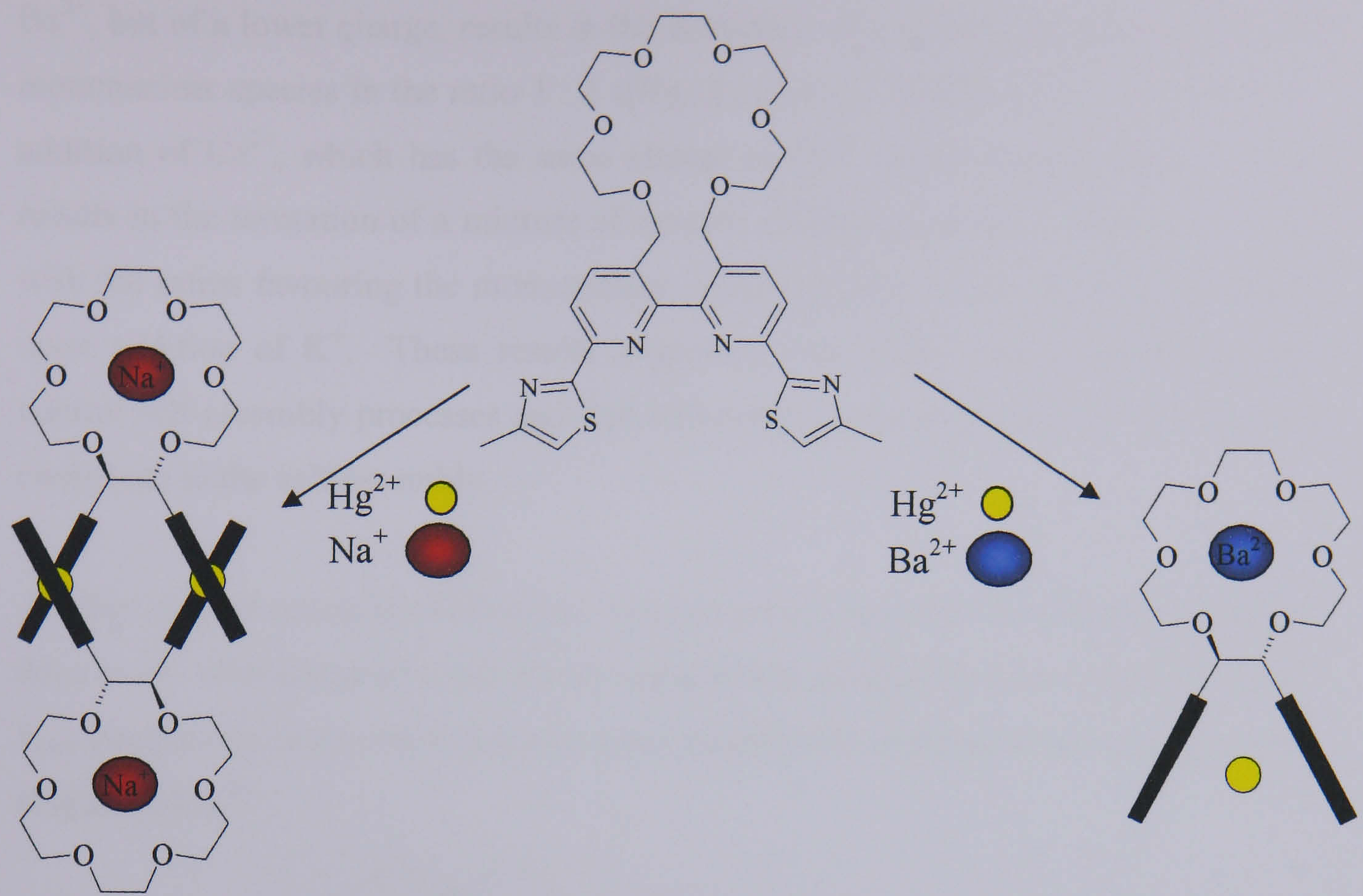

Figure 1.47. Allosteric reprogramming of the ditopic ligand, $\mathbf{L_{mm}}$.

In summary reaction of $\mathbf{L_{mm}}$ with Hg^{II} ions results in the formation of a dinuclear double helicate. The helicate retains its structure upon addition of sodium ions but upon addition of barium ions the helicate disassembles to give a mononuclear structure. Such control over self-assembly processes may be accounted to one of two factors. Firstly, an electrostatic effect as coordination of Ba^{2+} to the crown ether of the helicate species would lead to a highly charged 8+ ion, thus disassembly of the helicate species to a mononuclear system would reduce electrostatic repulsion and increase the entropy of the system. Secondly, an allosteric effect as coordination of the benzylic oxygen atoms induces a conformational change, thus preventing the ligand from acting as a bis-bidentate donor and so resulting in the formation of a mononuclear system with the ligand acting as a simple tetradentate donor. In an attempt to determine which of these factors controls the self-assembly of this ligand, various Group 1 and 2 metal cations were added to the ditopic helicate species $[Hg_2(\mathbf{L_{mm}})_2]^{4+}$. The helicate structure was retained upon addition of the smaller metal cations (M = Li^+, Na^+, or Mg^{2+}), thus forming $[Hg_2(\mathbf{L_{mm}})_2M_2]^{6+/8+}$, whereas upon addition of larger cations such as Ba^{2+} or Sr^{2+} results in the formation of the mononuclear system $[Hg(\mathbf{L_{mm}})M]^{4+}$. Upon addition of K^+, which is a similar size to

Ba^{2+}, but of a lower charge, results in the formation of a mixture of both helical and mononuclear species in the ratio 1 : 2 ($[Hg_2(\mathbf{L_{mm}})_2K_2]^{6+}$, $[Hg(\mathbf{L_{mm}})K]^{3+}$). However, addition of Ca^{2+}, which has the same charge as Ba^{2+} but is smaller then K^+, also results in the formation of a mixture of species, ($[Hg_2(\mathbf{L_{mm}})_2Ca_2]^{8+}$, $[Hg(\mathbf{L_{mm}})Ca]^{4+}$) with the ratios favouring the mononuclear system as observed to the helical system upon addition of K^+. These results suggested that neither factors independently control self-assembly processes and that both electrostatic and allosteric effects both contribute to the self-assembly.

Another elegant example of allosteric reprogramming has also been demonstrated by Rice *et al.*, who prepared a potentially tetradentate pyridyl-thiazole-bipyridyl ligand $\mathbf{L_{nn}}$, comprising of an external crown ether binding site attached to the bipyridyl unit (Figure 1.48).[98]

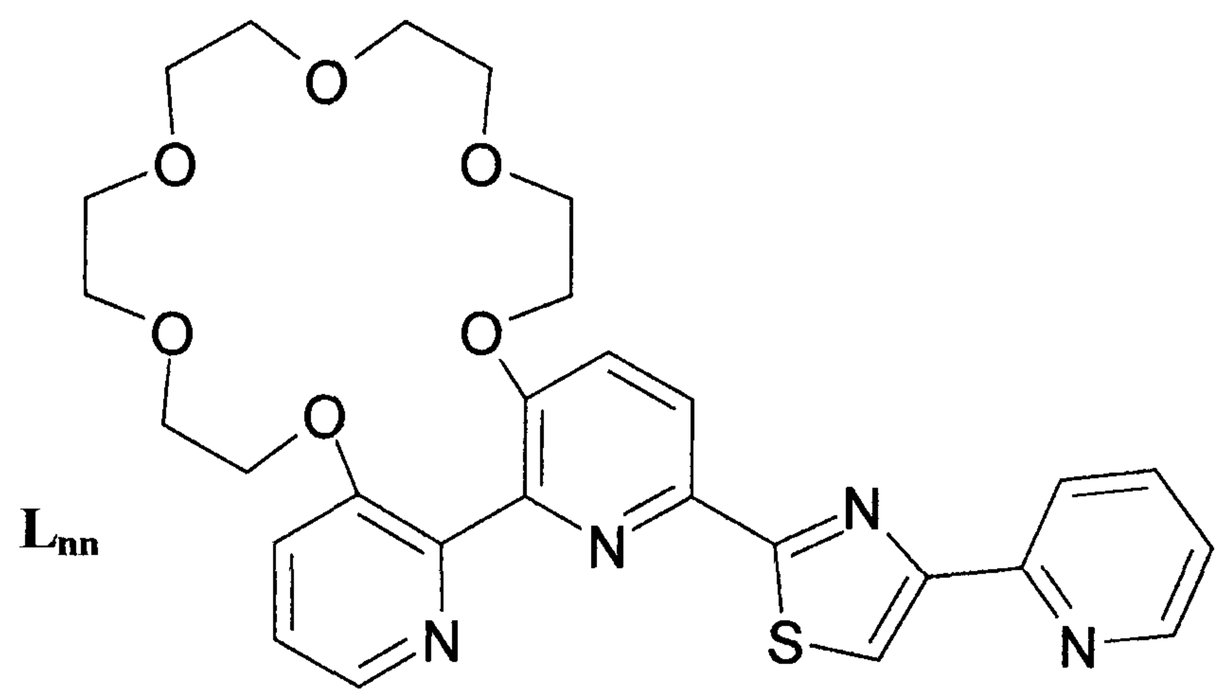

Figure 1.48. The potentially tetradentate ligand $\mathbf{L_{nn}}$.

Treatment of $\mathbf{L_{nn}}$ with an equimolar amount of Cu^I ions resulted in the formation of the dinuclear double helicate $[Cu_2(\mathbf{L_{nn}})_2]^{2+}$. The ligand partitions into two distinct bis-bidentate binding domains, a pyridyl-thiazole (head) and a bipyridyl domain (tail). Each copper centre occupies a distorted tetrahedral coordination geometry formed by one py-tz (head) and one bipy (tail) binding domain from two bridging ligands in a double helical arrangement. As a consequence of the formation of the HT helicate, both crown ether moieties are on the same side of the molecule, thus leading to the formation of a molecular cup that has the potential to bind various cations. Addition of Ba^{2+} ions to a solution of $[Cu_2(\mathbf{L_{nn}})_2]^{2+}$ resulted in the formation of $[Cu_2(\mathbf{L_{nn}})_2Ba_2]^{6+}$, observed through MS studies, thus providing evidence of the

helicate structure being retained while also coordinating Ba^{2+} ions to the crown ether moiety. However, X-ray crystallographic studies revealed that although the HT arrangement was still observed the bipyridyl unit was twisted about its backbone (C-N-N-C dihedral angle 81°) in such a manner that only the terminal pyridyl units coordinate the copper centres. The copper centres retain their distorted tetrahedral coordination geometry by coordination to the terminal pyridyl unit of one ligand and a thiazole-pyridyl domain of the second ligand, the copper centre completes its coordination sphere by coordination of a MeCN solvent molecule. The result of such a coordination mode results in the conversion of a helicate species to a side-by-side complex (Figure 1.49). A similar result was also observed upon addition of an excess of Na^{+} ions to $[Cu_2(\mathbf{L_{nn}})_2]^{2+}$, only this time a mixture of helicate and side-by-side species is observed in roughly the same quantities, suggesting an equilibrium exists between the two.

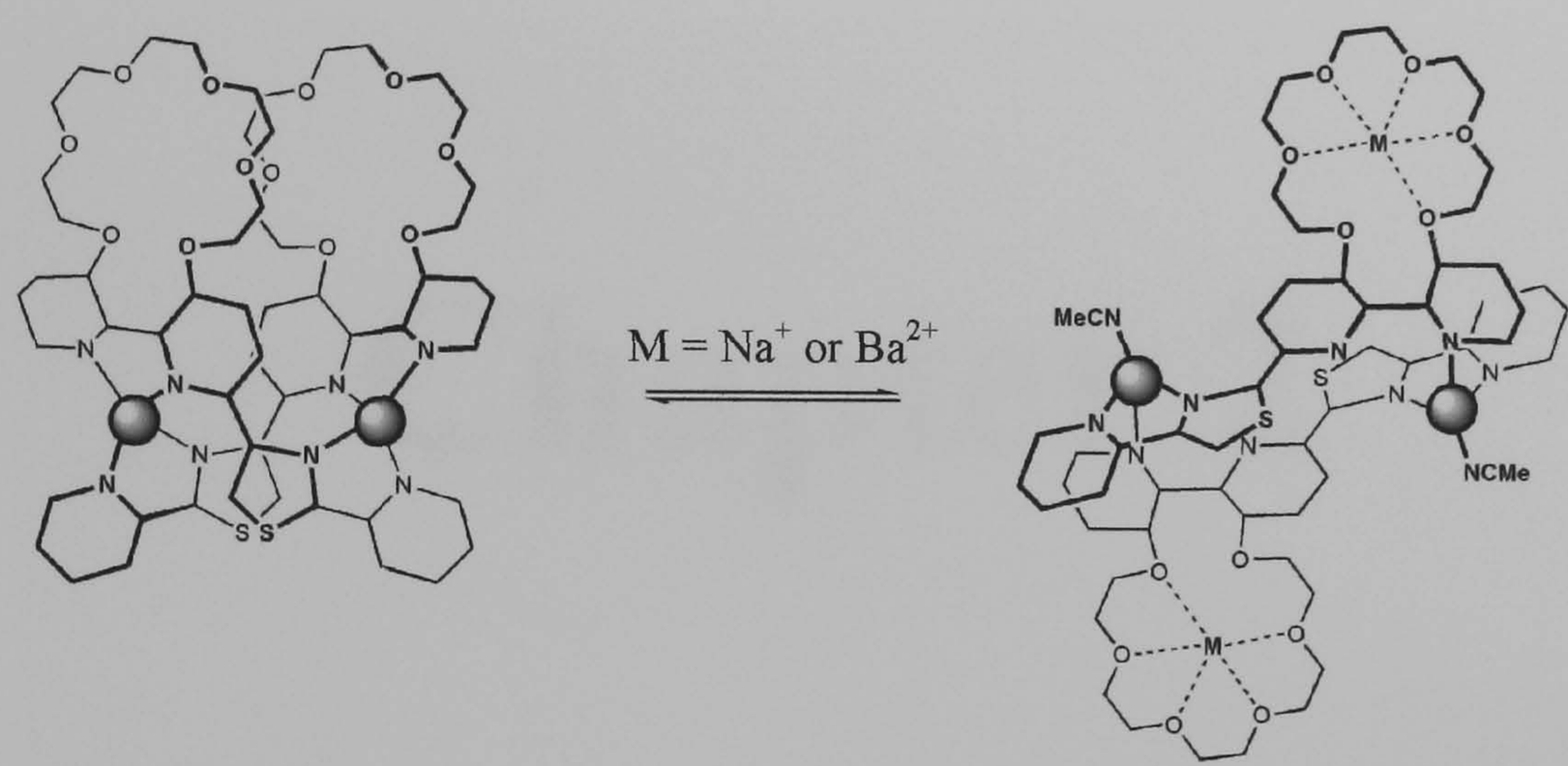

Figure 1.49. The conversion of the HT $\mathbf{L_{nn}}$ helicate species to a side-by-side species upon addition of Ba^{2+} or Na^{+} ions.

NMR studies also suggested an equilibrium existing between the two species even in the absence of an s-block metal cation. In the presence of Na^{+} ions this equilibrium is allosterically driven towards the side-by-side species, however, in the presence of Ba^{2+} ions only the side-by-side species is observed. This example elegantly demonstrates an allosteric effect, as coordination of the s-block metal cations to the crown ether unit causes a conformational change. The dramatic twisting of the bipyridyl unit means that it can no longer act as a bidentate domain and results in the formation of a side-by-side species. This system also has potential applications as a cation sensor as dramatic colour changes occur upon addition of various s-block metal cations to $[Cu_2(\mathbf{L_{nn}})_2]^{2+}$.

Chapter 2

2. Allosteric-Controlled Metal Specificity of a Ditopic Ligand

Described in this chapter is the synthesis and coordination chemistry of two potentially tetradentate N-donor ditopic ligands $\mathbf{L_1}$ and $\mathbf{L_2}$ (Figure 2.1) with selected transition metal cations. These particular ligands comprise of a tz-py-py-tz backbone, allowing the ligand to act as a simple tetradentate donor or partition into bis-bidentate tz-py binding domains.[97, 99] Also incorporated within these ligands is a crown ether receptor spanning the 3,3'-positions of the central bipyridine unit. However, the two crown ether moieties differ slightly as the crown ether in $\mathbf{L_1}$ is attached to the bipyridine unit via a methylene unit (O–CH_2–bipy), while in $\mathbf{L_2}$ the crown ether moiety is directly attached to the bipyridine unit (O–bipy).

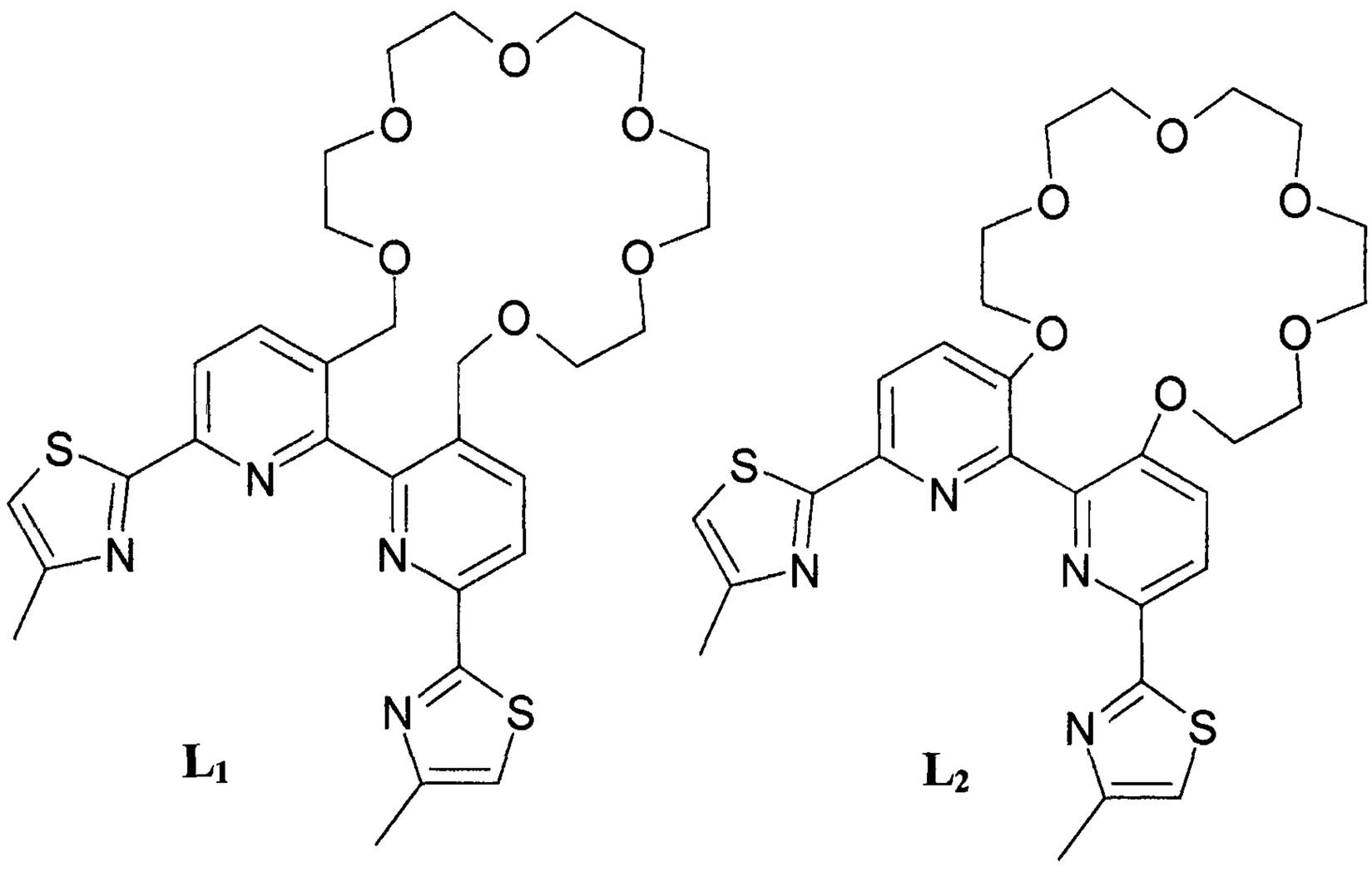

Figure 2.1. The potentially tetradentate ligands $\mathbf{L_1}$ and $\mathbf{L_2}$.

2.1 Ligand Synthesis

The synthesis of the two potentially tetradentate ligands $\mathbf{L_1}$ and $\mathbf{L_2}$ is very similar, with only the early stages of the synthesis differing and consists of relatively short eight- and seven-step synthetic routes, respectively. The most versatile compound en route to the preparation of these ligands is the synthesis of the thioamide which is formed by reaction of the appropriate nitrile group with hydrogen sulphide. The preparation of such a group, in principle allows the synthesis of a wide range of related polydentate (py-tz) based ligands as described in a number of recent publications by Rice *et al.*,[70, 72, 75]

2.1.1 Synthesis of $\mathbf{L_1}$

The synthesis of $\mathbf{L_1}$ is outlined in Scheme 1 and was carried out in a similar manner to the procedure described by Rebek *et al.*,[95] Thus, a basic solution containing 1,10-phenanthroline (**1**) and potassium permanganate was refluxed for two hours before acidification, forming the dicarboxylic acid (**2**). Esterification of (**2**) by reaction with *N*-methylmorpholine and methylchloroformate gave (**3**) in moderate yields. Complete reduction of the ester (**3**) to the diol (**4**) was achieved by slow addition of a sodium bis[2-methoxyethoxy] aluminium hydride solution to a solution of (**3**) in anhydrous THF. The appearance of a doublet at 4.45 ppm corresponding to a $-CH_2-$ group and the disappearance of the signal corresponding to the ester confirmed complete reduction to the diol. Reaction of the diol (**4**) with sodium hydride and penta-(ethylene glycol)-di-*p*-tosylate, resulted in the formation of bipyridyl crown ether (**5**) in moderate yields. Complete conversion of the bipyridyl crown ether to the *bis*-N,N'-oxide (**6**) using a slight excess of *meta*-chloroperoxybenzoic acid, gave a white solid after purification via column chromatography. The resulting bis-N,N'-oxide (**6**) was refluxed in DCM with excess trimethylsilyl cyanide in the presence of benzoyl chloride giving the dicarbonitrile derivative (**7**) in high yields. The dithioamide (**8**) was produced as a yellow solid by purging hydrogen sulphide through a solution of (**7**) in ethanol in the presence of triethylamine. The appearance of two singlets, corresponding to the dithioamide at 9.35 and 7.65 ppm in the H^1 NMR spectrum confirmed complete conversion of the dicarbonitrile derivative. Addition of an excess of chloroacetone to a refluxing solution of (**8**) in ethanol in the presence of TBA-Br resulted in the formation of pale yellow crystals of $\mathbf{L_1}$ on cooling.

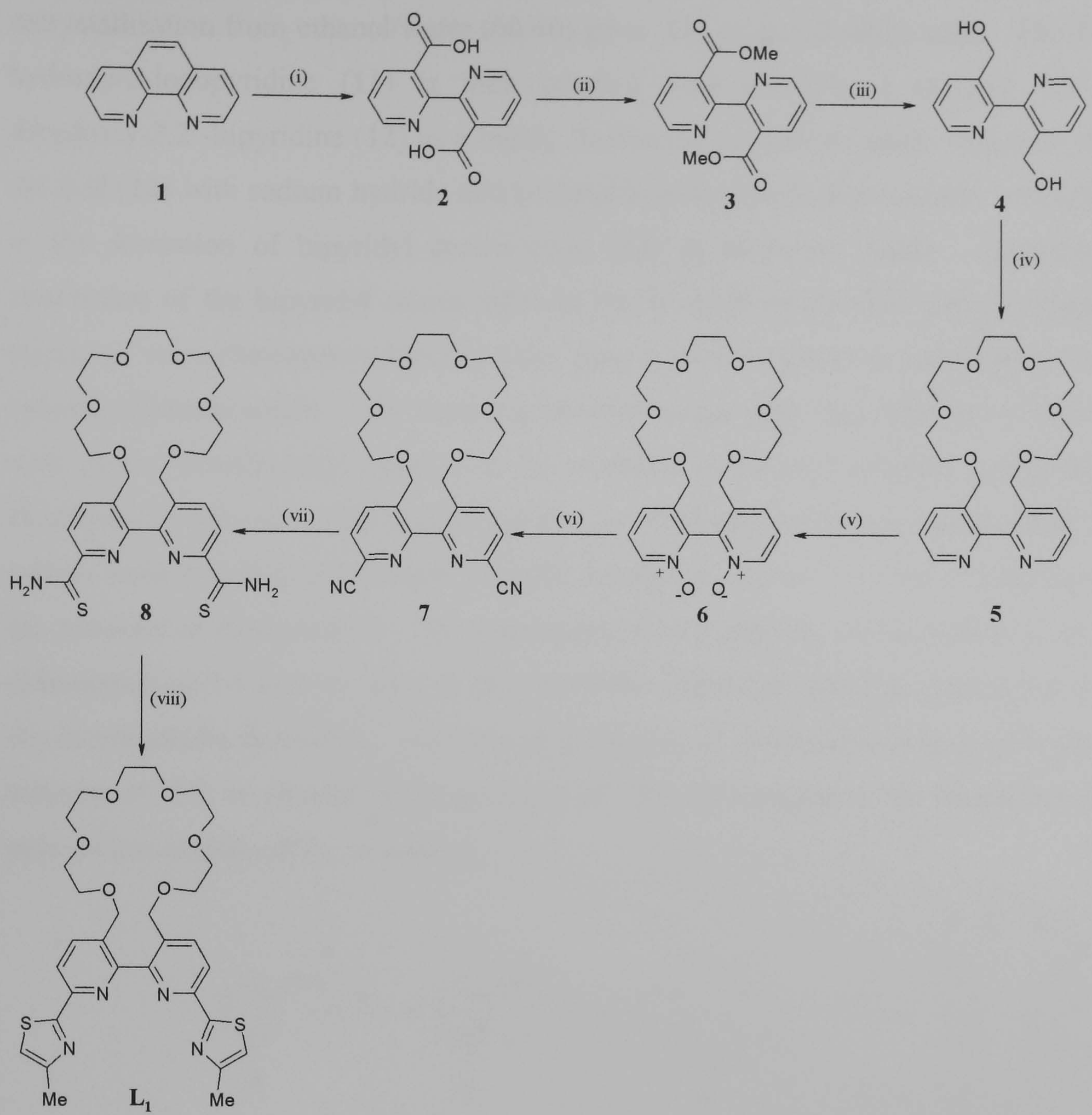

Scheme 1. Synthesis of $\mathbf{L_1}$ from 1,10-phenanthroline (**1**). Reagents and conditions: $KMnO_4$ and NaOH (at reflux in H_2O), $AgNO_3$ and $H_2S_{(g)}$, (ii) *N*-methylmorpholine and methylchloroformate, MeOH, 0°C, (iii) sodium bis[2-methoxyethoxy] aluminium hydride (Vitride), anhydrous THF, N_2, 0°C (iv) NaH, penta-(ethylene glycol)-di-*p*-tosylate, anhydrous DMF, N_2, 60°C, (v) *m*CPBA, DCM, RT, (vi) benzoyl chloride, TMSCN (at reflux in DCM), (vii) $H_2S_{(g)}$, Et_3N in EtOH, (viii) chloroacetone, TBA-Br (at reflux in EtOH).

2.1.2 Synthesis of $\mathbf{L_2}$

The synthesis of $\mathbf{L_2}$ is outlined in scheme 2 and was carried out in a similar manner to the procedure described by Rebek *et al.*,[95] Initially 3-hydroxypyridine (**10**) was converted to 3-hydroxy-2-iodopyridine (**11**) by reaction with sodium carbonate and iodine in water. Acidification using concentrated hydrochloric acid followed by

recrystallisation from ethanol/water (60/40) gave (**11**) as an off-white solid. The 3-hydroxy-2-iodopyridine (**11**) is then coupled with $[Ni(PPh_3)_4]$ to give 3,3'-dihydroxy-2,2'-bipyridine (**12**) as a highly fluorescent crystalline solid. Reaction of the diol (**12**) with sodium hydride and penta-(ethylene glycol)-di-*p*-tosylate, resulted in the formation of bipyridyl crown ether (**13**) in moderate yields. Complete conversion of the bipyridyl crown ether to the *bis*-N,N'-oxide (**14**) using a slight excess of *meta*-chloroperoxybenzoic acid, gave a white solid after purification via column chromatography. The resulting bis-N,N'-oxide (**14**) was refluxed in DCM with excess trimethylsilyl cyanide in the presence of benzoyl chloride giving the dicarbonitrile derivative (**15**) in high yields. The dithioamide (**16**) was produced as a yellow solid by purging hydrogen sulphide through a solution of (**15**) in ethanol in the presence of triethylamine. The appearance of two singlets, corresponding to the dithioamide at 9.4 and 7.6 ppm in the ^1H NMR confirmed complete conversion of the dicarbonitrile derivative. Addition of an excess of chloroacetone to a refluxing solution of (**16**) in ethanol in the presence of TBA-Br resulted in the formation of pale yellow crystals of $\mathbf{L_2}$ on cooling.

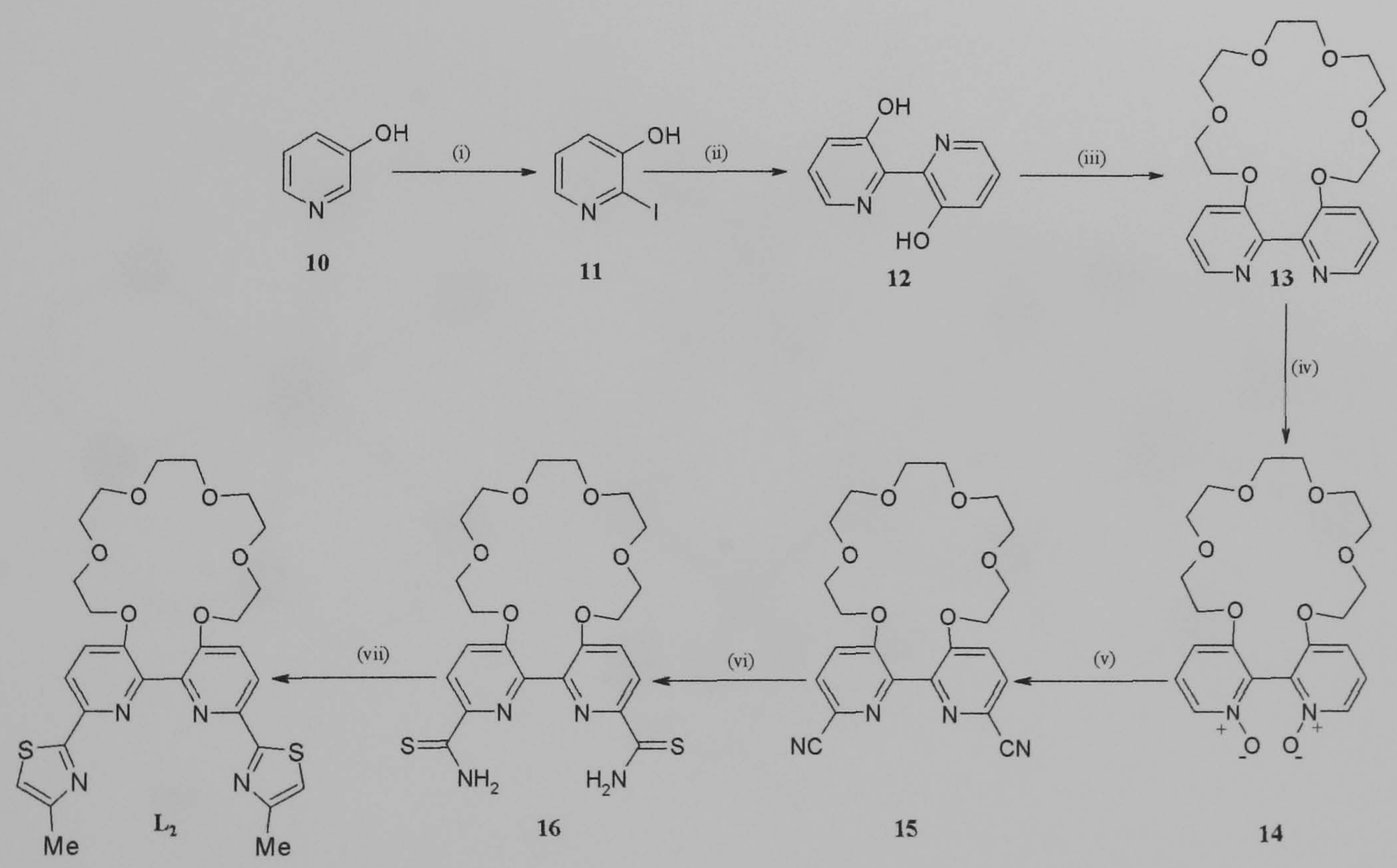

Scheme 2. Synthesis of $\mathbf{L_2}$ from 3-hydroxypyridine (**10**). Reagents and conditions: (i) Na_2CO_3, I_2, HCl, (ii) $NiCl_2.6H_2O$, PPh_3, zinc dust, anhydrous DMF, N_2, 50°C, (iii) NaH, penta-(ethylene glycol)-di-*p*-tosylate, anhydrous DMF, N_2, 60°C, (iv) DCM, *m*CPBA, RT, (v) benzoyl chloride, TMSCN (at reflux in DCM), (vi) $H_2S_{(g)}$, Et_3N in ethanol, (vii) chloroacetone, TBA-Br (at reflux in EtOH).

2.2 Coordination Chemistry

2.2.1 Complexes of $\mathbf{L_1}$ *with Copper(I)*

The reaction of $\mathbf{L_1}$ with an equimolar amount of $[Cu(MeCN)_4]PF_6$ in acetonitrile produced a dark red solution. ESI-MS of the resulting solution confirmed the formation of a dinuclear double helicate with an ion at *m/z* 1497 corresponding to the complex $\{[Cu_2(\mathbf{L_1})_2](PF_6)\}^+$. As previously established crown ether receptors of this type are capable of coordinating a range of s-block metal cations, thus upon addition of excess $Ba(ClO_4)_2$ to this solution results in the coordination of a barium ion by the crown ether moiety, forming the dinuclear double helicate $[Cu_2(\mathbf{L_1})_2Ba_2]^{6+}$. The presence of this helicate species has also been confirmed by ESI-MS by the presence of an ion at *m/z* 2124 corresponding to $\{[Cu_2(\mathbf{L_1})_2Ba_2](ClO_4)_5\}^+$. Slow diffusion of diethyl ether into this resulting solution afforded orange crystals of X-ray quality. The X-ray crystal structure of this complex has been previously reported by C. J. Baylies (Figure 2.2).[100]

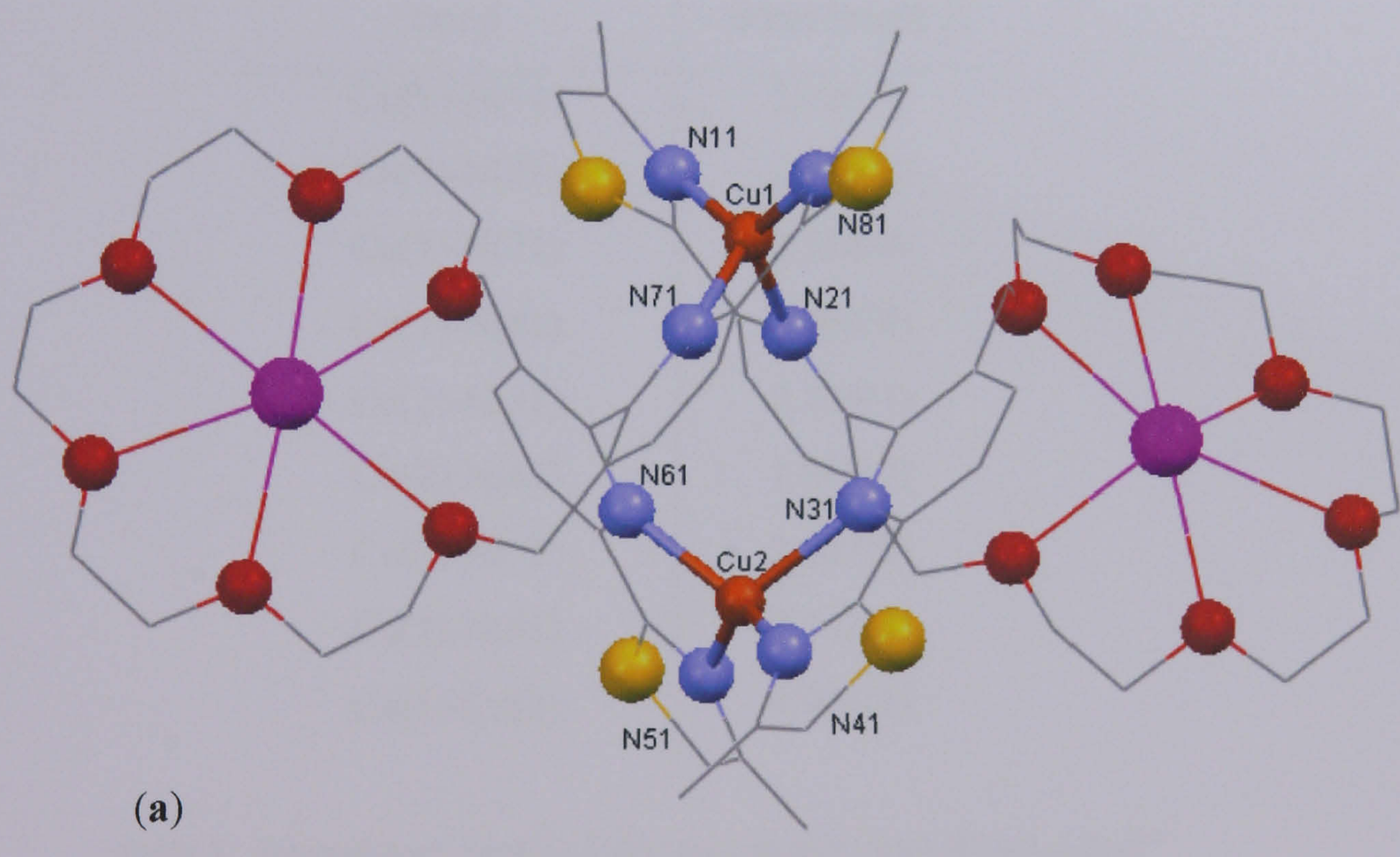

(a)

Figure 2.2(a). X-ray crystal structure of the complex cation $[Cu_2(\mathbf{L_1})_2Ba_2]^{6+}$ showing the structural framework.[100]

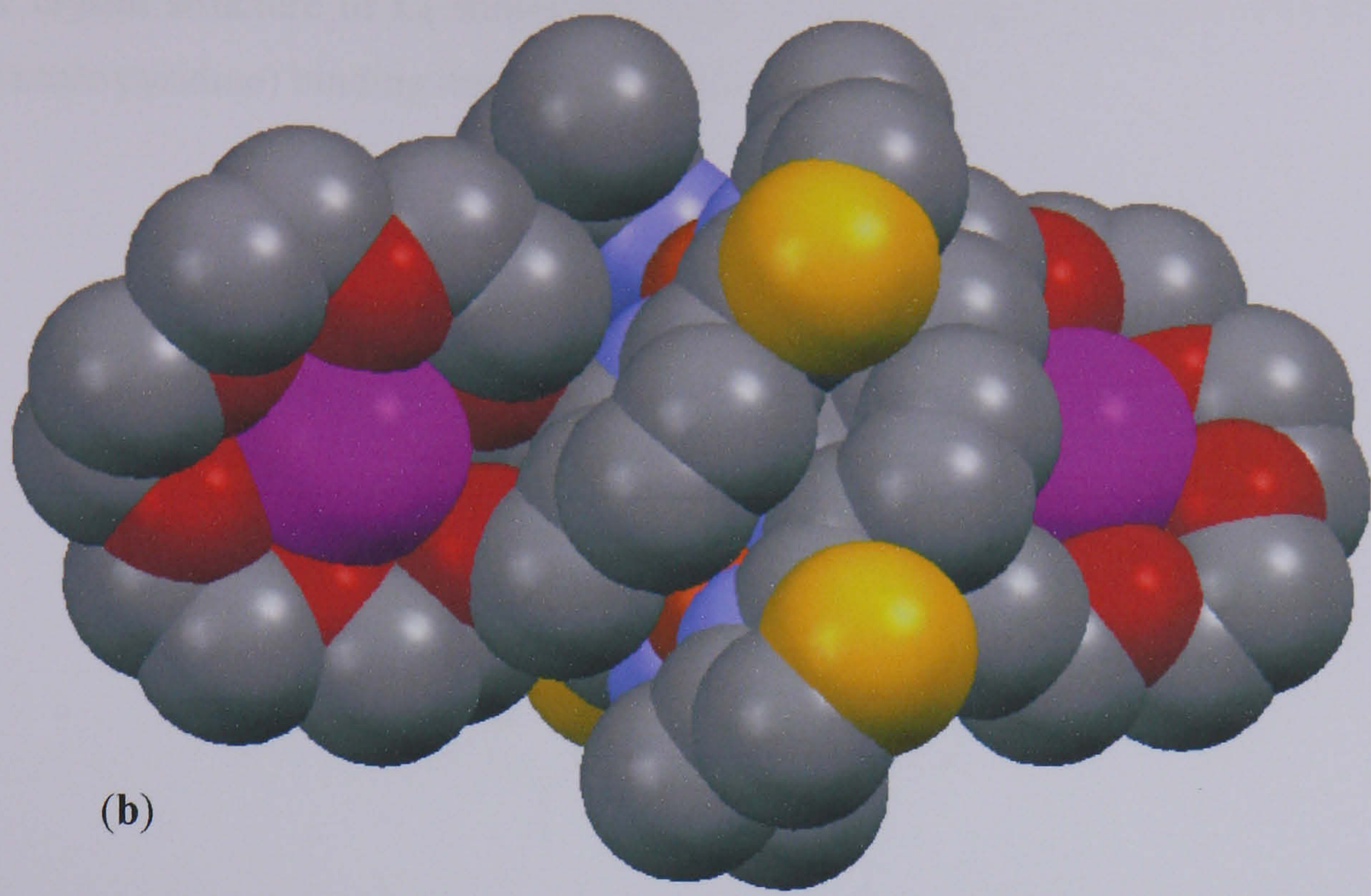

Figure 2.2(b). X-ray crystal structure of the complex cation $[Cu_2(\mathbf{L_1})_2Ba_2]^{6+}$ showing the space filling representation.[100]

Bond	Bond length Å
Cu(1)-N(11)	2.026(7)
Cu(1)-N(21)	2.109(7)
Cu(1)-N(71)	2.158(8)
Cu(1)-N(81)	2.002(9)
Cu(2)-N(31)	2.155(7)
Cu(2)-N(41)	1.985(7)
Cu(2)-N(51)	2.032(9)
Cu(2)-N(61)	2.102(7)
Cu(1)-Cu(2)	4.984(1)

Table 2. Selected bond lengths (Å) for the complex cation $[Cu_2(\mathbf{L_1})_2Ba_2]^{6+}$.

The crystal structure of $\mathbf{L_1}$ shows that each ligand partitions into two bis-bidentate (thiazole-pyridine) binding domains, as outlined in Figure 2.3.

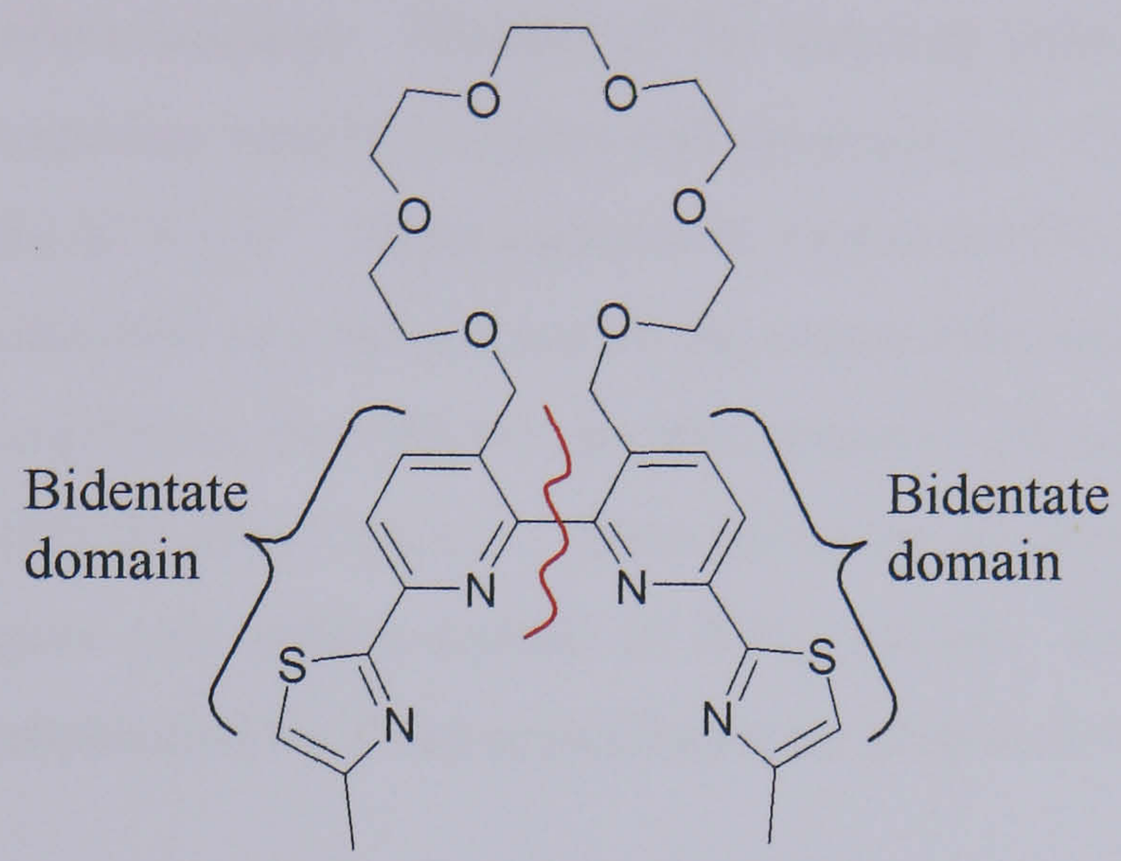

Figure 2.3. Structure of $\mathbf{L_1}$ showing the partitioning of the ligand into two bis-bidentate binding domains.

Each ligand coordinates two Cu^I centres *via* two bis-bidentate binding domains comprising of thiazole-pyridine units in a double helical arrangement. Each copper centre within the helicate species occupies a distorted tetrahedral coordination geometry formed by the coordination of two bidentate N-donor units, one from each ligand, with Cu–N bond distances ranging from 1.985(7)-2.158(8) Å, and the two copper(I) centres being 4.984(1) Å apart (Table 2). The partitioning of the potentially tetradentate ligand into two bis-bidentate binding domains is due to the preference of the copper(I) ions for a tetrahedral coordination geometry, thus the ligand partitions between the central bipyridine unit into tz-py domains. The partitioning of the ligand into bis-bidentate binding domains can be clearly seen by the NCCN torsion angle of 108.9°. In addition, all six of the O-donor units within both of the crown ether binding sites coordinate barium ions with O–Ba bond lengths ranging form 2.760(8)-2.978(12) Å, with the longest bond distances arising from coordination of the benzylic oxygen atoms.

2.2.2 Complexes of $\mathbf{L_1}$ *with Zinc(II)*

Reaction of $\mathbf{L_1}$ with an equimolar amount of $[Zn(H_2O)_6](ClO_4)_2$ in acetonitrile produced a pale yellow solution. ESI-MS of the resulting solution confirmed the formation of a mononuclear zinc(II) complex with an ion at *m/z* 776 corresponding to the complex $\{[Zn(\mathbf{L_1})](ClO_4)\}^+$. Upon addition of excess $Ba(ClO_4)_2$ to this solution resulted in the coordination of a barium ion by the crown ether moiety, thus forming $[Zn(\mathbf{L_1})Ba]^{4+}$, as established by ESI-MS by the presence of an ion at *m/z* 1112 corresponding to $\{[Zn(\mathbf{L_1})Ba](ClO_4)_3\}^+$. Slow diffusion of diethyl ether into the resulting solution gave pale yellow crystals of X-ray quality. The structure of this complex has been established by X-ray crystallography (Figure 2.4).

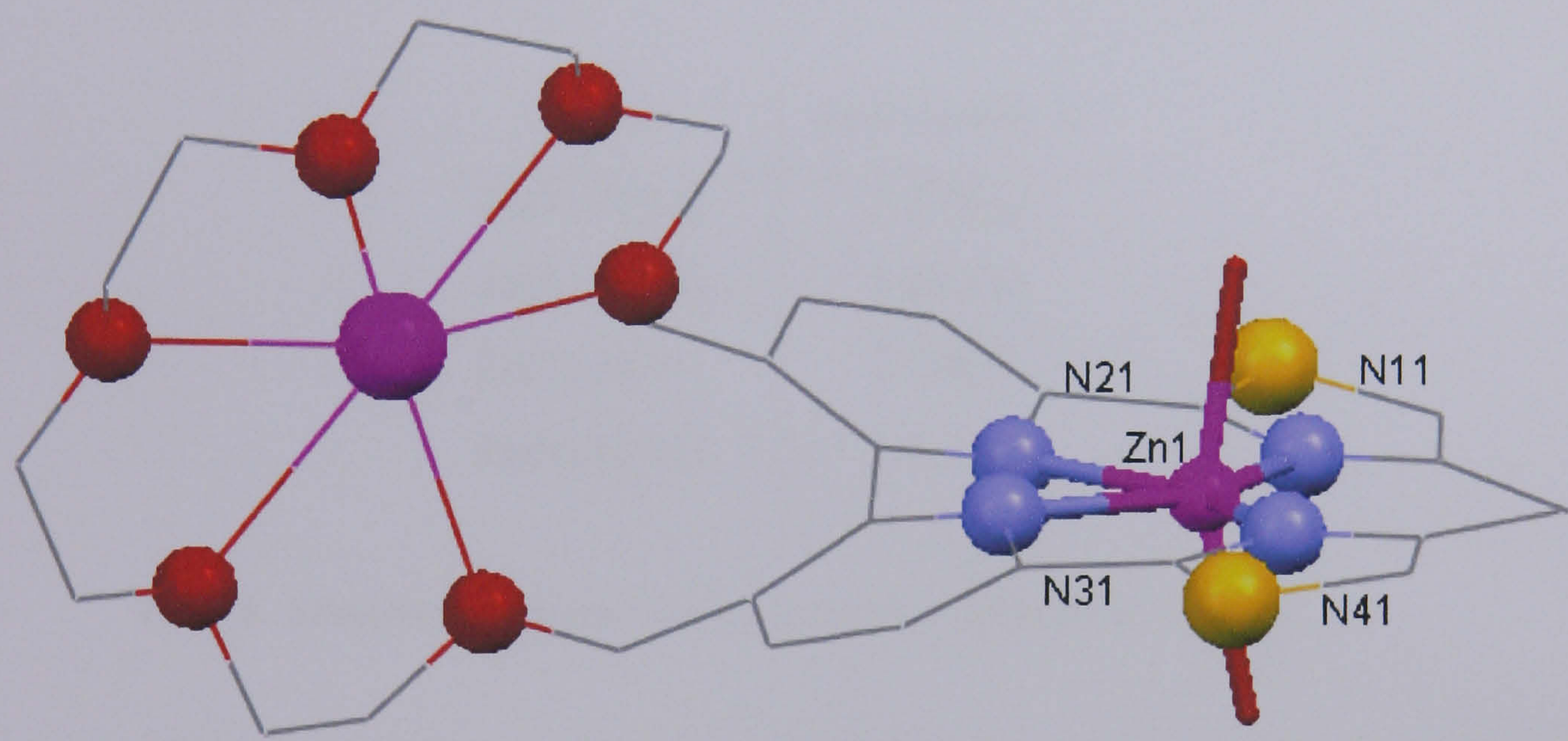

(a)

Figure 2.4(a). X-ray crystal structure of the complex cation $[Zn(\mathbf{L_1})Ba]^{4+}$ showing the structural framework.

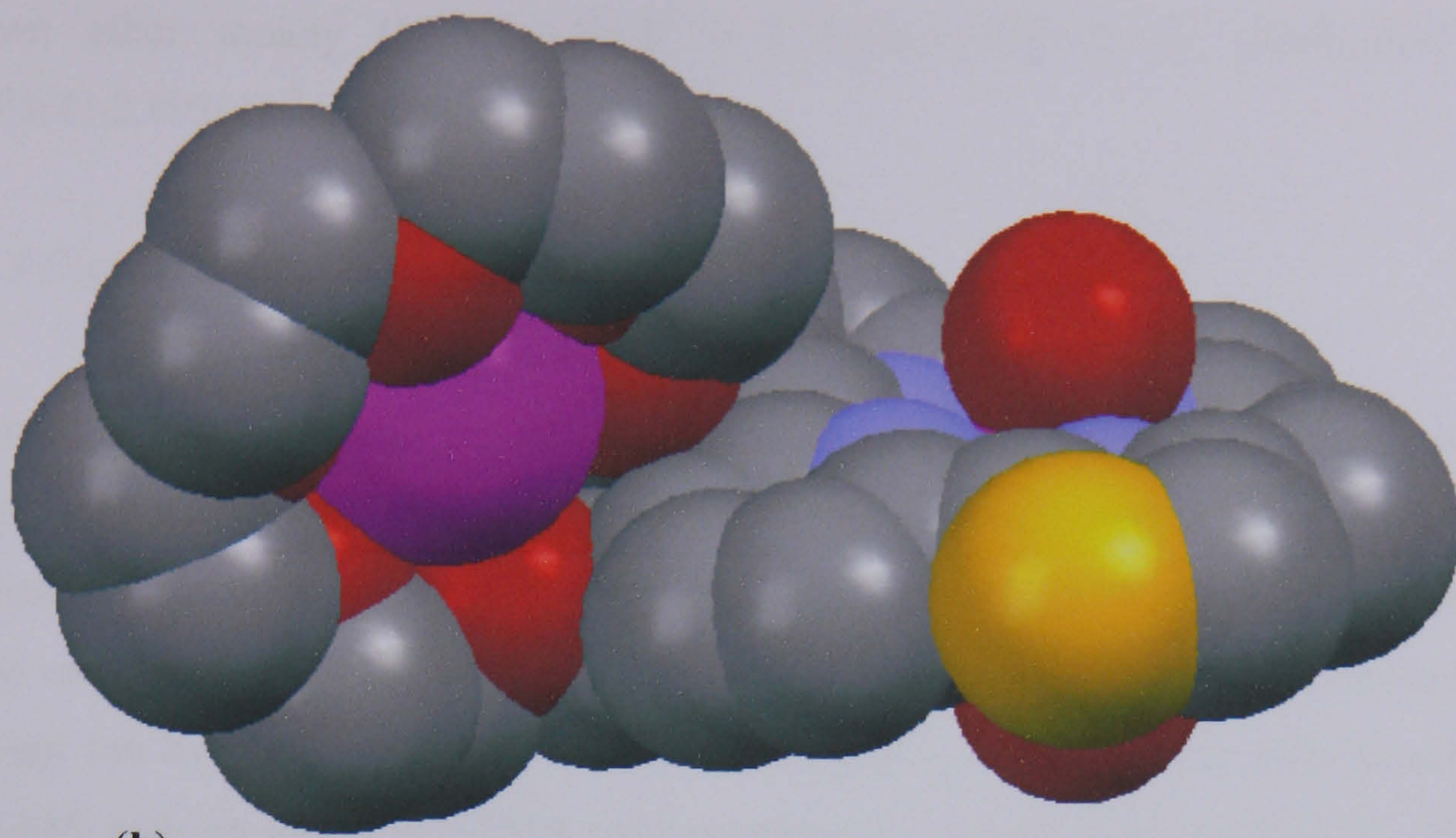

(b)
Figure 2.4(b). X-ray crystal structure of the complex cation $[Zn(\mathbf{L_1})Ba]^{4+}$ showing the space filling representation.

Bond	Bond length Å
Zn(1)-N(11)	2.237(6)
Zn(1)-N(21)	2.192(5)
Zn(1)-N(31)	2.178(5)
Zn(1)-N(41)	2.213(5)

Table 3. Selected bond lengths (Å) for the complex $[Zn(\mathbf{L_1})Ba]^{4+}$.

The crystal structure of $\mathbf{L_1}$ confirms the formation of the mononuclear species, with the ligand acting as a simple tetradentate donor and coordinating the equatorial plane of the zinc centre. The metal ion completes its coordination sphere by coordination to two water molecules, occupying the axial positions. As a result of coordination in the equatorial plane the ligand only exhibits a moderate twist about the central bipyridine unit, with an NCCN torsion angle of 31.0°. The inability of the potentially tetradentate ligand to adopt a planar coordination geometry is caused by unfavourable steric interactions between the substituents in the 3,3'-positions on the central bipyridine core. The zinc centre occupies a distorted tetragonal coordination geometry, with Zn–N bond distances ranging from 2.178(5)-2.237(6) Å (Table 3). In addition the Ba–O bond distances occur over a shorter range than those observed for $[Cu_2(\mathbf{L_1})_2Ba_2]^{6+}$, suggesting the barium ion is situated more centrally within the

crown ether moiety ($[Cu_2(\mathbf{L_1})_2Ba_2]^{6+}$: 2.760(8)-2.978(12) Å, $[Zn(\mathbf{L_2})Ba]^{4+}$: 2.803(4)-2.893(4) Å).

2.2.3 Complexes of $\mathbf{L_2}$ with Copper(I)

Upon reaction of $\mathbf{L_2}$ with an equimolar amount of $[Cu(MeCN)_4]PF_6$ in acetonitrile produced a dark red solution. ESI-MS confirmed the formation of a dinuclear double helicate with an ion at *m/z* 972 corresponding to $\{[Cu_2(\mathbf{L_2})_2](PF_6)\}^+$. Upon addition of an excess of $Ba(ClO_4)_2$ to a solution of $[Cu_2(\mathbf{L_2})_2]^{2+}$ results in the coordination of a barium ion by the crown ether moiety, forming $[Cu_2(\mathbf{L_2})_2Ba_2]^{6+}$, as established by ESI-MS with an ion at *m/z* 2068 corresponding to $\{[Cu_2(\mathbf{L_2})_2Ba_2](ClO_4)_5\}^+$. Slow diffusion of diethyl ether into the resulting solution afforded orange crystals of X-ray quality. X-ray crystallography confirmed the formation of the dinuclear double helicate $[Cu_2(\mathbf{L_2})_2Ba_2]^{6+}$ (Figure 2.5).

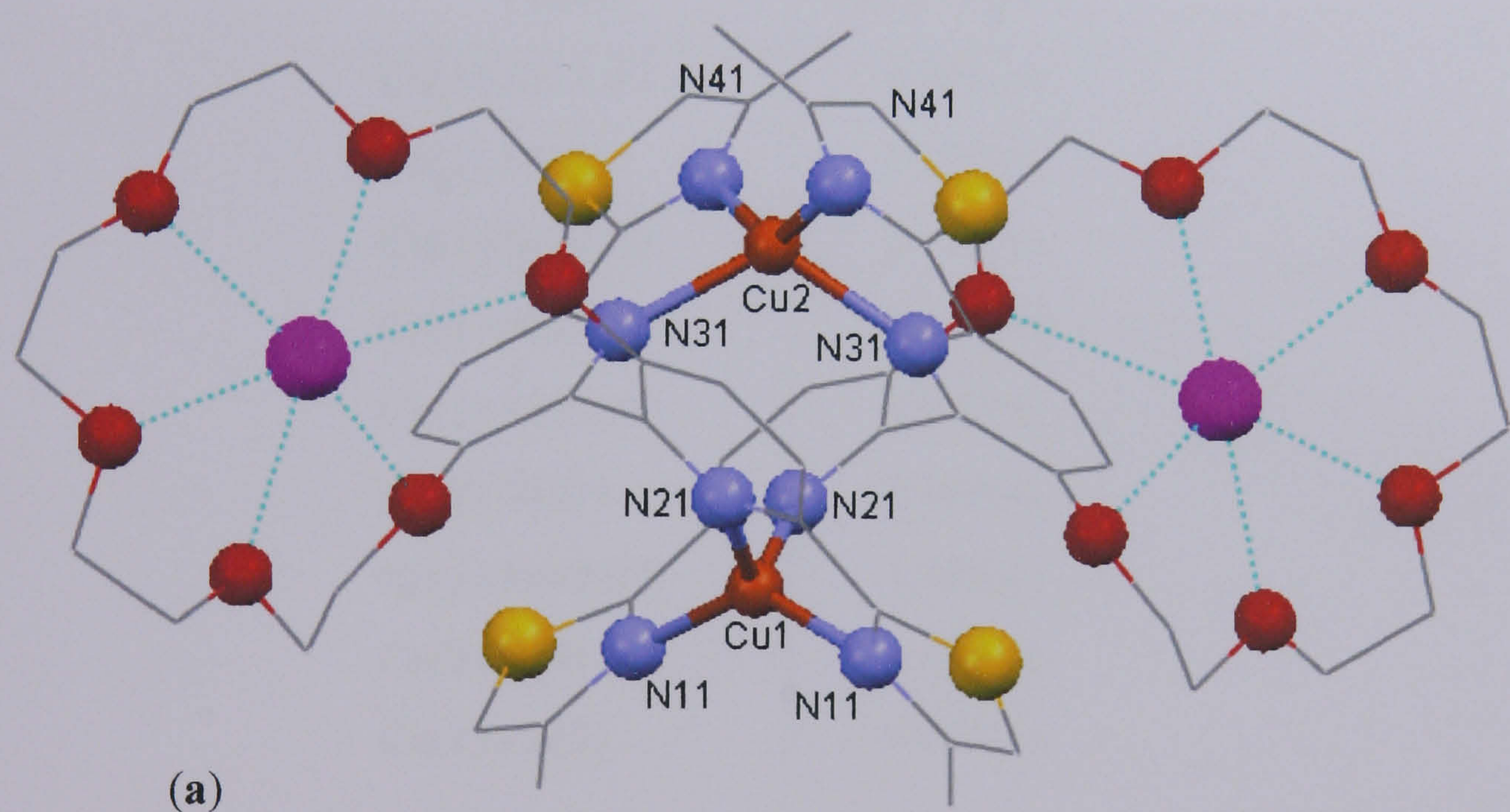

Figure 2.5(a). X-ray crystal structure of the complex cation $[Cu_2(\mathbf{L_2})_2Ba_2]^{6+}$ showing the structural framework.

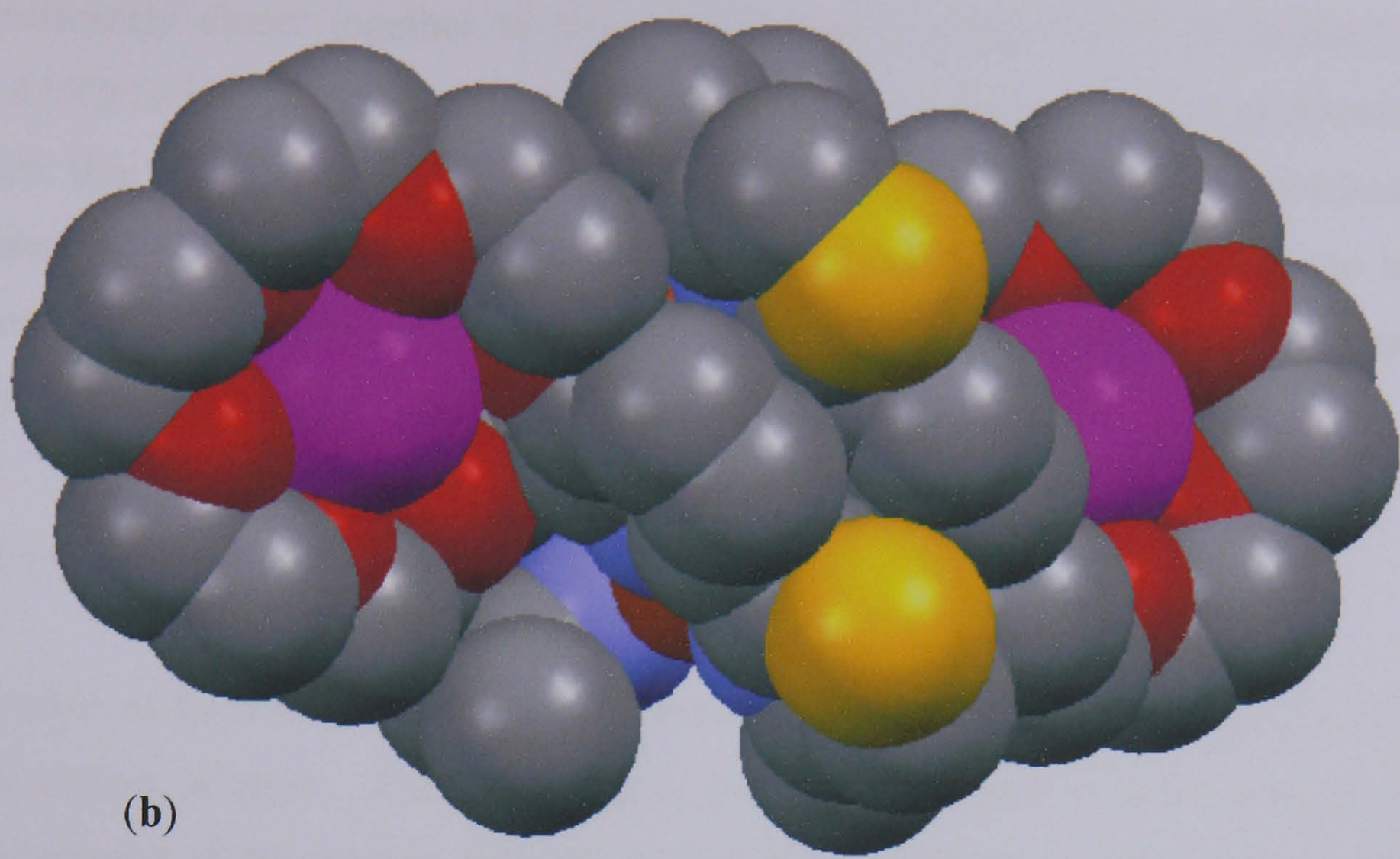

(b)

Figure 2.5(b). X-ray crystal structure of the complex cation $[Cu_2(\mathbf{L_2})_2Ba_2]^{6+}$ showing the space filling representation.

Bond	Bond length Å
Cu(1)-N(11)#2	2.001(4)
Cu(1)-N(11)	2.001(4)
Cu(1)-N(21)#2	2.119(4)
Cu(1)-N(21)	2.119(4)
Cu(2)-N(31)#2	2.087(4)
Cu(2)-N(31)	2.087(4)
Cu(2)-N(41)#2	1.988(4)
Cu(2)-N(41)	1.988(4)
Cu(1)-Cu(2)	4.092(1)

Table 4. Selected bond lengths (Å) for the complex cation $[Cu_2(\mathbf{L_2})_2Ba_2]^{6+}$.

Each ligand coordinates two Cu^I centres *via* two bis-bidentate binding domains comprising of thiazole-pyridine units in a double helical arrangement. Each of the copper centres occupies a distorted tetrahedral coordination geometry, formed by the coordination of two bidentate N-donor units, one from each ligand, with similar Cu–N bond distances to that observed in $[Cu_2(\mathbf{L_1})_2Ba_2]^{6+}$ ($\mathbf{L_1}$:1.985(7)-2.158(8) Å, $\mathbf{L_2}$:1.988(4)-2.119(4) Å) (Table 4). In addition the two copper(I) centres are

significantly closer together to that observed in $[Cu_2(\mathbf{L_1})_2Ba_2]^{6+}$ ($\mathbf{L_1}$:4.984(1) Å, $\mathbf{L_2}$:4.092(1) Å). The partitioning of the ligand into bis-bidentate binding domains is again due to the preference of the copper(I) ions for a tetrahedral coordination geometry, thus the ligand partitions between the central bipyridine unit into tz-py domains. The partitioning of the ligand into bis-bidentate binding domains can be clearly seen by the average NCCN torsion angle of 78.36°.

2.2.4 Complexes of $\mathbf{L_2}$ with Zinc(II)

Reaction of $\mathbf{L_2}$ with an equimolar amount of $Zn(CF_3SO_3)_2$ in acetonitrile produced a pale yellow solution. Although there is no crystallographic evidence that supports the presence of this species, ESI-MS studies of the resulting solution have confirmed the formation of the mononuclear complex with an ion at *m/z* 799 corresponding to $\{[Zn(\mathbf{L_2})](CF_3SO_3)\}^+$. In such a case the ligand acts as a simple tetradentate donor in a similar manner to that of the mononuclear, $\mathbf{L_1}$ zinc-containing species, where the ligand coordinates the equatorial plane of the metal ion. Addition of excess $Ba(ClO_4)_2$ to a solution of $[Zn(\mathbf{L_2})]^{2+}$ resulted in the coordination of a barium ion by the crown ether moiety, thus forming $[Zn(\mathbf{L_2})Ba]^{4+}$. The presence of the barium containing species is also supported by ESI-MS, studies revealed the presence of an ion at *m/z* 1085 corresponding to $\{[Zn(\mathbf{L_2})Ba](ClO_4)_3\}^+$.

2.3 ^{1}H NMR Studies

2.3.1 Complexes with $\mathbf{L_1}$

The 500 MHz ^{1}H NMR spectrum of the complex $[Cu_2(\mathbf{L_1})_2]^{2+}$ in CD_3CN shows six aromatic protons occurring in three environments between 7.55 and 7.80 ppm, confirming the formation of a symmetrical double helicate species with all four thiazole-pyridyl units in chemically equivalent environments. Furthermore, the diastereotopic "benzylic" (–O–CH_2–bipy) protons occur as sharp doublets between 4.00 and 4.20 ppm (Figure 2.6a). The 500 MHz ^{1}H NMR spectrum of the mononuclear zinc(II) complex $[Zn(\mathbf{L_1})]^{2+}$ in CD_3CN shows six aromatic protons occurring in three different environments between 7.60 and 8.60 ppm, consistent with the formation of a symmetrical mononuclear system (Figure 2.6b). The notable

downfield shift of the pyridyl proton resonances in relation to the copper helicate $[Cu_2(\mathbf{L_1})_2]^{2+}$ reflects the absence of aromatic shielding caused by extensive π-stacking of overlapping ligand strands found in the helicate species. In addition the benzylic (–O–CH_2–bipy) protons appear as a single broad singlet, suggesting rapid conformational movement about the bipyridyl backbone.

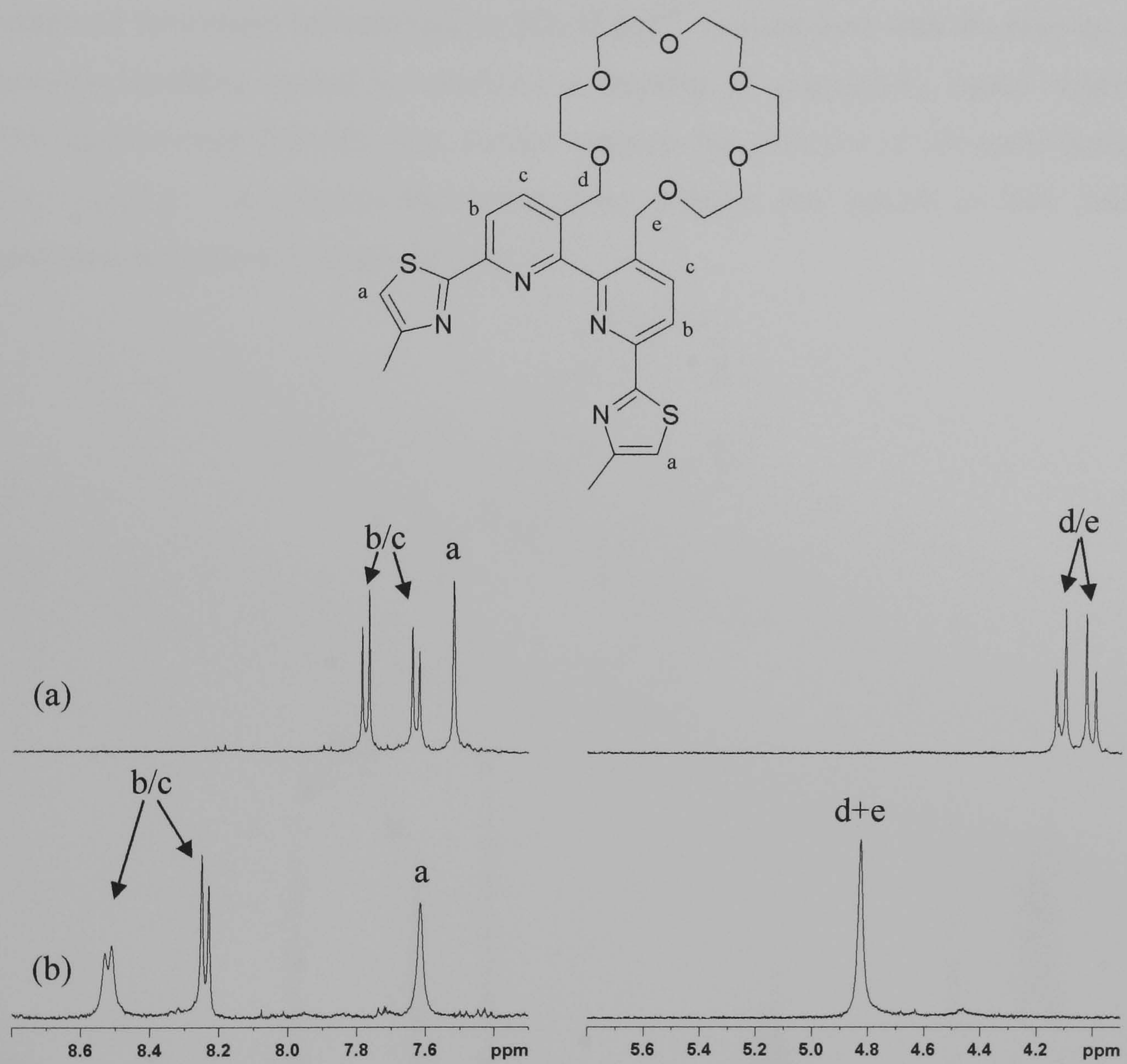

Figure 2.6. Selected regions of the ^{1}H NMR spectra (CD_3CN) of (a) $[Cu_2(\mathbf{L_1})_2]^{2+}$, and (b) $[Zn(\mathbf{L_1})]^{2+}$.

2.3.2 Complexes with $\boldsymbol{L_2}$

The 500 MHz ^{1}H NMR spectrum of the complex $[Cu_2(\mathbf{L_2})_2]^{2+}$ in CD_3CN shows twelve aromatic signals occurring in three different environments between 7.22 and 7.70 ppm, consistent with the formation of a symmetrical double helicate species (Figure 2.7a). In addition, the crown ether protons give rise to the expected

multiplets between 3.45 and 4.30 ppm. The presence of this helicate species is further supported by ESI-MS studies. The 500 MHz ^{1}H NMR spectrum of the mononuclear zinc(II) complex $[Zn(\mathbf{L_2})]^{2+}$ in CD_3CN shows six aromatic signals occurring in three different environments between 7.50 and 8.21 ppm, also consistent with the formation of a symmetrical mononuclear species (Figure 2.7b). As observed with $\mathbf{L_1}$ the notable downfield shift for the pyridyl proton resonances compared the copper helicate species $[Cu_2(\mathbf{L_2})_2]^{2+}$, is associated with the absence of aromatic shielding caused by extensive π stacking of overlapping ligand strands. This together with ESI-MS data, further supports the presence of the mononuclear zinc complex. In addition the crown ether protons also appear as their usual multiplets between 3.55 and 4.53 ppm.

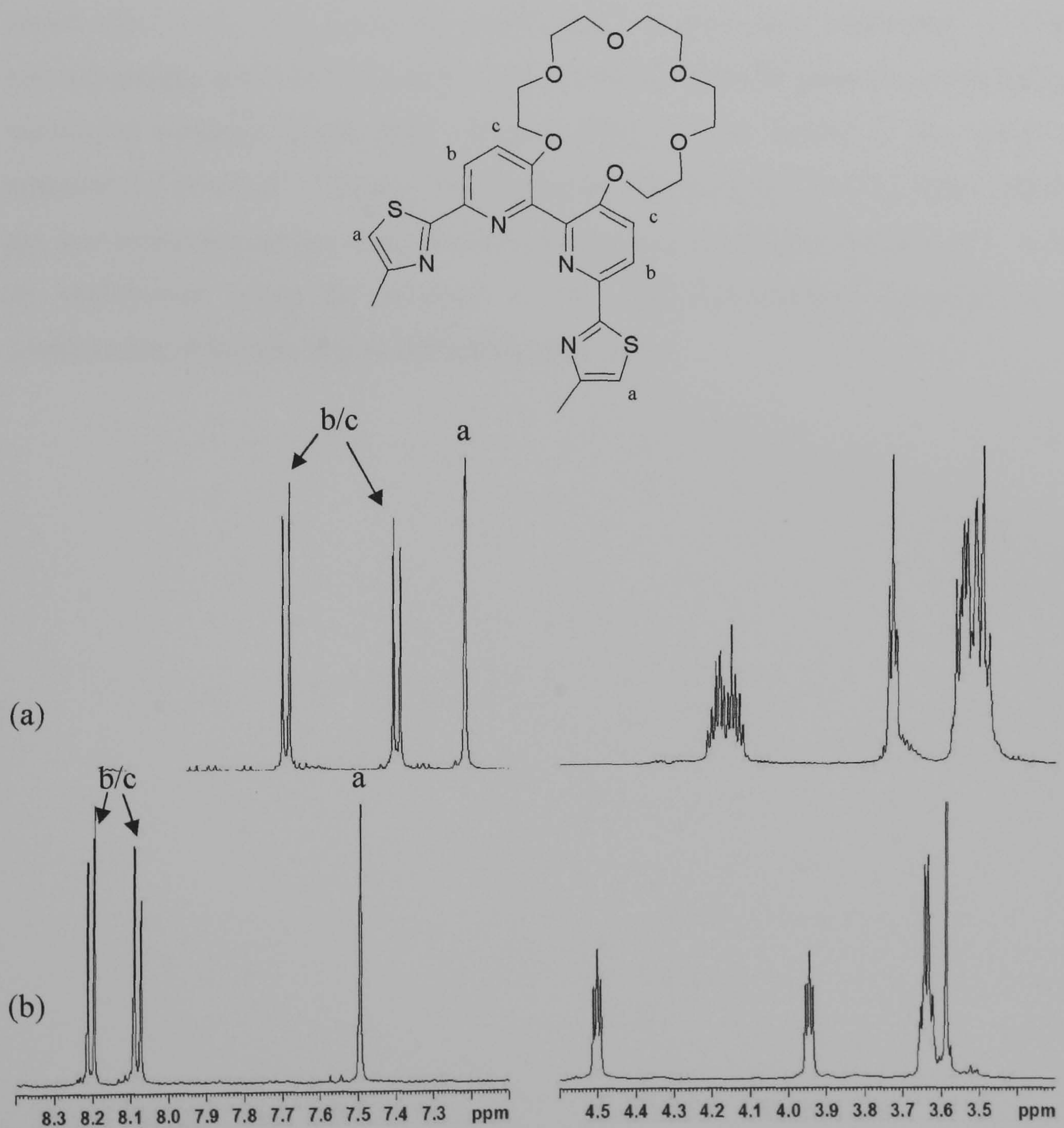

Figure 2.7. Selected regions of the ^{1}H NMR spectra (CD_3CN) of (a) $[Cu_2(\mathbf{L_2})_2]^{2+}$, and (b) $[Zn(\mathbf{L_2})]^{2+}$.

2.3.3 Addition of $Ba(ClO_4)_2$ to Complexes with $\mathbf{L_1}$

Addition of excess $Ba(ClO_4)_2$ to $[Cu_2(\mathbf{L_1})_2]^{2+}$ resulted in coordination of barium ions within the crown ether cavity, thus producing $[Cu_2(\mathbf{L_1})_2Ba_2]^{6+}$, as previously established by X-ray crystallography and ESI-MS studies. The 500 MHz ^{1}H NMR spectrum of the resulting barium containing complex $[Cu_2(\mathbf{L_1})_2Ba_2]^{6+}$ (Figure 2.8b) affords a similar spectrum to that observed for the complex $[Cu_2(\mathbf{L_1})_2]^{2+}$ (Figure 2.8a), with a slight occurrence of a downfield shift for the benzylic (O–CH_2–bipy) protons associated with the coordination of the electronegative Ba^{2+} ions to the crown ether moiety. Addition of excess $Ba(ClO_4)_2$ ions to the mononuclear zinc complex $[Zn(\mathbf{L_1})]^{2+}$, also resulted in the coordination of barium ions within the crown ether cavity, thus producing $[Zn(\mathbf{L_1})Ba]^{4+}$, as previously established by X-ray crystallography and ESI-MS studies. The 500 MHz ^{1}H NMR spectrum of the barium containing complex $[Zn(\mathbf{L_1})Ba]^{4+}$ (Figure 2.8d) is also similar to the spectrum obtained for $[Zn(\mathbf{L_1})]^{2+}$ (Figure 2.8c), however, the benzylic (O–CH_2–bipy) protons are now resonating as two sharp doublets as apposed to a singlet in $[Zn(\mathbf{L_1})]^{2+}$. Such an observation could be ascribed to the rigid environment produced upon coordination of barium ions to the crown ether cavity.

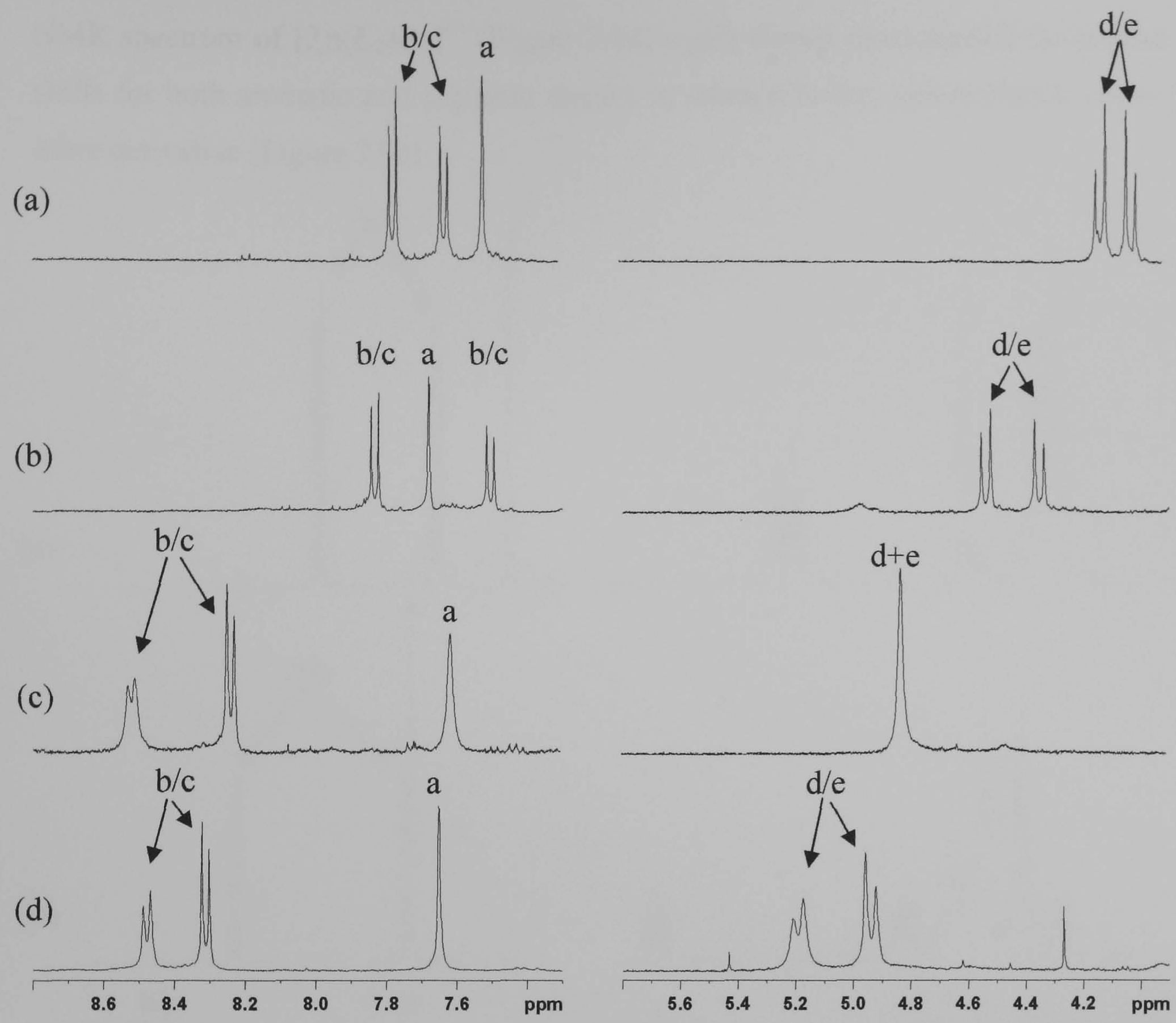

Figure 2.8. Selected regions of the ^{1}H NMR spectra (CD_3CN) of (a) $[Cu_2(\mathbf{L_1})_2]^{2+}$ (b) $[Cu_2(\mathbf{L_1})_2Ba_2]^{6+}$, (c) $[Zn(\mathbf{L_1})]^{2+}$ and (c) $[Zn(\mathbf{L_1})Ba]^{4+}$.

2.3.4 Addition of $Ba(ClO_4)_2$ to Complexes with $\mathbf{L_2}$

Reaction of $[Cu_2(\mathbf{L_2})_2]^{2+}$ with excess $Ba(ClO_4)_2$ resulted in the coordination of barium ions within the crown ether binding site, thus forming $[Cu_2(\mathbf{L_2})_2Ba_2]^{6+}$, as previously established by X-ray crystallography and ESI-MS studies. The 500 MHz ^{1}H NMR spectrum of the resulting barium containing complex $[Cu_2(\mathbf{L_2})_2Ba_2]^{6+}$ (Figure 2.9b) shows a characteristic downfield shift for both the aromatic and crown ether protons in relation to the uncoordinated crown ether derivative $[Cu_2(\mathbf{L_2})_2]^{2+}$ (Figure 2.9a). This downfield shift is typical for the coordination of the electronegative Ba^{2+} ions to the crown ether moiety. In addition, reaction of $[Zn(\mathbf{L_2})]^{2+}$ with excess $Ba(ClO_4)_2$ also results in the coordination of barium ions within the crown ether binding site, thus forming $[Zn(\mathbf{L_2})Ba]^{4+}$. The 500 MHz ^{1}H

NMR spectrum of $[Zn(\mathbf{L_2})Ba]^{4+}$ (Figure 2.9d) again shows characteristic downfield shifts for both aromatic and aliphatic signals in relation to the uncoordinated crown ether derivative (Figure 2.9c).

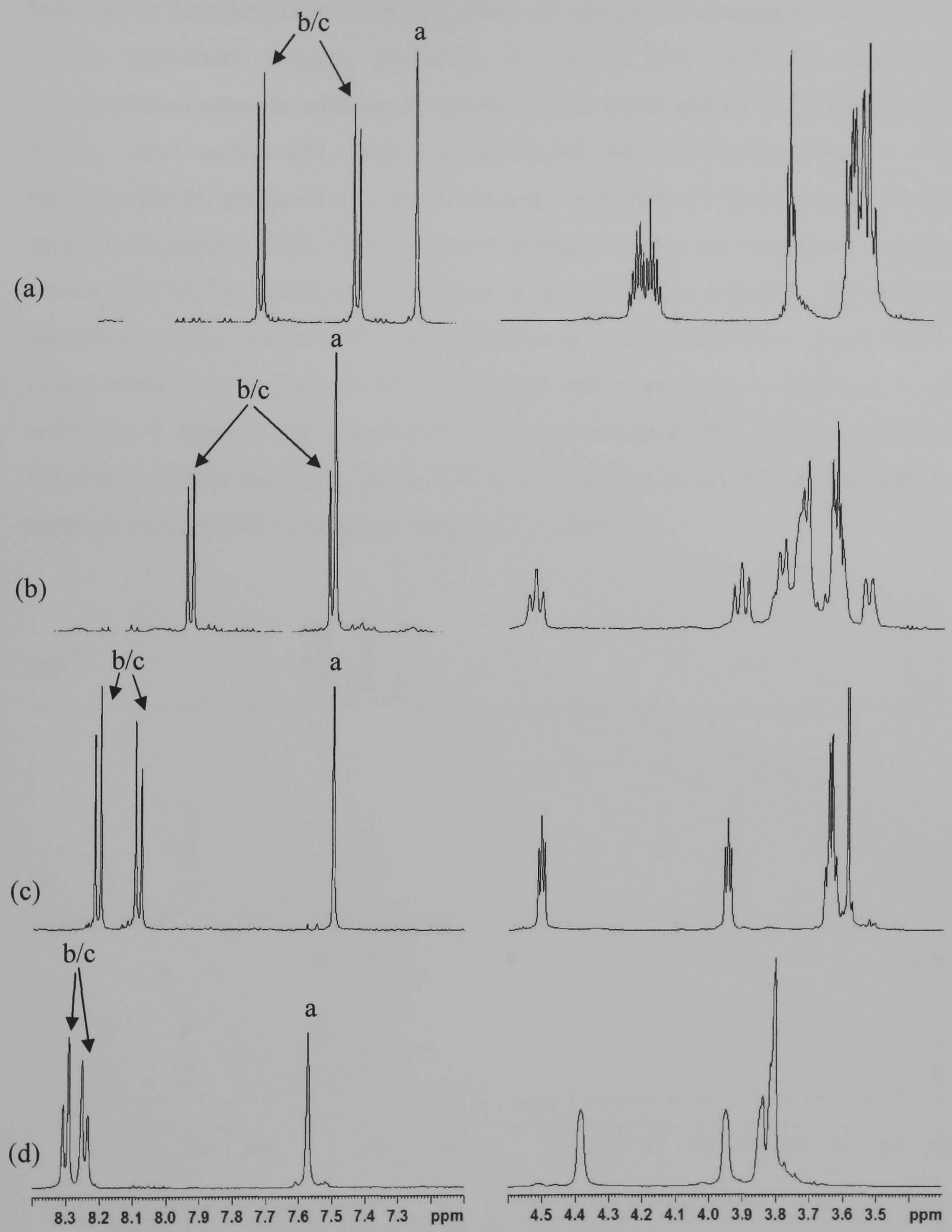

Figure 2.9. Selected regions of the ^1H NMR spectra (CD_3CN) of (a) $[Cu_2(\mathbf{L_2})_2]^{2+}$ (b) $[Cu_2(\mathbf{L_2})_2Ba_2]^{6+}$ (c) $[Zn(\mathbf{L_2})]^{2+}$ and (d) $[Zn(\mathbf{L_2})Ba]^{4+}$.

2.3.5 Reaction of $\mathbf{L_1}$ *with a Mixture of Copper(I) and Zinc(II)*

Given that both $\mathbf{L_1}$ and $\mathbf{L_2}$ can vary their coordination modes and act as either bis-bidentate or tetradentate coordinating units, we decided to investigate whether the ligands specificity towards copper(I) or zinc(II) ions could be effectively reprogrammed upon the addition of various s-block metal cations to the crown ether moiety. Thus reaction of $\mathbf{L_1}$ with $[Cu(MeCN)_4]PF_6$ and $[Zn(CF_3SO_3)_2]$ in a 1 : 1 : 1 ratio in CD_3CN, produced an orange solution. 500 MHz ^1H NMR studies on this solution revealed a total of six different aromatic proton environments. Careful comparison of this spectrum with those obtained for the copper(I) helicate and zinc(II) mononuclear structures (Figures 2.10a and 2.10b respectively) shows that the mixed metal system contains both the helical and mononuclear complexes in the ratio 1.5 : 1, respectively (Figure 2.10c). The presence of both of these species in solution is further supported by the ESI mass spectrum in which ions for both the copper(I) and zinc(II) containing complexes are observed.

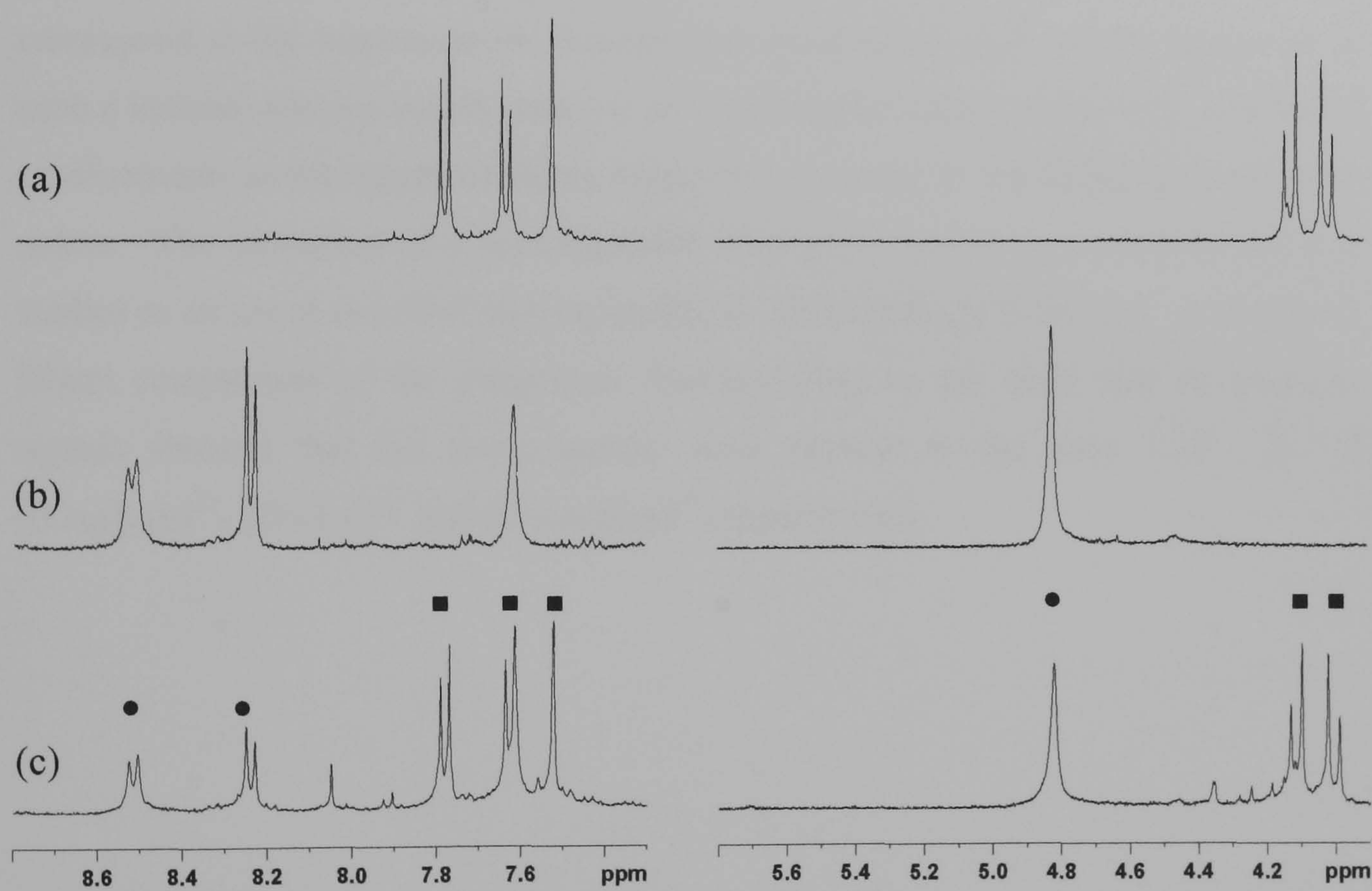

Figure 2.10. Selected regions of the ^1H NMR spectra (CD_3CN) of (a) $[Cu_2(\mathbf{L_1})_2]^{2+}$ (b) $[Zn(\mathbf{L_1})]^{2+}$ and (c) $\mathbf{L_1}$ + Cu^+ and Zn^{2+} ions. ● and ■ correspond to $[Zn(\mathbf{L_1})]^{2+}$ and $[Cu_2(\mathbf{L_1})_2]^{2+}$ respectively.

2.3.6 Reaction of $\mathbf{L_2}$ *with a Mixture of Copper(I) and Zinc(II)*

Reacting $\mathbf{L_2}$ with both $[Cu(MeCN)_4]PF_6$ and $[Zn(CF_3SO_3)_2]$ in a 1 : 1 : 1 ratio in CD_3CN produced an orange solution and the 500 MHz ^1H NMR studies revealed the presence of twelve different aromatic proton resonances, corresponding to the formation of three different $\mathbf{L_2}$ containing complexes (Figure 2.11c). Comparison of the ^1H NMR spectrum for the mixed metal system with the spectra recorded for the individual complex systems $[Cu_2(\mathbf{L_2})_2]^{2+}$ and $[Zn(\mathbf{L_2})]^{2+}$ (Figure 2.11a and 2.11b respectively) confirmed the presence of both of these species in solution. ESI-MS studies also confirmed the presence of $[Cu_2(\mathbf{L_2})_2]^{2+}$ and $[Zn(\mathbf{L_2})]^{2+}$ with ions at *m/z* 1441 and 797 corresponding to $\{[Cu_2(\mathbf{L_2})_2](PF_6)\}^+$ and $\{[Zn(\mathbf{L_2})](PF_6)\}^+$ respectively. However, six aromatic proton resonances are still unaccounted for. As these unaccounted signals have the same integration, it suggests that these signals correspond to the same species (presuming the identical integration is not just a co-incidence). Given there are six signals of identical integration suggests that they correspond to the heterometallic helicate species $[CuZn(\mathbf{L_2})_2]^{3+}$ as the formation of such a helicate species would result in all six aromatic protons occurring in different environments as the ligand would no longer be symmetrical due to the heterometallic nature. The formation of a heterometallic helicate is further supported by ESI-MS studies as an ion at *m/z* 1010 corresponding to $\{[CuZn(\mathbf{L_2})](CF_3SO_3)_2\}^+$ is observed. Direct comparison of the integration corresponding to the three sets of aromatic signals showed that the three species were present in the ratio 1.25 : 2 : 1 ($[Cu_2(\mathbf{L_2})_2]^{2+}$, $[Zn(\mathbf{L_2})]^{2+}$ and $[CuZn(\mathbf{L_2})_2]^{3+}$ respectively).

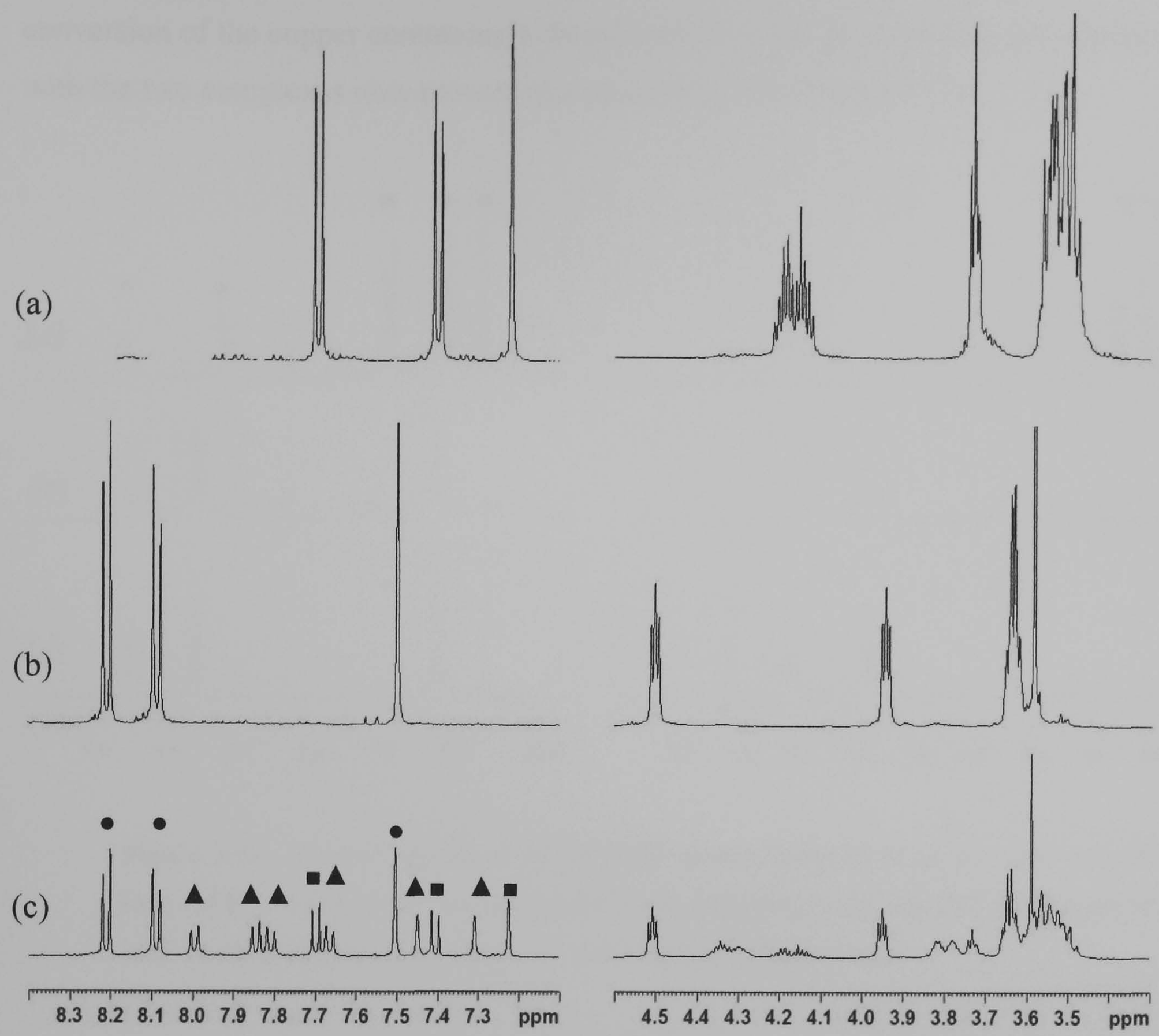

Figure 2.11. Selected regions of the ^{1}H NMR spectra (CD_3CN) of (a) $[Cu_2(\mathbf{L_2})_2]^{2+}$ (b) $[Zn(\mathbf{L_2})]^{2+}$ and (c) $\mathbf{L_2}$ + Cu^+ and Zn^{2+} ions. ●, ■ and ▲correspond to $[Zn(\mathbf{L_2})]^{2+}$, $[Cu_2(\mathbf{L_2})_2]^{2+}$ and $[CuZn(\mathbf{L_2})_2]^{3+}$ respectively.

2.3.7 Addition of s-block Metal Cations to the $\mathbf{L_1}$ Mixed Metal System

Addition of excess $Ba(ClO_4)_2$ to the 1 : 1 : 1 mixture of $\mathbf{L_1}$ with $[Cu(MeCN)_4]PF_6$ and $[Zn(CF_3SO_4)_2]$ produced a significant change to the ^{1}H NMR spectrum, as the two complexes $[Cu_2(\mathbf{L_1})_2Ba_2]^{6+}$ and $[Zn(\mathbf{L_1})Ba]^{4+}$ are now present in the ratio 1 : 10 respectively (ratio 1.5 : 1 prior to addition of barium ions) (Figure 2.12b). ESI-MS studies of the resulting solution confirmed the presence of $\{[Zn(\mathbf{L_1})Ba](ClO_4)_3\}^+$ as the major species, with ions corresponding to the copper containing helicate species almost nonexistent. Interestingly, upon addition of excess $Sr(ClO_4)_2$ to the mixture of $\mathbf{L_1}$ with $[Cu(MeCN)_4]PF_6$ and $[Zn(CF_3SO_3)_2]$, resulted in an almost complete

conversion of the copper containing helicate species to the mononuclear zinc species, with the two complexes now present in a ratio of 1 : >20 (Figure 2.12c).

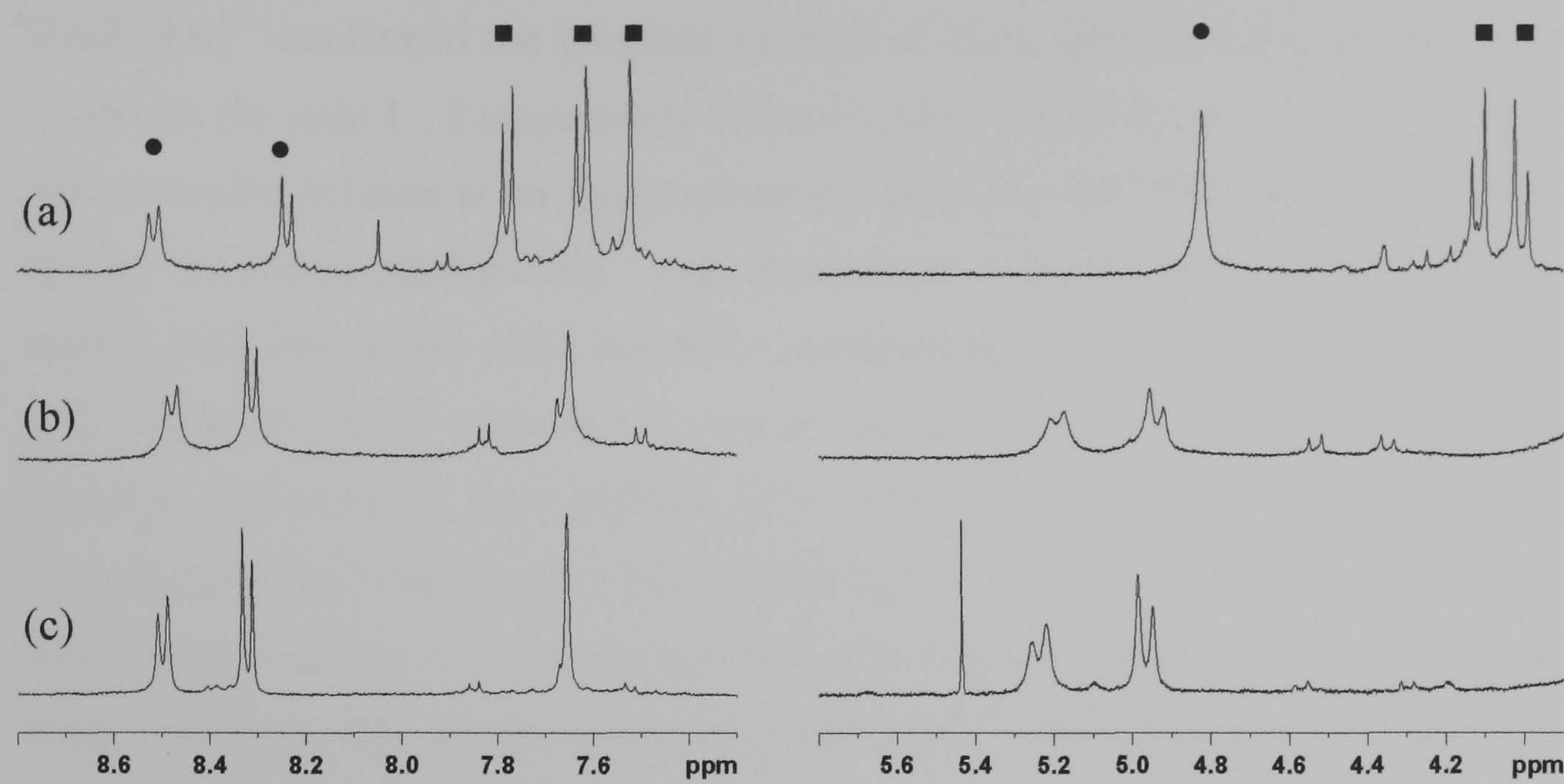

Figure 2.12. Selected regions of the ^{1}H NMR spectra (CD_3CN) of (a) $\mathbf{L_1}$ + Cu^+ and Zn^{2+} ions, (b) $\mathbf{L_1}$ + Cu^+ and Zn^{2+} plus excess Ba^{2+} ions, and (c) $\mathbf{L_1}$ + Cu^+ and Zn^{2+} plus excess St^{2+} ions. ● and ■ correspond to $[Zn(\mathbf{L_1})]^{2+}$ and $[Cu_2(\mathbf{L_1})_2]^{2+}$ respectively.

Addition of an excess of Li^+ and Na^+ ions to the mixed metal system gave a very different result to that obtained following the addition of excess barium and strontium ions, with equal amounts of both the copper(I) helical and zinc(II) mononuclear complexes being observed. However, upon addition of excess K^+ ions, the zinc(II) mononuclear complex $[Zn(\mathbf{L_1})K]^{3+}$ is again favoured over the copper(I) helicate complex $[Cu_2(\mathbf{L_1})_2K_2]^{4+}$, with the two species present in the ratio 4 : 1 respectively.

2.3.8 Addition of s-block Metal Cations to the $\mathbf{L_2}$ Mixed Metal System

Addition of excess $Ba(ClO_4)_2$ to the 1 : 1 : 1 mixture of $\mathbf{L_2}$ with $[Cu(MeCN)_4]PF_6$ and $[Zn(CF_3SO_4)_2]$ produced a significant change to the ^{1}H NMR spectrum. Prior to the addition of barium ions, twelve aromatic proton resonances were observed, corresponding to three different $\mathbf{L_2}$ containing species ($[Zn(\mathbf{L_2})Ba]^{4+}$, $[Cu_2(\mathbf{L_2})_2Ba_2]^{6+}$ and $[CuZn(\mathbf{L_2})_2]^{3+}$). However, following the addition of excess barium ions to the

mixed metal system resulted in the observation of only six aromatic proton resonances. Direct comparison of the ^{1}H NMR spectrum for the mixed metal system with the spectra recorded for the individual complex systems $[Cu_2(\mathbf{L_2})_2Ba_2]^{6+}$ and $[Zn(\mathbf{L_2})Ba]^{4+}$ confirmed the presence of both of these species in the mixed metal sample in the ratio 1 : 2 respectively (Figure 2.13b). Thus, the previously observed heterometallic helicate is no longer observed following the coordination of barium ions to the crown ether moiety. This observation is further supported by ESI-MS studies with ions at *m/z* 1084 and 984 corresponding to $\{[Zn(\mathbf{L_2})Ba](ClO_4)_3\}^+$ and $\{[Cu(\mathbf{L_2})Ba](ClO_4)_2\}^{2+}$ respectively, and no ions are observed for the heterometallic complex. Furthermore, upon addition of excess $Sr(ClO_4)_2$ to the 1 : 1 : 1 mixture of $\mathbf{L_2}$ with $[Cu(MeCN)_4]PF_6$ and $[Zn(CF_3SO_4)_2]$ gave a similar result to that observed following the edition of excess barium ions with only six aromatic proton resonances being observed, thus corresponding to $[Cu_2(\mathbf{L_2})_2Sr_2]^{6+}$ and $[Zn(\mathbf{L_2})Sr]^{4+}$ in the ratio 1 : 6 respectively (Figure 2.13c).

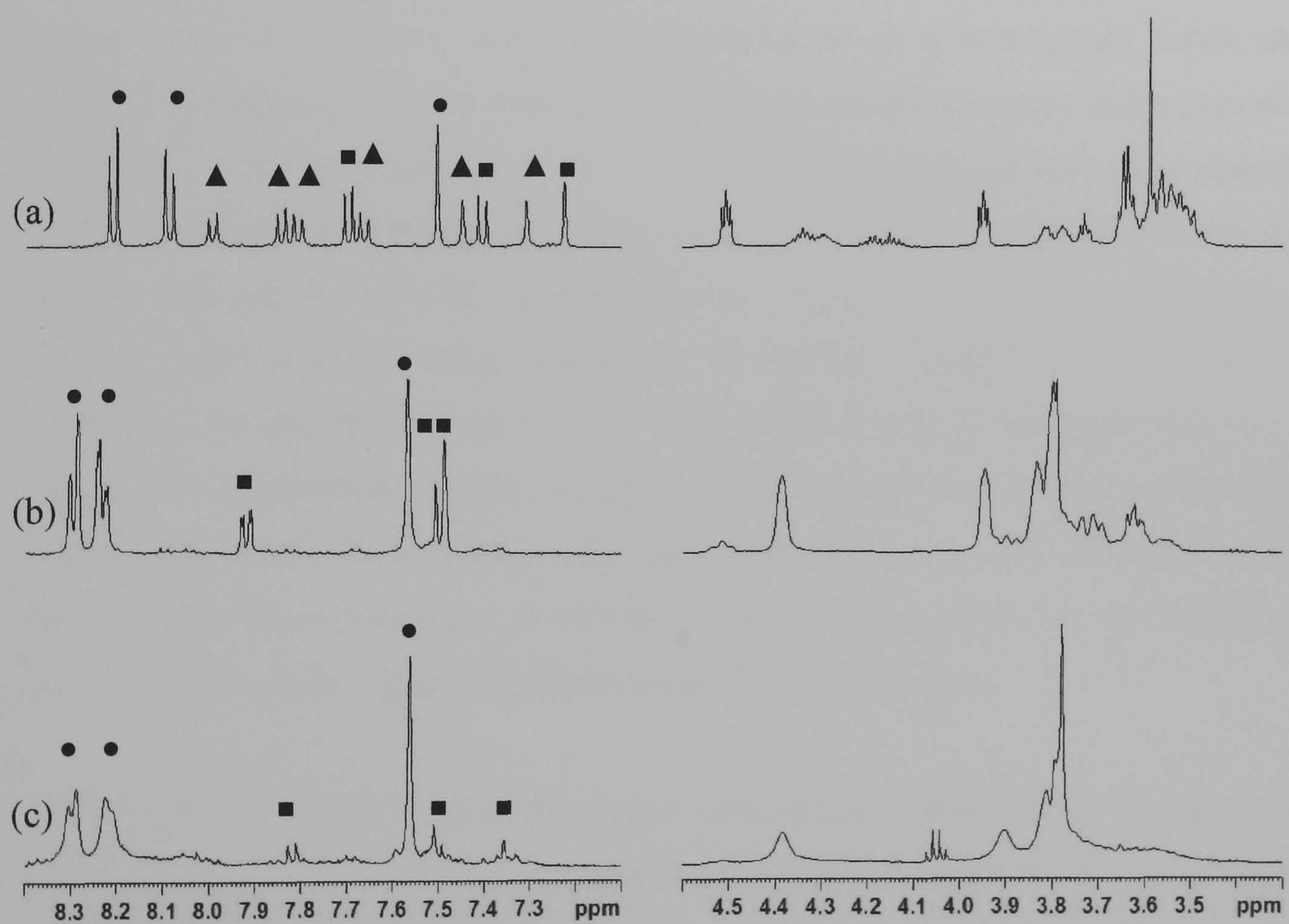

Figure 2.13. Selected regions of the ^{1}H NMR spectra (CD_3CN) of (a) $\mathbf{L_2}$ + Cu^+ and Zn^{2+} ions, (b) $\mathbf{L_2}$ + Cu^+ and Zn^{2+} plus excess Ba^{2+} ions, and (c) $\mathbf{L_2}$ + Cu^+ and Zn^{2+} plus excess St^{2+} ions. ●, ■ and ▲corresponds to the zinc(II), copper(I) species and the heterometallic species respectively.

2.4 Discussion

2.4.1 Discussion of the Ditopic Ligand $\mathbf{L_1}$

Reaction of the potentially tetradentate ligand, $\mathbf{L_1}$, with both copper(I) and zinc(II) ions afforded a mixture of both the dinuclear double helicate $[Cu_2(\mathbf{L_1})_2]^{2+}$ and the mononuclear zinc(II) complex $[Zn(\mathbf{L_1})]^{2+}$, with the copper(I) helicate complex being the major component. However, addition of either barium or strontium ions to the crown ether moiety resulted in virtually total conversion to the zinc(II) mononuclear complex, thus effectively reprogramming $\mathbf{L_1}$ to act as a tetradentate donor specific to zinc(II) ions. As previously established, such control over ligand coordination domains may be attributed to either electrostatic, allosteric or a combination of both of these factors. Although the crystal structures of both the copper(I) and the zinc(II) complexes clearly demonstrates that barium ions can coordinate the crown ether moiety when the ligand is acting as a bis-bidentate or a tetradentate donor, the copper(I) complex is virtually non-existent in the mixed metal system in the presence of barium. Close examination of the X-ray crystal structures of both the copper(I) and zinc(II) barium containing complex revealed that the separations between the barium ions and the benzylic oxygen atoms are marginally different, with the Ba–$O_{(benzylic)}$ bond distances being shorter in the zinc(II) complex ($[Cu_2(\mathbf{L_1})_2Ba_2]^{6+}$: 2.895(2) Å; $[Zn(\mathbf{L_1})Ba]^{4+}$: 2.863(9) Å). Such an observation could imply that when acting as a tetradentate donor, coordination of barium ions by the crown ether binding site contracts the crown ether unit, thus optimizing the Ba^{2+}/crown-ether interactions. This contraction of the crown ether could account for the change in equilibrium from the copper(I) helicate to the zinc(II) monomer.

Addition of Li^+ and Na^+ ions to the mixed metal system resulted in the formation of an equal amount of both the copper(I) and zinc(II) complexes. However, upon addition of K^+ ions the zinc(II) mononuclear complex $[Zn(\mathbf{L_1})K]^{3+}$ is again favoured over the copper(I) helicate complex $[Cu_2(\mathbf{L_1})_2K_2]^{4+}$, in the ratio 4 : 1 respectively. Comparison of the effects observed upon addition of Ba^{2+} with K^+ ions, shows that both ions change the equilibrium composition in favour of the mononuclear zinc(II) complex. However, the equilibrium is significantly more affected in favour of the zinc-containing species when Ba^{2+} is added. Given the fact that both these metal

cations have very similar atomic radii, the change in favour of the mononuclear complex must be associated with the difference in ionic charge.

In conclusion, it has been demonstrated how a ditopic ligand system can effectively be reprogrammed upon addition of various s-block metal cations to change its coordination preference for different transition metal cations. Given the fact that the addition of both Ba^{2+} and K^{+} ions to the crown ether unit changes equilibrium composition in favour of the zinc(II) mononuclear complex, this highlights the importance of both electrostatic and allosteric factors within ligand specificity. The reprogramming of the ligand upon addition of various s-block metal cations can be elegantly highlighted by a cartoon (Figure 2.14).

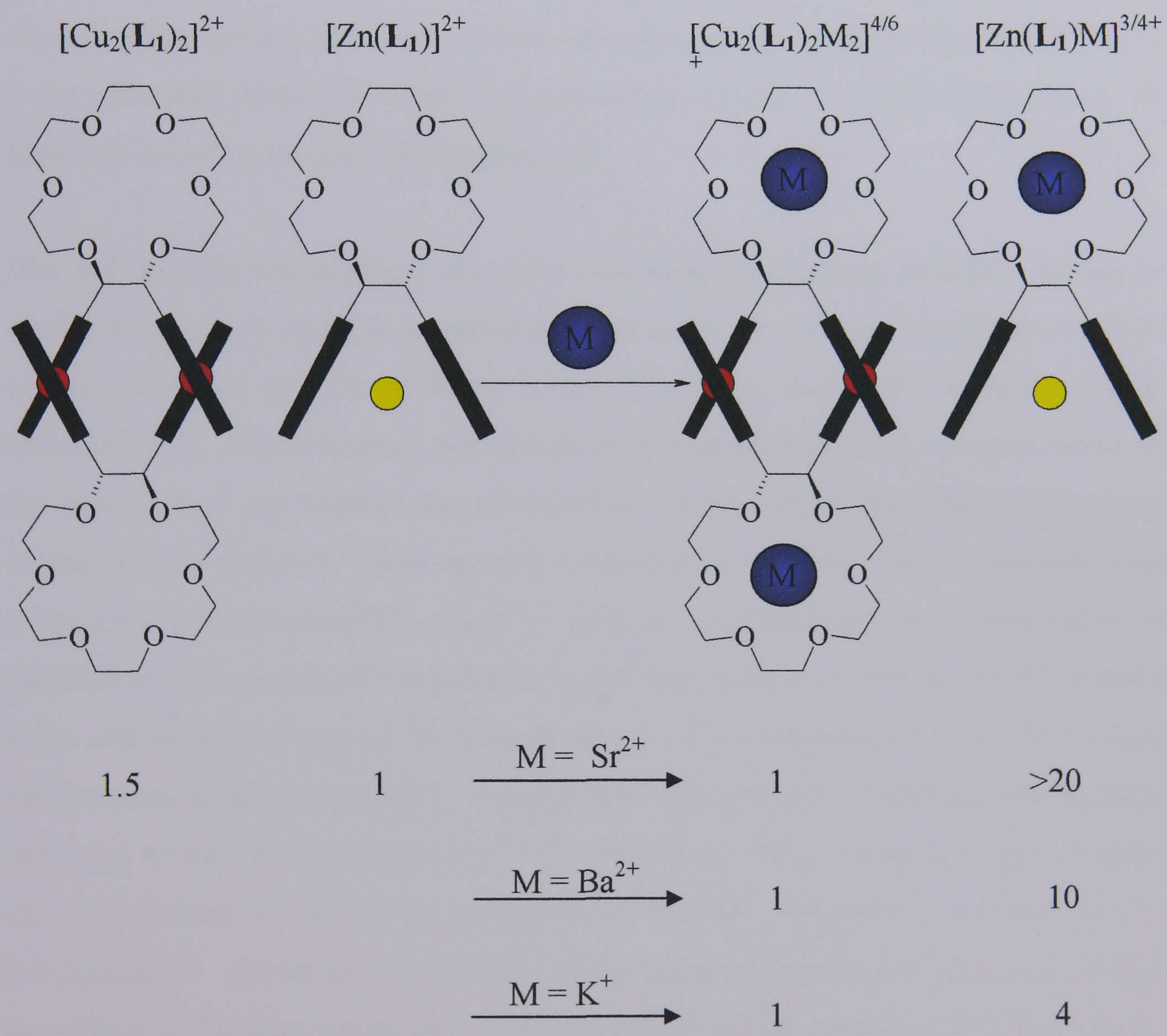

Figure 2.14. Cartoon representation of the distribution of products following the addition of various s-block metal cations to $\mathbf{L_1}$.

2.4.2 Discussion of the Ditopic Ligand $\mathbf{L_2}$

Reaction of the potentially tetradentate ligand $\mathbf{L_2}$, with equimolar amounts of both copper(I) and zinc(II) resulted in the formation of three different $\mathbf{L_2}$ containing species ($[Cu_2(\mathbf{L_2})_2]^{2+}$, $[Zn(\mathbf{L_2})]^{2+}$ and $[CuZn(\mathbf{L_2})_2]^{3+}$ in the ratio 1.25 : 2 : 1 respectively). However, addition of either barium or strontium ions to the crown ether moiety resulted in the formation of only the homoleptic species $[Cu_2(\mathbf{L_2})_2M]^{6+}$ and $[Zn(\mathbf{L_2})M]^{4+}$ (where M = Ba^{2+} or Sr^{2+}), with the zinc(II) mononuclear species being the major component in both cases ($[Cu_2(\mathbf{L_2})_2Ba]^{6+}$ and $[Zn(\mathbf{L_2})Ba]^{4+}$ in the ratio 1 : 2; $[Cu_2(\mathbf{L_2})_2Sr]^{6+}$ and $[Zn(\mathbf{L_2})Sr]^{4+}$ in the ratio 1 : 6 respectively). In a similar manner to that observed with $\mathbf{L_1}$ the crystal structure of the copper(I) containing helicate species clearly demonstrates that the ligand can easily accommodate barium ions within the crown ether moiety when the ligand is acting as a bis-bidentate donor, the zinc(II) mononuclear species is clearly favoured in the presence of both strontium and barium ions.

The redistribution of products observed following the addition of either barium or strontium ions may again be a consequence of either electrostatic or allosteric effects or a combination of both of these factors. However, unlike the allosteric effects observed in $\mathbf{L_1}$, which favours the formation of a tetradentate unit as coordination of the crown ether unit reduces the inter-domain torsion angle, the mode of allosteric action in $\mathbf{L_2}$ is different. Thus upon coordination of either barium or strontium ions to the crown ether unit of $[Cu_2(\mathbf{L_2})_2]^{2+}$ would, due to the oxygen atoms being directly attached to the pyridine unit, result in a significant increase to both the NCCN torsion angle and the pitch length of the helicate species. This lengthening of the pitch length and increase in the torsion angle of complexes containing this chelating unit has been observed in similar ligand systems.[98, 101] The same effect would be expected upon the coordination of barium or strontium ions to the heteroleptic helicate species $[CuZn(\mathbf{L_2})_2]^{3+}$. However, an increase in the torsion angle about the two bidentate coordination domains would favour the formation of the dinuclear double helicates (either homo- or heterometallic). However, the ^1H NMR studies demonstrate that this is clearly not the case and the formation of the mononuclear Zn(II) complex, with the ligand acting as a planar tetradentate donor, is favoured.

The other possibility for the observed change in the preference for metal ions is an electrostatic effect. Thus the reaction of $[Cu_2(\mathbf{L_2})_2]^{2+}$, $[CuZn(\mathbf{L_2})_2]^{3+}$ and $[Zn(\mathbf{L_2})]^{2+}$ with a divalent metal ion would result in the formation of $[Cu_2(\mathbf{L_2})_2M_2]^{6+}$, $[CuZn(\mathbf{L_2})_2M_2]^{7+}$ and $[Zn(\mathbf{L_2})M]^{4+}$ (where M = Ba^{2+} or Sr^{2+}). As can be clearly seen from the distribution of products following the addition of barium ions to the mixed metal system, none of the 7+ heterometallic species is observed and the two homometallic complexes are present in the ratio 1 : 2 ($[Cu_2(\mathbf{L_2})_2Ba_2]^{6+}$ and $[Zn(\mathbf{L_2})Ba]^{4+}$ respectively). A similar observation is also observed following the coordination of strontium ions to the crown ether unit with the two homometallic complexes being observed in the ratio 1 : 6 ($[Cu_2(\mathbf{L_2})_2Sr_2]^{6+}$ and $[Zn(\mathbf{L_2})Sr]^{4+}$ respectively).

Reaction of the mixed metal system with smaller s-block metal cations, such as Na^+, Ca^{2+} and Mg^{2+} has very little effect on the distribution of the $\mathbf{L_2}$ containing species as both the homometallic and the heterometallic complexes are present in roughly the same ratios. As these metal ions have a much smaller ionic radii than both barium and strontium it is highly likely that they only coordinate the "outer" oxygen atoms of the crown ether unit as has been observed in similar systems.[101] As this mode of coordination will result in a larger distance between the s-block and transition metal ions, it is likely that any electrostatic interactions will be less and the resulting overall distribution of species will be unaffected. However, upon addition of K^+ which is univalent but has a very similar size to Ba^{2+} (resulting in coordination of all the crown ether oxygen atoms) results in the formation of all three species $[Cu_2(\mathbf{L_2})_2K_2]^{4+}$, $[Zn(\mathbf{L_2})K]^{3+}$ and $[CuZn(\mathbf{L_2})_2K_2]^{5+}$ in the ratio of 1 : 8 : 2. Again the zinc-containing species is favoured, but in this case the mixed metal species is still present which is presumably a consequence of the lower overall charge (c.f. $[CuZn(\mathbf{L_2})_2Ba_2]^{7+}$ and $[CuZn(\mathbf{L_2})_2K_2]^{5+}$).

Thus, as allosteric effects would favour the formation of the helicate species (due to an increase in the torsion angle) and electrostatic effects would favour the formation of the mono-nuclear systems, it would appear that in the $\mathbf{L_2}$ system electrostatic effects are dominant. The fact that the heterometallic species is present upon addition of K^+ and not upon addition of Ba^{2+} further supports this assumption.

The reprogramming of the ligand upon addition of various s-block metal cations can again be elegantly highlighted by the use of a cartoon (Figure 2.15).

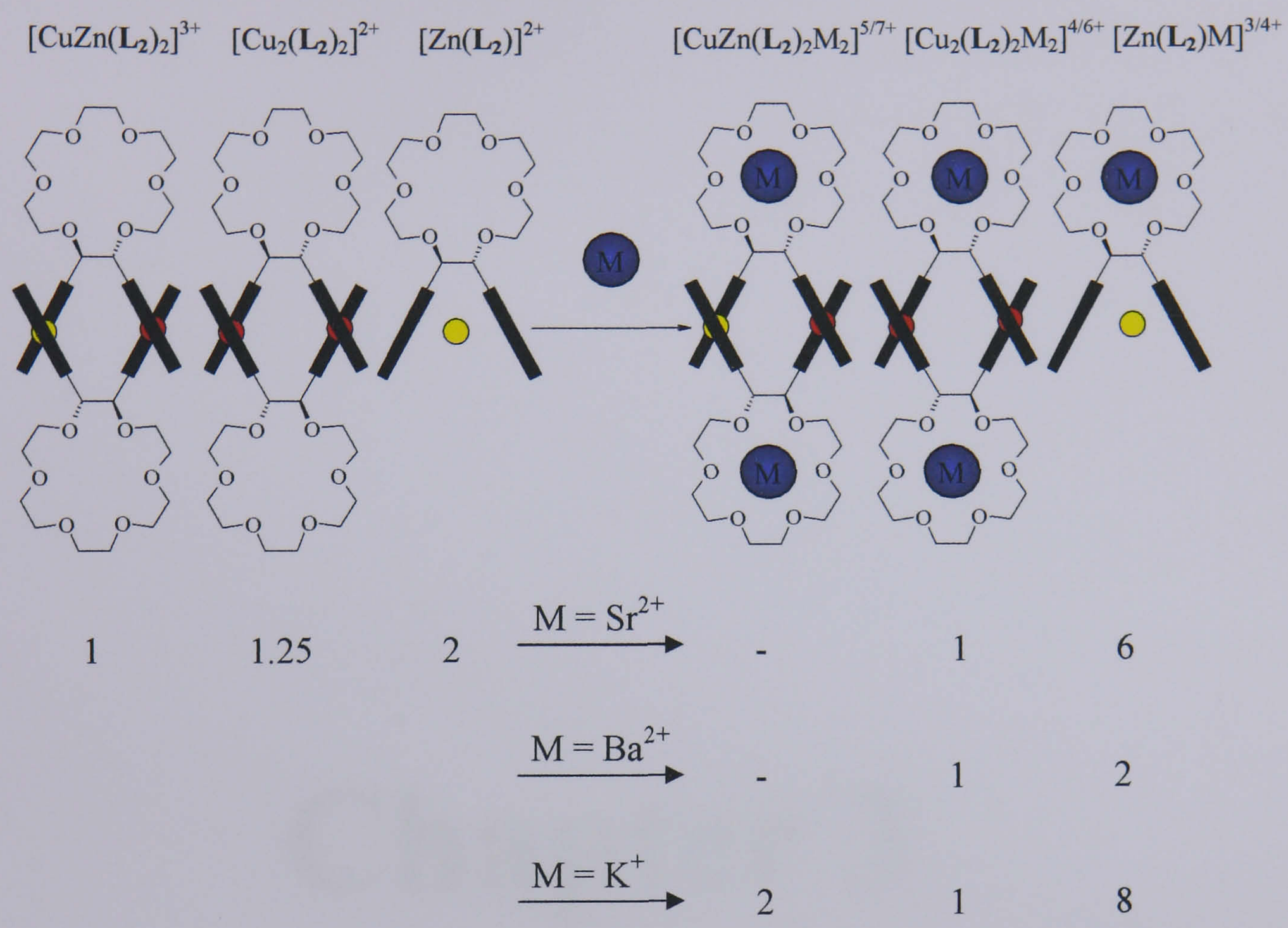

Figure 2.15. Cartoon representation of the distribution of products following the addition of various s-block metal cations to $\mathbf{L_2}$.

Chapter 3

3. Electrostatic Control of the Formation of Heteroleptic Helicates

Described in this chapter is the synthesis of a potentially hexadentate ligand $\mathbf{L_3}$, (Figure 3.1) and its coordination chemistry with zinc(II) cations. This hexadentate ligand contains two pyridyl-thiazole-pyridyl (py-tz-py) binding domains and an external crown ether binding site that spans the 3,3'-positions of the central bipyridyl unit, in a similar manner to the potentially tetradentate ligands described in Chapter 2.

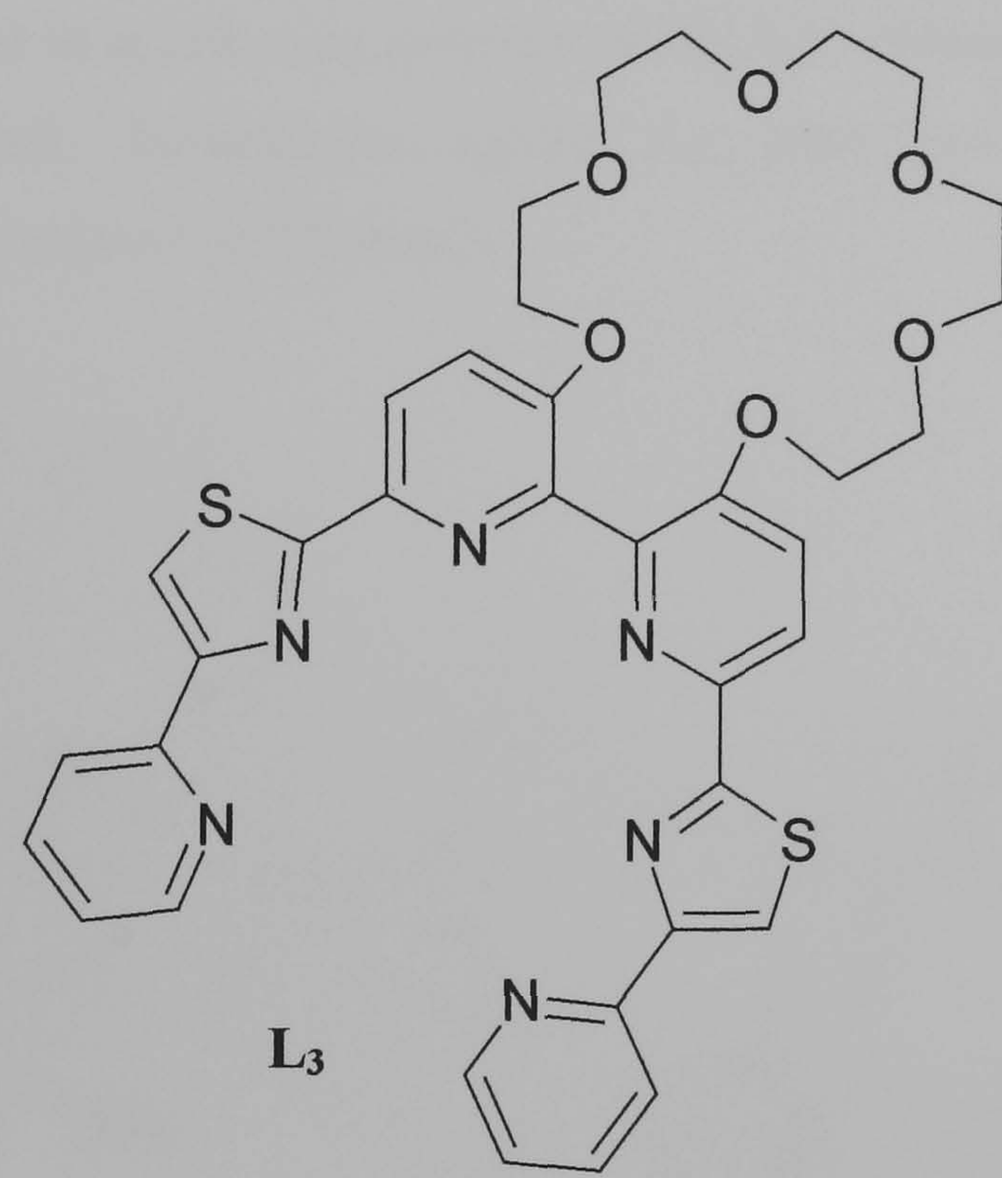

Figure 3.1. The potentially hexadentate ligand $\mathbf{L_3}$.

3.1 Ligand Synthesis

3.1.1 Synthesis of L_3

As previously established, the versatility of the thioamide derivative allows many other ligands to be easily synthesised from one compound. Such is the case here as the potentially hexadentate ligand, L_3, can be easily synthesised in one step from the thioamide (**16**) described in chapter two. Addition of a slight excess of 2-(α-bromoacetyl)pyridine to a refluxing solution of the 6,6'-dithioamide (**16**) in ethanol affords the potentially hexadentate ligand, L_3, after purification via column chromatography, as outlined in Scheme 3.

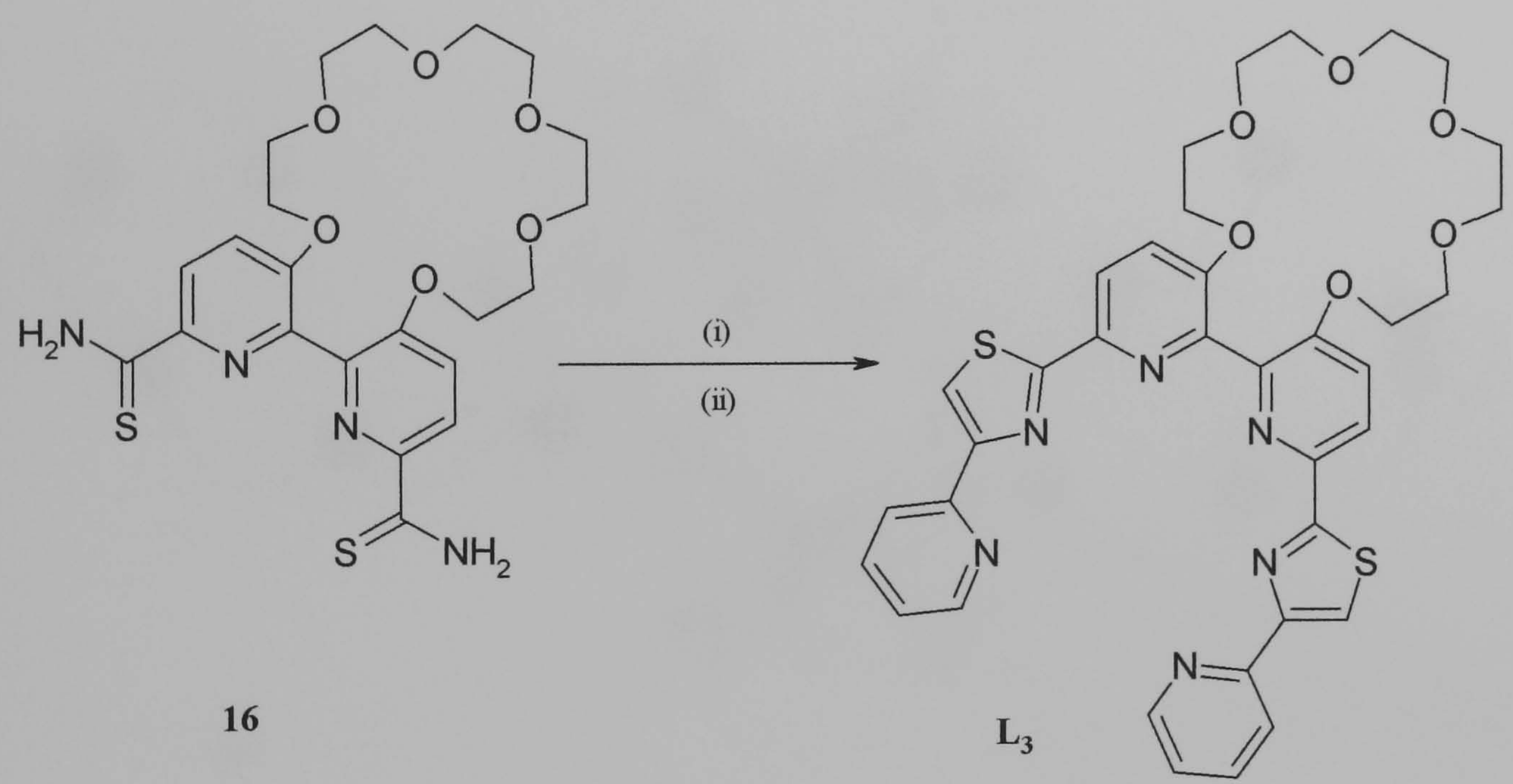

Scheme 3. Synthesis of L_3 from 6,6'-dithioamide (**16**). Reagents and conditions: (i) 2-(α-bromoacetyl)pyridine, at reflux in EtOH and (ii) $NH_{3(aq)}$.

3.2 Coordination Chemistry

3.2.1 Complexes of $\mathbf{L_3}$ *with Zinc(II)*

Reaction of the potentially hexadentate ligand, $\mathbf{L_3}$, with an equimolar amount of $[Zn(H_2O)_6](ClO_4)_2$ in acetonitrile produced a colourless solution. ESI-MS of the resulting solution confirmed the formation of a dinuclear double helicate with an ion at *m/z* 1851 corresponding to the complex $\{[Zn_2(\mathbf{L_3})_2](ClO_4)_3\}^+$. Slow diffusion of ethyl acetate vapour into the resulting colourless solution afforded colourless crystals of X-ray quality. The structure of which has been established by X-ray crystallography (Figure 3.2).

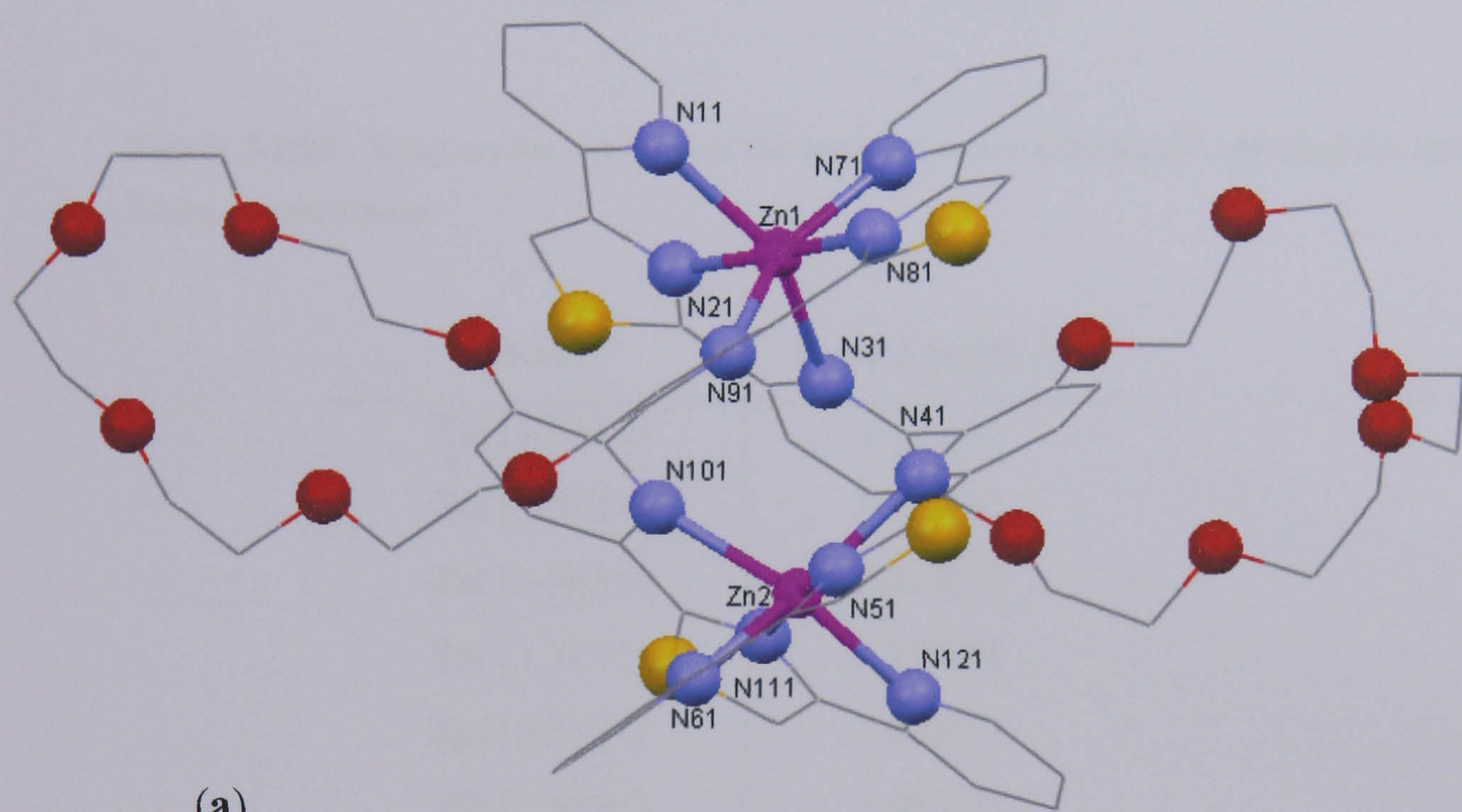

(a)

Figure 3.2(a). X-ray crystal structure of the complex cation $[Zn_2(\mathbf{L_3})_2]^{4+}$ showing the structural framework.

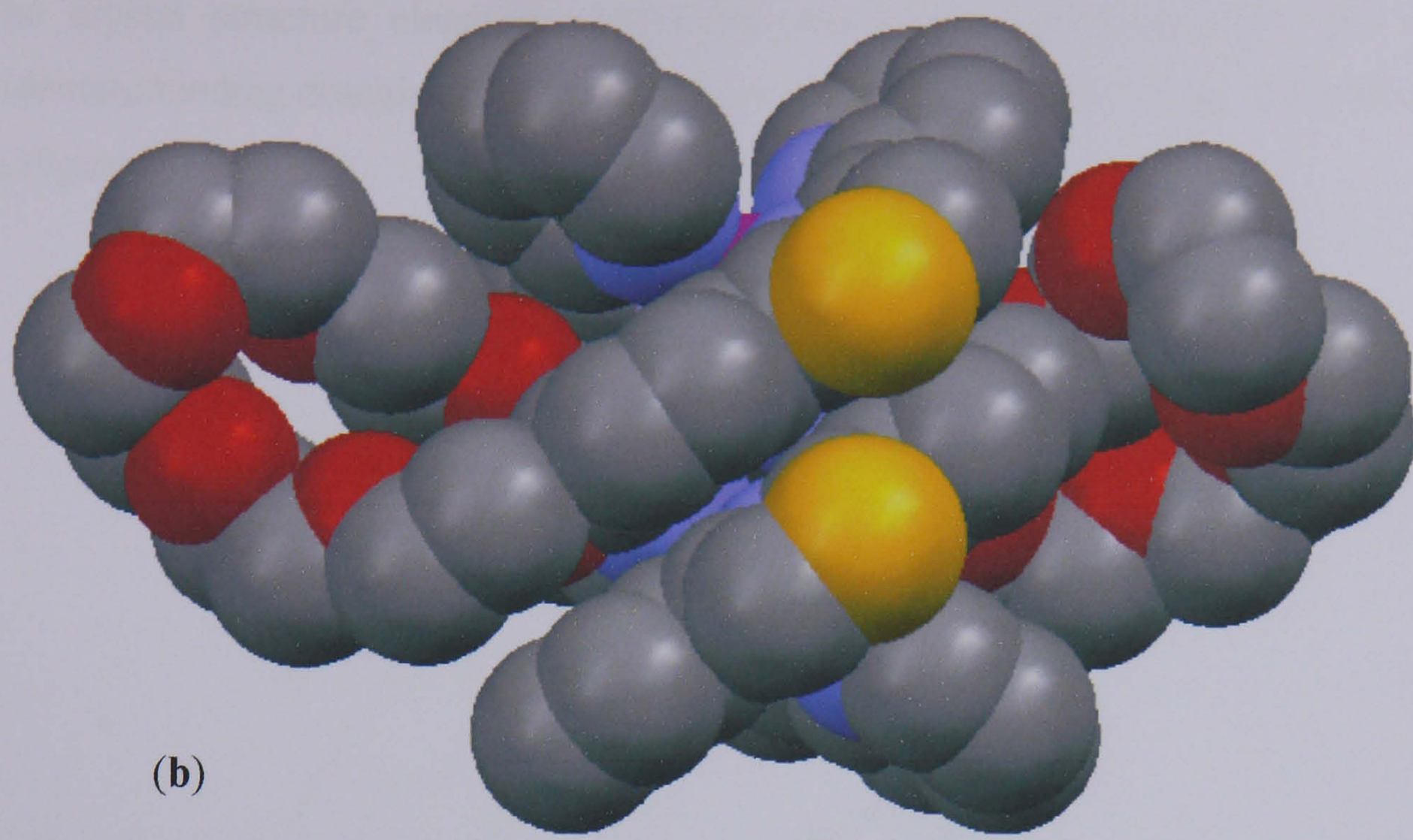

Figure 3.2(b). X-ray crystal structure of the complex cation $[Zn_2(\mathbf{L_3})_2]^{4+}$ showing the space filling representation.

Bond	Bond Length Å
Zn(1)-N(11)	2.264(3)
Zn(1)-N(21)	1.999(3)
Zn(1)-N(31)	2.413(3)
Zn(1)-N(71)	2.176(4)
Zn(1)-N(81)	2.001(3)
Zn(1)-N(91)	2.465(3)
Zn(2)-N(41)	2.376(3)
Zn(2)-N(51)	1.997(3)
Zn(2)-N(61)	2.243(4)
Zn(2)-N(101)	2.382(3)
Zn(2)-N(111)	1.999(3)
Zn(2)-N(121)	2.243(3)
Zn(1)-Zn(2)	4.812(1)

Table 5. Selected bond lengths (Å) for the complex cation $[Zn_2(\mathbf{L_3})_2]^{4+}$.

The crystal structure elegantly shows that each ligand partitions into two bis-tridentate binding domains comprising of pyridyl-thiazole-pyridyl units, as illustrated in Figure 3.3.

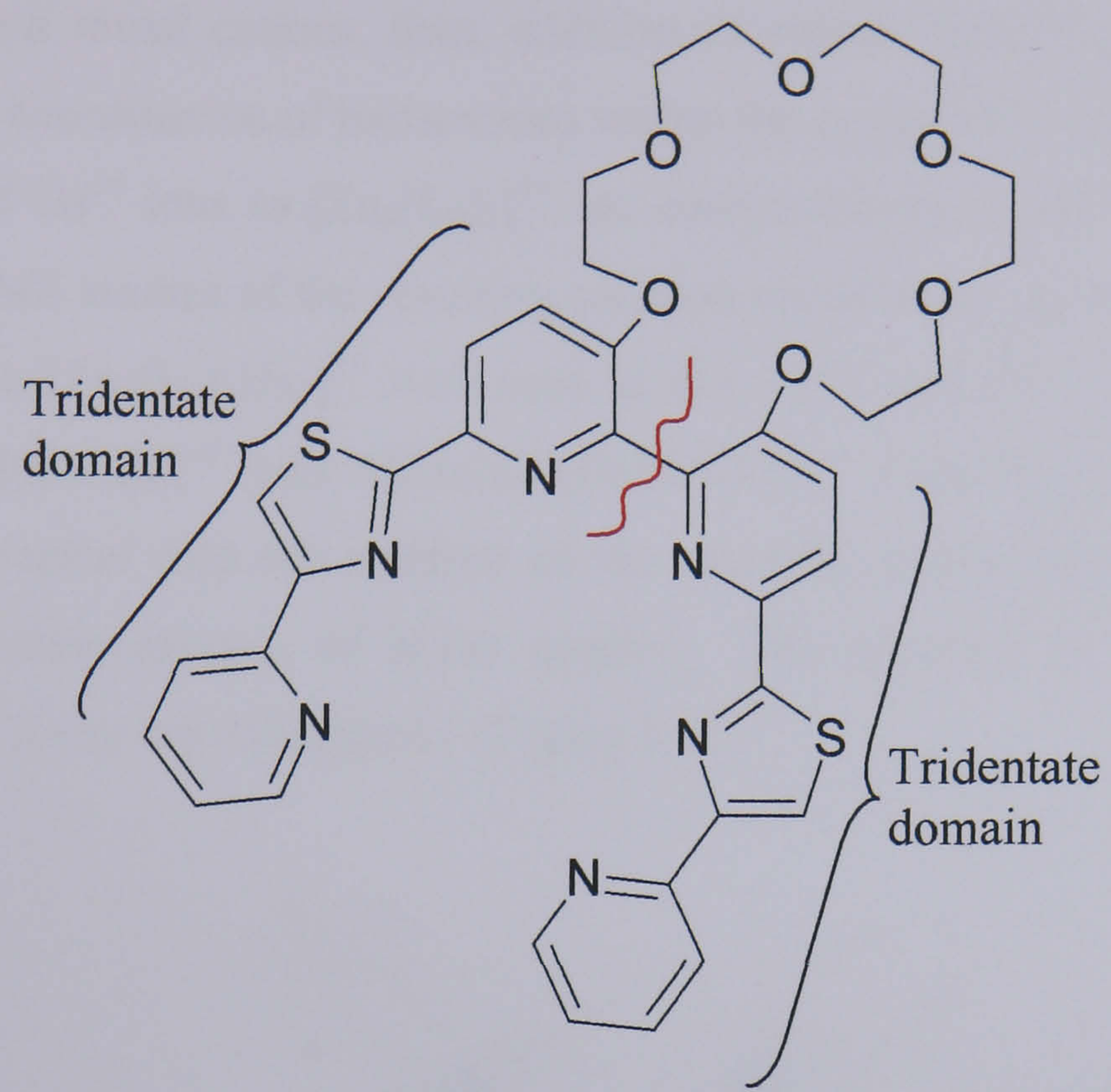

Figure 3.3. Structure of $\mathbf{L_3}$ showing the partitioning of the ligand into two bis-tridentate binding domains.

In the crystal, each ligand partitions into two bis-tridentate binding domains as a consequence of the of the steric interactions between the oxygen atoms spanning the 3,3'-positions of the central bipyridine core. The two bis-tridentate domains are coordinated by two bridging ligands in a double helical arrangement, with NCCN interdomain torsion angles of 64.91° and 67.54°. Each of the two zinc centres occupies a distorted octahedral coordination geometry formed by two tridentate binding domains, one from each ligand with Zn–N bond distances ranging from 1.997(3) to 2.456(3) Å, and with a Zn–Zn distance of 4.812(1) Å (Table 5). With the shortest bond distances arising from the coordination between $Zn–N_{(thiazole)}$ units.

3.2.2 Addition of $Ba(ClO_4)_2$ to Complexes with $\mathbf{L_3}$

As established in the previous chapters, crown ether units can further coordinate a range of s-block metal cations, thus, addition of excess $Ba(ClO_4)_2$ to $[Zn_2(\mathbf{L_3})_2]^{4+}$ resulted in the coordination of barium ions within the crown ether moiety. Following the addition of Ba^{2+} ions to $[Zn_2(\mathbf{L_3})_2]^{4+}$, no colour change is observed in solution, although ESI-MS studies of the resulting solution revealed the presence of dinuclear double helicate $[Zn_2(\mathbf{L_3})_2Ba_2]^{8+}$ with ions at *m/z* 1213 and 2187 corresponding to $\{[Zn_2(\mathbf{L_3})_2Ba_2](ClO_4)_6\}^{2+}$ and $\{[Zn_2(\mathbf{L_3})_2Ba](ClO_4)_5\}^{+}$ respectively. Diffusion of ethyl acetate vapour into the solution of the resulting barium-containing complex afforded colourless crystals of X-ray quality. The structure of which has been established by X-ray crystallography (Figure 3.4).

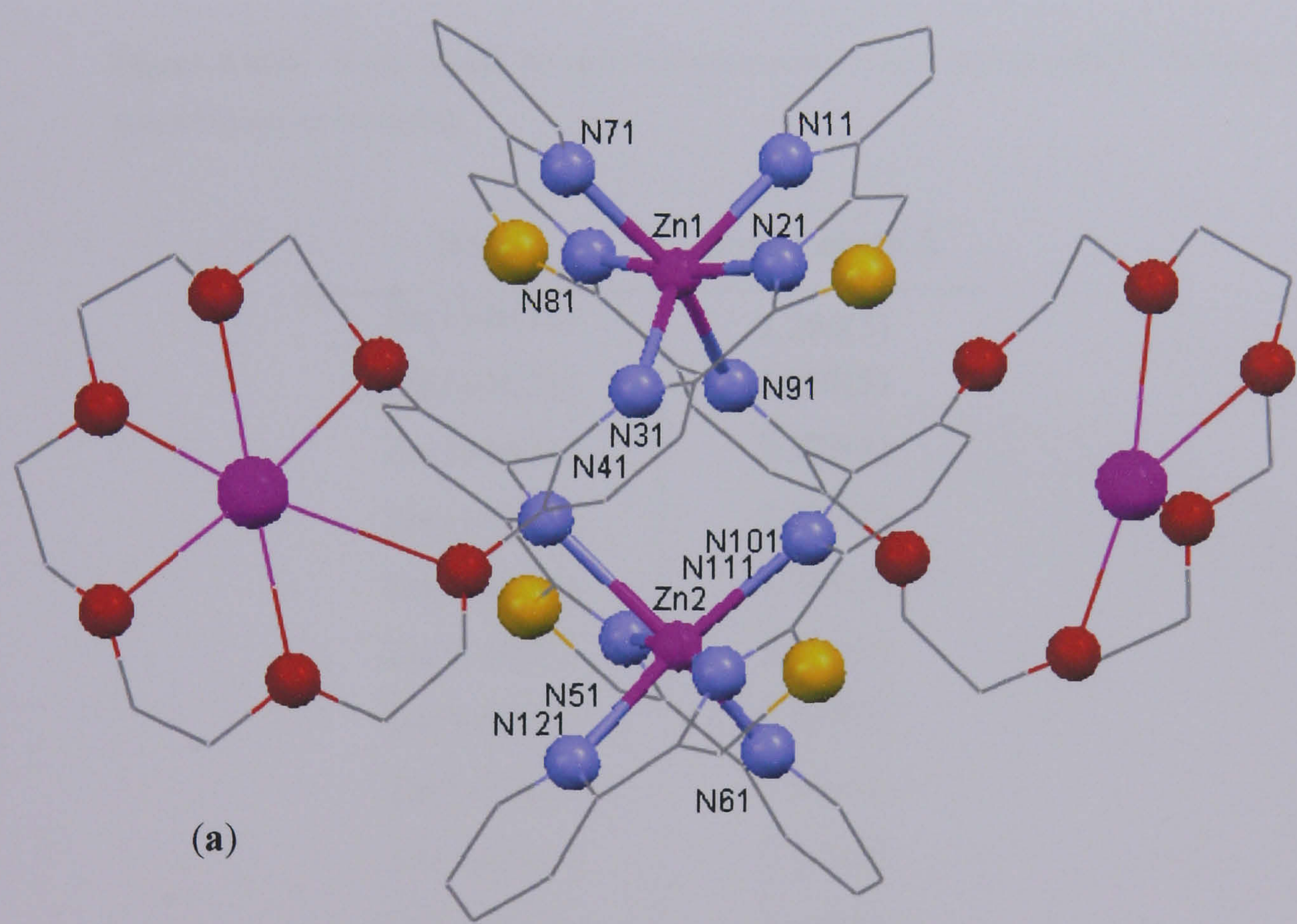

Figure 3.4(a). X-ray crystal structure of the complex cation $[Zn_2(\mathbf{L_3})_2Ba_2]^{8+}$ showing the structural framework.

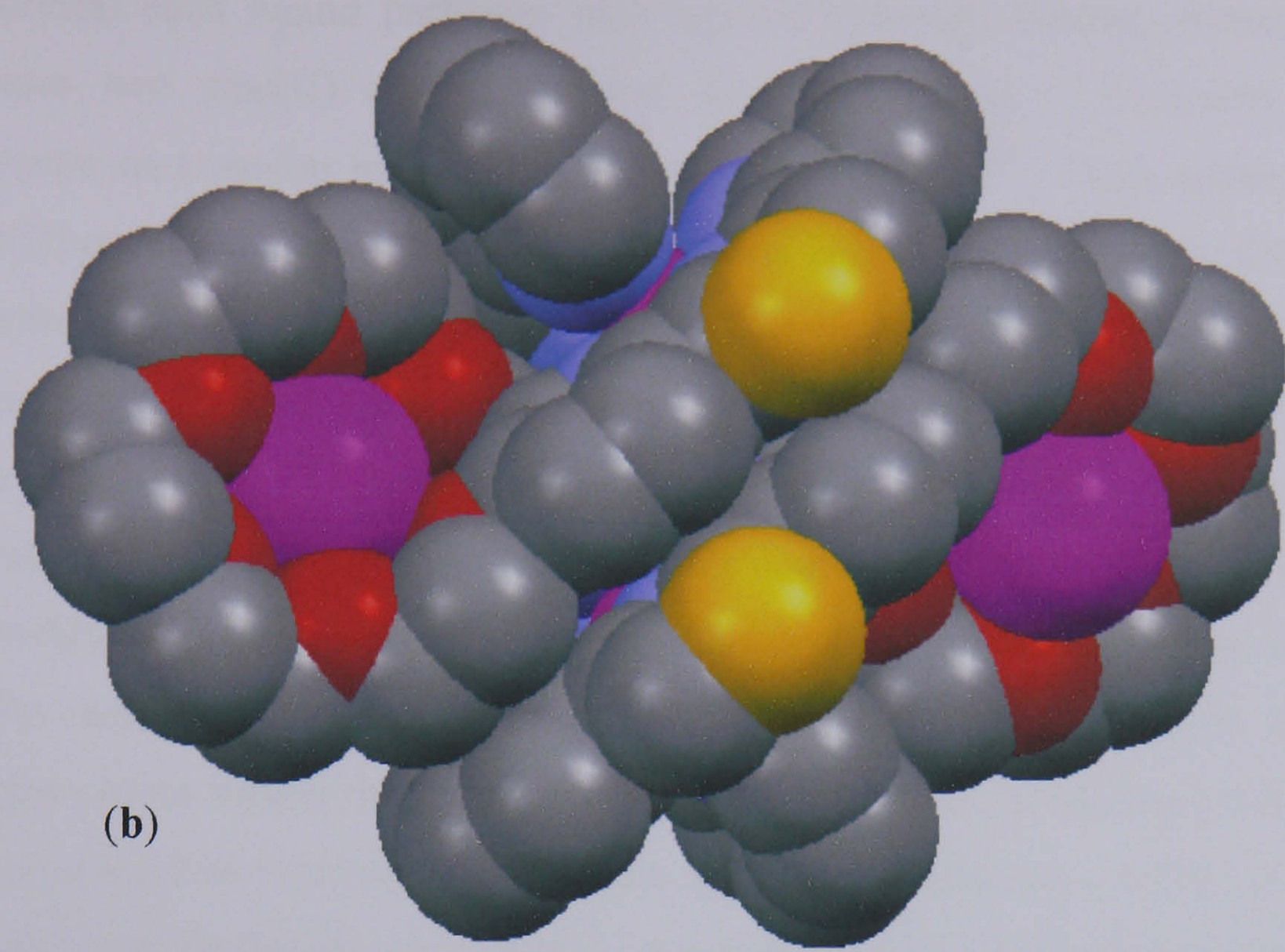

Figure 3.4(b). X-ray crystal structure of the complex cation $[Zn_2(\mathbf{L_3})_2Ba_2]^{8+}$ showing the space filling representation.

Bond	Bond Length Å
Zn(1)-N(11)	2.286(5)
Zn(1)-N(21)	1.986(5)
Zn(1)-N(31)	2.377(4)
Zn(1)-N(71)	2.197(5)
Zn(1)-N(81)	1.989(5)
Zn(1)-N(91)	2.549(5)
Zn(2)-N(41)	2.525(5)
Zn(2)-N(51)	1.994(5)
Zn(2)-N(61)	2.173(5)
Zn(2)-N(101)	2.368(5)
Zn(2)-N(111)	1.985(5)
Zn(2)-N(121)	2.289(5)
Zn(1)-Zn(2)	5.142(1)

Table 6. Selected bond lengths (Å) for the complex cation $[Zn_2(\mathbf{L_3})_2Ba_2]^{8+}$.

In the crystal each ligand partitions into two bis-tridentate binding domains, and coordinates two zinc(II) centres via two bridging ligands in a double helical arrangement, in a similar manner to the complex $[Zn_2(\mathbf{L_3})_2]^{4+}$. Once again each of the zinc(II) centres occupies a distorted octahedral coordination geometry formed by the coordination of two tridentate (py-tz-py) N-donor units, one from each ligand with Zn–N bond distances ranging from 1.985(5) to 2.549(5) Å, and a Zn–Zn distance of 5.142(1) Å (4.812(1) Å; $[Zn_2(\mathbf{L_3})_2]^{4+}$) (Table 6). As previously established, barium ions are of an ideal size for coordination to all six of the oxygen atoms within a [18]crown-6 ether fragment; however, this is not the case here. In one of the crown ether units the barium ion is nine coordinate and bonds to all six of the oxygen atoms within the crown ether fragment and the remaining coordination sites are occupied by two perchlorate anions and a water molecule. In the remaining crown ether unit, the barium ion is seven coordinate and this time is only coordinated by four "outer" oxygen atoms of the crown ether fragment. The Ba–O distances between the two uncoordinated oxygen atoms are 3.312 and 3.442 Å, and are too long to be considered as bonding interactions. The three remaining coordination sites are occupied by three perchlorate anions.

In addition to the differences observed between the coordination of barium ions within the two crown ether moieties, only two other major differences between the two structures have been observed. These differences are the NCCN torsion angles between the two tridentate domains and the pitch lengths of the two helicate structures. The inter-domain NCCN torsion angles observed within the helicate $[Zn_2(\mathbf{L_3})_2]^{4+}$ are 64.91° and 67.54° and for the barium containing species $[Zn_2(\mathbf{L_3})_2Ba_2]^{8+}$ the torsion angles are 78.35° and 80.85°, thus representing a significant average increase of 13°. This increase has a direct effect on the pitch length of the helicate (defined as the Zn···Zn distance) with the pitch lengths for the two structures also increasing from 4.812 to 5.142 Å for $[Zn_2(\mathbf{L_3})_2]^{4+}$ and $[Zn_2(\mathbf{L_3})_2Ba_2]^{8+}$ respectively. This increase in torsion angle is due to a combination of both electrostatic and allosteric effects that occur following the coordination of barium ions within the external crown ether moiety. This observation has also been seen in similar helicate systems.[97, 98, 101]

3.3 ^{1}H NMR Studies

3.3.1 Complexes with $\boldsymbol{L_3}$

The 500 MHz ^{1}H NMR spectrum of the complex $[Zn_2(\mathbf{L_3})_2]^{4+}$ in CD_3CN shows fourteen aromatic signals occurring in seven different environments between 7.19 and 8.6 ppm, consistent with the formation of a highly symmetrical dinuclear double helicate species. Furthermore the crown ether protons occur as their usual multiplets between 2.9 and 3.85 ppm (Figure 3.5).

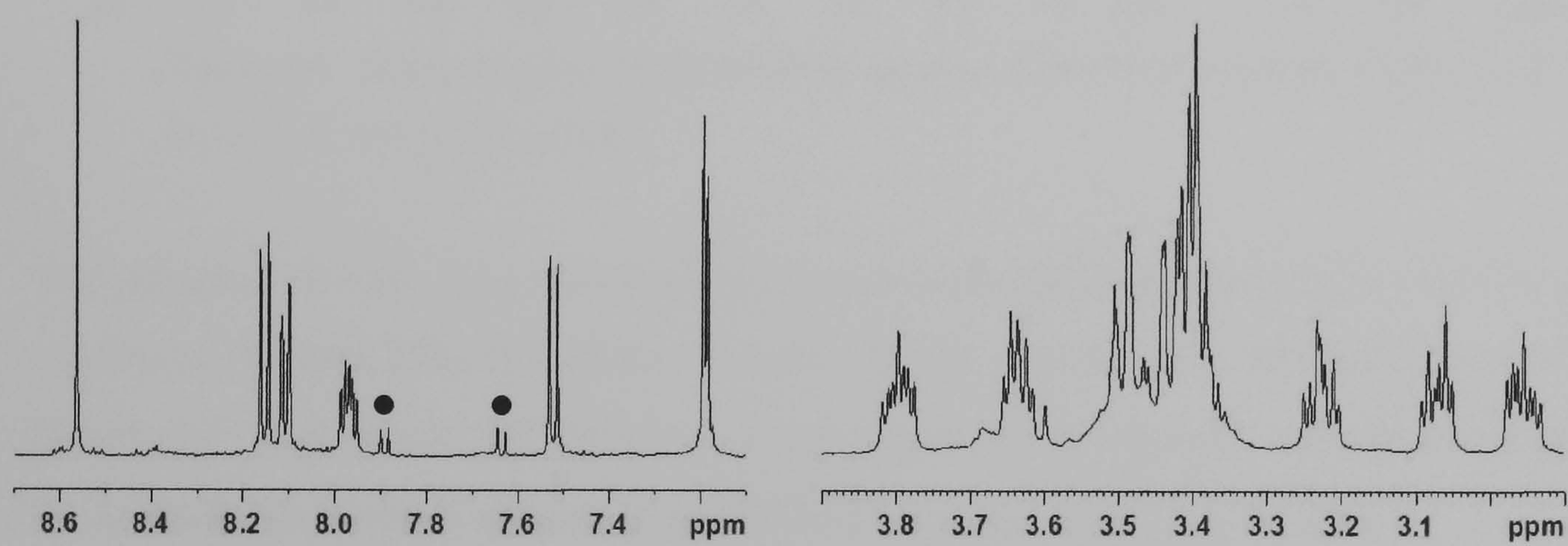

Figure 3.5. Selected regions of the ^{1}H NMR spectrum of $[Zn_2(\mathbf{L_3})_2]^{4+}$. • corresponds to a small amount of impurities.

3.3.2 Formation of Heteroleptic Complexes

Given that $\mathbf{L_3}$ contains identical N-donor binding domains as the previously reported parent ligand $\mathbf{L_z}$ (which does not contain the external crown ether binding site),[75] and both ligands are capable of forming the dinuclear double helicates $[Zn_2(\mathbf{L_3})_2]^{4+}$ and $[Zn_2(\mathbf{L_z})_2]^{4+}$ upon reaction with zinc(II) ions. Therefore it was decided to investigate their ability to form double stranded heteroleptic complexes. Thus, reaction of $\mathbf{L_3}$, $\mathbf{L_z}$ and Zn(II) (1 : 1 : 2 molar ratio) in CD_3CN produced a colourless solution, and 400 MHz ^{1}H NMR studies of the resulting solution gave a rather complex spectrum, with aromatic signals occurring between 6.98 and 8.71 ppm (Figure 3.6). Careful comparison of this spectrum with those obtained for the $\mathbf{L_3}$ and $\mathbf{L_z}$ homoleptic complexes shows that the mixed ligand system contains both homoleptic complexes $[Zn_2(\mathbf{L_3})_2]^{4+}$ and $[Zn_2(\mathbf{L_z})_2]^{4+}$ and a very small amount of the heteroleptic complex $[Zn_2(\mathbf{L_3})(\mathbf{L_z})]^{4+}$ (approximately 5%). The most diagnostic signals present within the spectrum are those corresponding to the thiazole ring, which occur as sharp singlets

at 8.57 and 8.60 ppm for $[Zn_2(\mathbf{L_3})_2]^{4+}$ and $[Zn_2(\mathbf{L_z})_2]^{4+}$ respectively. The weak singlets at 8.71 and 8.56 ppm correspond to a small amount of the heteroleptic complex $[Zn_2(\mathbf{L_3})(\mathbf{L_z})]^{4+}$ being present.

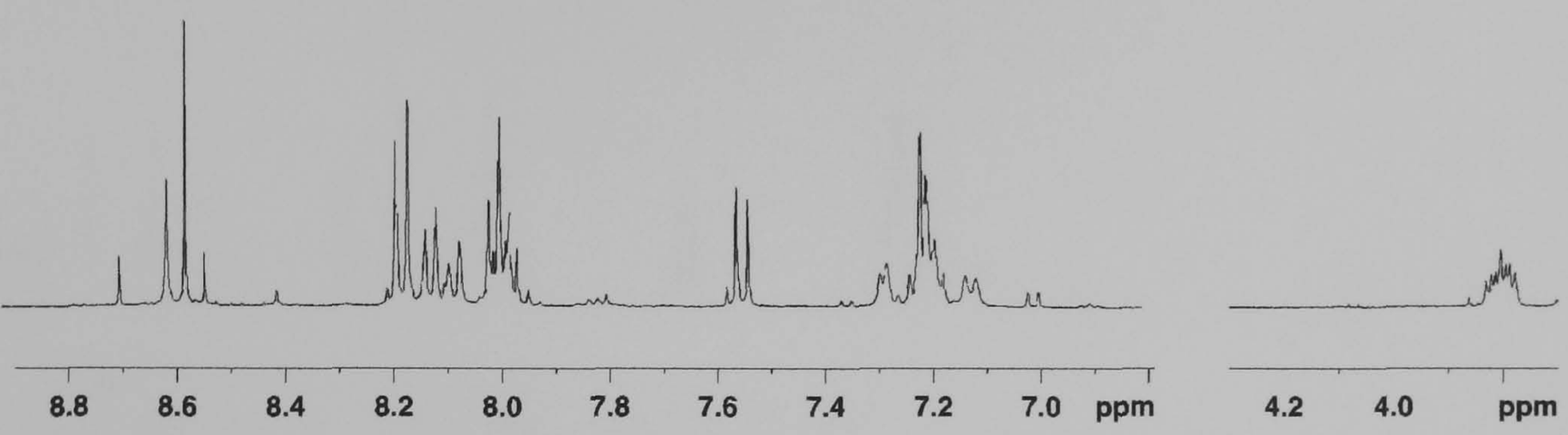

Figure 3.6. Selected regions of the ^{1}H NMR spectrum (CD_3CN) of a mixture of $[Zn_2(\mathbf{L_3})_2]^{4+}$, $[Zn_2(\mathbf{L_z})_2]^{4+}$ and $[Zn_2(\mathbf{L_3})(\mathbf{L_z})]^{4+}$.

The presence of both the homoleptic and heteroleptic helicate species has also been confirmed through ESI-MS studies, where intense signals were observed for both $[Zn_2(\mathbf{L_3})_2]^{4+}$ and $[Zn_2(\mathbf{L_z})_2]^{4+}$ helicates and a signal of low intensity was observed for the heteroleptic helicate species $[Zn_2(\mathbf{L_3})(\mathbf{L_z})]^{4+}$.

3.3.3 Addition of $Ba(ClO_4)_2$ to the Mixed Ligand System

Addition of twenty equivalents of $Ba(ClO_4)_2$ to the mixed ligand system not only shows changes to the chemical shifts, but also shows an increase in intensity of the heteroleptic helicate species which now accounts for approximately 25% of the species present (Figure 3.7b). The changes observed to the chemical shifts are a typical observation for the coordination of an electronegative Ba^{2+} ion within the crown ether binding site. Addition of a further twenty equivalents of $Ba(ClO_4)_2$ affords another increase in the amount of the heteroleptic helicate species present, thus the three helicate species are now present in the ratio 1 : 1 : 2 ($[Zn_2(\mathbf{L_3})_2]^{4+}$, $[Zn_2(\mathbf{L_z})_2]^{4+}$ and $[Zn_2(\mathbf{L_3})(\mathbf{L_z})]^{4+}$ respectively) (Figure 3.7c). No changes are observed to the distribution of products following a further addition of $Ba(ClO_4)_2$.

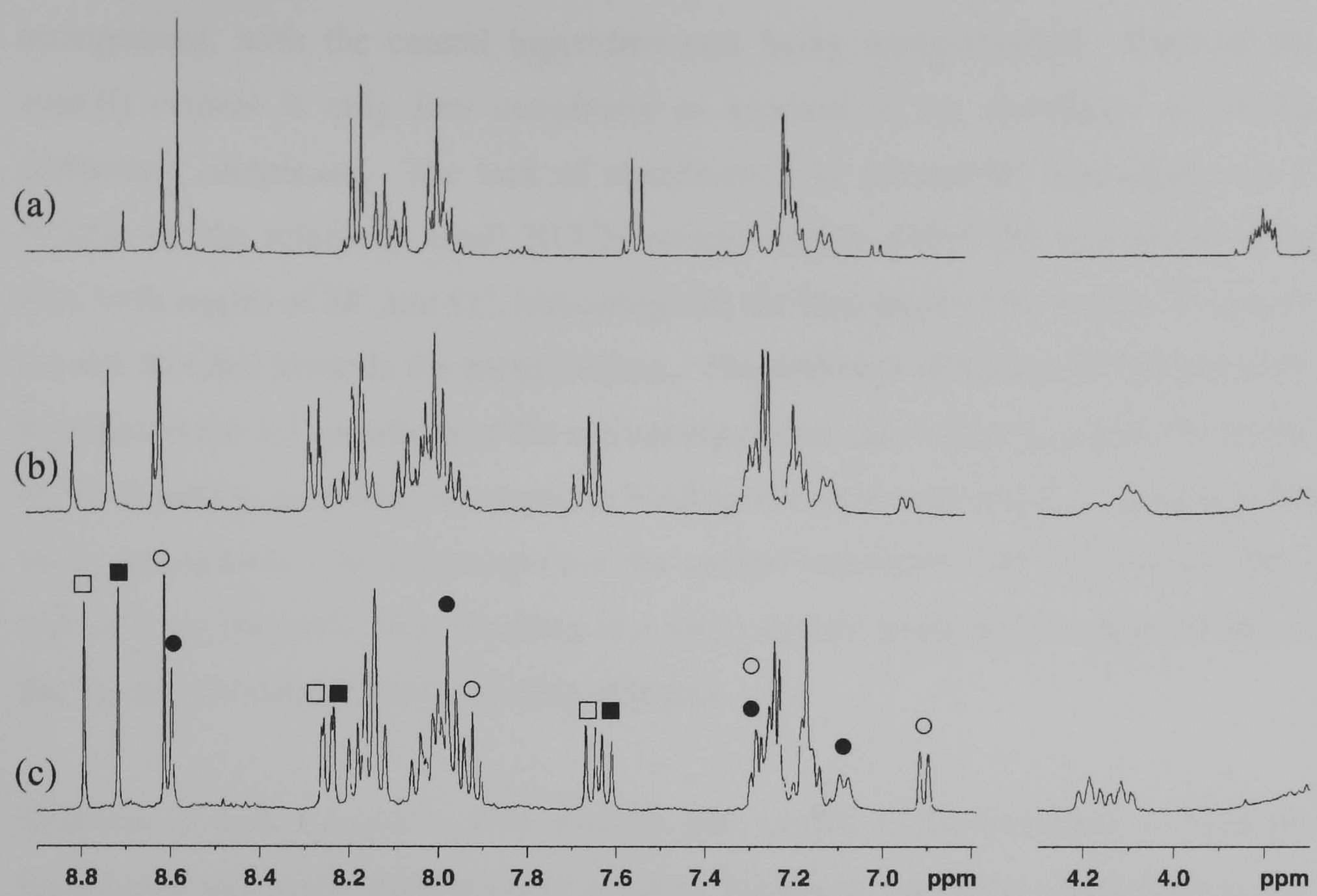

Figure 3.7. Selected regions of the ^{1}H NMR spectrum of a mixture of ($[Zn_2(\mathbf{L_3})_2]^{4+}$, $[Zn_2(\mathbf{L_z})_2]^{4+}$ and $[Zn_2(\mathbf{L_3})(\mathbf{L_z})]^{4+}$ following the addition of (a) 0, (b) 20 and (c) 40 equivalents of $Ba(ClO_4)_2$. ■ $[Zn_2(\mathbf{L_3})_2]^{4+}$, ● $[Zn_2(\mathbf{L_z})_2]^{4+}$, □ $[Zn_2(\mathbf{L_3})(\mathbf{L_z})]^{4+}$, ○ $[Zn_2(\mathbf{L_3})(\mathbf{L_z})]^{4+}$.

The aromatic region, in particular the thiazole singlets are very useful in determining the distribution of products. Thus following the addition of forty equivalents (Figure 3.7c) of barium ions, the four thiazole singlets are of similar intensity, as would be expected if a statistical mixture of species is formed (8.72 $[Zn_2(\mathbf{L_3})_2]^{4+}$ and 8.60 $[Zn_2(\mathbf{L_z})_2]^{4+}$; 8.62 and 8.80 ppm $[Zn_2(\mathbf{L_3})(\mathbf{L_z})]^{4+}$). In addition the doubling up of the methylene (crown ether) signals at 4.12 and 4.19 ppm is also observed.

3.4 Discussion

Although both $\mathbf{L_3}$ and $\mathbf{L_z}$ contain the same basic ligand chain and both ligands form dinuclear double helicates, the crystal structure of $[Zn_2(\mathbf{L_z})_2]^{4+}$, which has been presented in a recent publication, reveals that the two structures obtained are subtly different.[71, 75] Although $\mathbf{L_z}$ forms a dinuclear double helicate upon reaction with zinc(II) ions, the crystal structure of the complex $[Zn_2(\mathbf{L_z})_2]^{4+}$ reveals that each ligand partitions into bis-bidentate binding domains as apposed to bis-tridentate binding domains in $\mathbf{L_3}$. As a consequence of this, the two zinc(II) centres are coordinated by two bis-bidentate (py-tz) binding domains, one from each ligand in a double helical

arrangement, with the central bipyridine unit being uncoordinated. Each of the zinc(II) centres is only four coordinate as apposed to six coordinate in the $\mathbf{L_3}$ containing complexes. The lack of coordination to the central bipyridine unit is evident by the relatively small NCCN torsion angles within the non-coordinating unit, with angles of 38° and 51°, indicating that the lone pairs of the pyridyl N-donors are not directed towards the metal centres. The presence of the crown ether moiety attached to the 3,3'-positions of the central bipyridine unit within $\mathbf{L_3}$ alters the ability of the ligand to partition into separate binding domains and is due to unfavourable steric interactions. As a consequence the central bipyridine unit is prevented from approaching planarity, thus resulting in a large torsion angle and the partitioning of the ligand into two tridentate binding domains.

Reaction of both $\mathbf{L_3}$ and $\mathbf{L_z}$ with zinc(II) ions results in the formation of both the homoleptic and heteroleptic helicate species. However, very little of the heteroleptic helicate species $[Zn_2(\mathbf{L_3})(\mathbf{L_z})]^{4+}$ is observed. This observation could be due to electronic effects, as the formation of a heteroleptic helicate species would lead to an unfavourable five-coordinate zinc(II) centre, formed by the tridentate pyridyl-thiazol-pyridyl domain from $\mathbf{L_3}$ and the terminal bidentate pyridyl-thiazole domain from $\mathbf{L_z}$. Although the formation of a five-coordinate zinc(II) centre is feasible, only 4- and 6-coordinate species have been previously observed within pyridyl-thiazole ligands.[71, 75] Other factors, however, such as inter-ligand interactions may affect ligand recognition properties.

Following the addition of forty equivalents of barium ions to this mixed ligand system, the distribution of species changes and the three helicates are now present in a statistical ratio of 1 : 1 : 2 ($[Zn_2(\mathbf{L_3})_2]^{4+}$, $[Zn_2(\mathbf{L_z})_2]^{4+}$ and $[Zn_2(\mathbf{L_3})(\mathbf{L_z})]^{4+}$ respectively). This observation suggests that all ligand recognition between the ligand strands is lost. There are two possible reasons as to why the ligand recognition is lost between the two ligand strands following the addition of excess barium ions. Firstly an allosteric effect, as coordination of barium ions to the crown ether unit of $\mathbf{L_3}$ changes the partitioning of the ligands N-donor domains and as a consequence the ligand acts as a bis-bidentate donor unit, in a similar fashion to $\mathbf{L_z}$. However, the crystal structure of $[Zn_2(\mathbf{L_3})_2Ba_2]^{8+}$ clearly shows that this is not the case as the zinc(II) centres are still six-coordinate and occupy a distorted octahedral

coordination geometry formed by two pyridyl-thiazole-pyridyl donor units, one from each ligand. Secondly the ligand recognition may be lost due to electrostatic effects. The coordination of barium ions within the crown ether units of $\mathbf{L_3}$ would result in the formation of a highly charged 8+ ion. Such a high charge could destabilise the helicate species in such a manner that the formation of the heteroleptic helicate species $[Zn_2(\mathbf{L_3})(\mathbf{L_z})Ba]^{6+}$ is favoured. Furthermore, upon reaction of the mixed ligand system with K^+ ions, which are virtually identical size to the Ba^{2+} ions but only monocationic results in no change to the distribution of helicate species with the three complexes $[Zn_2(\mathbf{L_3})_2]^{4+}$, $[Zn_2(\mathbf{L_z})_2]^{4+}$ and $[Zn_2(\mathbf{L_3})(\mathbf{L_z})]^{4+}$ still being observed in their original quantities. As a consequence of this observation it would seem most likely that the formation of a statistical mixture of species is solely due to electrostatic and not allosteric effects. The ability to change the ligand's recognition properties upon addition of excess barium ions can be elegantly demonstrated by the use of a cartoon (Figure 3.8).

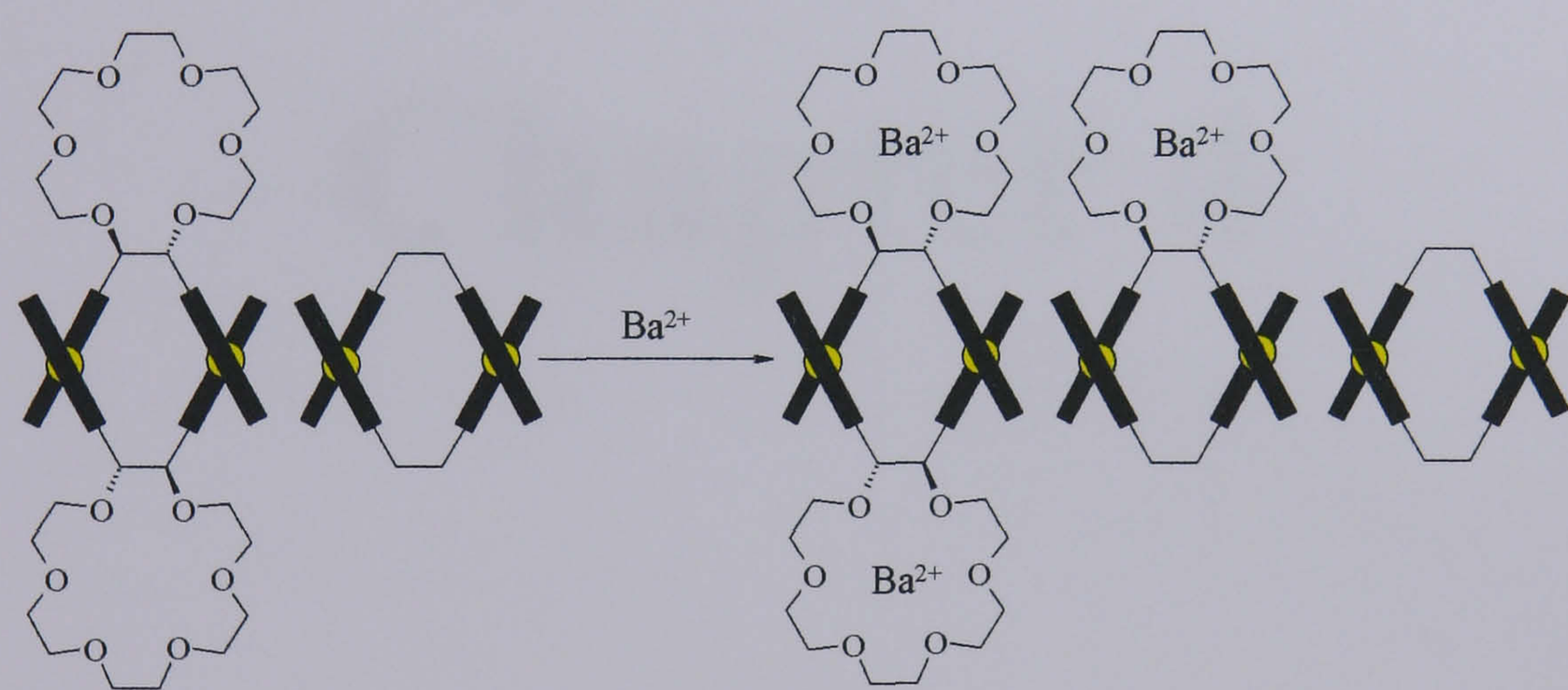

Figure 3.8. Cartoon representation showing the change in the ligand recognition properties between $\mathbf{L_3}$ and $\mathbf{L_z}$ following the addition of excess barium ions.

Chapter 4

4. Deprogrammable Heterometallic Helicates

Described in this chapter is the synthesis and coordination chemistry of three novel multidentate N-donor ligands $\mathbf{L_4}$, $\mathbf{L_5}$ and $\mathbf{L_6}$ (Figure 4.1) with selected transition metal cations. Each of these ligands contain pyridyl-thiazole (py-tz) binding domains similar to those seen in previous chapters. In these ligands methylene spacers have been introduced along the ligand chain, in a similar manner to those employed by Jean-Marie Lehn *et al.*,[65] and Cohen *et al.*,[102] where a number of bidentate units are linked by these methylene spacers. The incorporation of these methylene units along the ligand chain partitions the ligand into distinct tridentate and bidentate binding domains. These methylene units also offer more flexibility within the ligand strand unlike the rigid ortho-linked polydentate (tz-py-py-tz) ligands introduced by Baxter and co-workers.[103]

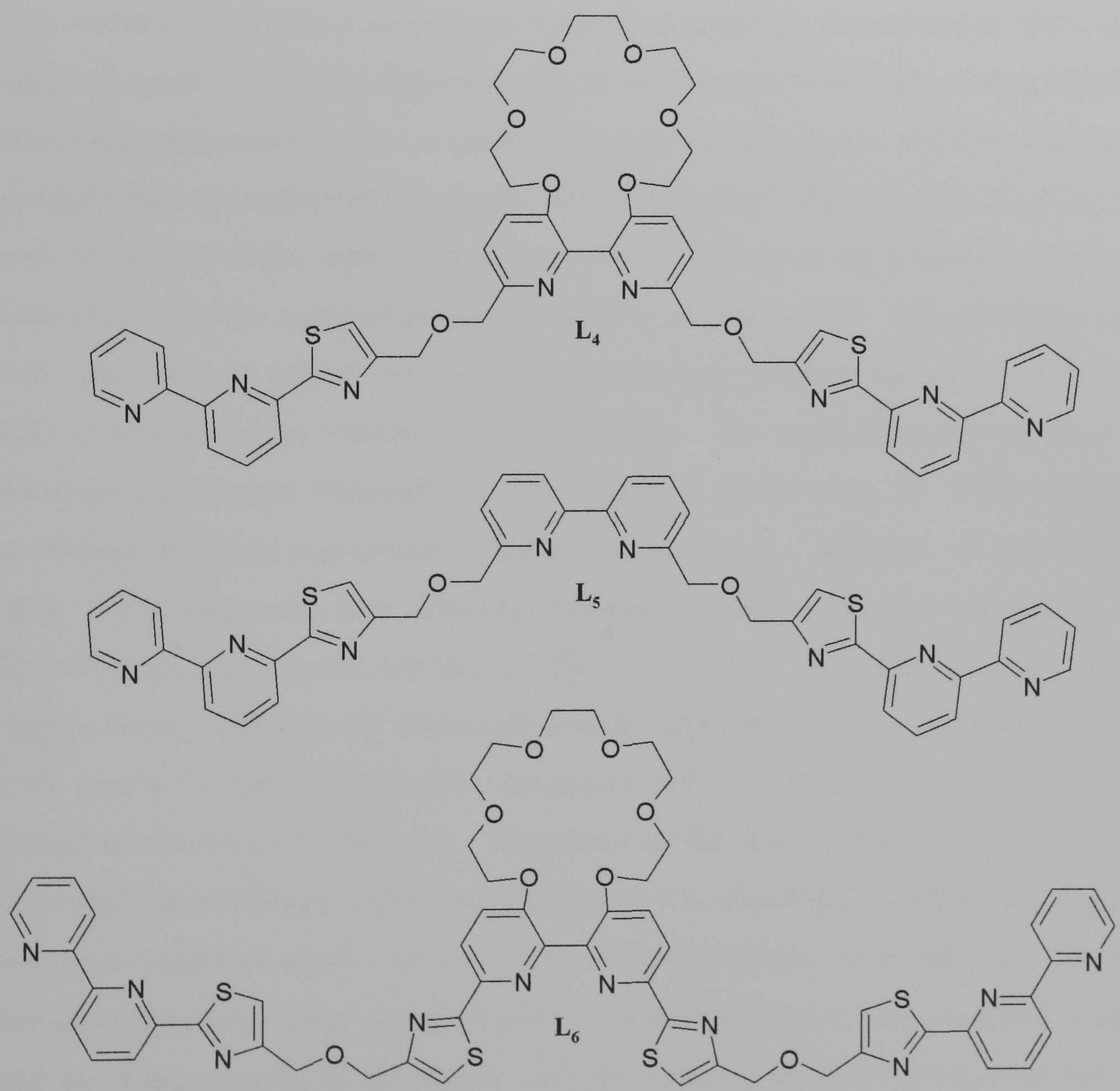

Figure 4.1. Structures of ligands $\mathbf{L_4}$, $\mathbf{L_5}$ and $\mathbf{L_6}$.

4.1 Ligand Synthesis

4.1.1 Synthesis of L_4

One of the main advantages of pyridyl-thiazole type ligands is their relative ease of synthesis and the availability of the starting materials. This particular ligand involves a convergent synthesis of two separate compounds which, when coupled together, gives the novel ligand, L_4. The most versatile compound en route to the preparation of this particular ligand is the synthesis of the thioamide by reaction of the appropriate nitrile group with hydrogen sulphide. The preparation of such a group, in principle allows the synthesis of a wide range of related polydentate (py-tz) based ligands as described in a number of recent publications by Rice *et al.*[70, 72, 75]

The synthesis of the first compound required to make L_4 is outlined in Scheme 4. Mono-N-oxidation of 2,2'-bipyridine (**9**) by slow addition of half an equivalent of *meta*-chloroperoxybenzoic acid gave a mixture of both mono and bis substituted products that was separated by column chromatography. The resulting N-oxide (**20**) was refluxed in DCM with excess trimethylsilyl cyanide in the presence of benzoyl chloride giving the carbonitrile-derivative (**21**) in high yields. The thioamide (**22**) was produced as a yellow solid by purging hydrogen sulphide through a solution of (**21**) in ethanol in the presence of triethylamine. The appearance of two singlets, corresponding to the thioamide at 9.59 and 7.74 ppm in the H^1 NMR spectrum confirmed complete conversion of the nitrile derivative. Addition of an excess of ethyl 3-bromopyruvate to a refluxing solution of (**22**) in ethanol, resulted in the formation of large brown crystals of (**23**) on cooling. The disappearance of the signals corresponding to the thioamide and the appearance of a triplet and quartet at 1.45 and 4.45 ppm respectively, consistent with an ethyl group, confirms the complete conversion to the ester. Reduction of the ester to the alcohol of (**24**) by slow addition of lithium aluminium hydride at 0°C afforded the target compound in moderate yields of approximately 50%. The appearance of singlet at 4.88 ppm corresponding to a $-CH_2-$ group together with the presence of eight aromatic signals and the disappearance of the signals corresponding to an ethyl group confirms the formation of our target compound.

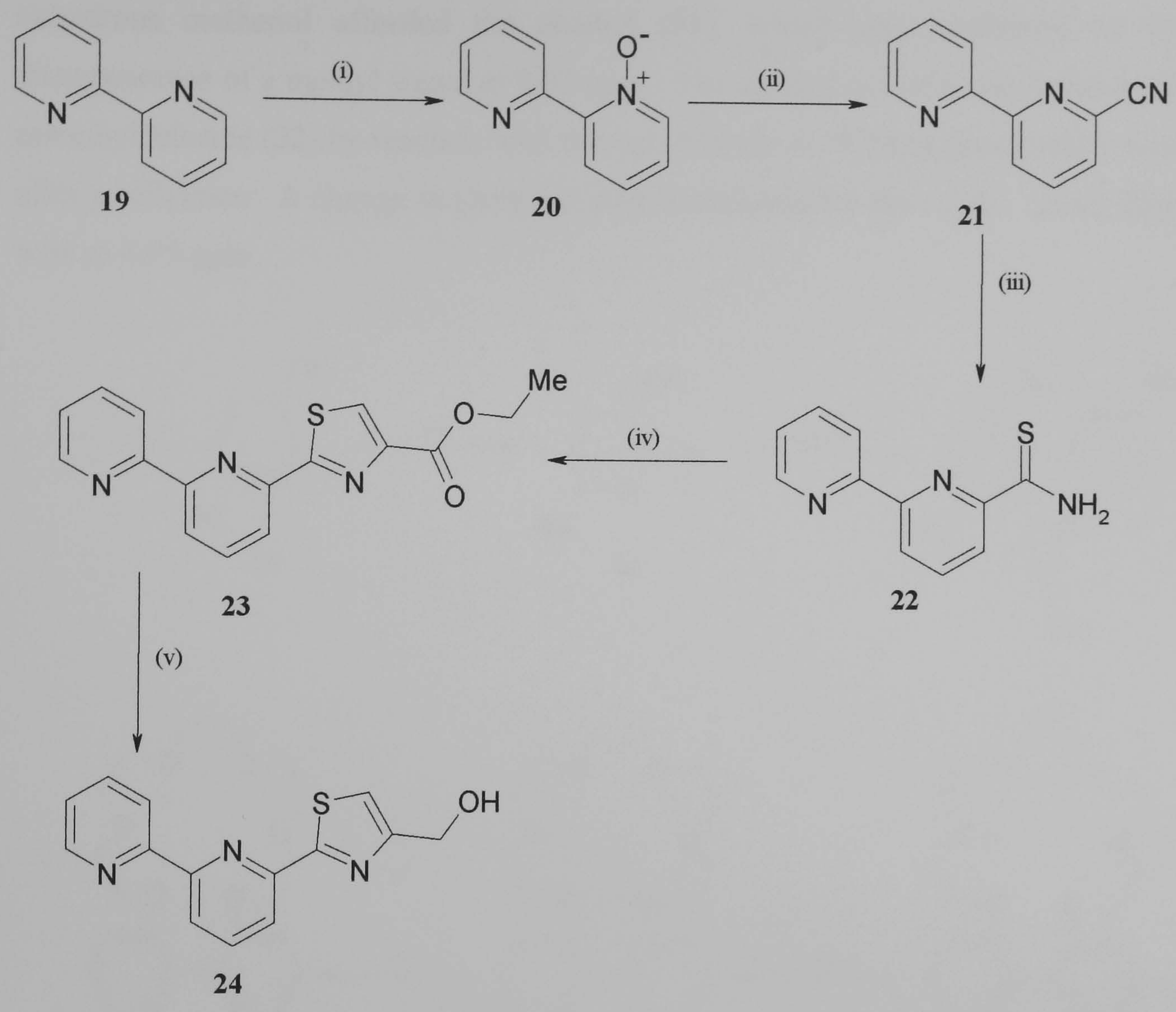

Scheme 4. Synthesis of compound (**24**) from 2,2'-bipyridine (**19**). Reagents and conditions: (i) DCM, *m*CPBA, RT, (ii) benzoyl chloride, TMSCN (at reflux in DCM), (iii) $H_2S_{(g)}$, Et_3N in EtOH, (iv) ethyl 3-bromopyruvate (at reflux in EtOH), (v) $LiAlH_4$, 0°C, N_2, anhydrous THF.

The synthesis of the second compound required to make $\mathbf{L_4}$ is outlined in Scheme 5. The 6,6'-dimethyl-2,2'-bipyridine-3,3'-diol precursor (**27**) was prepared from 5-hydroxy-2-methylpyridine (**25**), following the procedures described by Rebek *et al.*,[94, 104] Reaction of the diol (**27**) with sodium hydride (used to deprotonate the alcohol groups) and penta-(ethylene glycol)-di-*p*-tosylate, resulted in the formation of bipyridyl crown ether (**28**) in moderate yields of 50%. Complete conversion of the bipyridyl crown ether to the bis-N,N'-oxide (**29**) using a slight excess of *meta*-chloroperoxybenzoic acid, gave a white solid after purification. Acetylation of the methyl groups by reaction with acetic anhydride gave (**30**), the structure of which was confirmed by the appearance of a $-CH_2-$ signal at 5.13 ppm in the H^1 NMR spectrum. Complete hydrolysis of (**30**) using an excess of potassium carbonate in

anhydrous methanol afforded the alcohol (**31**), which was confirmed by the disappearance of a methyl signal at 2.03 ppm. The alcohol is easily converted to the dimethylchloride (**32**) by reaction with thionyl chloride in DCM to give a white solid after purification. A change in chemical shift is observed for the $-CH_2-$ group from 4.68 to 4.75 ppm.

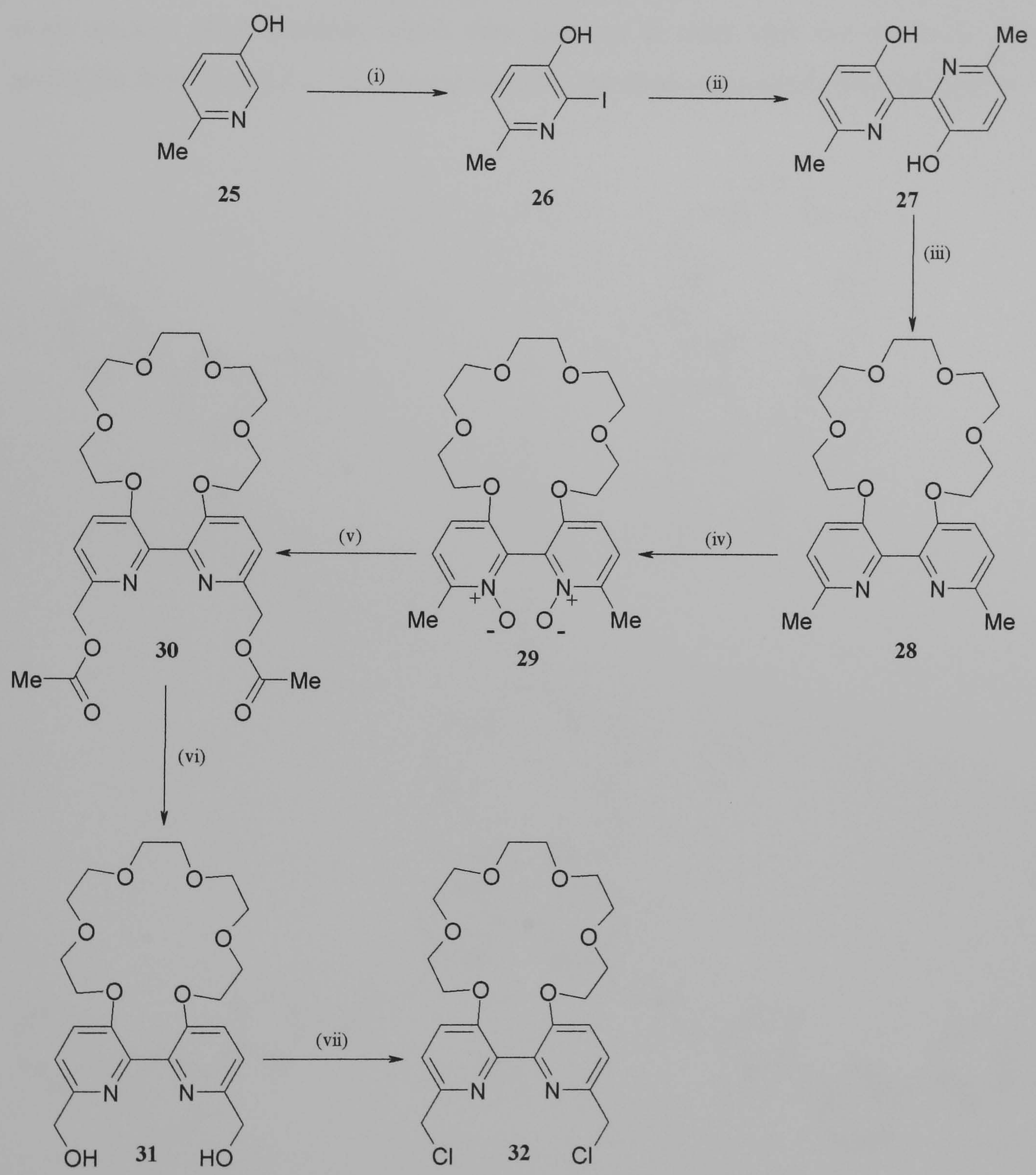

Scheme 5. Synthesis of compound (**32**) from 5-hydroxy-2-methylpyridine (**25**). Reagents and conditions: (i) Na_2CO_3, I_2, HCl, (ii) $[NiCl_2(PPh_3)_2]$, TBA-I, zinc dust, anhydrous DMF, N_2, 80°C, (iii) NaH, penta-(ethylene glycol)-di-*p*-tosylate, anhydrous DMF, N_2, 60°C, (iv) DCM, *m*CPBA, RT, (v) acetic anhydride, N_2, 120°C, (vi) K_2CO_3, anhydrous methanol, RT, (vii) thionyl chloride (at reflux in DCM).

The formation of the methylene links via the Williamson ether synthesis is outlined in Scheme 6. Deprotonation of the alcohol group of (**24**) using an excess of sodium hydride followed by the addition of half an equivalent of the dimethylchloride (**32**) and lengthy reflux times did not give the desired ligand $\mathbf{L_4}$. However, the addition of a catalytic amount of TBA-Br (a source of Br^-) results in a nucleophilic substitution reaction between the alkyl chloride of (**32**) and the bromide ion. This gave rise to a more reactive alkyl bromide which then goes on to react with the anion of (**24**) giving the final ligand $\mathbf{L_4}$. The ligand was then purified via column chromatography.

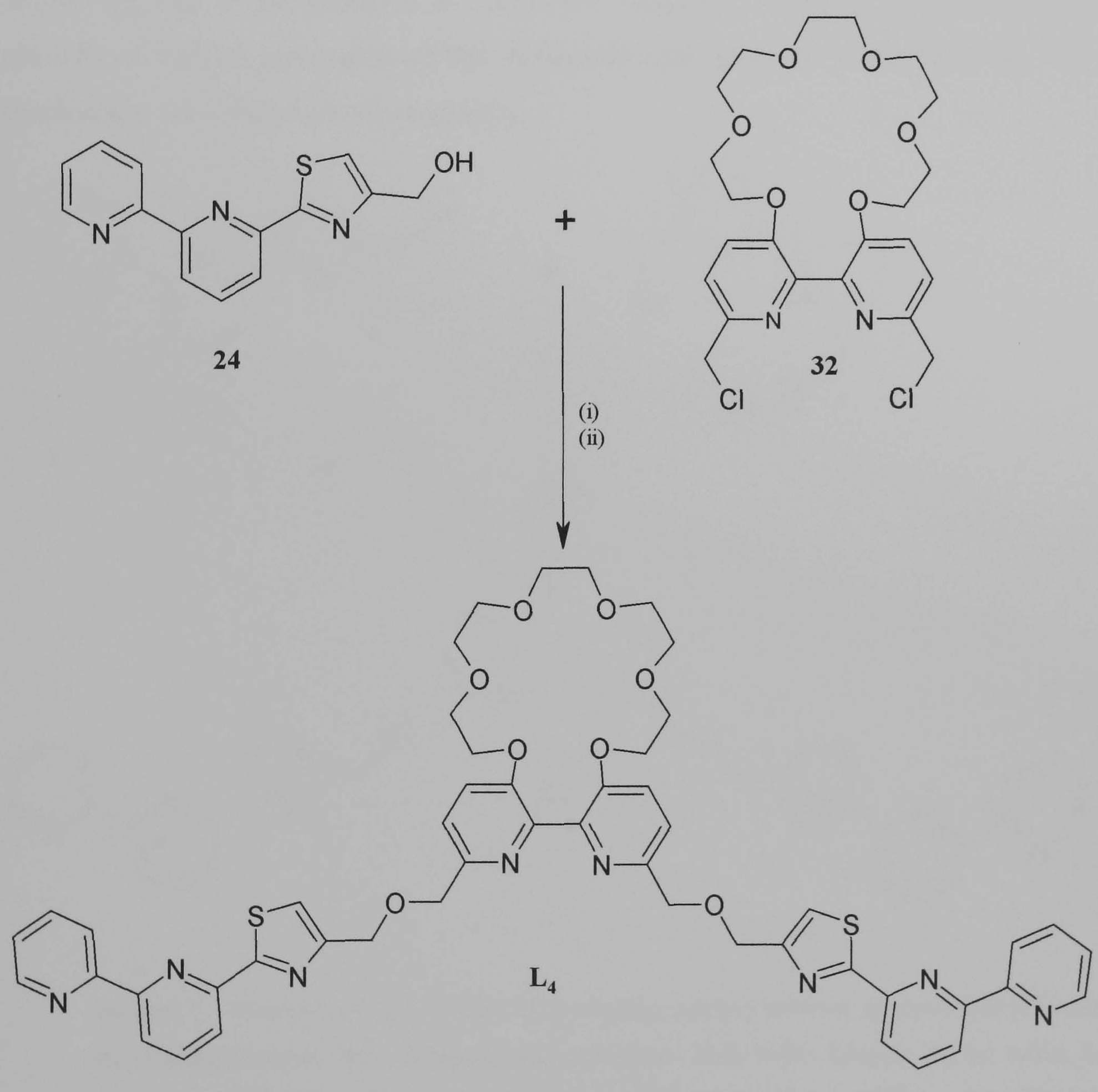

Scheme 6. Synthesis of the ligand $\mathbf{L_4}$ by means of a coupling reaction between py-py-tz-OH (**24**) and the dimethylchloride (**32**). Reagents and conditions: (i) (**24**), NaH, TBA-Br, N_2 (at reflux in anhydrous THF), (ii) addition of (**32**) (as a solution in anhydrous THF) to the refluxing solution of (i).

All compounds used in the synthesis of $\mathbf{L_4}$ were characterised using elemental analysis, mass spectroscopy and ^{1}H NMR (see experimental section).

4.1.2 Synthesis of $\boldsymbol{L_5}$

The synthesis of this ligand was achieved by the Williamson ether synthesis reaction between the previously synthesised tridentate unit (**24**) and the 2,2'-bipyridine-6,6'-dimethly dimethylchloride (**34**), outlined in Scheme 7, in a similar manner to the synthesis of $\mathbf{L_4}$. Deprotonation of the alcohol group of (**24**) using an excess of sodium hydride in the presence of a catalytic amount of TBA-Br, followed by the addition of half an equivalent of the dichloride (**34**) gave the final ligand $\mathbf{L_5}$ after purification via column chromatography.

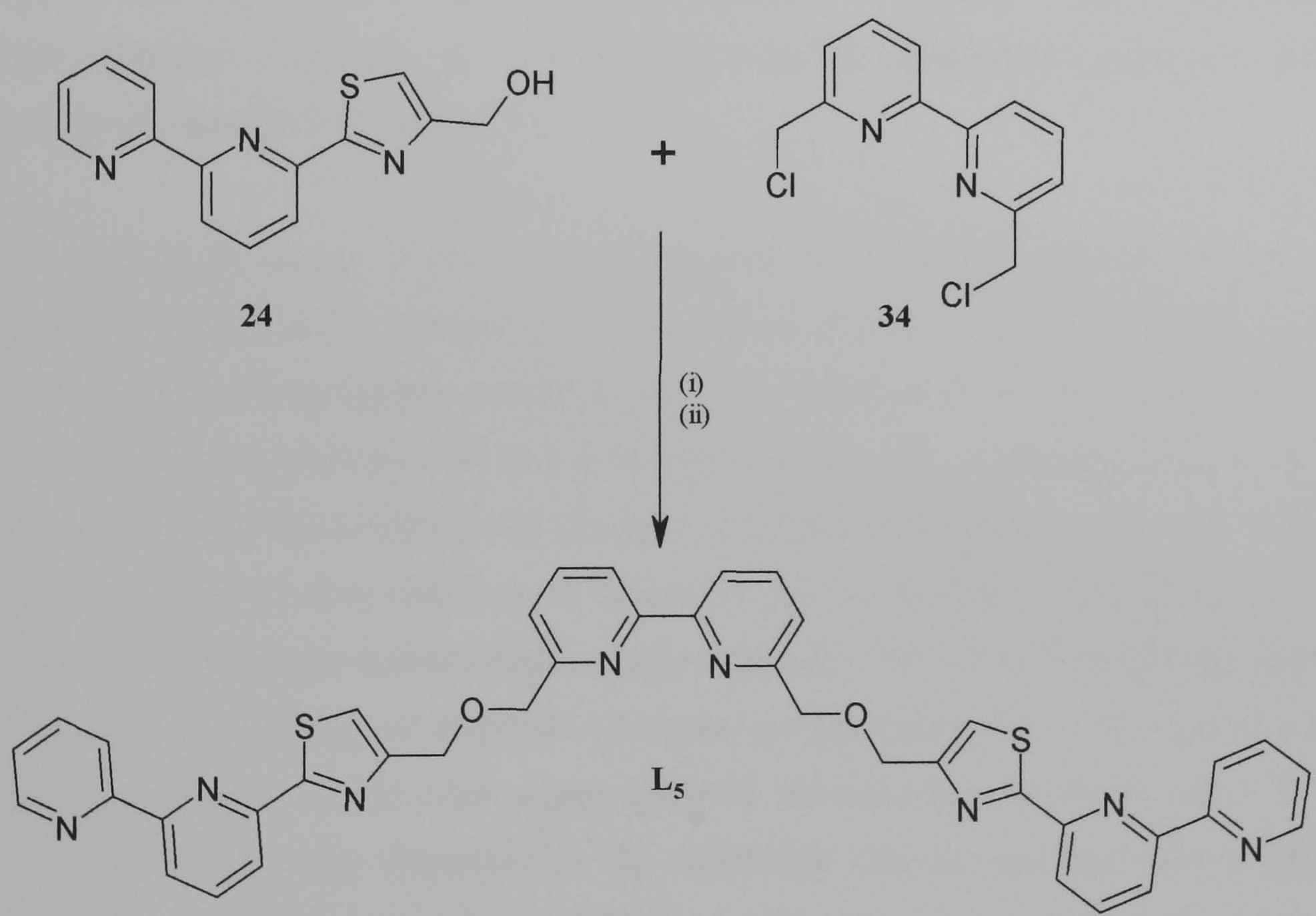

Scheme 7. Synthesis of $\mathbf{L_5}$ by means of a coupling reaction between py-py-tz-OH (**24**) and the dimethylchloride (**34**). Reagents and conditions: (**24**), NaH, TBA-Br, N_2 (at reflux in anhydrous THF), (ii) addition of (**34**) (as a solution in anhydrous THF) to the refluxing solution of (i).

All compounds used in the synthesis of $\mathbf{L_5}$ were characterised using elemental analysis, mass spectroscopy and ^{1}H NMR spectroscopy (see experimental section).

4.1.3 Synthesis of L_6

This novel ligand is very similar to L_4 as both ligands contain the same tridentate (py-py-tz) binding domains at the ends of the ligand chain. However, a subtle change has been made by the introduction of two thiazole rings, one either side of the central pyridyl-pyridyl bidentate domain seen in L_4. The introduction of such a group allows the central part of the ligand to partition into two bis-bidentate (py-tz) binding domains, in a similar manner to the recent example by Rice *et al.*,[105]

The synthesis of this ligand also uses a convergent synthesis technique like that seen in the formation of previous ligands. The synthesis of the tridentate unit (**24**) remains exactly the same, outlined earlier in Scheme 4, and the central bis-bidentate unit (outlined in Scheme 8) is synthesised from the dithioamide precursor (**16**), previously described in section 2.1.2.

Addition of an excess of ethyl 3-bromopyruvate to a refluxing solution of (**16**) in ethanol, resulted in the formation of large brown crystals of (**36**) on cooling. The disappearance of the signals corresponding to the dithioamide and the appearance of a triplet and a quartet at 1.45 and 4.48 ppm respectively, consistent with an ethyl group, confirms the complete conversion to the ester. Reduction of the ester to the alcohol of (**37**) by slow addition of lithium aluminium hydride at 0°C afforded the target compound in moderate yields of approximately 50%. The ^{1}H NMR spectrum reveals the appearance of singlet at 4.85 ppm corresponding to a $-CH_2-$ group and the disappearance of the ethyl signal confirms the formation of the alcohol. The alcohol (**37**) is easily converted to the dichloride (**38**) by reaction with thionyl chloride in DCM to give a white solid after purification. Conversion of the alcohol to the dichloride is accompanied by a change in the chemical shift for the $-CH_2-$ group from 4.85 to 4.68 ppm.

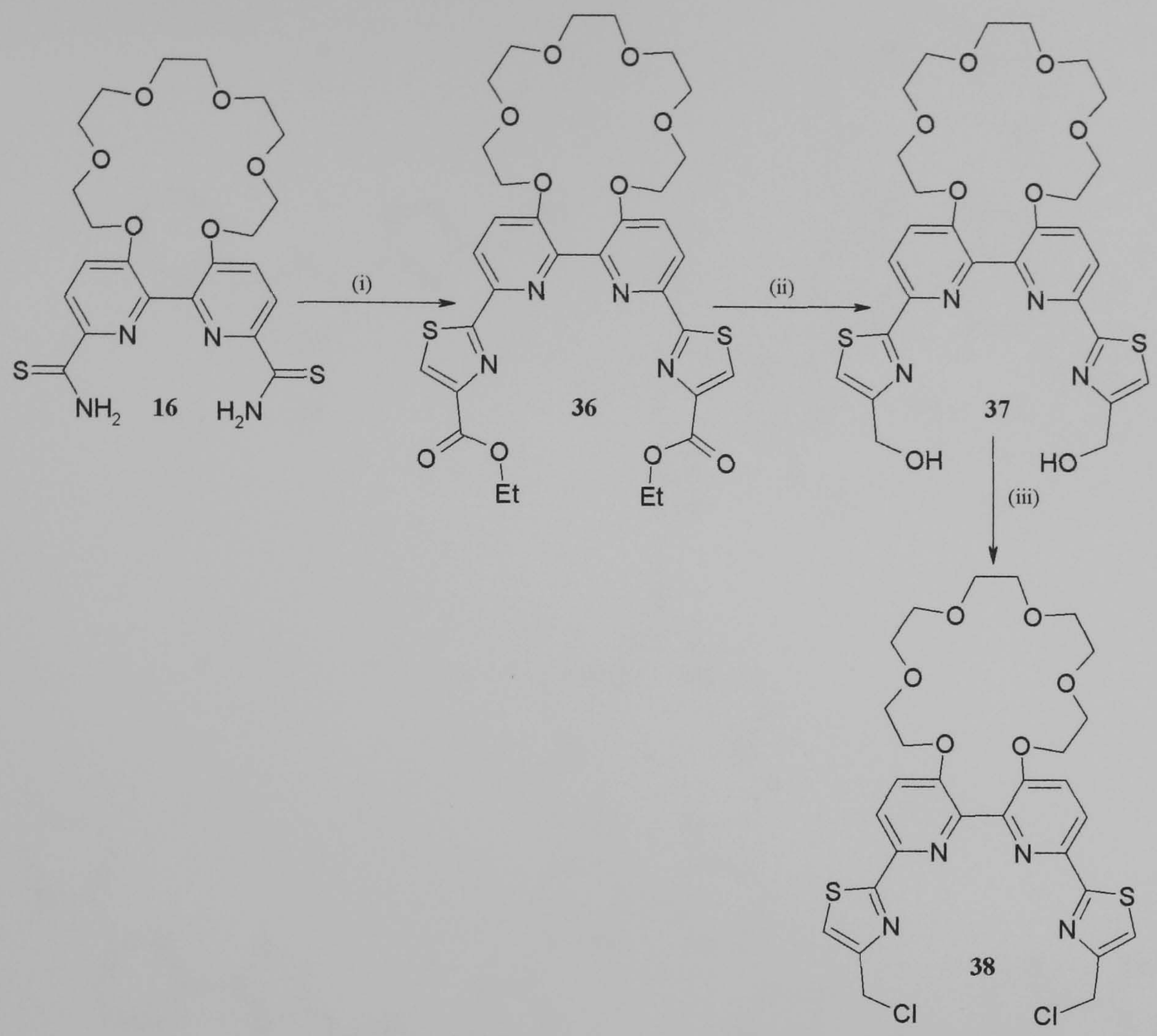

Scheme 8. Synthesis of compound (**38**) from the dithioamide (**16**). Reagents and conditions: (i) ethyl 3-bromopyruvate (at reflux in ethanol), (ii) $LiAlH_4$, 0°C, N_2, anhydrous THF, (iii) thionyl chloride (at reflux in DCM).

The formation of the ether spacers via the Williamson ether synthesis is outlined in Scheme 9. Deprotonation of the alcohol group of (**24**) using an excess of sodium hydride in the presence of a catalytic amount of TBA-Br, followed by the addition of half an equivalent of the dimethylchloride (**38**) gave the final ligand $\mathbf{L_6}$ after purification via column chromatography.

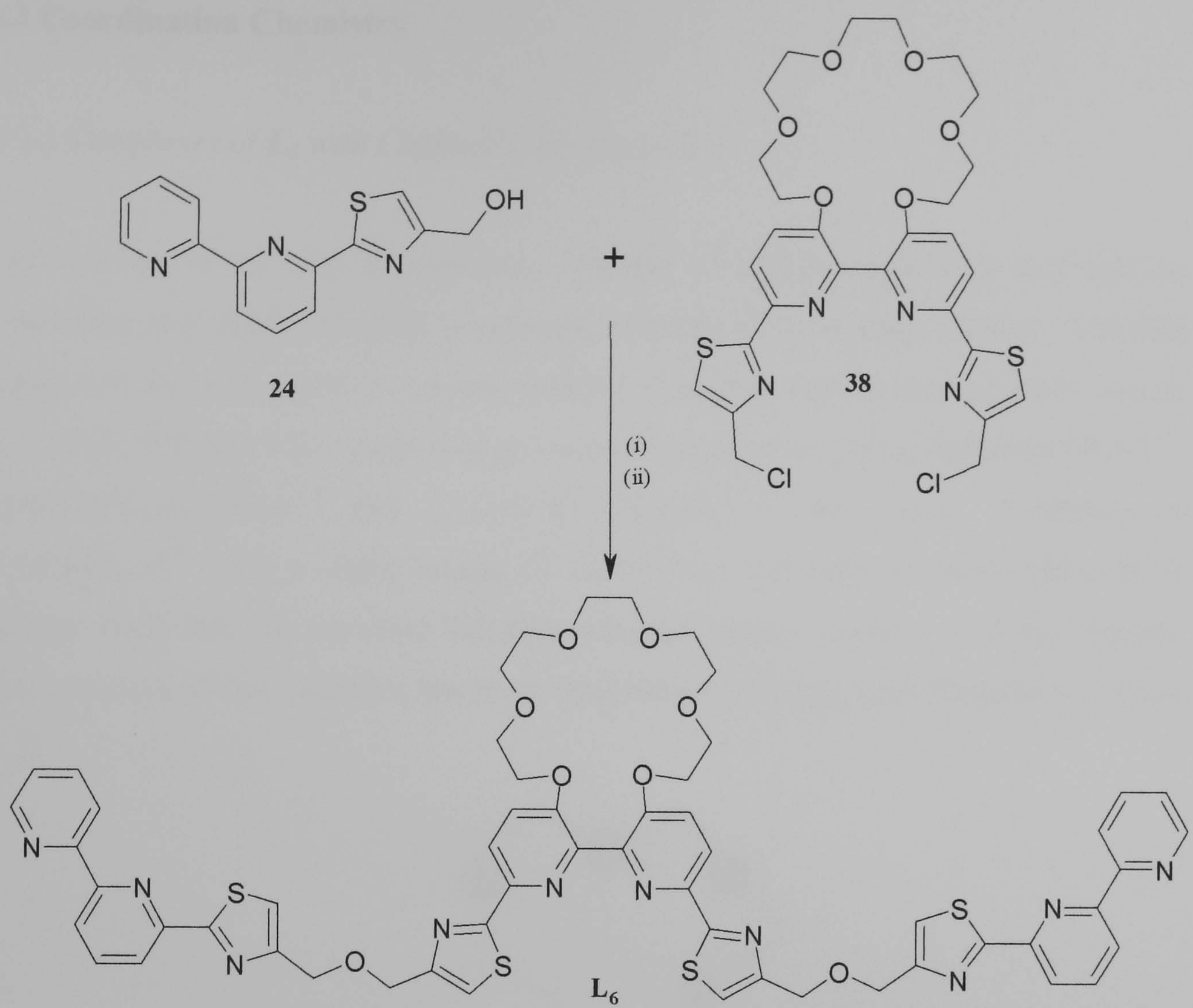

Scheme 9. Synthesis of the ligand $\mathbf{L_6}$ by means of a coupling reaction between the alcohol (**24**) and the dimethylchloride (**38**). Reagents and conditions: (i) (**24**), NaH, TBA-Br, N_2 (at reflux in anhydrous THF), (ii) addition of (**38**) (as a solution in anhydrous THF) to the refluxing solution of (i).

All compounds used in the synthesis of $\mathbf{L_6}$ were characterised using elemental analysis, mass spectroscopy and ^{1}H NMR (see experimental section).

4.2 Coordination Chemistry

4.2.1 Complexes of $\mathbf{L_4}$ *with Copper(I) and Zinc(II)*

The reaction of $\mathbf{L_4}$ with an equimolar amount of $[Zn(H_2O)_6](ClO_4)_2$ and half an equivalent of $[Cu(MeCN)_4]PF_6$ in acetonitrile produced an orange solution. ESI-MS confirmed the formation of a heterometallic trinuclear double helicate with ions at *m/z* 1273, 799 and 562 whose charge states correspond to $\{[Zn_2Cu(\mathbf{L_4})_2](ClO_4)_3\}^{2+}$, $\{[Zn_2Cu(\mathbf{L_4})_2](ClO_4)_2\}^{3+}$ and $\{[Zn_2Cu(\mathbf{L_4})_2](ClO_4)\}^{4+}$ respectively. Treatment of $[CuZn_2(\mathbf{L_4})_2]^{5+}$ with a slight excess of $TBA(ClO_4)$ followed by slow diffusion of diethyl ether into the resulting solution afforded orange crystals of X-ray quality. The structure of this complex has been established by X-ray crystallography (Figure 4.2).

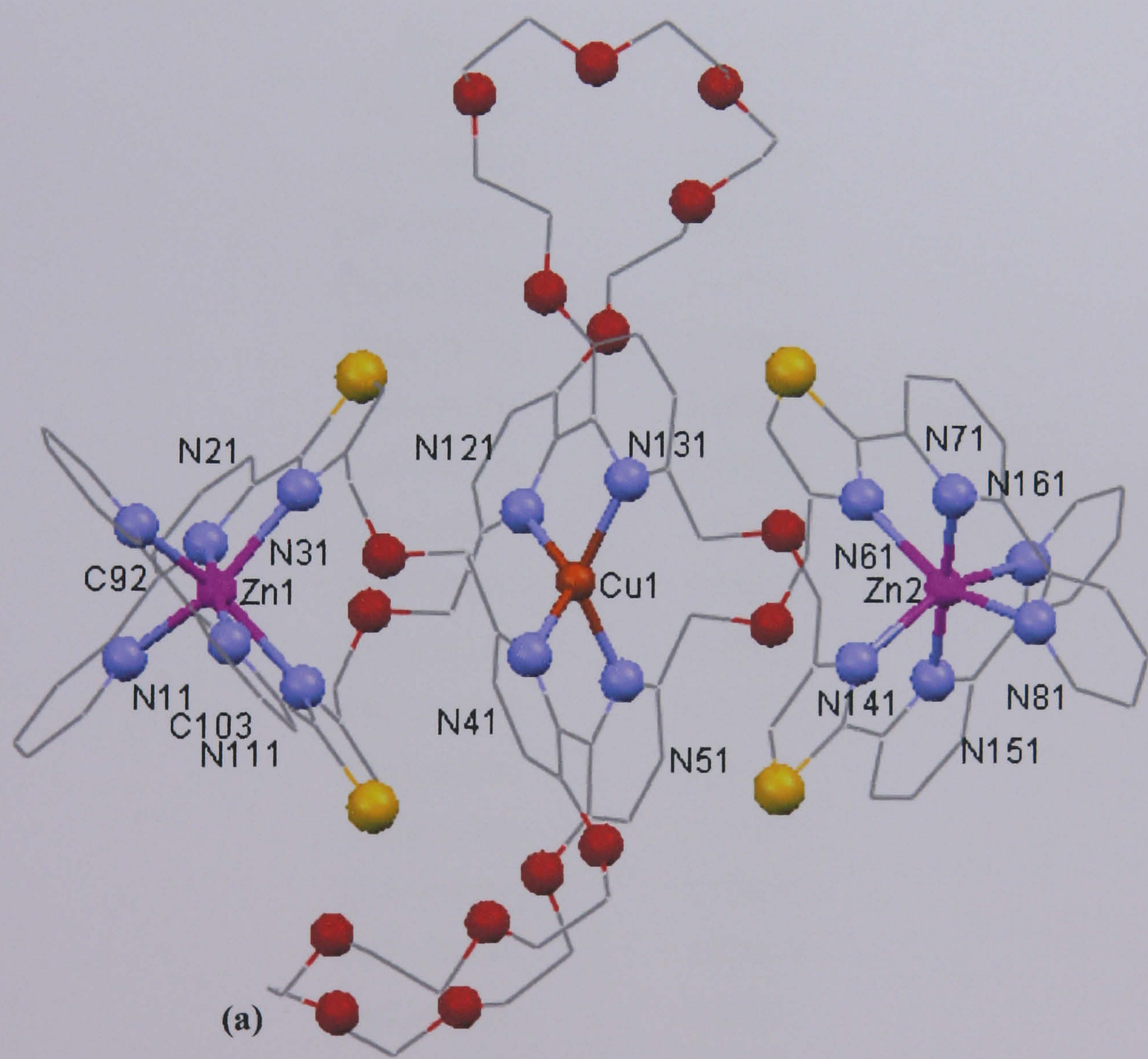

Figure 4.2(a). X-ray crystal structure of the complex cation $[CuZn_2(\mathbf{L_4})_2]^{5+}$ showing the structural framework.

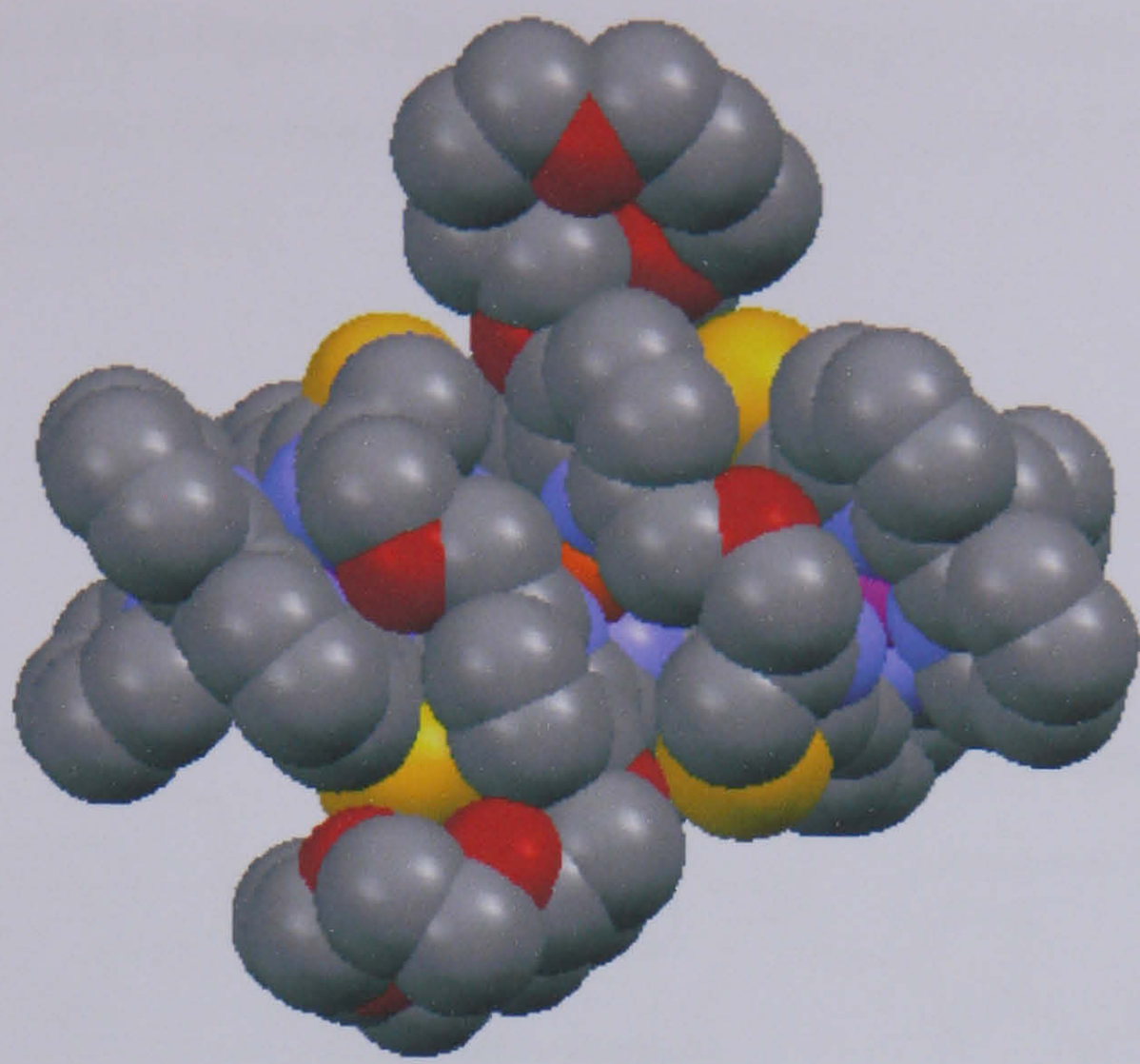

(b)

Figure 4.2(b). X-ray crystal structure of the complex cation $[CuZn_2(\mathbf{L_4})_2]^{5+}$ showing a space filling representation.

Bond	Bond Length Å
Cu(1)-N(41)	2.020(7)
Cu(1)-N(51)	2.030(7)
Cu(1)-N(121)	2.027(7)
Cu(1)-N(131)	2.043(6)
Zn(1)-N(11)	2.179(7)
Zn(1)-N(21)	2.086(7)
Zn(1)-N(31)	2.199(7)
Zn(1)-N(91)	2.183(8)
Zn(1)-N(101)	2.066(7)
Zn(1)-N(111)	2.255(7)
Zn(2)-N(61)	2.217(7)
Zn(2)-N(71)	2.081(7)
Zn(2)-N(81)	2.174(7)
Zn(2)-N(141)	2.228(7)
Zn(2)-N(151)	2.073(7)
Zn(2)-N(161)	2.201(7)
Zn(1)-Cu(1)	6.148(1)
Zn(2)-Cu(1)	6.356(1)

Table 7. Selected bond lengths (Å) for the complex $[CuZn_2(\mathbf{L_4})_2]^{5+}$.

The crystal structure of $\mathbf{L_4}$ (Figure 4.2a) shows that the ligand is naturally partitioned by the methylene spacers into two bis-tridentate and one central bidentate binding domains, outlined in Figure 4.3.

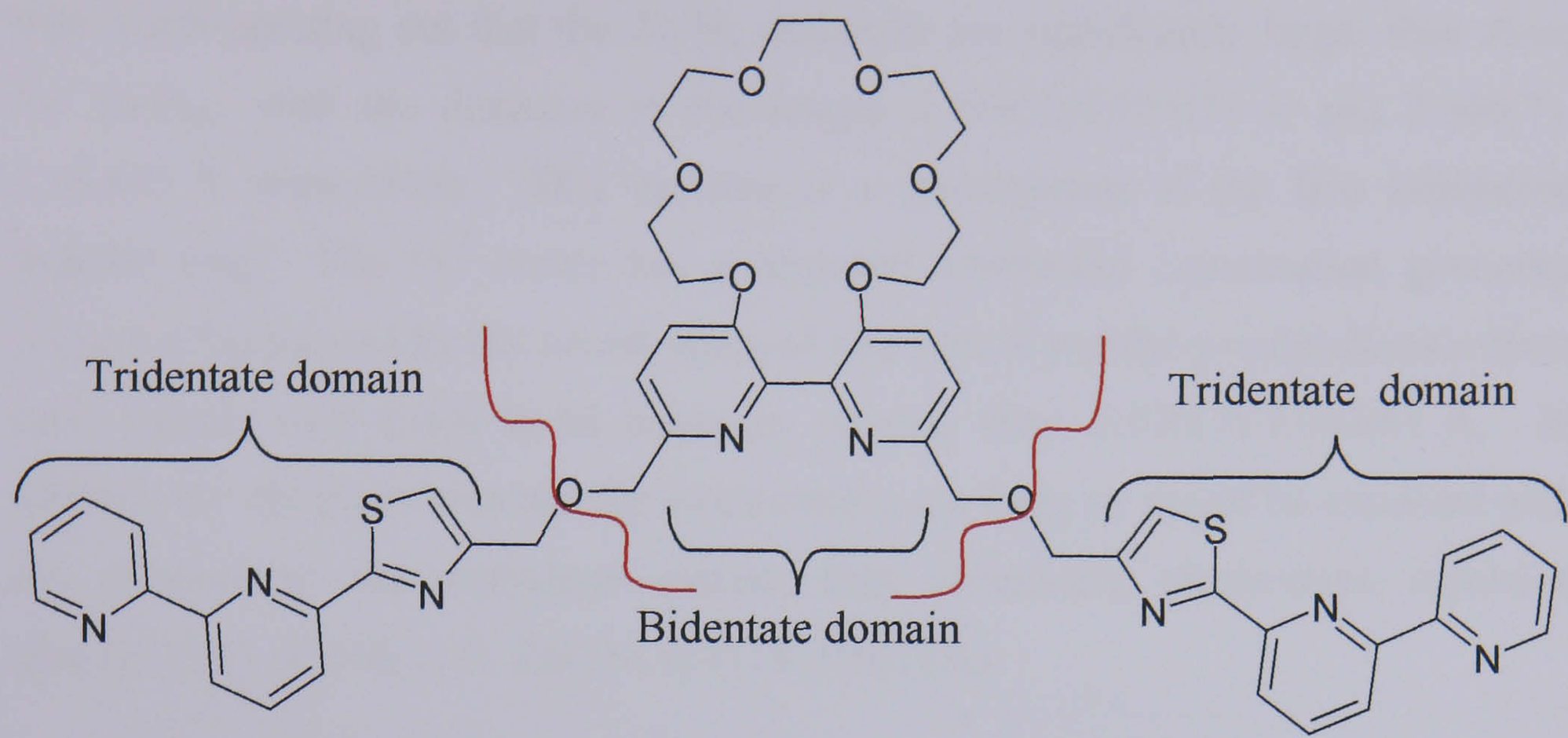

Figure 4.3. Structure of $\mathbf{L_4}$ showing the partitioning of the ligand into two bis-tridentate and one central bidentate binding domains.

In the crystal each ligand is coordinated by two Zn^{II} centres *via* two bis-tridentate binding domains comprising of pyridyl-pyridyl-thiazole units at each end of the ligand chain, in between the two Zn^{II} centres is a Cu^{I} centre coordinated by the central bidentate binding domain comprising of a pyridyl-pyridyl unit. The three metal centres are coordinated by two bridging ligands in a double helicate arrangement. Even though the central bidentate unit does act as a bidentate donor a substantial twist away from planarity is observed, with NCCN torsion angles of 33.41° and 30.56° (Figure 4.4). This twist is caused by unfavourable steric interactions between the subunits in the 3,3'-positions of the central bipyridyl unit.

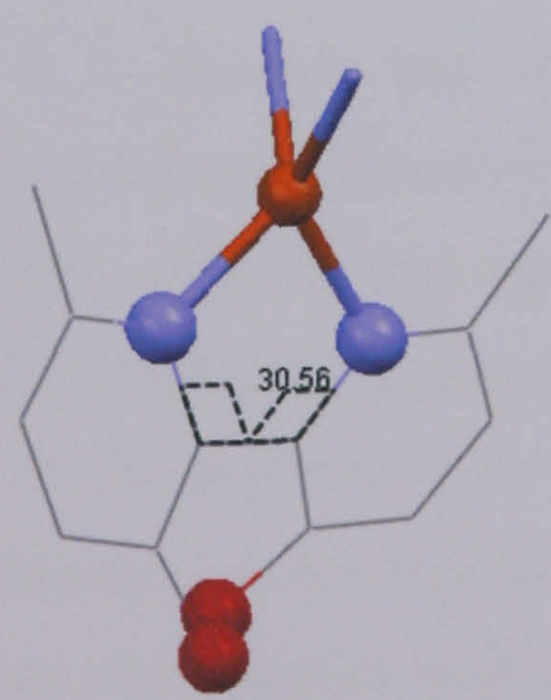

Figure 4.4. The central bipyridyl unit from the crystal structure of $\mathbf{L_4}$ showing the NCCN torsion angle of 30.56°.

Each of the Zn^{II} centres has a distorted octahedral coordination geometry (Figure 4.5b) formed by the coordination of one pyridyl-pyridyl-thiazole binding domain from each ligand, with Zn-N bond distances ranging from 2.066(7)-2.255(7) Å. It is also worth pointing out that the $Zn\text{-}N_{tz}$ distances are significantly larger than those for $Zn\text{-}N_{py}$, with the distances in the ranges 2.199(7)-2.255(7) Å and 2.066(7)-2.183(8) Å respectively. This increase is a consequence of the five membered thiazole ring. The Cu^{I} centre has a distorted tetrahedral coordination geometry (Figure 4.5a) formed by the coordination of one central pyridyl-pyridyl domain from each ligand, with Cu-N bond distances ranging from 2.020(7)-2.043(6) Å. In addition the distances between the metal centres are large as would be expected with the presence of the methylene spacers, thus minimising electrostatic repulsion (Zn(1)-Cu(1) : 6.148(1) Å, Zn(2)-Cu(1) : 6.356(1) Å).

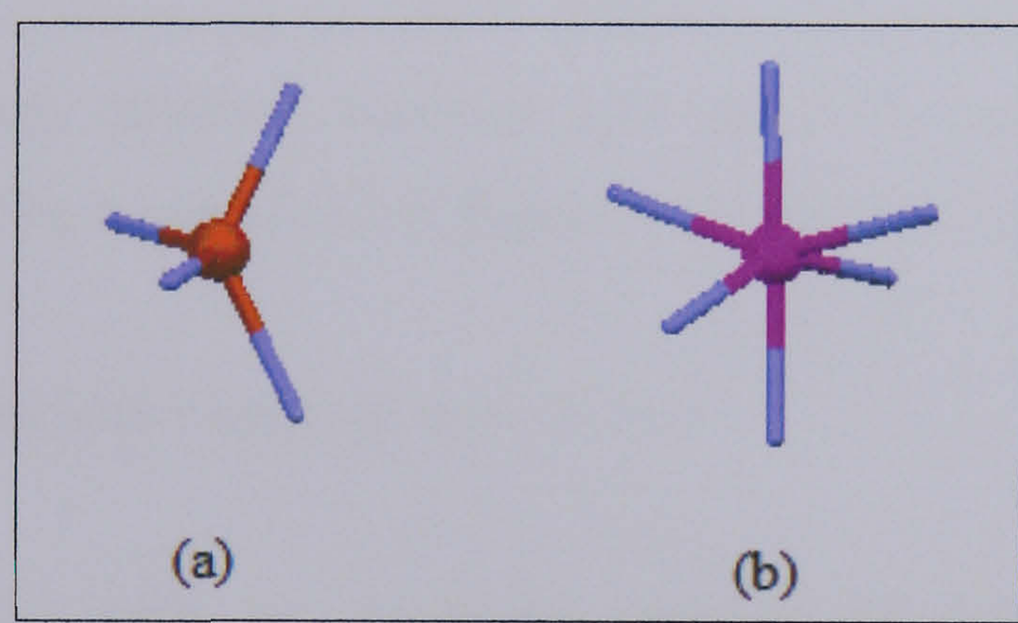

Figure 4.5. Part of the crystal structure of $\mathbf{L_4}$ showing (a) the distorted tetrahedral and (b) octahedral metal centres.

Due to the isoelectronic nature of the Cu^{I} and Zn^{II} transition metal cations, differentiation between the two metal ions is rather difficult through the X-ray crystallographic data. Thus it is possible that the complexes $[Zn_3(\mathbf{L_4})_2]^{6+}$ or $[ZnCu_2(\mathbf{L_4})_2]^{5+}$ are present in the solid state. However, as Cu^{I} ions favour tetrahedral coordination geometry it is highly unlikely that the terminal tridentate units are coordinated by Cu^{I} ions, thus discounting the presence of the homometallic copper species $[Cu_3(\mathbf{L_4})_2]^{3+}$. Furthermore the presence of the homometallic zinc species can also be ruled out as five perchlorate counter ions are observed within the crystal structure, suggesting the presence of a complex with a 5+ charge, this together with the ESI-MS data strongly supports the presence of the heterometallic complex $[Zn_2Cu(\mathbf{L_4})_2]^{5+}$.

4.2.2 Complexes of $\mathbf{L_5}$ *with Copper(I) and Zinc(II)*

The reaction of $\mathbf{L_5}$ with an equimolar amount of $[Zn(H_2O)_6](ClO_4)_2$ and half an equivalent of $[Cu(MeCN)_4]PF_6$ in acetonitrile produced an orange solution. As the ligand contains identical binding domains to $\mathbf{L_4}$ it would be expected that this ligand would behave in a similar manner. Thus the terminal tridentate domains will react with zinc(II) ions and the central bidentate domain will react with copper(I) ions in a double helical arrangement. ESI-MS confirmed the formation of a heterometallic trinuclear double helicate with ions at *m/z* 964, 610 and 432 corresponding to $\{[Zn_2Cu(\mathbf{L_5})_2](ClO_4)_3\}^{2+}$, $\{[Zn_2Cu(\mathbf{L_5})_2](ClO_4)_2\}^{3+}$ and $\{[Zn_2Cu(\mathbf{L_5})_2](ClO_4)\}^{4+}$ respectively. As would be totally expected the absence of the crown ether unit has no effect on the ability of $\mathbf{L_5}$ to form a heterometallic trinuclear double helicate. The ^1H NMR (CD_3CN) also supports the formation of this helicate species with twenty two aromatic signals occurring in eleven different environments between 7.0 and 8.75 ppm and signals observed between 3.25 and 3.70 ppm correspond to the methylene protons (See section 3.3.2.1, Figure 4.13a, for the ^1H NMR spectrum).

4.2.3 Complexes of $\mathbf{L_6}$ *with Copper(I) and Zinc(II)*

The reaction of $\mathbf{L_6}$ with an equimolar amount of $[Zn(H_2O)_6](ClO_4)_2$ and $[Cu(MeCN)_4]PF_6$ in acetonitrile produced an orange solution. ESI-MS confirmed the formation of a heterometallic tetranuclear double helicate with an ions at *m/z* 1542, 979 and 698 whose charge states correspond to $\{[Zn_2Cu_2(\mathbf{L_6})_2](ClO_4)_4\}^{2+}$, $\{[Zn_2Cu_2(\mathbf{L_6})_2](ClO_4)_3\}^{3+}$ and $\{[Zn_2Cu_2(\mathbf{L_6})_2](ClO_4)_2\}^{4+}$ respectively. Treatment of $[Cu_2Zn_2(\mathbf{L_6})_2]^{6+}$ with a slight excess of $TBA(ClO_4)$ followed by slow diffusion of diethyl ether into the resulting solution afforded orange crystals of X-ray quality. The structure of this complex has been established by X-ray crystallography (Figure 4.6).

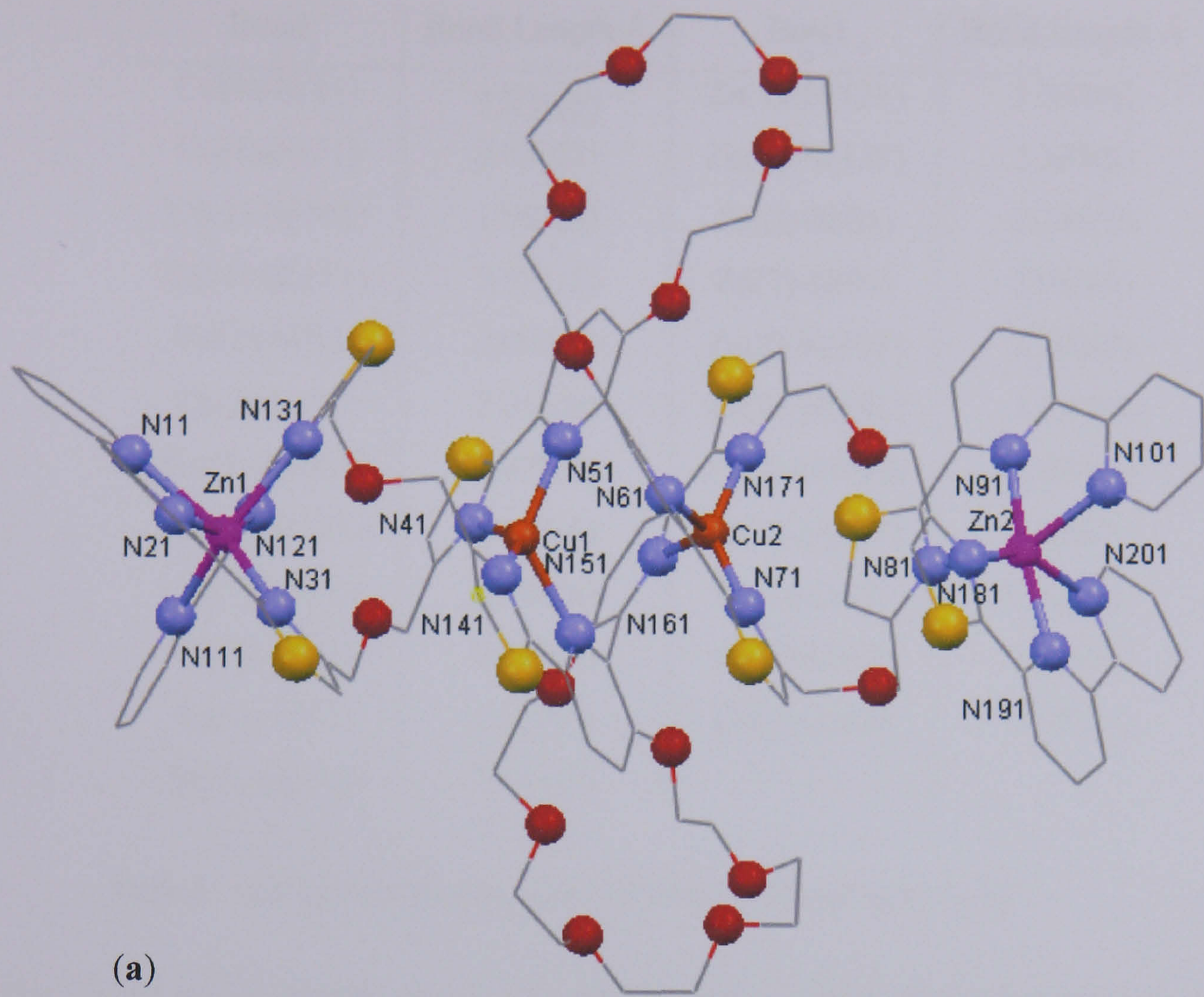

(a)

Figure 4.6(a). X-ray crystal structure of the complex cation $[Cu_2Zn_2(\mathbf{L_6})_2]^{6+}$ showing the structural framework.

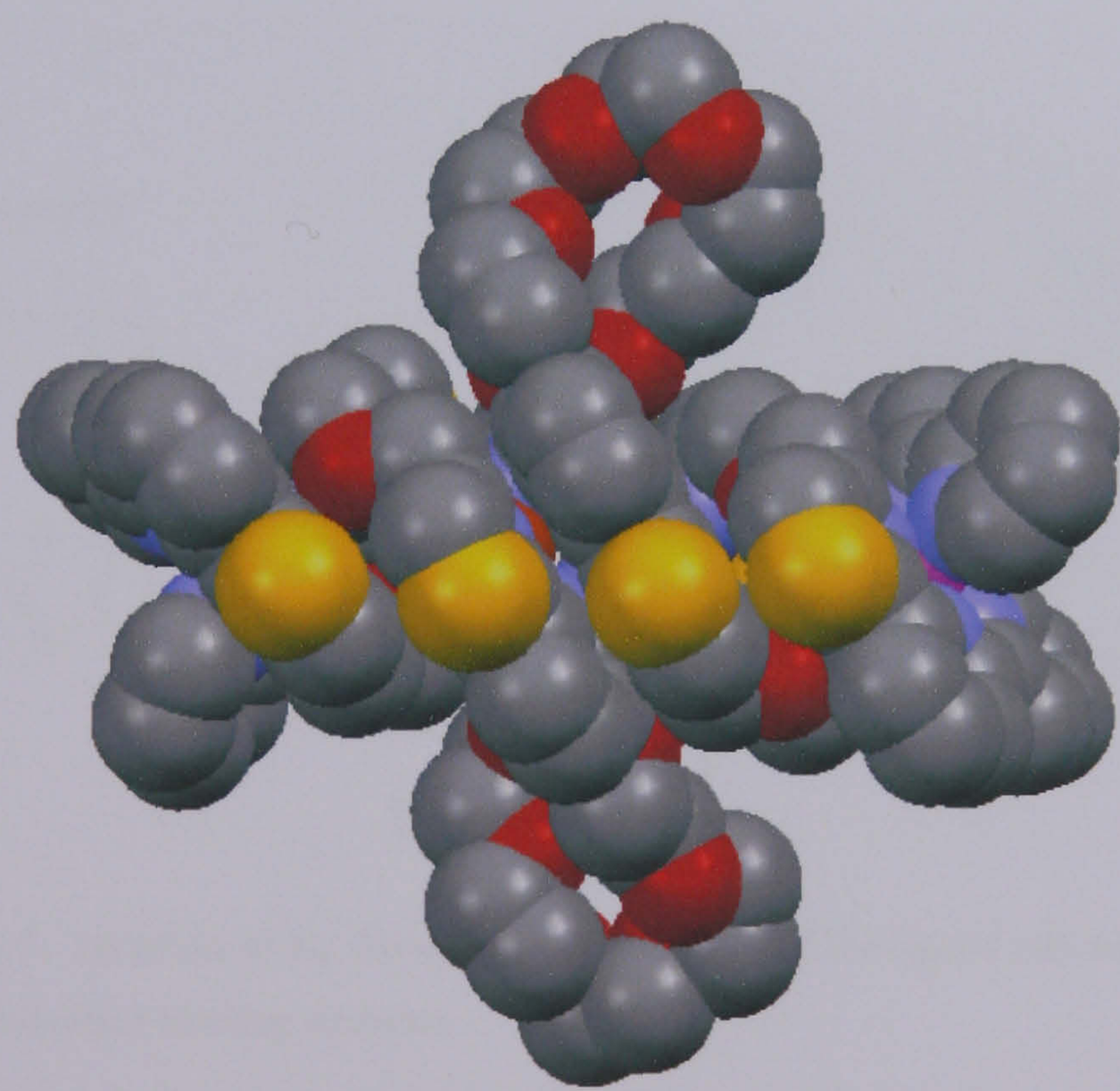

(b)

Figure 4.6(b). X-ray crystal structure of the complex cation $[Cu_2Zn_2(\mathbf{L_6})_2]^{6+}$ showing the space filling representation.

Bond	Bond Length Å	Bond	Bond Length Å
Cu(1)-N(41)	2.031(5)	Zn(1)-N(121)	2.038(6)
Cu(1)-N(51)	2.060(5)	Zn(1)-N(131)	2.339(6)
Cu(1)-N(141)	1.982(5)	Zn(2)-N(81)	2.185(5)
Cu(1)-N(151)	2.095(5)	Zn(2)-N(91)	2.080(6)
Cu(2)-N(61)	2.097(5)	Zn(2)-N(101)	2.182(6)
Cu(2)-N(71)	2.016(6)	Zn(2)-N(181)	2.190(6)
Cu(2)-N(161)	2.078(5)	Zn(2)-N(191)	2.095(6)
Cu(2)-N(171)	2.033(6)	Zn(2)-N(201)	2.205(7)
Zn(1)-N(11)	2.348(6)	Zn(1)-Cu(1)	5.622(1)
Zn(1)-N(21)	2.079(6)	Cu(1)-Cu(2)	3.608(1)
Zn(1)-N(31)	2.127(7)	Cu(2)-Zn(2)	5.982(1)
Zn(1)-N(111)	2.151(7)		

Table 8. Selected bond lengths (Å) for the complex cation $[Cu_2Zn_2(\mathbf{L_6})_2]^{6+}$.

The crystal structure of $\mathbf{L_6}$ shows that the ligand is naturally partitioned by the ether linkages into two bis-tridentate and two bis-bidentate binding domains, outlined in Figure 4.7.

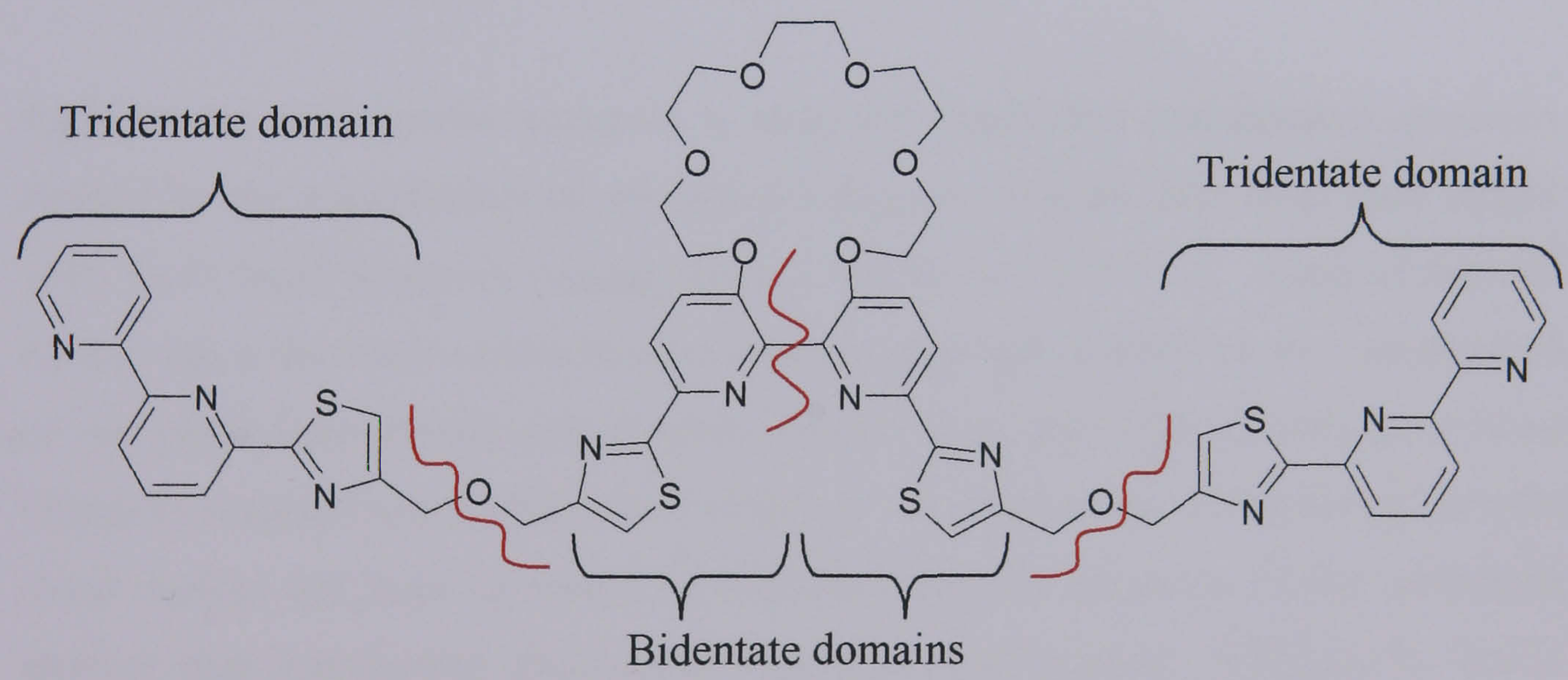

Figure 4.7. Structure of $\mathbf{L_6}$ showing the partitioning of the ligand into two bis-tridentate and two bis-bidentate binding domains.

In a similar manner to $\mathbf{L_4}$ the ligand $\mathbf{L_6}$ coordinates two zinc(II) ions via both of the two terminal bis-tridentate (py-py-tz) domains. However the central, potentially tetradentate unit, partitions into two separate bidentate (py-tz) domains each of which

coordinates a copper(I) ion. The formation of these two bidentate domains is a consequence of the oxygen atoms in the 3,3'-positions on the central bipyridine core, which due to unfavourable steric interactions prevents the ligand from adopting a planar conformation. This causes the central binding domain of the ligand to split into two bidentate pyridyl-thiazole donor units. This can be clearly seen in the torsion angle formed by the NCCN unit which is significantly more twisted about the central bond between the two pyridyl rings than that seen in $\mathbf{L_4}$. Where $\mathbf{L_4}$ is has NCCN torsion angles of 33.41° and 30.56°, $\mathbf{L_6}$ has NCCN torsion angles of 58.62° and 57.86° (Figure 4.8).

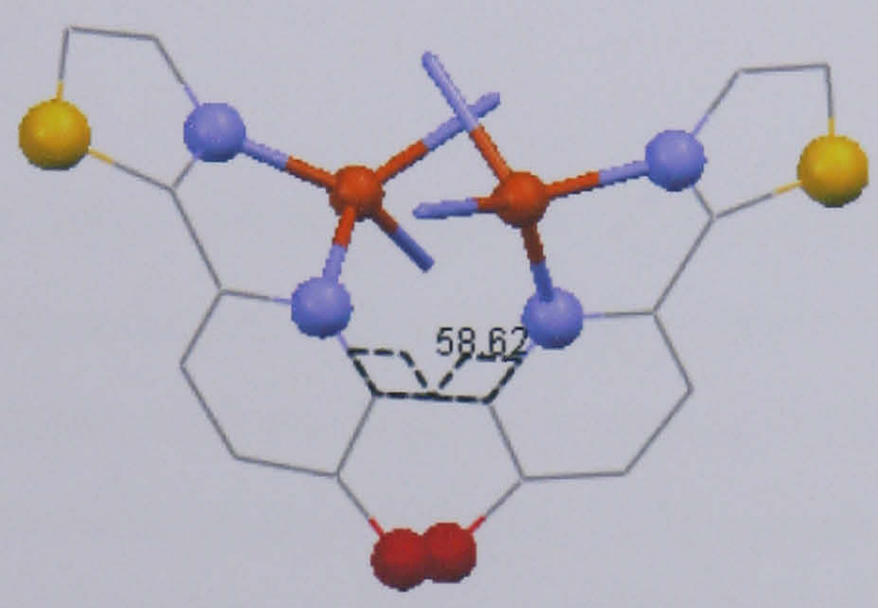

Figure 4.8. The central bipyridyl unit from the crystal structure of $\mathbf{L_6}$ showing the NCCN torsion angle of 58.62°.

Each of the Cu^I centres occupies a distorted tetrahedral coordination geometry formed by the coordination of one pyridyl-thiazole N-donor unit from each ligand, with Cu-N bond distances ranging from 1.982(5) to 2.097(5) Å. Each of the Zn^{II} centres has a distorted octahedral coordination geometry formed by the coordination of one pyridyl-pyridyl-thiazole binding domain from each ligand, with Zn-N bond distances ranging from 2.038(6) to 2.348(6) Å. In addition the distances between the metal centres are large as would be expected with the presence of the methylene spacers, thus minimising electrostatic repulsion (Zn(1)-Cu(1) : 5.622(1) Å, Cu(1)-Cu(2) : 3.608(1) Å, Cu(2)-Zn(2) : 5.982(1) Å).

As with the heterometallic trinuclear helicate it is difficult to distinguish between Cu^I and Zn^{II} ions though X-ray crystallographic date alone, due to their isoelectronic nature. Although the crystal structure confirmed the presence of one complex cation $[Zn_2Cu_2(\mathbf{L_6})_2]^{6+}$ and six interstitial perchlorate counter anions, the anions are very

disordered and several residual peaks in the electron density map were assigned and satisfactorily refined as an additional ca. 0.5 site-occupancy perchlorate moiety. The presence of such may be due to a small amount of ClO_4H co-crystallate, or an indication that the bis-bidentate copper(I) sites are occasionally occupied by a Zn^{II} dication. Regardless of these observations no homometallic zinc helicate species was observed in the ESI-MS, suggesting the major species present is the heterometallic helicate $[Zn_2Cu_2(\mathbf{L_6})_2]^{6+}$.

4.3 ^{1}H NMR Studies

4.3.1 Complexes with $\boldsymbol{L_4}$

The 500 MHz ^{1}H NMR spectrum (Figure 4.9) of the crystals of $[CuZn_2(\mathbf{L_4})_2]^{5+}$ in CD_3CN shows twenty aromatic protons occurring in ten environments between 6.8 and 8.7 ppm. This confirms that the ligand is symmetrical, as would be expected upon formation of a trinuclear double helicate. The crown ether protons occur as their usual multiplets between 3.6-4.7 ppm and the protons for the methylene spacers occur as sharp doublets between 2.9-3.6 ppm. Assignment of the aromatic protons was aided by the ^{1}H/^{1}H COSY spectrum (Figure 4.10).

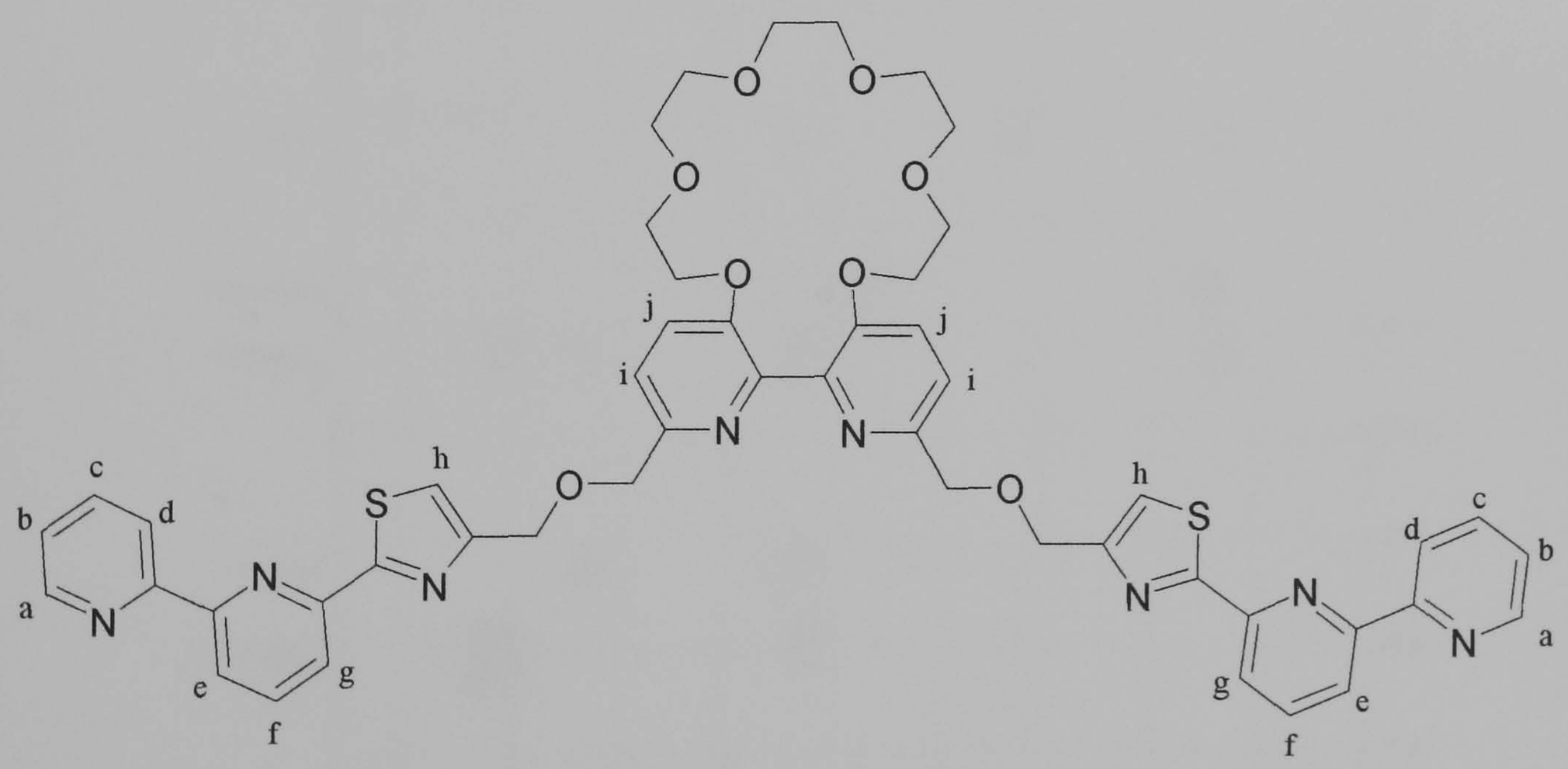

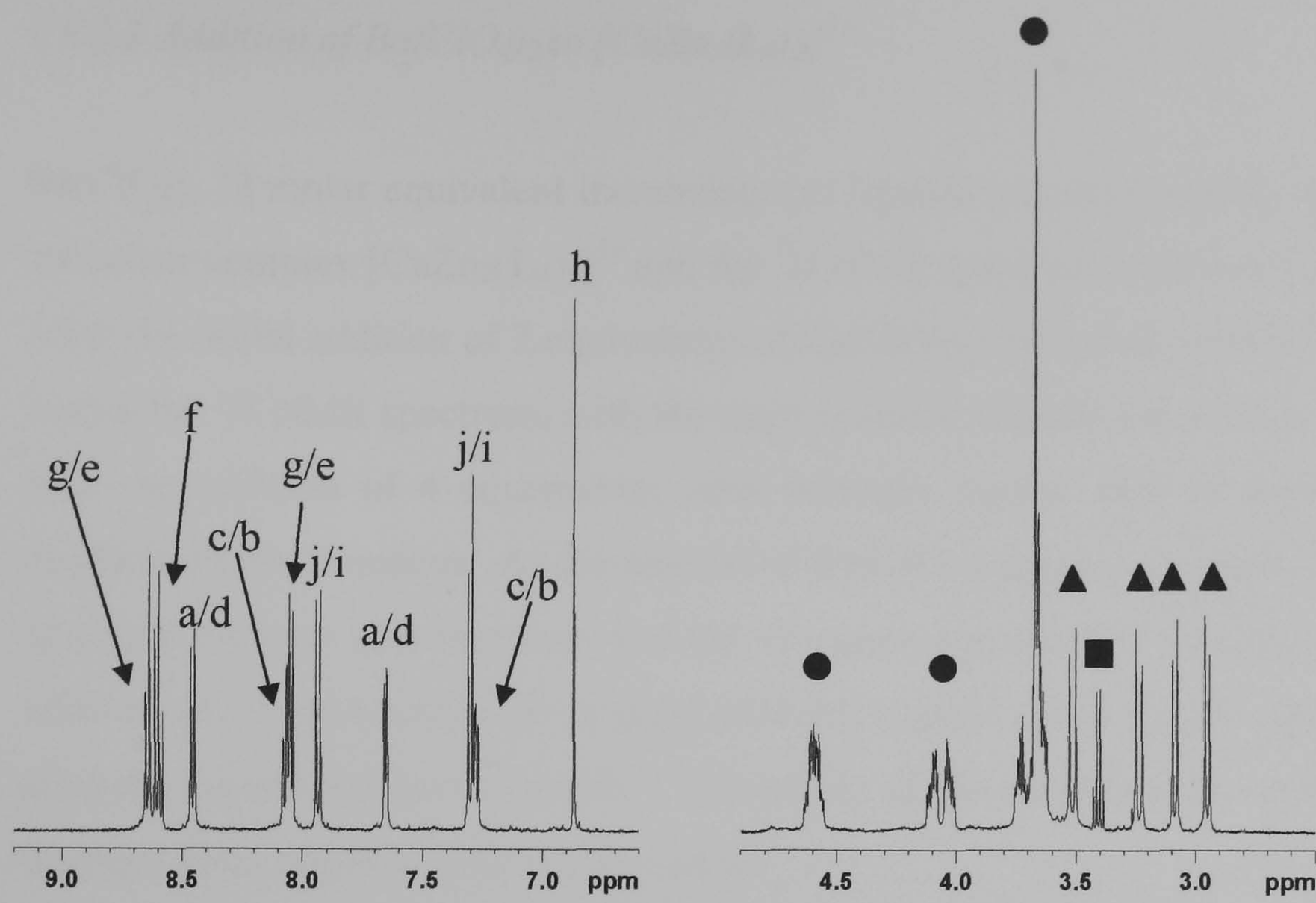

Figure 4.9. Selected regions of the ^{1}H NMR spectrum of $[CuZn_2(\mathbf{L}_4)_2]^{5+}$. ● corresponds to the crown ether signals, ▲ corresponds to methylene signals and ■ correspond to diethyl ether solvent impurity.

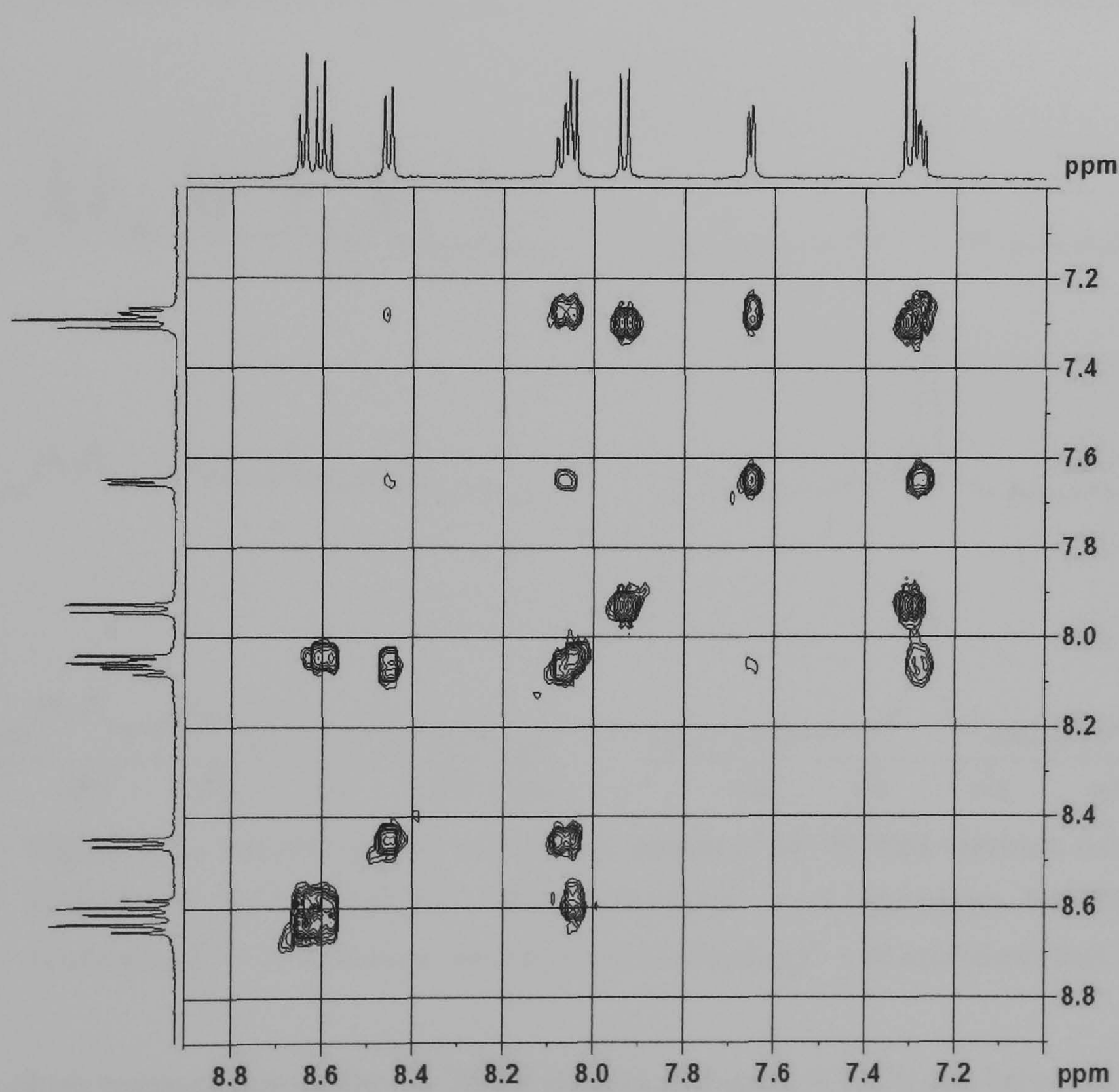

Figure 4.10. Aromatic region from the $^{1}H/^{1}H$ COSY spectrum of $[CuZn_2(\mathbf{L}_4)_2]^{5+}$ recorded in CD_3CN.

4.3.1.1 Addition of $Ba(ClO_4)_2$ to $[CuZn_2(\mathbf{L_4})_2]^{5+}$

$Ba(ClO_4)_2$ (2 molar equivalent increments per ligand) was successively added to the trinuclear complex $[CuZn_2(\mathbf{L_4})_2]^{5+}$ and the ^1H NMR spectrum recorded (Figure 4.11). After the initial addition of 2 equivalents of $Ba(ClO_4)_2$, very little change is observed within the ^1H NMR spectrum, with the main aromatic signals still present. However, after the addition of 4 equivalents, new aromatic signals start to appear and the aliphatic region broadens. As the amount of $Ba(ClO_4)_2$ present increases, the number of signals present also increases and the spectrum significantly broadens. After the addition of 10 equivalents, the original aromatic signals are no longer present and the aliphatic signals are barely visible. The colour of the sample at this point has also changed from bright orange to pale yellow.

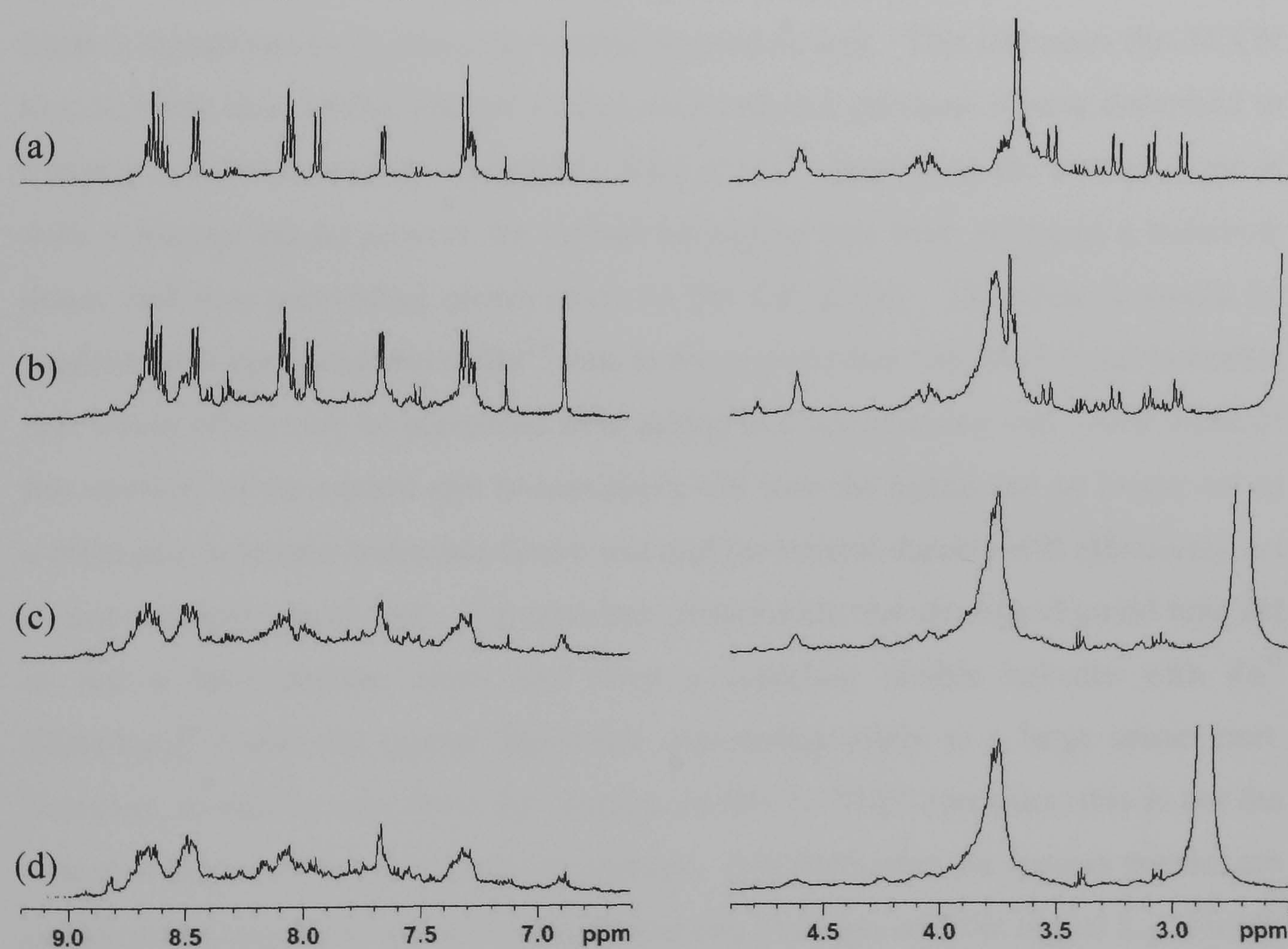

Figure 4.11. Selected aromatic and aliphatic regions of the ^1H NMR spectrum, recorded in CD_3CN, of (a) $[CuZn_2(\mathbf{L_4})_2]^{5+}$, (b) $[CuZn_2(\mathbf{L_4})_2]^{5+}$ + 4 equivalents $Ba(ClO_4)_2$, (c) $[CuZn_2(\mathbf{L_4})_2]^{5+}$ + 10 equivalents $Ba(ClO_4)_2$, (d) $[CuZn_2(\mathbf{L_4})_2]^{5+}$ + 20 equivalents $Ba(ClO_4)_2$.

Upon close examination of the ^1H NMR spectra in Figure 4.11, it can be seen that the spectrum changes dramatically upon addition of Ba^{2+} ions to $[CuZn_2(\mathbf{L_4})_2]^{5+}$. The signals corresponding to the complex $[CuZn_2(\mathbf{L_4})_2]^{5+}$ (Figure 4.11a) gradually

disappear as the amount of Ba^{2+} ions present increases. After the addition of 20 equivalents of Ba^{2+} ions the ^1H NMR spectrum (Figure 4.11d) becomes very disordered, with the original peaks no longer distinguishable and the peaks that are present becoming significantly broadened. It can therefore be concluded from the ^1H NMR changes that in the presence of Ba^{2+} ions the original helicate $[CuZn_2(\mathbf{L_4})_2]^{5+}$ is no longer present. This is also supported by the ESI-MS, as the original ion at *m/z* 1273 corresponding to $\{[Zn_2Cu(\mathbf{L_4})_2](ClO_4)_3\}^{2+}$, is no longer observed following addition of Ba^{2+} ions. Thus, after addition of such an excess of Ba^{2+} ions, the complex does not result in the formation of a new *singular* species but results in the formation of a large number of different species.

It would be expected that coordination of Ba^{2+} ions to the crown ether unit would cause a significant twist about the central bipyridine unit. This increases the NCCN torsion angle in a similar manner to that observed in a previous system described in Chapter 2 and that recently reported by Rice *et al.*,[98] Increasing the torsion angle in such a manner would prevent the central bipyridine unit from acting as a bidentate donor and thus preventing coordination to the Cu^I centre. Therefore it would be expected that upon addition of Ba^{2+} ions to the crown ether unit, the central bidentate unit would effectively be prevented from acting as a coordinating unit. As a result of this inability of the central unit to coordinate Cu^I ions the ligand can no longer act as a tridentate-bidentate-tridentate donor unit and the central domain will effectively act as just a simple spacer unit. It is therefore conceivable that the ligand could now act as just a bis-tridentate donor and form a dinuclear double helicate with Zn^{II} ($[Zn_2(\mathbf{L_4})_2]^{4+}$) with the central bipyridine unit acting solely as a large spacer unit. However, as can be seen from the changes in the ^1H NMR spectrum, this is not the case as a large number of species are present. It is likely that the species present are coordination oligomers and polymers containing zinc ions and the ligand $\mathbf{L_4}$. This is supported to some extent by the ^1H NMR as the signals corresponding to the tridentate unit are still observed but now as broad multiplets at roughly the same chemical shifts as the helicate species. This indicates that this unit is still coordinated to the zinc ions but in many different environments. The inability of a ligand of this type, *i.e.* two coordination domains separated by a large space unit, to form helicates has been observed previously by Cohen *et al.*,[49] Here the binding domains of a bis-bidentate ligand are separated by a bridging biphenyl group acting

as a large spacer unit (similar to the deprogrammed unit in $\mathbf{L_4}$). Reaction of this bis-bidentate ligand with Cu^I ions does not result in a single transition metal helicate but produces a number of different complexes. This demonstrates that some ligands, where a large spacer unit separates the binding domains, are insufficiently "programmed" to act as helicating ligands.

In conclusion, $\mathbf{L_4}$ reacts with Zn^{II} and Cu^I ions to form a trinuclear double helicate. Addition of Ba^{2+} ions to this species prevents the central bipyridine unit from coordinating Cu^I ions and results in the formation of coordination polymers of the type $[(\mathbf{L_4})ZnBa]_n$. Consequently the ligand, which is initially programmed to form a trinuclear double helicate, now has insufficient programming to form a helicate and has correspondingly been "*deprogrammed*". The disassembly of the helicate species is outlined by means of a cartoon in Figure 4.12.

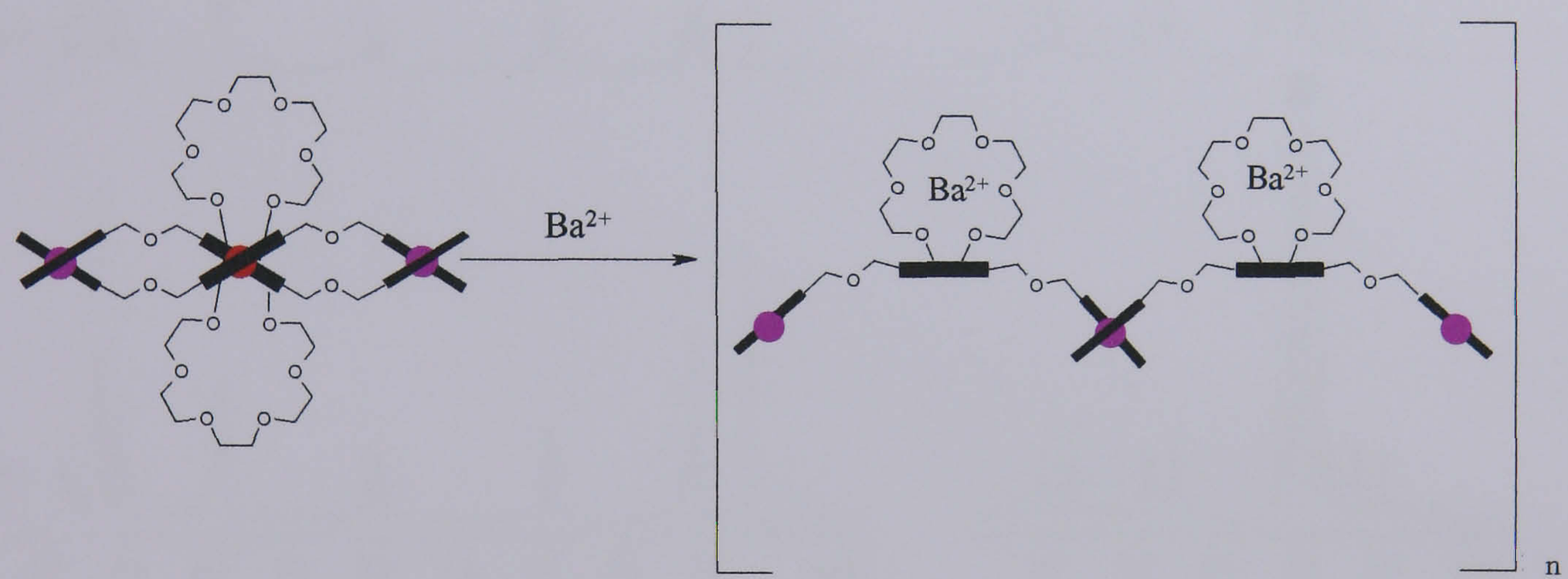

Figure 4.12 Cartoon representation of the deprogramming of the $\mathbf{L_4}$ helicate species upon addition of Ba^{2+} ions, which leads to the formation of a series of coordination polymers.

4.3.2 Complexes with $\boldsymbol{L_5}$

The 400 MHz ^1H NMR spectrum (Figure 4.13a) of the crystals of $[CuZn_2(\mathbf{L_5})_2]^{5+}$ in CD_3CN shows twenty two aromatic protons occurring in eleven environments between 7.0 and 8.80 ppm. This confirms that the ligand is symmetrical, as would be expected upon formation of a trinuclear double helicate. The protons for the methylene spacers occur as their usual sharp doublets between 3.25 and 3.70 ppm.

4.3.2.1 Addition of $Ba(ClO_4)_2$ to $[CuZn_2(\mathbf{L_5})_2]^{5+}$

Addition of $Ba(ClO_4)_2$ to $[CuZn_2(\mathbf{L_5})_2]^{5+}$ was carried out to determine whether or not the coordination of Ba^{2+} ions to the crown ether unit of $\mathbf{L_4}$ was responsible for the deprogramming that resulted in the disassembly of the helicate. If the crown ether unit is instrumental in the deprogramming then no changes should be observed within the ^{1}H NMR spectrum upon addition of 20 equivalents of Ba^{2+} to $\mathbf{L_5}$ (Figure 4.13b).

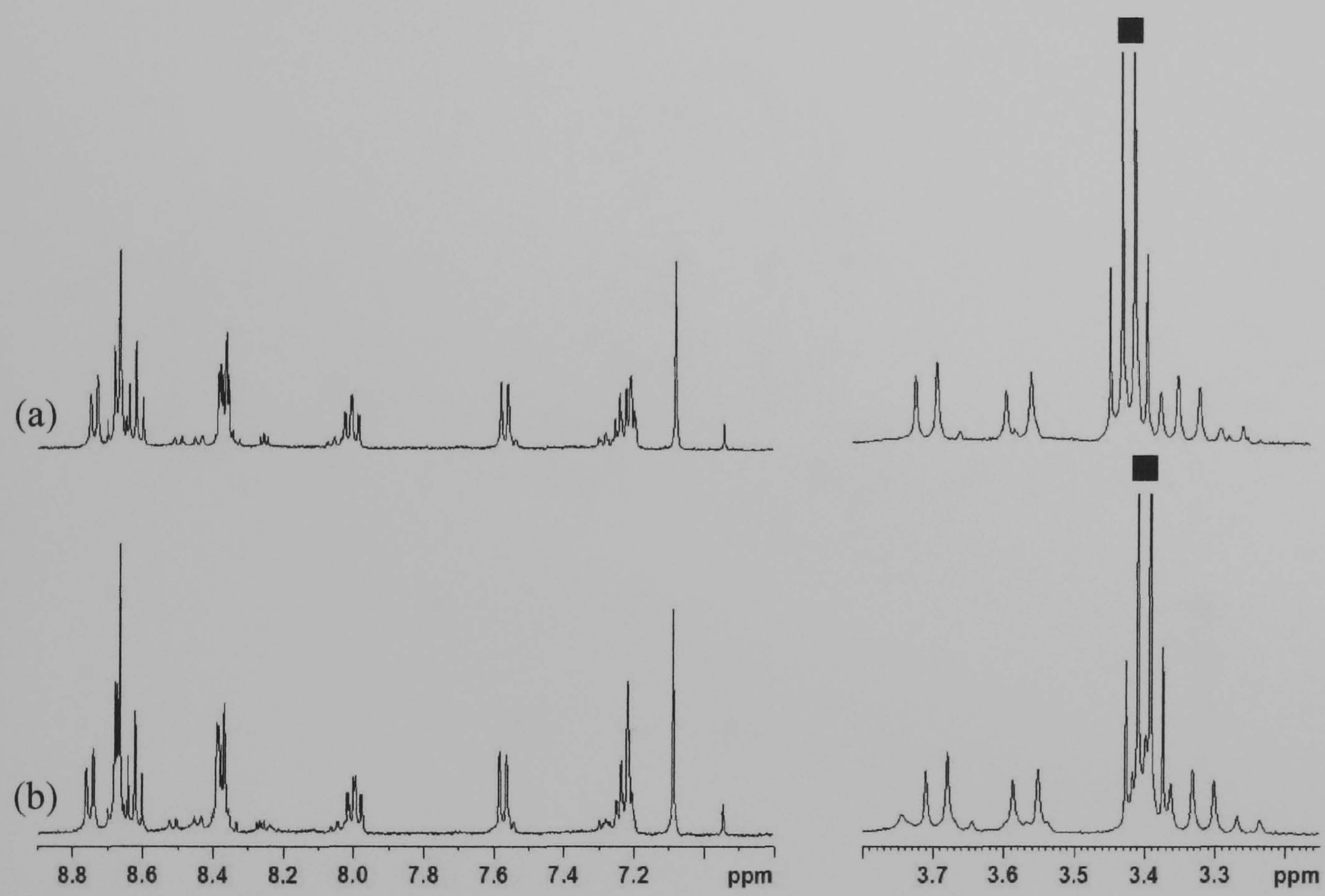

Figure 4.13. Selected aromatic and aliphatic regions of the ^{1}H NMR spectra recorded in CD_3CN of (a) $[CuZn_2(\mathbf{L_5})_2]^{5+}$ and (b) $[CuZn_2(\mathbf{L_5})_2]^{5+}$ + 20 equivalents of $Ba(ClO_4)_2$. The symbol ■ corresponds to diethyl ether solvent impurity.

It can be clearly seen from the ^{1}H NMR spectra that upon addition of 20 equivalents of Ba^{2+} ions to $[CuZn_2(\mathbf{L_5})_2]^{5+}$ no change is observed to either the aromatic or aliphatic protons. This provides more evidence that the coordination of Ba^{2+} ions to the crown ether fragment of $\mathbf{L_4}$ deprogrammes the helicate resulting in the disassembly and the formation of coordination polymers.

4.3.3 Complexes with $\boldsymbol{L_6}$

The 500 MHz ^{1}H NMR spectrum (Figure 4.14) of the crystals of $[Cu_2Zn_2(\mathbf{L_6})_2]^{6+}$ in CD_3CN shows twenty two aromatic protons occurring in eleven environments between 6.75 and 8.70 ppm. This confirms that the ligand is symmetrical, as would be expected upon formation of a tetranuclear double helicate. The crown ether protons occur as their usual multiplets between 3.45-4.2 ppm and the protons for the methylene spacers occur as sharp doublets between 3.11-3.60 ppm.

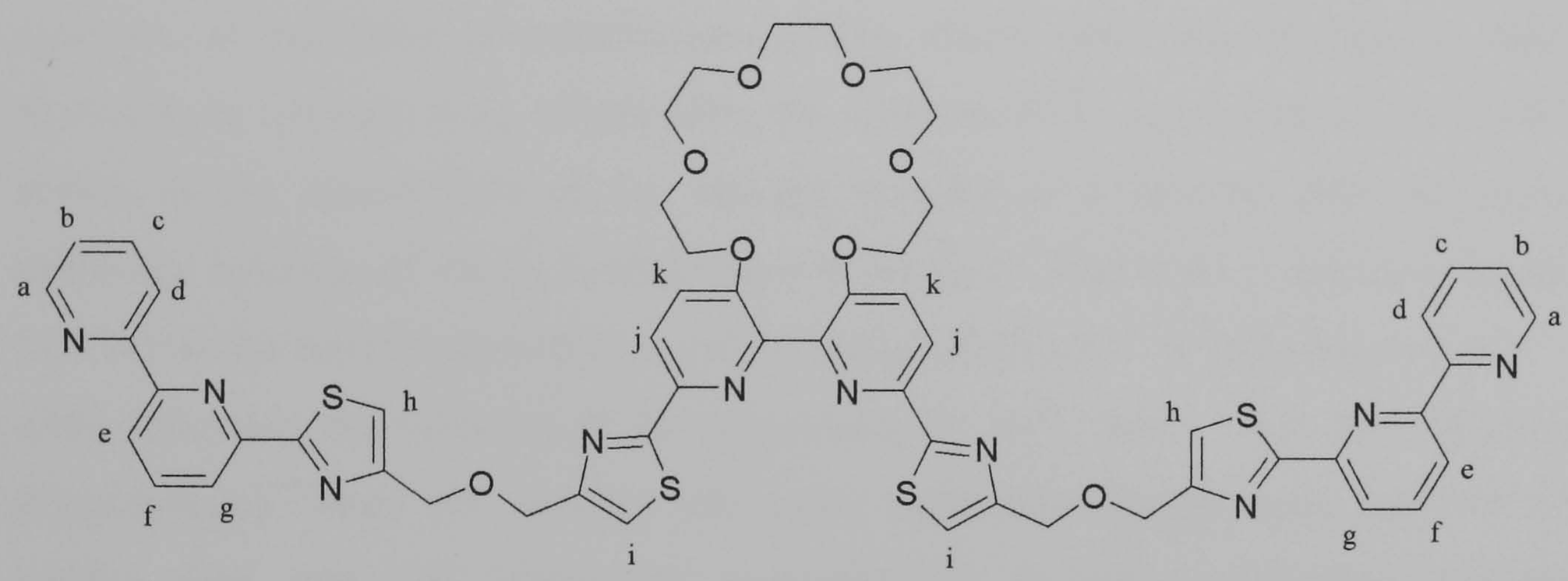

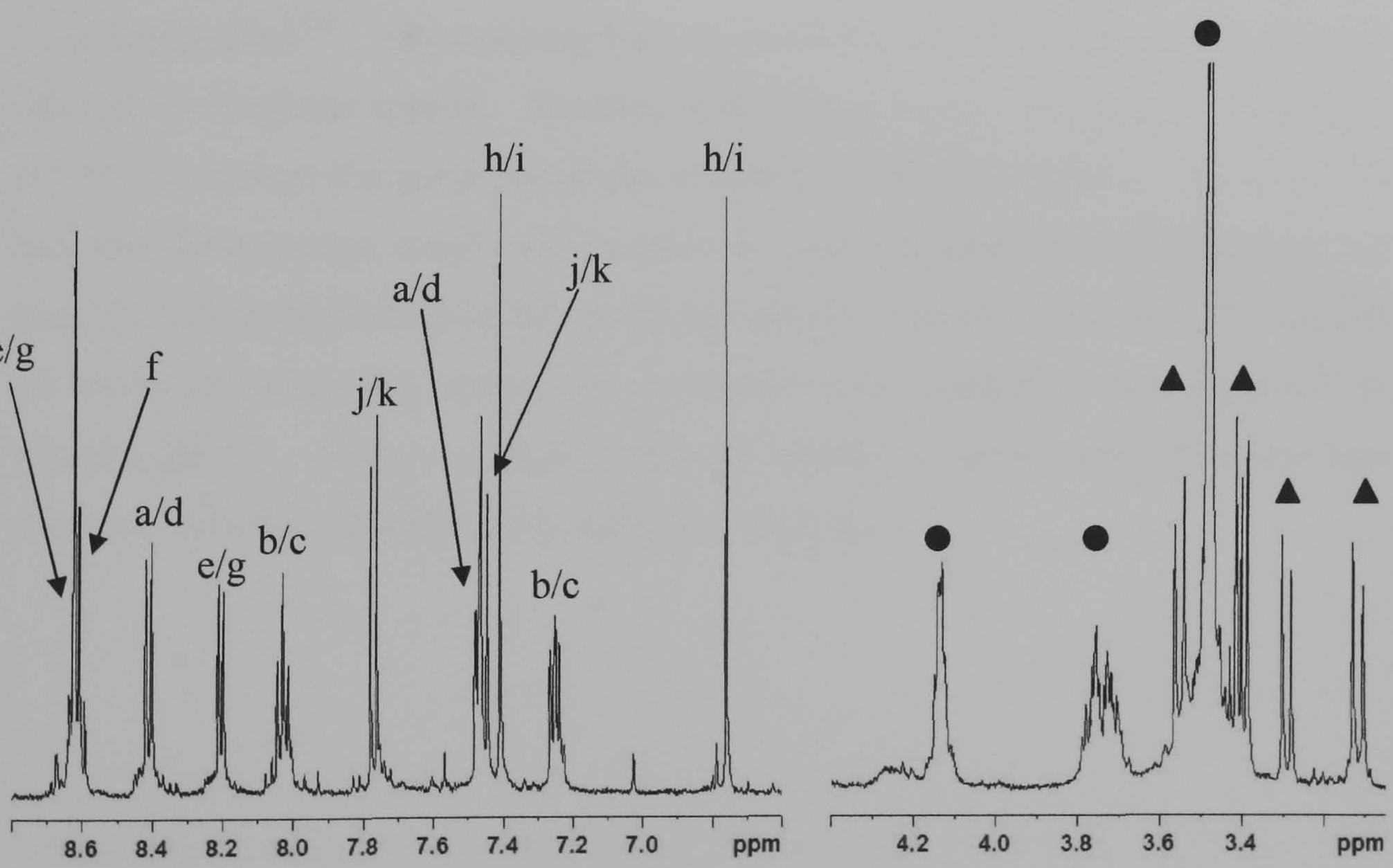

Figure 4.14. Selected aromatic regions of the ^{1}H NMR spectrum of $[Cu_2Zn_2(\mathbf{L_6})_2]^{6+}$. ● corresponds to the crown ether signals and ▲ correspond to the methylene signals.

4.3.3.1 Addition of $Ba(ClO_4)_2$ to $[Cu_2Zn_2(\mathbf{L_6})_2]^{6+}$

Upon addition of 20 equivalents of $Ba(ClO_4)_2$ (per ligand) to $[Cu_2Zn_2(\mathbf{L_6})_2]^{6+}$ very little change is observed to the colour of the sample. Furthermore, the ^1H NMR spectrum of the barium-containing sample shows a slight change in the chemical shifts of the aromatic signals and more significant changes to the crown ether signals (Figure 4.15). The assignment of the aromatic protons was aided by the $^1H/^1H$ COSY following addition of 20 equivalents of Ba^{2+} ions (Figure 4.16). The lack of colour change and the changes observed in the chemical shifts of the ^1H NMR spectrum is indicative of coordination of the crown ether unit by barium ions. However, in contrast to $\mathbf{L_4}$, where after the addition of 20 equivalents of Ba^{2+} ions results in the disassembly of the helicate species; it is obvious that the gross molecular structure of the $\mathbf{L_6}$ helicate has not changed. This is also supported by the ESI-MS as the ion corresponding to $\{[Zn_2Cu_2(\mathbf{L_6})_2](ClO_4)_4\}^{2+}$ is still observed at *m/z* 1542 following the addition of 20 equivalents of Ba^{2+} ions. Thus the complex $[Cu_2Zn_2(\mathbf{L_6})_2]^{6+}$ does not undergo any gross molecular change upon addition of barium ions and just forms the corresponding barium coordinated helicate $[Cu_2Zn_2(\mathbf{L_6})_2Ba_2]^{10+}$. The resulting barium-containing species gives rise to a highly charged 10+ helicate species. Previous studies have shown that such an increase in charge can change the gross molecular structure of helicate systems.[97] However, in this case the transition metal ions are quite far apart (separated by ether linkers) and thus the electrostatic effect on this particular helicate will be minimised. The core of the molecule, where the barium ions are bound, only changes from $[Cu_2(\mathbf{L_6})_2]^{2+}$ to $[Cu_2(\mathbf{L_6})_2Ba_2]^{6+}$. Such a change, which is similar to those outlined in previous chapters, does not affect the gross molecular structure.

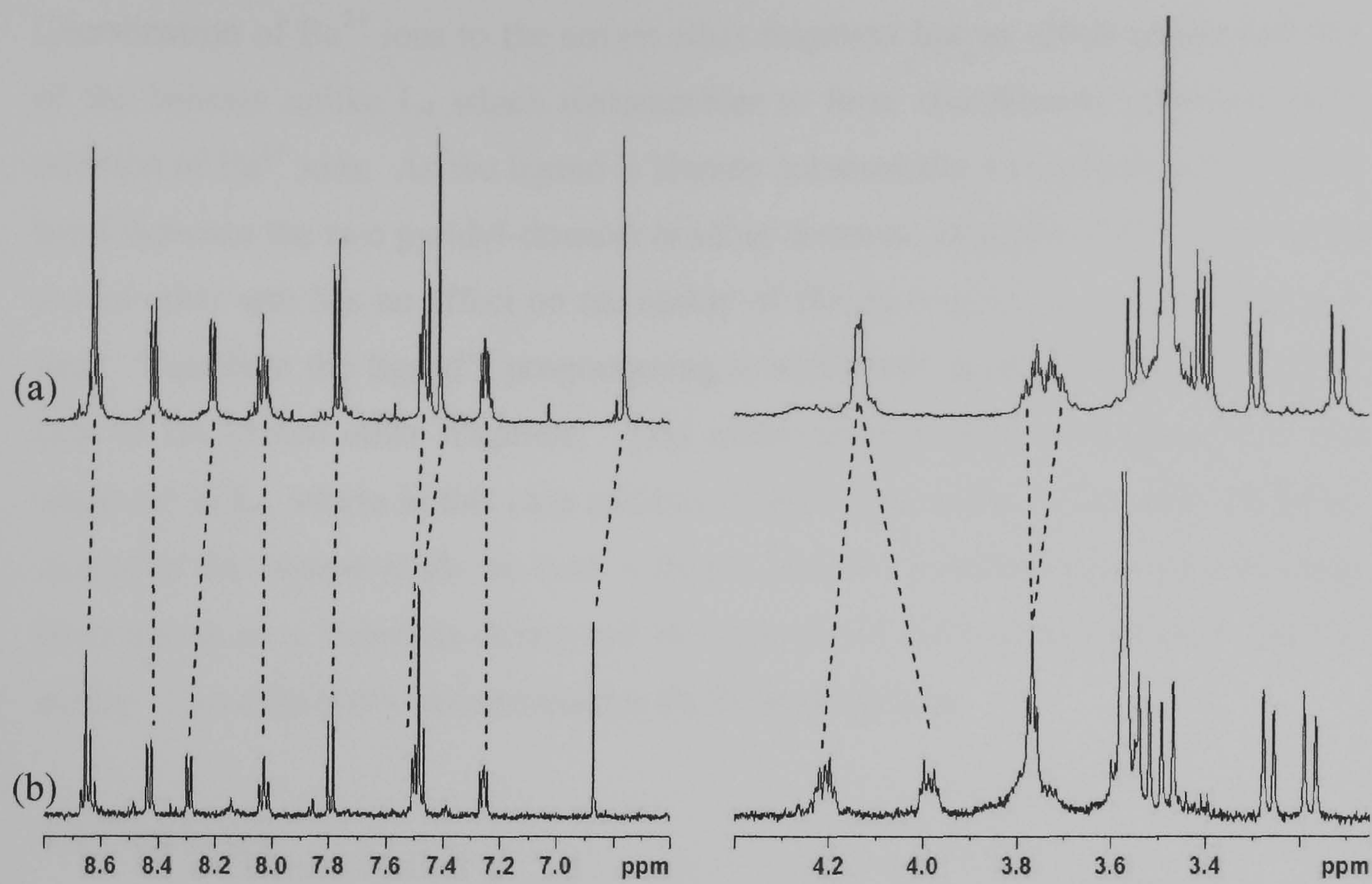

Figure 4.15. Selected aromatic and aliphatic regions of the ^{1}H NMR spectra recorded in CD_3CN of (a) $[Cu_2Zn_2(\mathbf{L_6})_2]^{6+}$ and (b) $[Cu_2Zn_2(\mathbf{L_6})_2]^{6+}$ + 20 equivalents of Ba^{2+} ions.

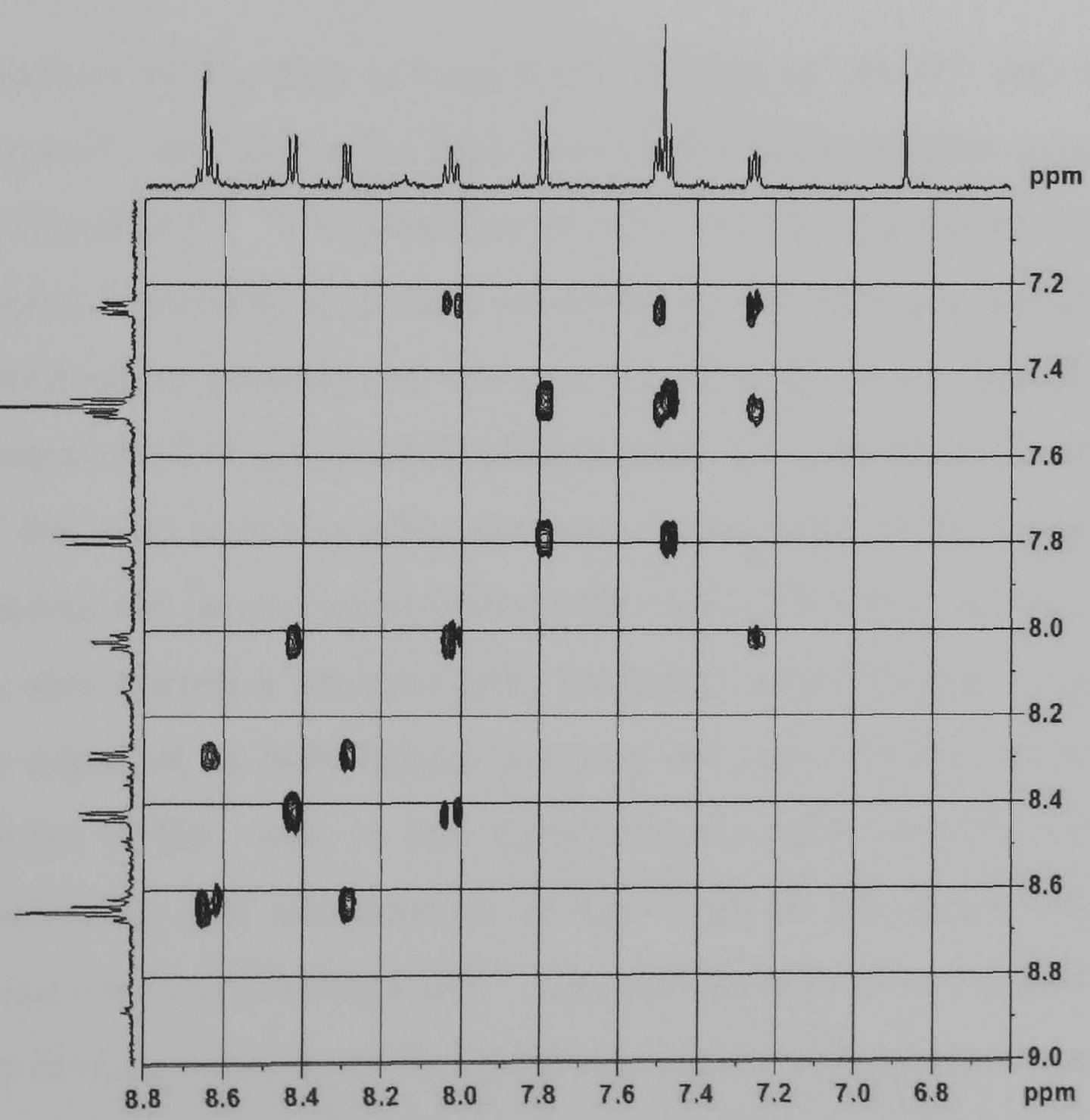

Figure 4.16. Aromatic region from the ^{1}H/^{1}H COSY spectrum of $[Cu_2Zn_2(\mathbf{L_6})_2]^{6+}$ + 20 equivalents of Ba^{2+} ions, recorded in CD_3CN.

Coordination of Ba^{2+} ions to the crown ether fragment has no effect on the stability of the helicate unlike $\mathbf{L_4}$ which disassembles to form coordination polymers upon addition of Ba^{2+} ions. As the ligand is already substantially twisted about the central bond between the two pyridyl-thiazole binding domains, addition of Ba^{2+} ions to the crown ether unit has no effect on the ability of the py-tz domains to coordinate Cu^{I} ions. Therefore the ligand's programming is unaffected upon coordination of Ba^{2+} ions to the crown ether fragment. This observation is quite the opposite of that observed in $\mathbf{L_4}$, where in this case addition of Ba^{2+} ions to the crown ether fragment increased the torsion angle by such a degree that the bidentate unit was prevented from acting as a bidentate donor and thus prevented from coordination to the Cu^{I} centre. This effectively deprogrammes the helicate species.

4.4 Conclusion

Three novel ligands $\mathbf{L_4}$, $\mathbf{L_5}$ and $\mathbf{L_6}$ were successfully synthesised and their abilities to form heterometallic helicates with zinc(II) and copper(I) were investigated.

Reaction of $\mathbf{L_4}$ with an equimolar amount of zinc(II) and half an equivalent of copper(I) resulted in the formation of the heterometallic trinuclear double helicate $[CuZn_2(\mathbf{L_4})_2]^{5+}$. Coordination of Ba^{2+} ions to the crown ether unit prevents the central bipyridine unit from coordinating Cu^{I} ions and results in the formation of coordination polymers of the type $[(\mathbf{L_4})ZnBa]_n$, as the ligand is now insufficiently programmed to act as a helicating ligand. To determine whether or not coordination of Ba^{2+} ions to crown ether unit was instrumental in the disassembly of the helicate species, the parent ligand without the crown ether unit, $\mathbf{L_5}$ was synthesised. Like $\mathbf{L_4}$, $\mathbf{L_5}$ also formed a heterometallic trinuclear double helicate $[CuZn_2(\mathbf{L_5})_2]^{5+}$ as would be expected as both ligands possess the same binding domains. Addition of an excess of Ba^{2+} ions to this species had no effect on the stability of the helicate, confirming that coordination of Ba^{2+} ions to the crown ether of $\mathbf{L_4}$ lead to the disassembly of $[CuZn_2(\mathbf{L_4})_2]^{5+}$. The introduction of two thiazole units in $\mathbf{L_5}$ changed the binding domains of the ligand so reaction with equimolar amounts of zinc(II) and copper(I) resulted in the formation of the heterometallic tetranuclear double helicate $[Cu_2Zn_2(\mathbf{L_6})_2]^{6+}$. Coordination of Ba^{2+} ions to the crown ether unit of $\mathbf{L_6}$ had no

effect on the stability of the helicate as the ligand is still sufficiently programmed to act as a helicating ligand in the presence of Ba^{2+} ions.

Chapter 5

5. Conclusion

In conclusion seven multidentate N-donor ligands $\mathbf{L_1}$–$\mathbf{L_6}$ and $\mathbf{L_z}$, have been successfully synthesised and although the ligands $\mathbf{L_1}$–$\mathbf{L_3}$, $\mathbf{L_z}$ have been previously synthesised some of the synthetic steps have been significantly improved. Furthermore, the coordination chemistry of these four ligands has been further investigated to reveal some interesting results. The multidentate N-donor ligands $\mathbf{L_4}$–$\mathbf{L_6}$ are, however, novel ligands and are previously un-reported. The synthesis of these ligands involves a multi-step synthetic methodology and has correspondingly received considerable attention in order to maximise the yields of each step to allow production of reasonable quantities of the final ligands. Following the successful synthesis of $\mathbf{L_4}$–$\mathbf{L_6}$, their ability to form heterometallic helicates has been investigated.

Following the successful synthesis of these multidentate N-donor ligands it has been shown how the ditopic ligand $\mathbf{L_1}$ can form a mixture of both dinuclear double helicate $[Cu_2(\mathbf{L_1})_2]^{2+}$ and the mononuclear zinc species $[Zn(\mathbf{L_1})]^{2+}$ in a competitive experiment. Coordination of various s-block metal cations to the crown ether unit of $\mathbf{L_1}$ effectively reprograms the inherent ligand information so that a change to the distribution of products is observed, with the mononuclear zinc species being the major component. The difference in the distribution of products observed following the addition of barium and potassium ions highlights the importance of both allosteric and electrostatic factors within ligand specificity.

The potentially tetradentate ditopic ligand $\mathbf{L_2}$ also forms a mixture of species in a competitive experiment, forming the dinuclear double helicates $[Cu_2(\mathbf{L_2})_2]^{2+}$ and $[CuZn(\mathbf{L_2})_2]^{3+}$ and the mononuclear zinc species $[Zn(\mathbf{L_2})]^{2+}$. However, coordination of either barium or strontium ions to the crown ether units within this mixed metal system resulted in a redistribution of products, with only the homometallic species observed $[Cu_2(\mathbf{L_2})_2]^{2+}$, $[Zn(\mathbf{L_2})]^{2+}$ and none of the heterometallic species $[CuZn(\mathbf{L_2})_2]^{3+}$ was observed. As was observed with $\mathbf{L_1}$ the mononuclear zinc species is again favoured, however, in this case the mode of allosteric action in $\mathbf{L_2}$ is different to that of $\mathbf{L_1}$, with electrostatic effects being dominant.

Reaction of the potentially hexadentate ligands $\mathbf{L_3}$ and $\mathbf{L_z}$ with zinc(II) ions in a competitive experiment resulted in the formation of both homoleptic helicates $[Zn_2(\mathbf{L_3})_2]^{4+}$ and $[Zn_2(\mathbf{L_z})_2]^{4+}$ and a very small amount of the heteroleptic helicate species $[Zn_2(\mathbf{L_3})(\mathbf{L_z})]^{4+}$. Coordination of barium ions to the crown ether unit of $\mathbf{L_3}$ results in all ligand recognition being lost and the three helicate species being observed in a ratio of 1 : 2 : 1. In this ligand system the redistribution of products occurs as a consequence of electrostatic effects as apposed to allosteric effects.

The potentially octadentate ditopic ligand $\mathbf{L_4}$, forms the heterometallic trinuclear double helicate $[Zn_2Cu(\mathbf{L_4})_2]^{5+}$ upon reaction with copper(I) and zinc(II) ions. Coordination of barium ions to the external crown ether binding site of $\mathbf{L_4}$ causes the helicate species to disassemble as the ligand is no longer sufficiently programmed to act as a helicating ligand, resulting in the formation of coordination polymers of the type $[(\mathbf{L_4})ZnBa]_n$. The potentially decadentate ditopic ligand $\mathbf{L_6}$ also forms a heterometallic helicate species, $[Zn_2Cu_2(\mathbf{L_6})_2]^{6+}$. However, coordination of barium ions to this species results in the formation of the barium containing helicate species $[Zn_2Cu_2(\mathbf{L_6})_2Ba_2]^{10+}$. Thus the potentially decadentate ligand $\mathbf{L_6}$ is sufficiently programmed to accommodate barium ions. This elegantly demonstrates how a subtle change to the ligands binding domains dramatically affects the ability of $\mathbf{L_4}$ and $\mathbf{L_6}$ to act as a helicating ligand in the presence of barium ions.

Having obtained all these results for the six multidentate N-donor ligands $\mathbf{L_1}$–$\mathbf{L_6}$, the evidence suggests that electrostatic effects are most important in the reprogramming of ligand helicate systems. However, this is not always the case as although electrostatic effects are more dominant in the reprogramming of $\mathbf{L_2}$ and $\mathbf{L_3}$ ligand systems both electrostatics and allosteric effects are important in the reprogramming of $\mathbf{L_1}$. In addition the deprogramming of the heterometallic helicate $[Zn_2Cu(\mathbf{L_4})_2]^{5+}$ is solely due to allosteric effects and not electrostatic effects as the potentially decadentate ligand $\mathbf{L_6}$ is capable of forming a highly charged 10+ species $[Zn_2Cu_2(\mathbf{L_6})_2Ba_2]^{10+}$.

All these results highlight that the ability to reprogramme helicate species by addition of s-block metal ions to remote crown ether units is system specific. Thus if a system *can be reprogrammed* and whether this reprogramming is due to

electrostatic or allosteric effects depends greatly upon the position of the crown ether within the ligand chain and the disposition of the N-donor binding domains.

Chapter 6

6. Experimental

6.1 Synthesis of 2,2'-bipyridine-3,3'-dicarboxylic acid, (2)

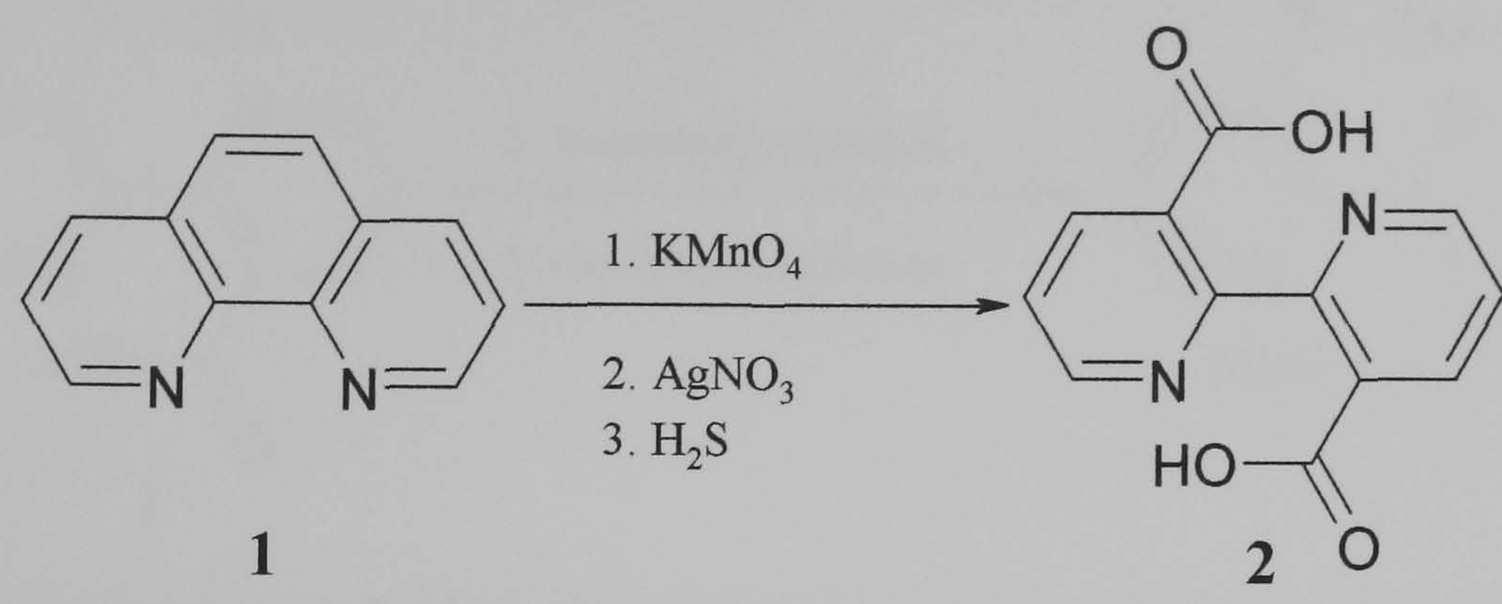

To a solution of sodium hydroxide (3.2 g, 0.08 mol) in distilled water (700 ml), 1,10-phenanthroline (**1**) (8.0 g, 0.04 mol) was added with stirring. Potassium permanganate (19.0 g, 0.12 mol) was slowly added to this aqueous solution at room temperature using a powder dropping funnel, before being refluxed for 2 hours, during which time the solution turned brown. This hot solution was filtered through a sintered glass funnel charged with celite, giving a clear yellow solution which was reduced to half its volume by rotary evaporation. Acidification of this concentrated solution with acetic acid followed by the slow addition of a silver nitrate solution (13.6 g, 0.08 mol, dissolved in a minimum amount of distilled water), formed a white precipitate which was collected by vacuum filtration. The white solid was transferred to a 1 litre flask together with distilled water (500 ml) and boiled with vigorous stirring. The boiling solution was then saturated with $H_2S_{(g)}$, during which time a black precipitate formed before the solution cleared. Once again the hot solution was then filtered through a sintered glass funnel charged with celite to give a pale red solution. This red solution was reduced in volume to around 50 ml by rotary evaporation, on cooling of the reduced solution gave colourless crystals of (**2**) which were collected by vacuum filtration and dried (4.22 g, 0.017 mol, 39%). The synthesis of 2,2'-bipyridine-3,3'-dicarboxylic acid, (**2**) was carried out with reference to the procedure described by Rebek and co-workers.[95]

^{1}H NMR [400 MHz, $CDCl_3$]: δ (ppm) 12.93 (s, 2H, -OH), 8.67 (dd, J = 4.78, 1.51, 2H), 8.27 (dd, J = 7.88, 1.51, 2H), 7.53 (dd, J = 7.83, 4.78 Hz, 2H).

6.2 Synthesis of 3,3'-dicarbomethoxy-2,2'-bipyridine, (3)

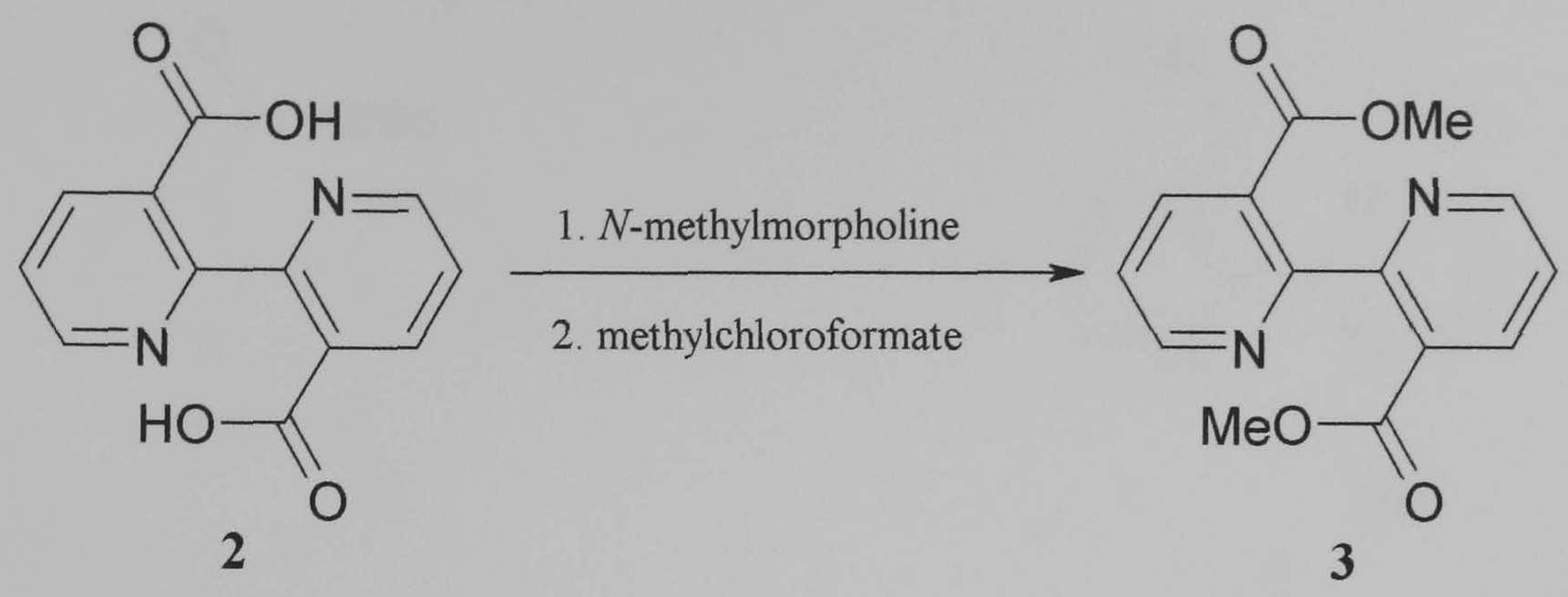

To a 100 ml round bottom flask charged with 2,2'-bipyridine-3,3'-dicarboxylic acid (**2**) (3.22 g, 0.013 mol) and *N*-methylmorpholine (2.90 ml, 0.026 mol), methanol was added and the reaction mixture cooled to 0°C. To this methylchloroformate (2.05 ml, 0.033 mol) was added drop wise over a period of 10 minutes with stirring. The reaction mixture was then stirred for a further 30 minutes at ambient temperature. Removal of the solvent by rotary evaporation gave thick oil to which $NaHCO_{3(aq)}$ (30 ml) was added and extracted with DCM (3 × 50 ml). Evaporation of the combined organic layers gave 2,2'-bipyridine-3,3'-dicarboxylic acid dimethyl ester (**3**) as white crystals (2.85 g, 0.010 mol, 79%). The synthesis of 3,3'-dicarbomethoxy-2,2'-bipyridine, (**3**) was carried out with reference to the procedure described by Rebek and co-workers.[95]

^{1}H NMR [400 MHz, $CDCl_3$]: δ (ppm) 8.80 (dd, J = 4.91, 1.81, 2H), 8.40 (dd, J = 7.96, 1.82, 2H), 7.47 (dd, 7.82, 4.75 Hz, 2H), 3.71 (s, 6H).

6.3 Synthesis of 2,2'-bipyridine-3,3'-dimethanol, (4)

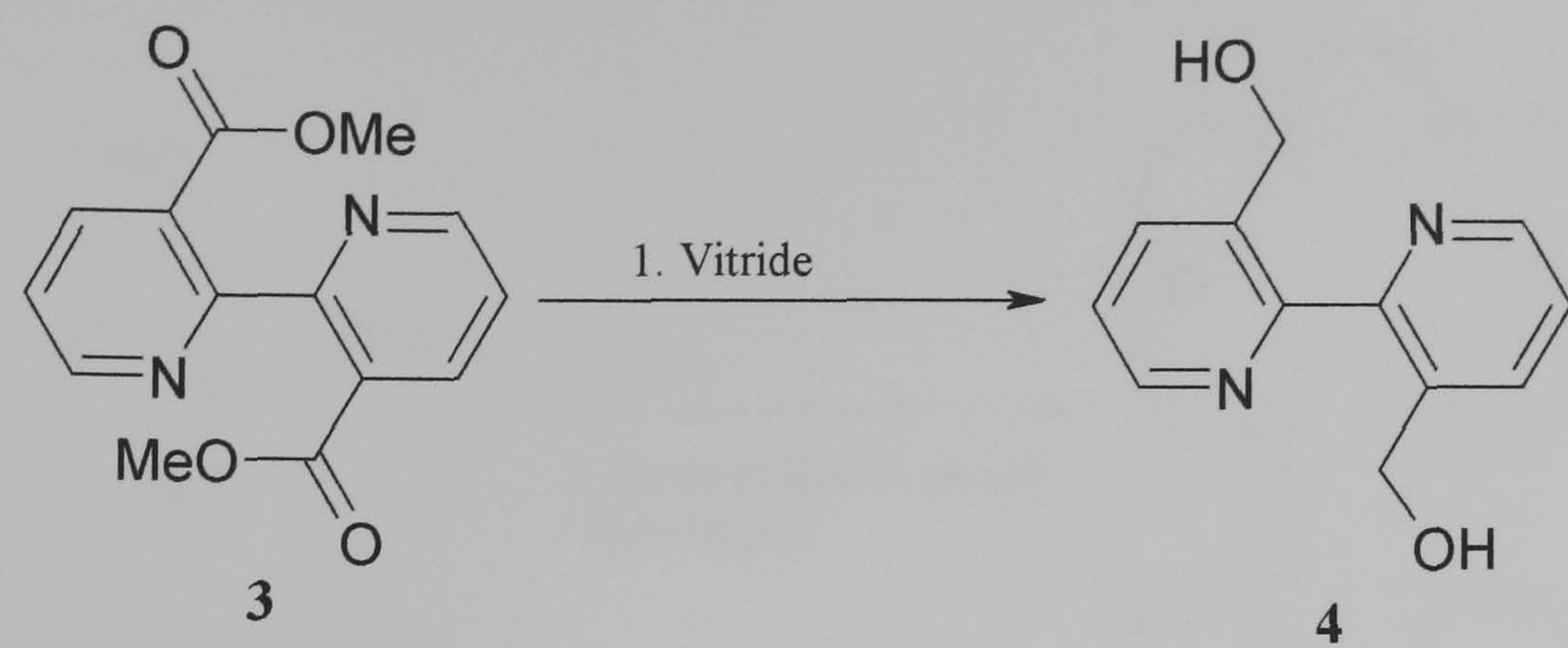

Under an atmosphere of nitrogen a 250 ml round bottom flask charged with 3,3'-dicarbomethoxy-2,2'-bipyridine (**3**) (1.0 g, 3.67 mmol). To this anhydrous THF (150 ml) was added and the reaction cooled to 0°C. A solution of sodium bis[2-methoxyethoxy] aluminium hydride (Vitride) (5.4 ml, 0.019 mol) in anhydrous THF (20 ml), was added drop wise to the reaction vessel over a period of 30 minutes with stirring. Stirring was continued for 1 hour at 0°C before addition of methanol (10 ml). Removal of the solvents by rotary evaporation gave a brown oil to which $NaHCO_{3(aq)}$ (40 ml) was added and extracted from DCM (3 × 50 ml). Evaporation of the combined organic layers gave a brown residue which was recrystalised from a minimum amount of toluene, affording large brown crystals of (**4**) on cooling (0.62 g, 2.86 mmol, 78%). The synthesis of 2,2'-bipyridine-3,3'-dimethanol, (**4**) was carried out with reference to the procedure described by Rebek and co-workers.[95]

^{1}H NMR [400 MHz, $CDCl_3$]: δ (ppm) 8.63 (dd, J = 4.78, 1.59, 2H), 7.93 (dd, J = 7.69, 1.58, 2H), 7.45 (dd, J = 7.7, 4.84, 2H), 6.05 (t, J = 6.93, 2H, -OH), 4.45 (d, J = 6.85 Hz, 4H).

*6.4 Synthesis of 2,2'-bipyridine-crown ether, (**5**)*

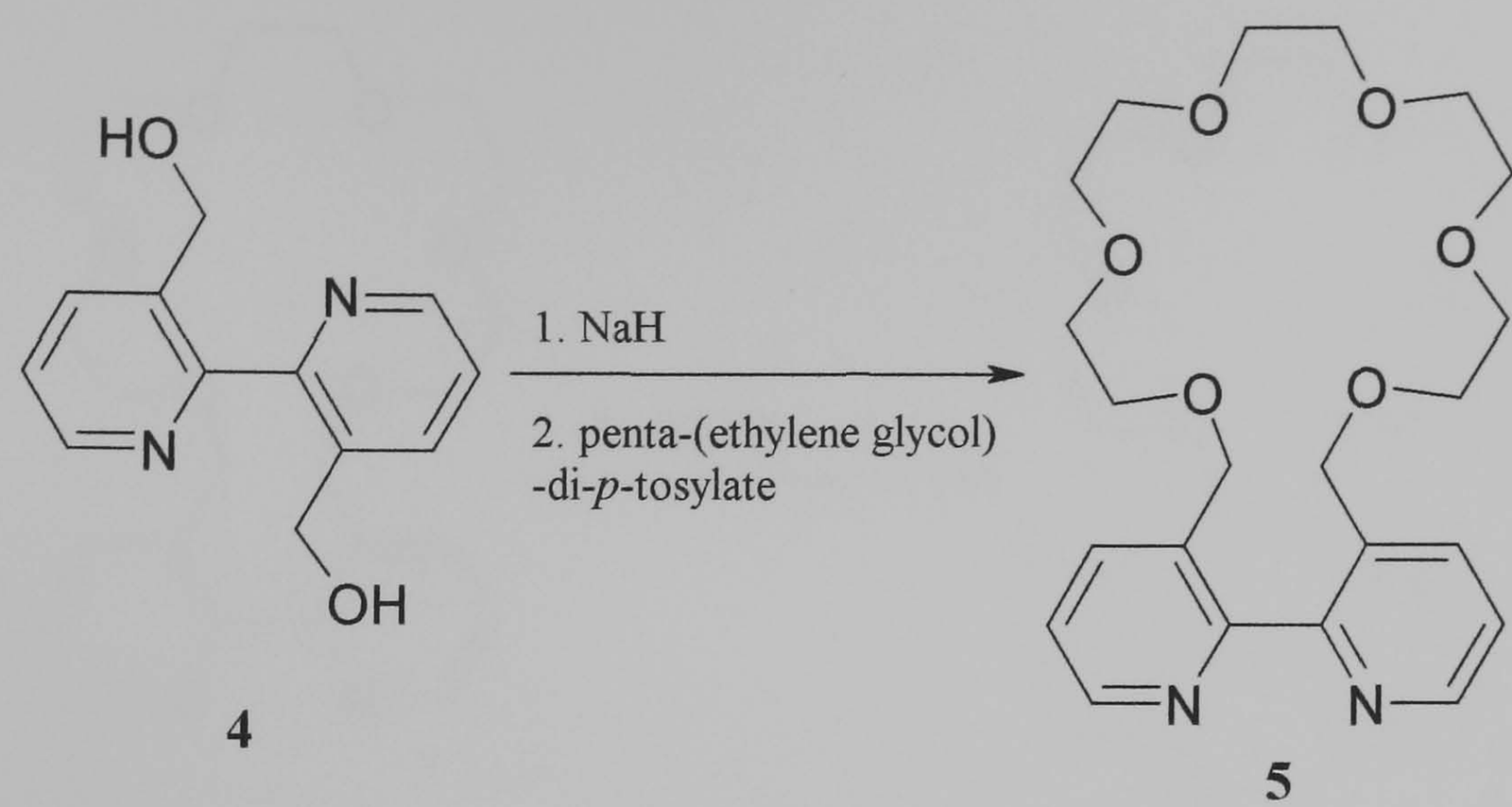

Under an atmosphere of nitrogen a 100 ml two neck round bottom flask was charged with 2,2'-bipyridine-3,3'-dimethanol (**4**) (1.0 g, 4.62 mmol) and sodium hydride (60% dispersion in oil, 0.41 g, 0.010 mol). To this anhydrous DMF (50 ml) was added and the reaction heated to 60°C with stirring for 1 hour. After this time penta-(ethylene glycol)-di-*p*-tosylate (2.53 g, 4.62 mmol) was added to the reaction mixture and heating continued for a further 24 hours. The reaction was allowed to cool before any remaining sodium hydride was quenched by addition of methanol (5 ml). Removal of the solvents by rotary evaporation gave a brown oil to which $NaHCO_{3(aq)}$ (40 ml) was added and extracted into DCM (3 × 50 ml). Evaporation of the combined organic layers gave a brown oil that was purified via column chromatography (10% MeOH in DCM, SiO_2) gave (**5**) as a viscous amber oil, which solidifies on standing to give a pale brown waxy solid (0.70 g, 1.67 mmol, 52%). The synthesis of of 2,2'-bipyridine-crown ether, (**5**) was carried out with reference to a procedure described by Rice and co-workers.[97]

^{1}H NMR [400 MHz, $CDCl_3$]: δ (ppm) 8.54 (d, J = 4.74, 2H), 7.95 (d, J = 7.83, 2H), 7.34 (dd, J = 7.7, 4.76, 2H), 4.55 (d, J = 12.67, 2H), 4.47 (d, J = 12.9 Hz, 2H), 3.65-3.35 (m, 20H).

ESI-MS: *m/z* 419.1 ($M + H^+$).

*6.5 Synthesis of bis-N,N'-oxide, (**6**)*

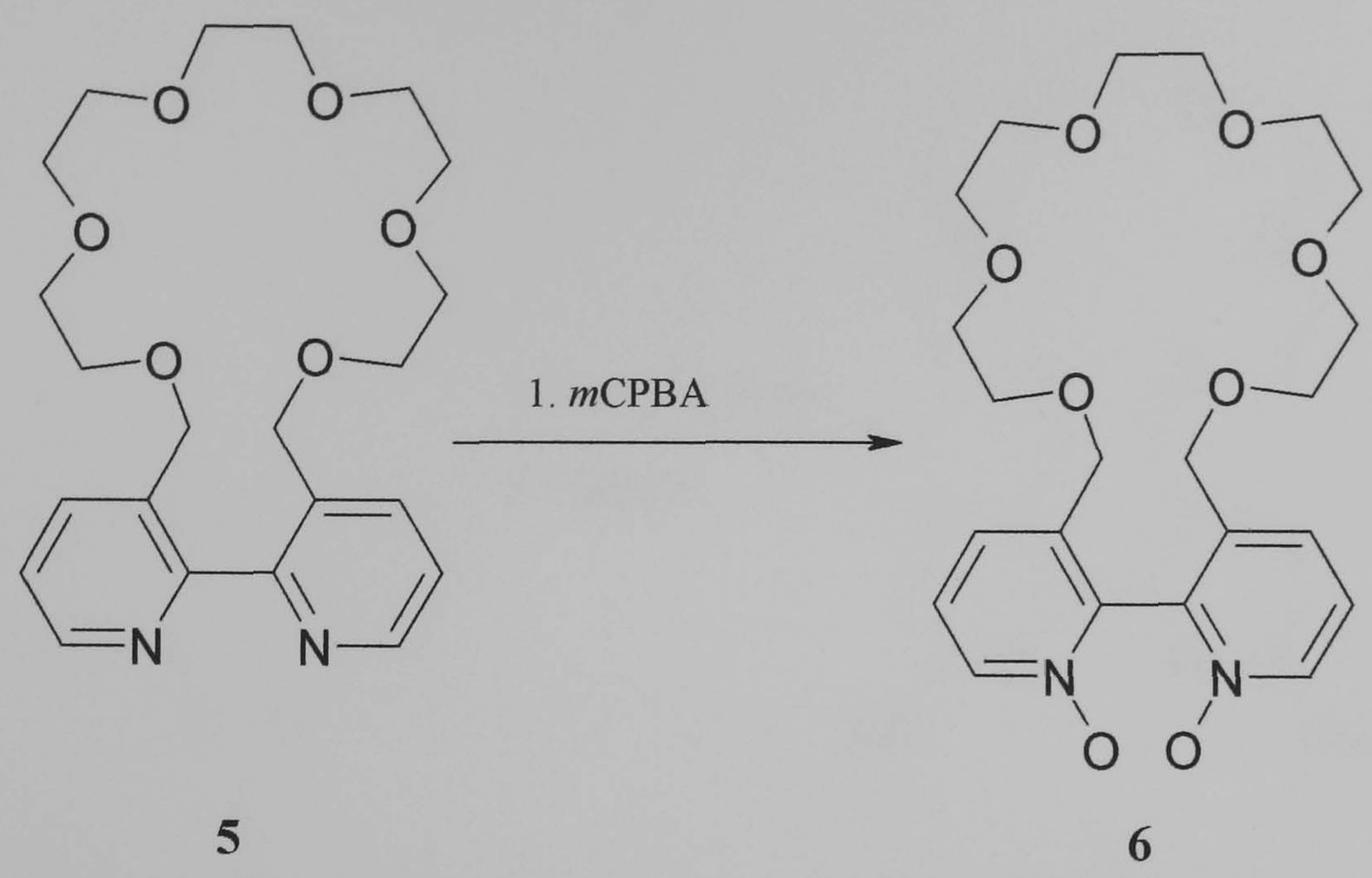

A solution of 2,2'-bipyridine-crown ether (**5**) (0.7 g, 1.67 mmol) and *m*CPBA (77%, 0.82 g, 3.68 mmol) in DCM (40 ml) was stirred at room temperature for 6 hours. The reaction was followed by TLC and upon completion the solvent was reduced to half its volume by rotary evaporation. The resulting solution was then purified by column chromatography (1% MeOH in DCM, Al_2O_3) giving (**6**) as a white solid (0.62 g, 1.37 mmol, 82%). The synthesis of the bis-N,N'-oxide, (**6**) was carried out with reference to the procedure described by Rice and co-workers.[97]

^{1}H NMR [400 MHz, $CDCl_3$]: δ (ppm) 8.25 (d, J = 5.95, 2H), 7.55 (d, J = 7.9, 2H), 7.40 (t, J = 6.52, 2H), 4.37 (d, J = 13.07, 2H), 4.32 (d, J = 13.05 Hz, 2H), 3.67-3.4 (m, 20H).

ESI-MS: *m/z* 451.1 ($M + H^+$).

6.6 Synthesis of 2,2'-bipyridine-crown ether-6,6'-dicarbonitrile, (7)

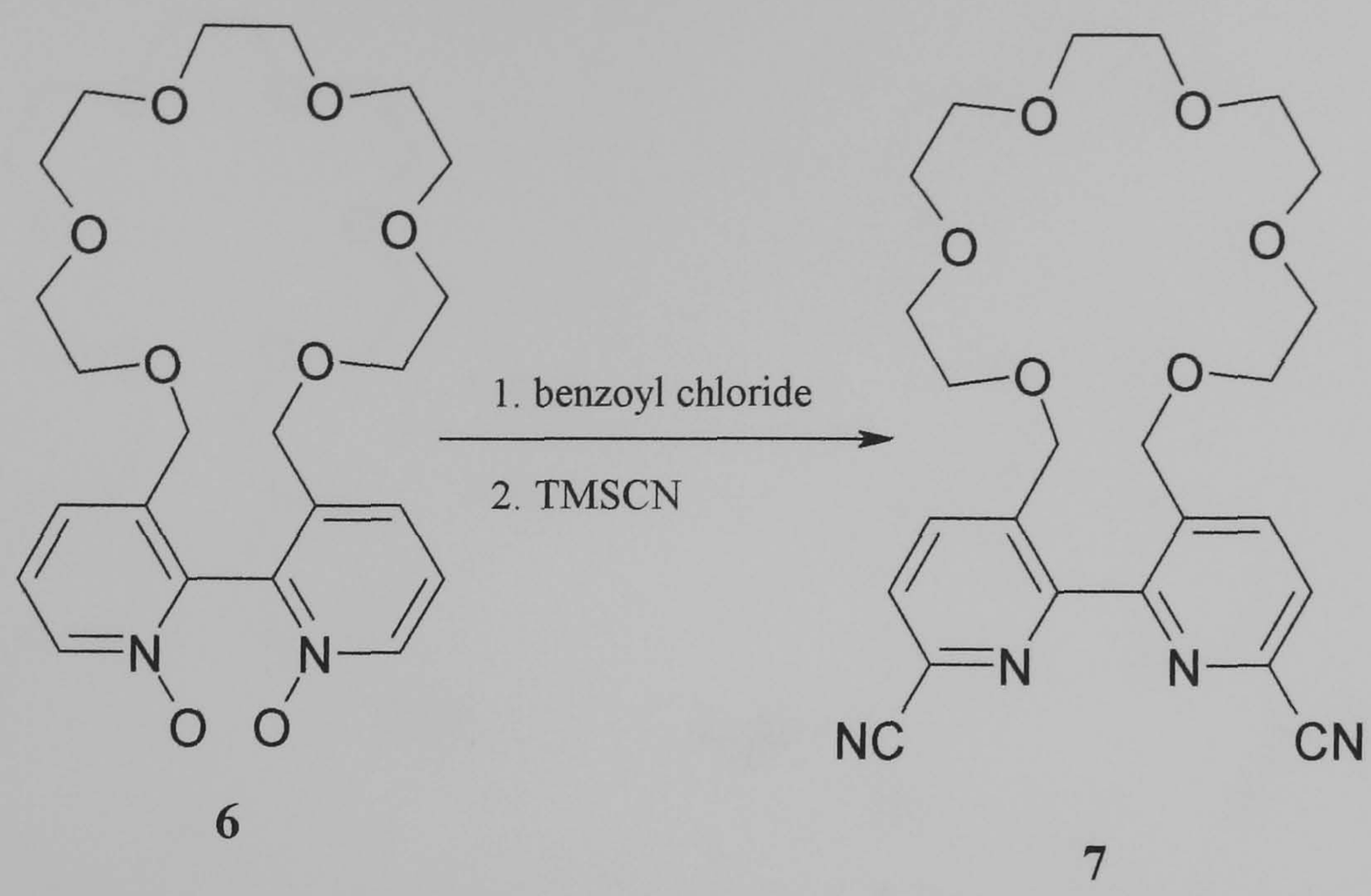

A solution of bis-N,N'-oxide (**6**) (0.6 g, 1.33 mmol) and benzoyl chloride (0.34 ml, 2.93 mmol) in DCM (50 ml) was refluxed, and trimethylsilyl cyanide (0.39 ml, 2.93 mmol) added slowly after a period of 30 minutes. The reaction was monitored by TLC and upon completion the solution was cooled and washed with $NaHCO_{3(aq)}$. Removal of the solvent by rotary evaporation give the crude product as a brown oil that was purified via column chromatography (1% MeOH in DCM, Al_2O_3) affording (**7**) as a white solid (0.60 g, 1.28 mmol, 96%). The synthesis of (**7**) was carried out with reference to the procedure described by Rice and co-workers.[97]

^{1}H NMR [400 MHz, $CDCl_3$]: δ (ppm) 8.19 (d, J = 8.01, 2H), 7.81 (d, J = 7.97, 2H), 4.69 (d, J = 13.73, 2H), 4.61 (d, J = 13.69 Hz, 2H), 3.75-3.4 (m, 20H).

ESI-MS: m/z 469.1 ($M + H^+$).

*6.7 Synthesis of 2,2'-bipyridine-crown ether 6,6'-dithioamide, (**8**)*

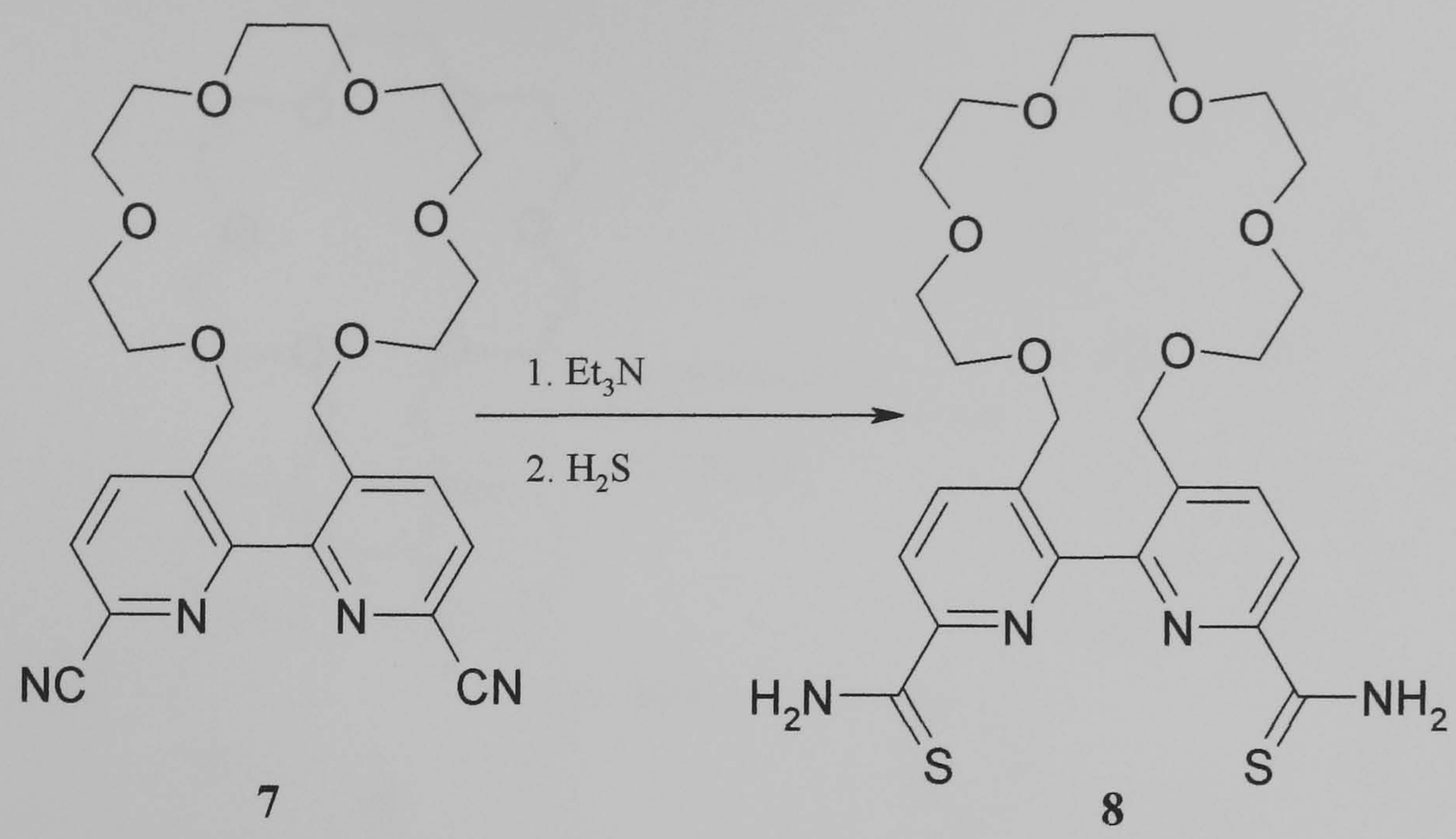

To a solution of 2,2'-bipyridine-crown ether-6,6'-dicarbonitrile (**7**) (0.6 g, 1.40 mmol) and triethylamine (1.0 g, 9.9 mmol) in ethanol (20 ml), H_2S was slowly bubbled through the solution for 15 minutes, during which time the solution turned yellow. The yellow solution was allowed to stand for 48 hours during which time a yellow solid slowly precipitated. Collection via filtration gave pure 2,2'-bipyridine dithioamide (**8**) as a yellow solid (0.63 g, 1.17 mmol, 92%). The synthesis of (**8**) was carried out with reference to the procedure described by Rice and co-workers.[97]

^{1}H NMR [400 MHz, $CDCl_3$]: δ (ppm) 9.2 (s, 2H), 8.76 (d, J = 8.09, 2H), 8.14 (d, J = 8.10, Hz, 2H), 7.65 (s, 2H), 4.53 (s, 4H), 3.6-3.35 (m, 20H).

ESI-MS: *m/z* 537.1 ($M + H^+$).

*6.8 Synthesis of (**L₁**)*

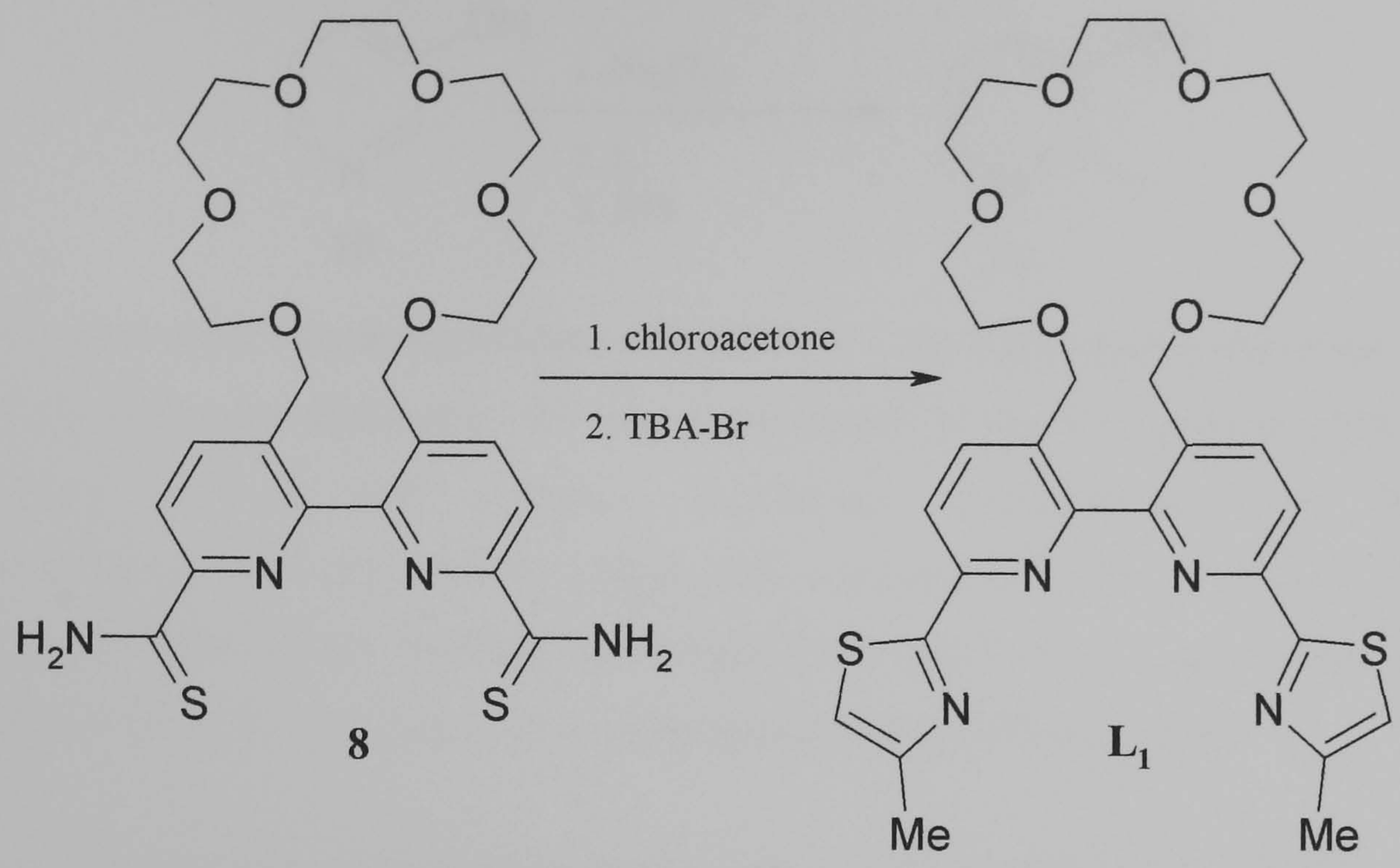

A solution of 2,2'-bipyridine-crown ether-6,6'-dithioamide (**8**) (0.2 g, 0.37 mmol) and chloroacetone (0.16 ml, 2.46 mmol) in ethanol (50 ml) was refluxed for 6 hours in the presence of a catalytic amount of TBA-Br. Removal of the solvent by rotary evaporation gave a yellow solid to which $NaHCO_{3(aq)}$ (30 ml) was added and extracted from DCM (3 × 50 ml). Evaporation of the combined organic layers gave the crude product as an off white solid that was then purified via column chromatography (1% MeOH in DCM, Al_2O_3) giving (**L₁**) as an off white solid (0.18 g, 0.29 mmol, 79%). The synthesis of (**L₁**) carried out with reference to the procedure described by Rice and co-workers.[97]

^{1}H NMR [400 MHz, $CDCl_3$]: δ (ppm) 8.19 (d, J = 8.07, 2H), 8.08 (d, J = 8.16 Hz, 2H), 6.96 (s, 2H), 4.81 (s, 4H), 3.6-3.35 (m, 20H), 1.57 (s, 6H).

^{13}C NMR [400 MHz, ($CDCl_3$)]: δ (ppm) 168.6 (th), 155.3 (py), 154.6 (py), 149.3 (py), 138.3 (py), 135.3 (py), 119.1 (th), 116.5 (th), 71.1 (cr), 71.0 (cr), 70.7 (cr), 70.6 (cr), 70.3 (cr), 66.3 (cr), 17.8 (Me).

ESI-MS: *m/z* 613.4 ($M + H^+$)

*6.9 Synthesis of 3-hydroxy-2-iodopyridine, (**11**)*

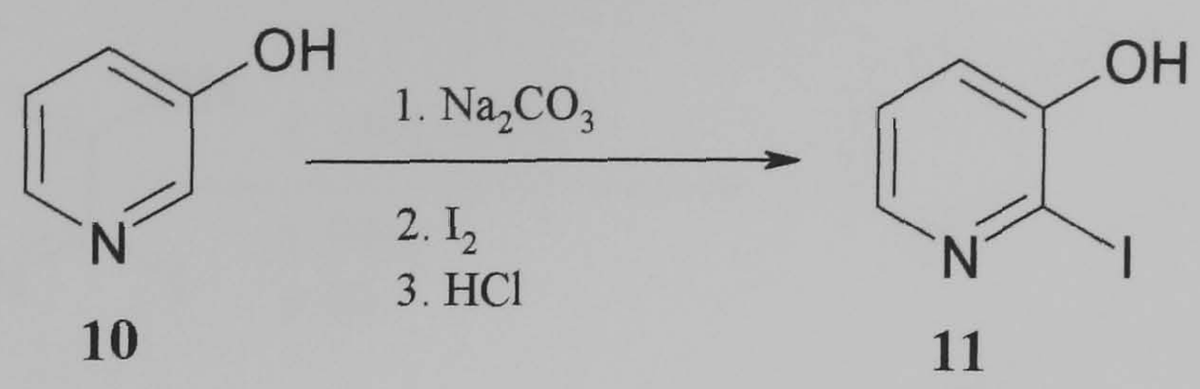

To a solution of 3-hydroxypyridine (**10**) (9.5 g, 0.1 mol) and sodium carbonate (22.3 g, 0.21 mol) in distilled water (400 ml), iodine bead (25.4 g, 0.1 mol) was added with vigorous stirring until complete dissolution (approximately two hours). Concentrated HCl was slowly added with stirring until pH 3. Filtration and recrystallisation of the resulting solid form 60:40 EtOH : H_2O gave 3-hydroxy-2-iodopyridine (**11**) as a creamy crystalline solid (12.4 g, 0.56 mol, 56%).

^{1}H NMR [400 MHz, DMSO]: δ (ppm) 10.83 (s, 1H), 7.80 (dd, J = 4.43, 1.80, 1H), 7.17 (dd, 8.03, 4.38, 1H), 7.13 (dd, 8.02, 1.63 Hz, 1H)

*6.10 Synthesis of 3,3-dihydroxy-2,2-bipyridine, (**12**)*

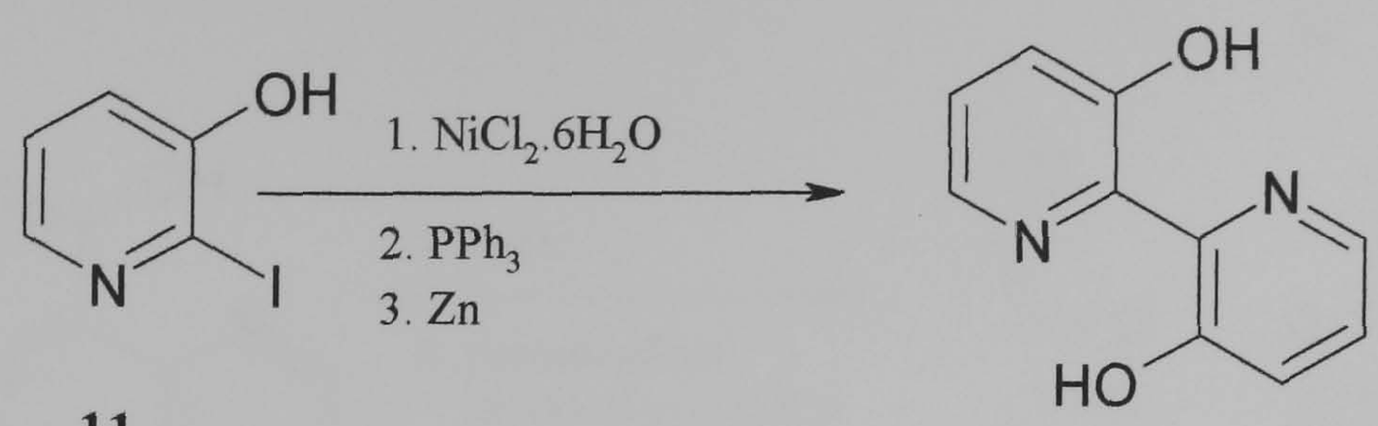

11 **12**

A mixture of $NiCl_2.6H_2O$ (4.0 g, 16.8 mmol) and triphenyl phosphine (17.92 g, 68.0 mmol) was completely dissolved in anhydrous DMF under an atmosphere of nitrogen at 50°C. Zinc powder (6.0 g, 91.7 mmol) was added with stirring and sonication for 15 minutes. Stirring was continued for 1 hour at 50°C. To this 3-hydroxy-2-iodopyridine (**11**) (6.0 g, 27.1 mmol) was added and stirring continued for 2 hours. The warm mixture was poured into 2 M NaOH (300 ml) with vigorous stirring. The solid was removed by filtration through a sintered glass funnel and acidification of the solution until pH 4 gave a yellow solid. Filtration and recrystallisation from toluene gave 3,3-dihydroxy-2,2-bipyridine (**12**) as a yellow crystalline solid (0.93 g, 4.94 mmol, 36%). The synthesis of 3,3-dihydroxy-2,2-bipyridine, (**12**) was prepared using the literature method.[106]

^{1}H NMR [400 MHz, $CDCl_3$]: δ (ppm) 14.68 (s, 2H), 8.05 (dd, J = 4.7, 1.33, 2H), 7.43 (dd, J = 8.5, 1.4, 2H), 7.30 (dd, J = 8.42, 4.6 Hz, 2H)

*6.11 Synthesis of 2,2'-bipyridine-crown ether, (**13**)*

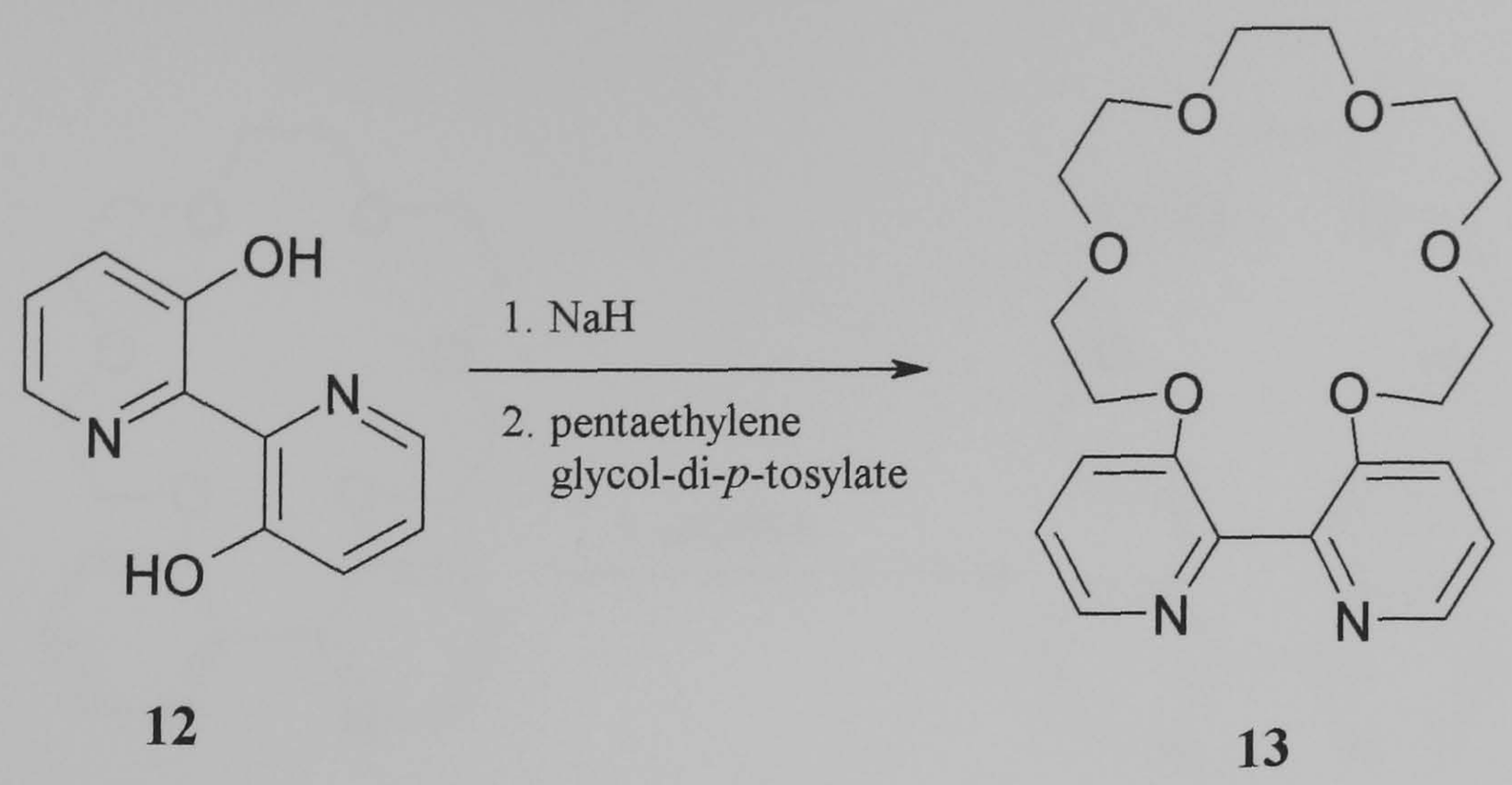

12 **13**

To a two neck round bottom flask that was under nitrogen, 3,3-dihydroxy-2,2-bipyridine (**12**) (1.0 g, 5.3 mmol) and sodium hydride (60% dispersion in oil) (0.85 g, 22.2 mmol) were added. Anhydrous DMF (50 ml) was added and the reaction heated to 60°C with stirring for 1 hour, after this time penta-(ethylene glycol)-di-*p*-tosylate (2.9 g, 5.3 mmol) was added to the reaction mixture and heating continued for a further 24 hours. Any remaining sodium hydride was then reacted by addition of methanol (5 ml). Removal of the solvents by rotary evaporation gave a brown oil to which $NaHCO_{3(aq)}$ (40 ml) was added and extracted into DCM (4 × 50 ml). Evaporation of the combined organic layers gave a brown oil that was purified via column chromatography (10% MeOH in DCM, SiO_2) giving (**13**) as a viscous amber oil. This solidifies on standing to give a pale brown waxy solid (1.3 g, 3.32 mmol, 62%). The synthesis of 2,2'-bipyridine-crown ether, (**13**) was carried out using literature methods.[104]

^{1}H NMR [400 MHz, $CDCl_3$]: δ (ppm) 8.35 (d, J = 4.2, Hz, 2H), 7.35 (m, 2H), 7.30 (m, 2H), 4.20-3.40 (m, 20H)

ESI-MS: *m/z* 391.1 ($M + H^+$)

*6.12 Synthesis of bis-N,N'-oxide, (**14**)*

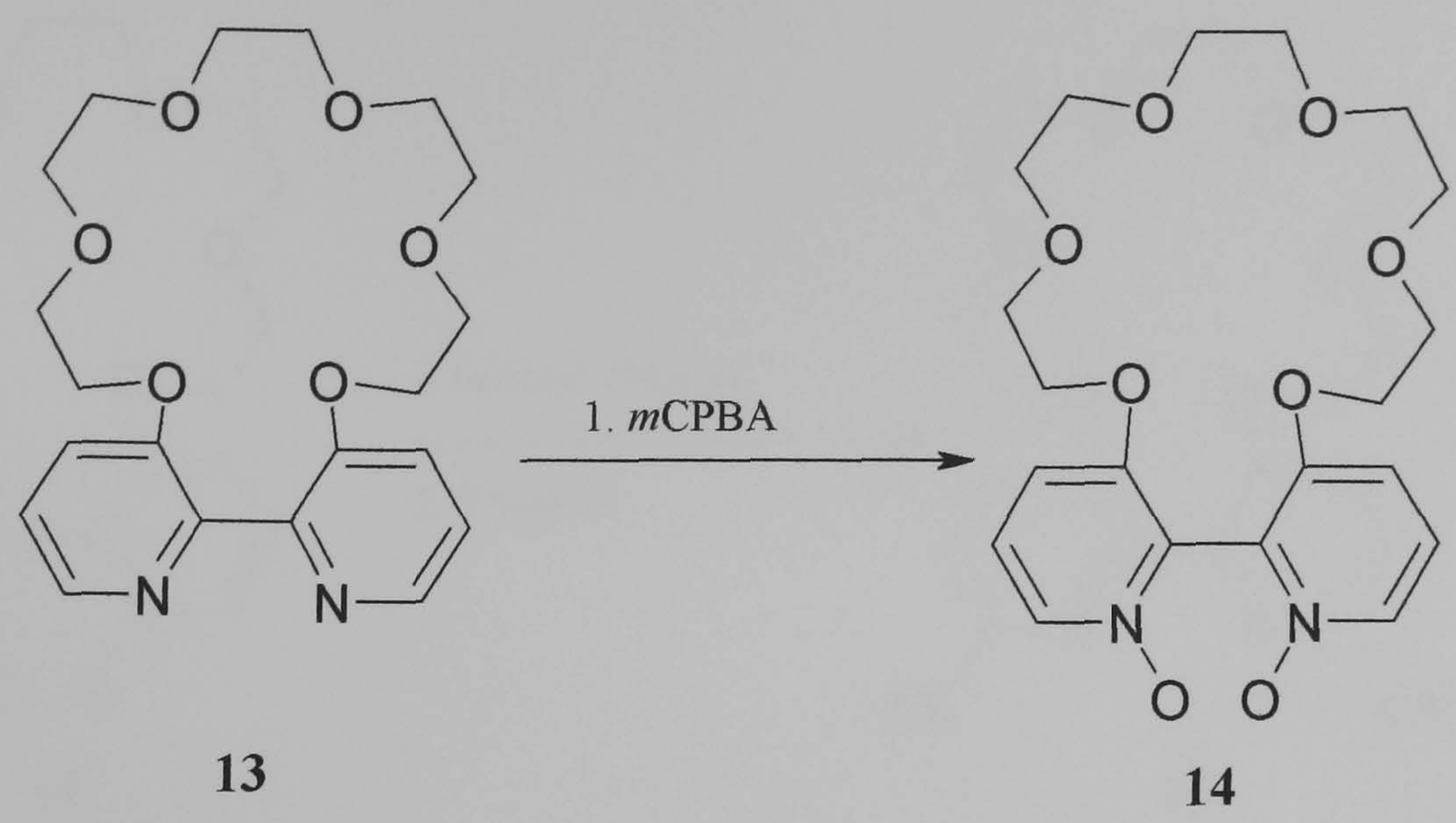

A solution of 2,2'-bipyridine-crown ether (**14**) (1.0 g, 2.56 mmol) and *m*CPBA (77%, 1.26 g, 5.63 mmol) in DCM (40 ml) was stirred at room temperature for 6 hours. The reaction was followed by TLC and upon completion the solvent was reduced to half its volume by rotary evaporation. The solution was then purified by column chromatography (1% MeOH in DCM, Al_2O_3) giving (**15**) as a white solid (0.94 g, 2.23 mmol, 87%).

^{1}H NMR [400 MHz, $CDCl_3$]: δ (ppm) 8.05 (d, J = 6.5, 2H), 7.25 (m, 2H), 7.0 (d, J = 8.6 Hz, 2H), 4.30-3.45 (m, 20H)

ESI-MS: *m/z* 419.2 ($M + H^+$)

*6.13 Synthesis of 2,2'-bipyridine-crown ether-6,6'-dicarbonitrile, (**15**)*

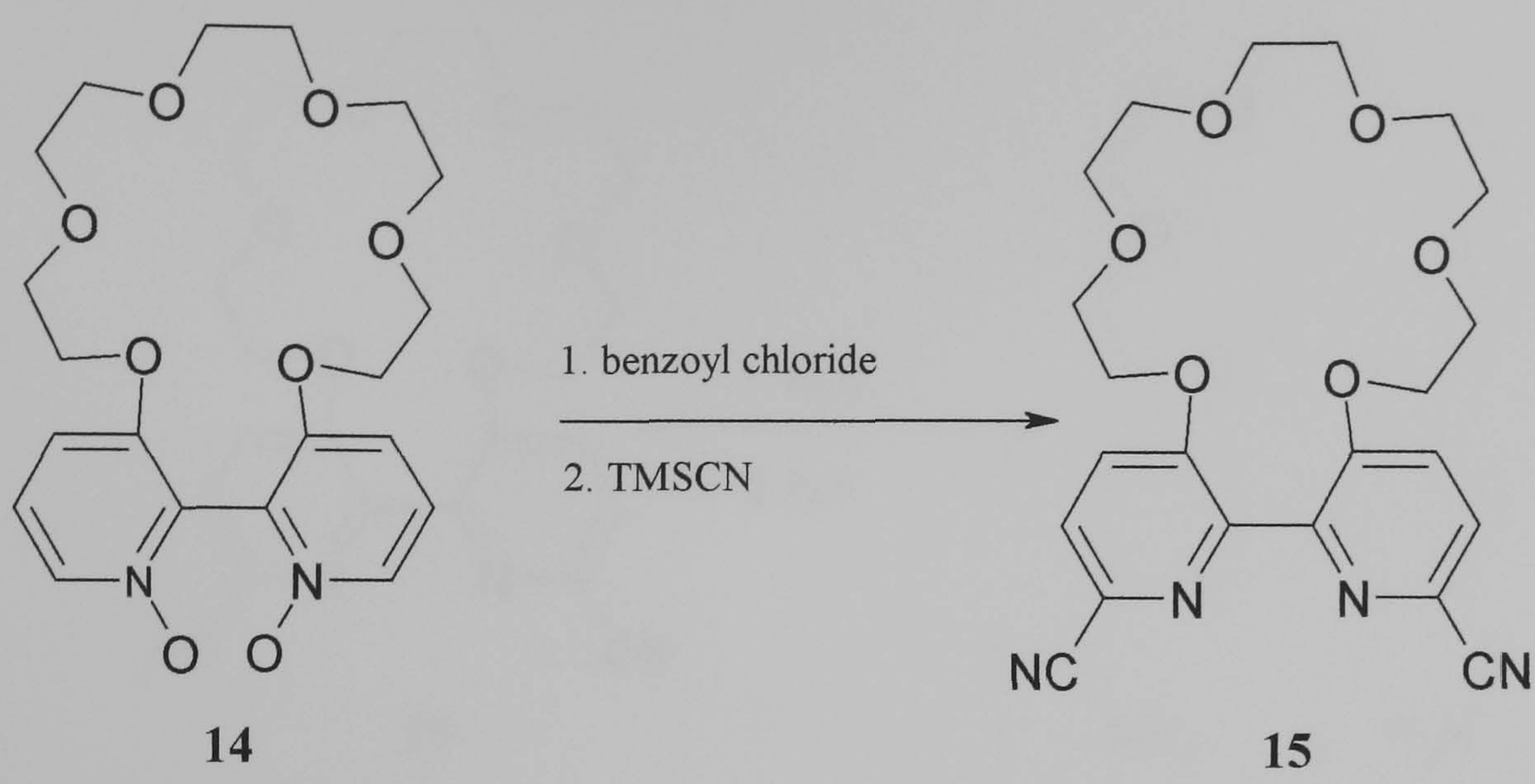

A solution of bis-N,N'-oxide (**14**) (0.8 g, 1.9 mmol) and benzoyl chloride (0.59 g, 4.16 mmol) in DCM (50 ml) was refluxed, and trimethylsilyl cyanide (0.41 g, 4.17 mmol) added slowly after a period of 30 minutes. The reaction was monitored by TLC and upon completion the solution was cooled and washed with $NaHCO_{3(aq)}$. Removal of the solvent by rotary evaporation give the crude product as a brown oil, this was then purified via column chromatography (1% MeOH in DCM, Al_2O_3) affording (**15**) as a white solid (0.71 g, 1.61 mmol, 85%).

^{1}H NMR [400 MHz, $CDCl_3$]: δ (ppm) 7.75 (d, J = 8.7, 2H), 7.45 (d, 8.6 Hz, 2H), 4.35-3.55 (m, 20H)

ESI-MS: m/z 441.4 ($M + H^+$)

*6.14 Synthesis of 2,2'-bipyridine-crown ether-6,6'- dithioamide, (**16**)*

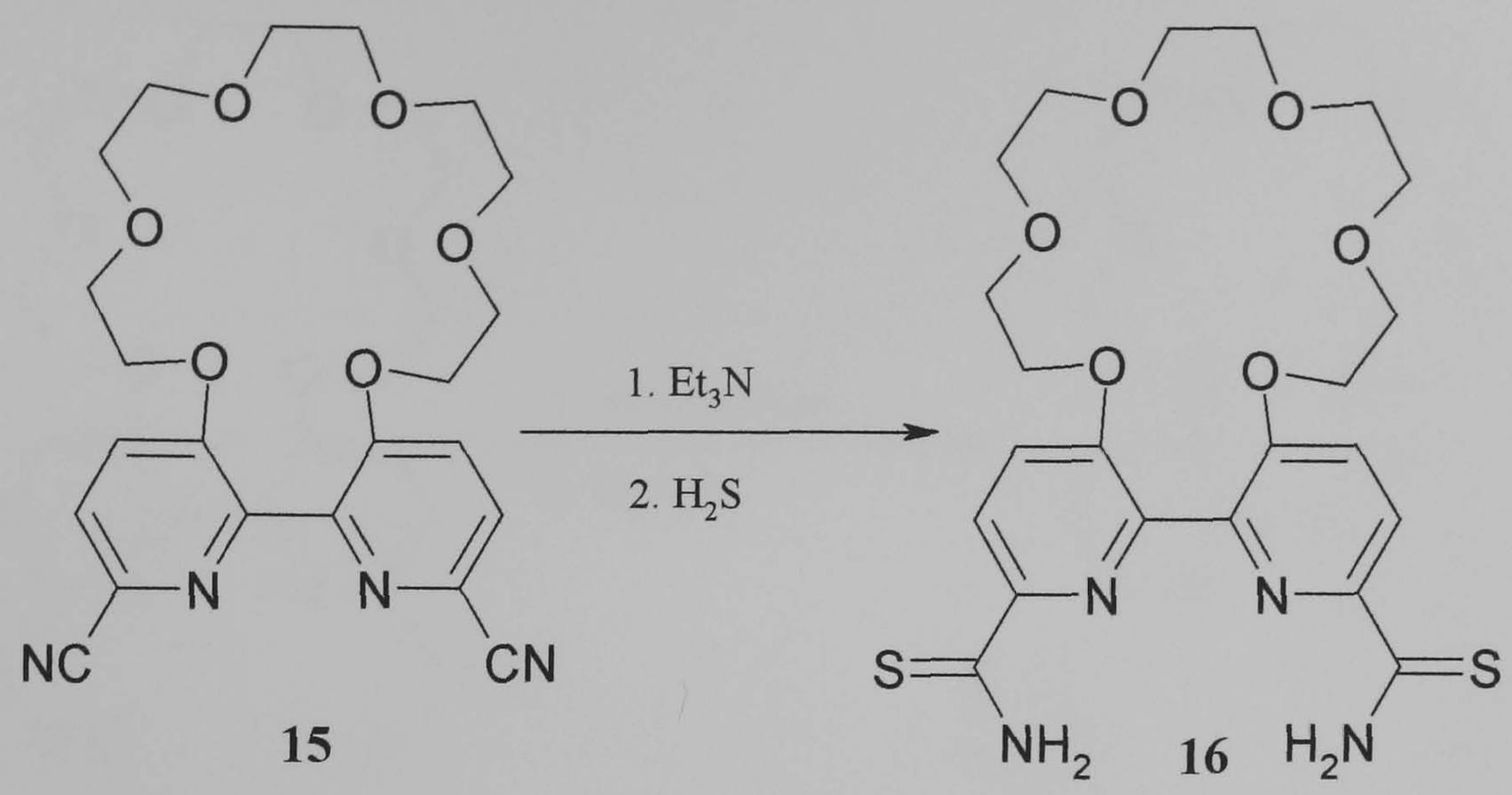

To a solution of 2,2'-bipyridine-crown ether-6,6'-dicarbonitrile (**15**) (0.7 g, 1.59 mmol) and triethylamine (1.0 g, 9.9 mmol) in ethanol (20 ml), H_2S was slowly bubbled through the solution for 15 minutes, during which time the solution turned yellow. The yellow solution was allowed to stand for 48 hours during which time a yellow solid slowly precipitated. Collection via filtration gave pure 2,2'-bipyridine-crown ether-6,6'-dithioamide (**16**) as a yellow solid(0.68 g, 1.33 mmol, 84%).

^{1}H NMR [400 MHz, $CDCl_3$]: δ (ppm) 9.40 (s, 2H), 8.50 (d, J = 9.2, 2H), 7.60 (s, 2H), 7.4 (d, J = 9.2 Hz, 2H) 4.50-3.50 (m, 20H)

ESI-MS: *m/z* 509.0 ($M + H^+$)

*6.15 Synthesis of (**L₂**)*

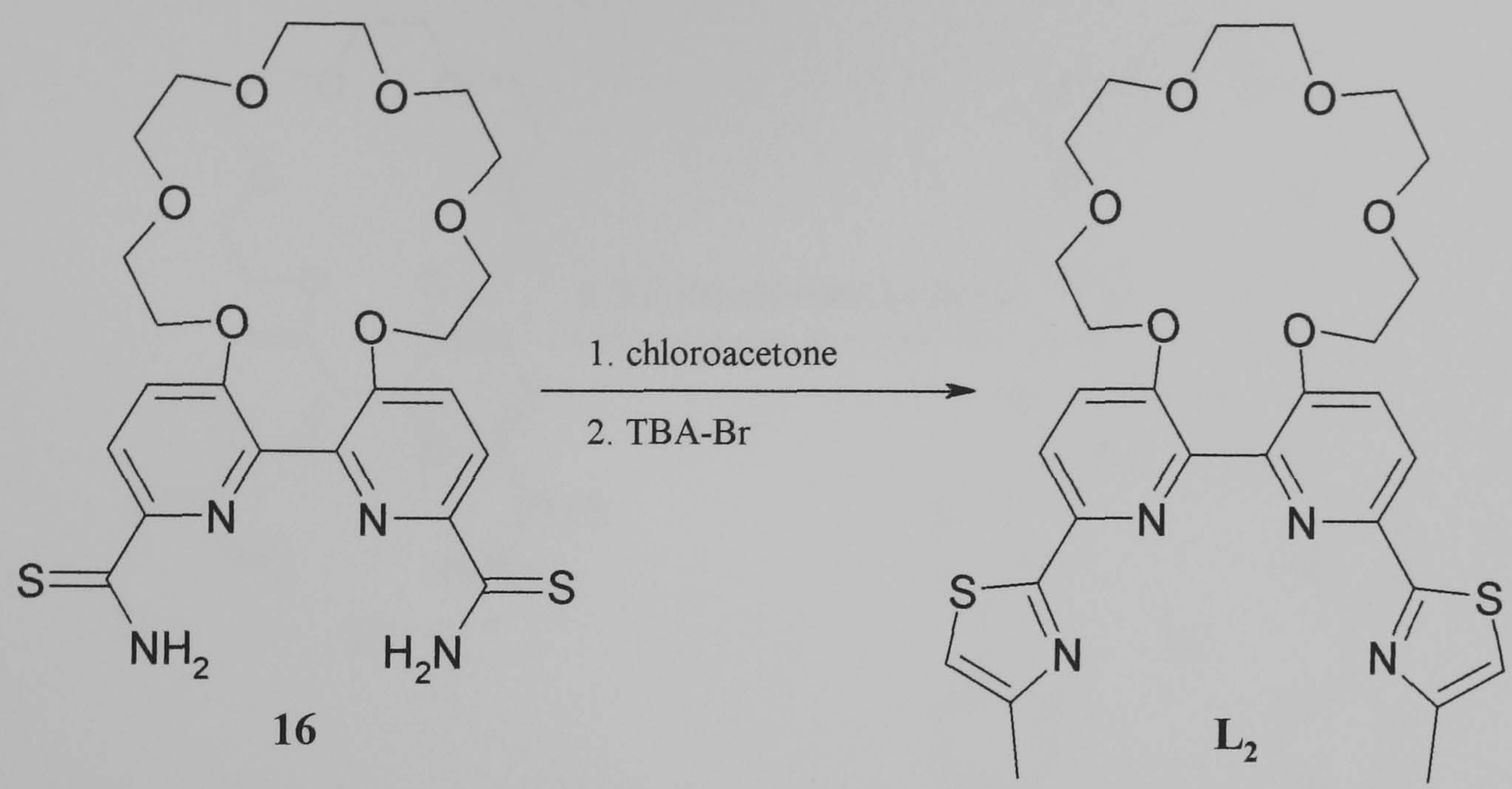

A solution of 2,2'-bipyridine-crown ether-6,6'-dithioamide (**16**) (0.2 g, 0.39 mmol) and chloroacetone (0.19 ml, 3.03 mmol) in ethanol (50 ml) was refluxed for 6 hours in the presence of a catalytic amount of TBA-Br. Removal of the solvent by rotary evaporation gave a yellow solid to which $NaHCO_{3(aq)}$ (30 ml) was added and extracted from DCM (3 × 50 ml). Evaporation of the combined organic layers gave the crude product as an off white solid, purification via column chromatography (1% MeOH in DCM, Al_2O_3) gave (**L₂**) as an off white solid (0.17 g, 0.29 mmol, 74%).

^{1}H NMR [400 MHz, $CDCl_3$]: δ (ppm) 8.2 (d, J = 8.65, 2H), 7.43 (d, J = 8.70 Hz, 2H), 6.9 (s, 2H), 4.3-3.5 (m, 20H), 2.52 (s, 6H).

^{13}C NMR [400 MHz, ($CDCl_3$)]: δ (ppm) 168.5 (th), 154.5(py), 153.5 (py), 146.1 (py), 143.9 (py), 120.3 (th), 120.1 (py), 115.2 (th), 70.9 (cr), 70.7 (cr), 70.6 (cr), 69.4 (cr), 68.8 (cr), 17.3 (Me).

ESI-MS: *m/z* 585.3 ($M + H^+$).

*6.16 Synthesis of (**L**$_3$)*

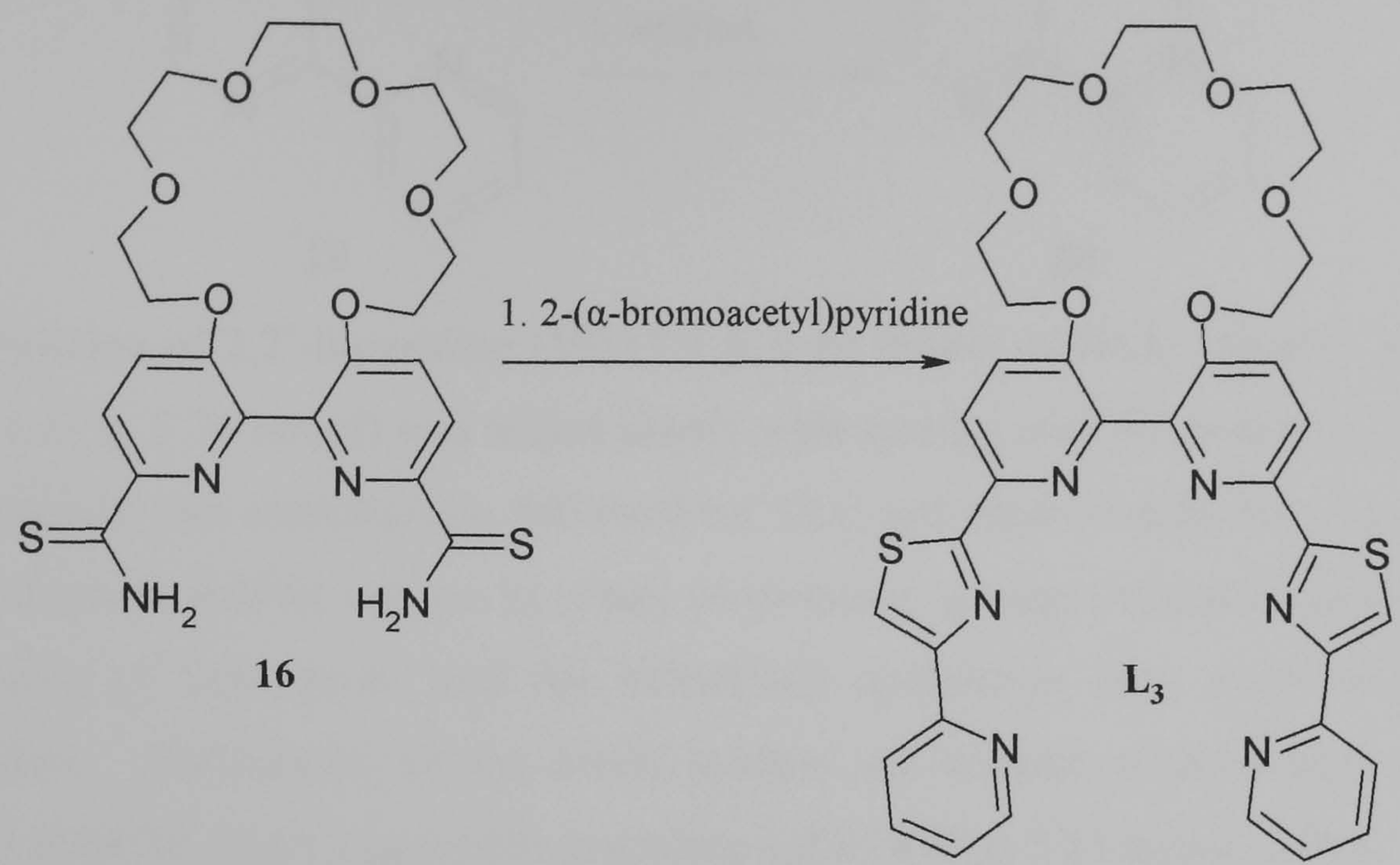

A solution of 2,2'-bipyridine-crown ether-6,6'-dithioamide (**16**) (0.2 g, 0.39 mmol) and 2-(α-bromoacetyl)pyridine (0.28 g, 1.37 mmol) in ethanol (50 ml) was refluxed for 8 hours. Removal of the solvent by rotary evaporation gave a brown residue which was dissolved in distilled water (20 ml) and neutralised with $NaHCO_{3(aq)}$ and extracted from DCM (3 × 50 ml). Evaporation of the combined organic layers gave the crude product as a pale oil. The oil was the treated with diethyl ether (5 ml) and the remaining solid was collected by filtration. The solid was then washed with two further portions of diethyl ether (2 ml) giving (**L**$_3$) as a tan solid. Further purification via column chromatography (1% MeOH in DCM, Al_2O_3) gave (**L**$_3$) as an off white solid (0.18 g, 0.25 mmol, 64%). The synthesis of (**L**$_1$) was carried out following the procedure described by Rice and co-workers.[101]

^{1}H NMR [400 MHz, $CDCl_3$]: δ (ppm) 8.67 (d, J = 4.18, 2H), 8.39 (d, J = 8.69, 2H), 8.29 (d, J = 7.76, 2H), 8.13 (s, 2H), 7.84 (t, J = 6.01, 2H), 7.51 (d, J = 8.7 Hz, 2H), 7.28 (m, 2H), 4.3-3.75 (m, 20H).

^{13}C NMR [400 MHz, ($CDCl_3$)]: δ (ppm) 169.2 (C), 154.8 (C), 152.8 (C), 149.4 (CH), 146.1 (C), 143.8 (C), 136.9 (CH), 122.6 (CH), 121.1 (CH), 120.6 (CH), 120.2 (CH), 118.7 (CH), 71.0 (CH_2), 70.7 (CH_2), 70.6 (CH_2), 69.5 (CH_2), 68.9 (CH_2).

ESI-MS: *m/z* 711.3 ($M + H^+$)

*6.17 Synthesis of 2,2'-bipyridine 1-N-oxide, (**20**)*

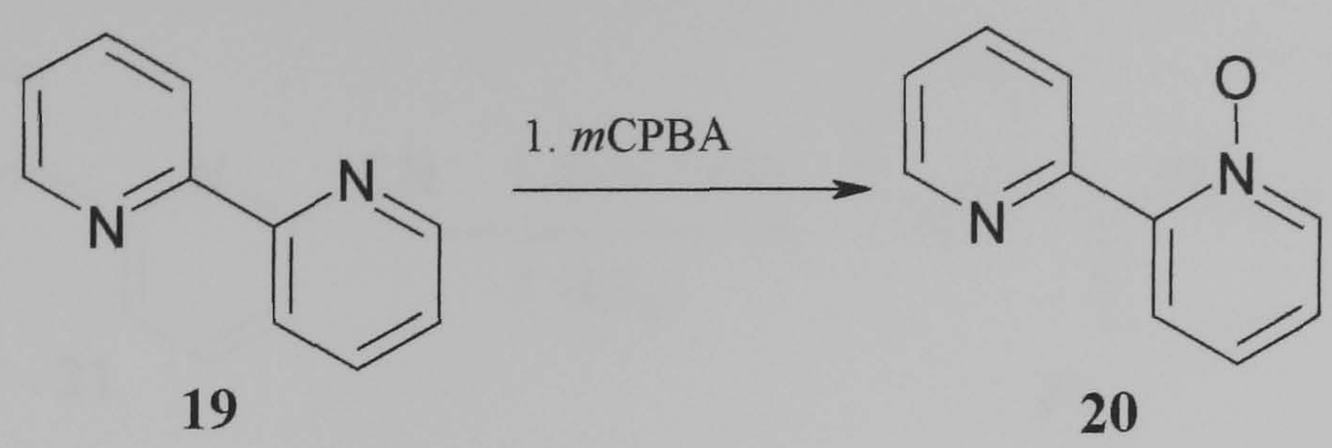

To a solution of 2,2'-bipyridine (**19**) (1.0 g, 6.40 mmol) in DCM (40 ml), *m*CPBA (77% 1.29 g, 5.76 mmol) was added slowly with stirring over the course of 3 hours. The reaction was continuously followed by TLC and upon completion the solvent was reduced to half its volume by rotary evaporation, giving a viscous oil containing a mixture of both *mono* and *bis* substituted derivatives plus some un-reacted bipyridine. Purification of the crude product via column chromatography (1% MeOH in DCM, Al_2O_3) gave (**20**) as a white solid (0.89 g, 5.11 mmol, 80%).

^{1}H NMR [500 MHz, $CDCl_3$]: δ (ppm) 8.93 (d, J = 8.95, 1H), 8.75 (ddd, J = 4.8, 0.85, 1H), 8.35 (dd, J = 6.55, 1.1, 1H), 8.20 (dd, J = 8.0, 2.1, 1H), 7.86 (dt, J = 7.85, 1.8, 1H), 7.40 (dt, J = 7.7, 1.2, 1H), 7.38 (dt, J = 7.55, 1.15 Hz, 1H), 7.30 (m, 1H)

*6.18 Synthesis of 2,2'-bipyridine-6-carbonitrile, (**21**)*

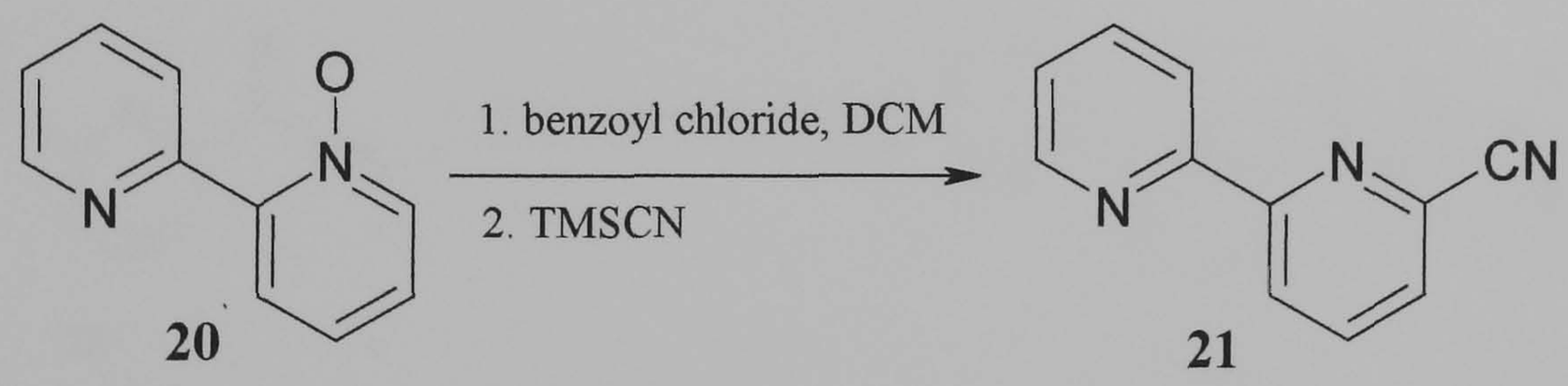

A solution of mono-N-oxide (**20**) (0.8 g, 4.65 mmol) and benzoyl chloride (0.71 g, 5.11 mmol) in DCM (50 ml) was refluxed, and trimethylsilyl cyanide (0.51 g, 5.11 mmol) added slowly after a period of 30 minutes. Upon completion the solution was cooled and washed with $NaHCO_{3(aq)}$. Removal of the solvent by rotary evaporation give the crude product as a brown oil, purification via column chromatography (1% MeOH in DCM, Al_2O_3) afforded (**21**) as a white solid (0.70 g, 3.86 mmol, 84%).

^{1}H NMR [500 MHz, $CDCl_3$]: δ (ppm) 8.72 (m, 2H), 8.50 (d, J = 9.95, 1H), 7.97 (t, J = 9.8, 1H), 7.88 (dt, J = 9.7, 2.25, 1H), 7.72 (dd, J = 9.5, 1.25, 1H), 7.40 (ddd, J = 9.4, 5.95, 1.4 Hz, 1H).

*6.19 Synthesis of 2,2'-bipyridine thioamide, (**22**)*

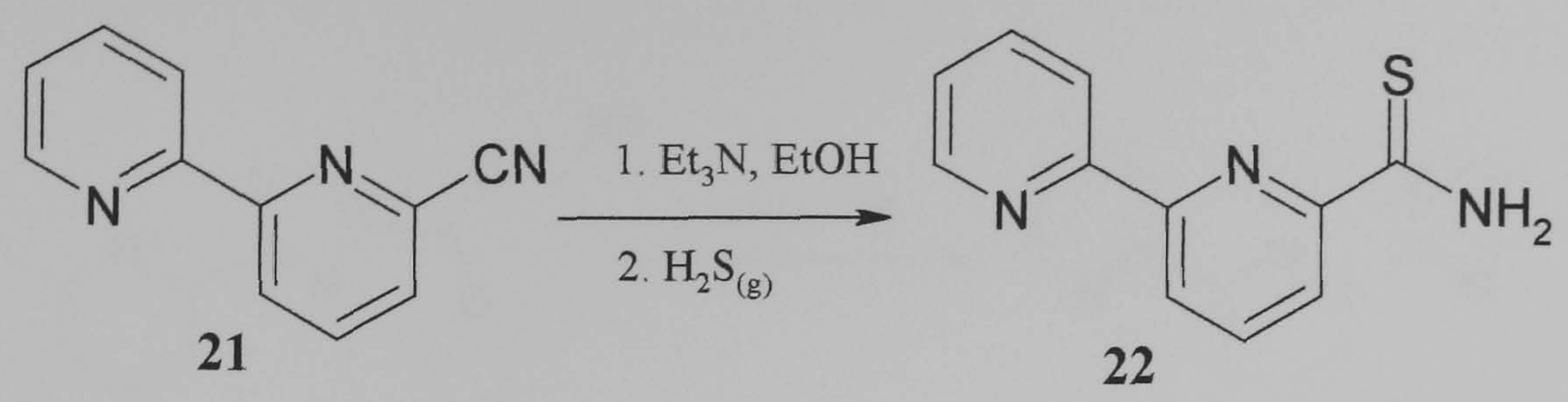

21 **22**

To a solution of 2,2'-bipyridine-6-carbonitrile (**21**) (0.7 g, 3.84 mmol) and triethylamine (1.0 g, 9.9 mmol) in ethanol (20 ml), H_2S was slowly bubbled through the solution for 15 minutes, during which time the solution turned yellow. The yellow solution was allowed to stand for 48 hours during which time a yellow solid slowly precipitated. Collection via filtration gave pure 2,2'-bipyridine thioamide (**22**) as a yellow solid (0.71 g, 3.30 mmol, 85%).

^{1}H NMR [500 MHz, $CDCl_3$]: δ (ppm) 9.61 (brs, 1H), 8.78 (d, J = 7.8, 1H), 8.73 (d, J = 4.7, 1H), 8.64 (d, J = 7.9, 1H), 8.38 (d, J = 7.95, 1H), 8.01 (t, J = 7.85, 1H), 7.88 (dt, J = 7.8, 1.5, 1H), 7.73 (bs, 1H), 7.39 (dd, J = 7.45, 4.85 Hz, 1H).

*6.20 Synthesis of tridentate ester, (**23**)*

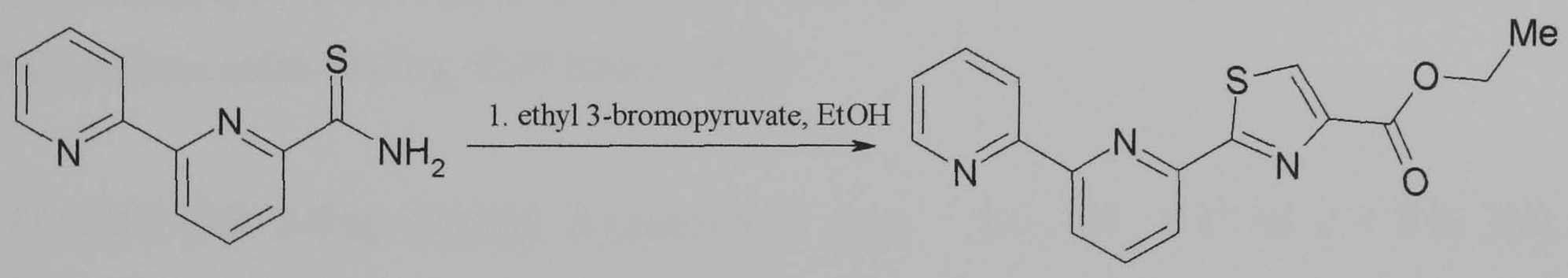

22 **23**

A solution of 2,2'-bipyridine thioamide (**22**) (0.6 g, 2.79 mmol) and ethyl 3-bromopyruvate (0.60 g, 3.07 mmol) in ethanol (50 ml) was refluxed for 6 hours. On cooling large brown crystals of (**23**) slowly formed which were filtered and washed with ethanol (2 ml) (0.63 g, 2.02 mmol, 73%).

^{1}H NMR [500 MHz, $CDCl_3$]: δ (ppm) 9.19 (d, J = 5.5, 1H), 9.12 (d, J = 8.0, 1H), 8.85 (d, J = 8.0, 1H), 8.56 (d, J = 8.0, 1H), 8.54 (m, 1H), 8.33 (s, 1H), 8.18 (t, J = 8.0, 1H), 7.98 (t, J = 6.5, 1H), 4.45 (q, J = 7.0, 2H), 1.44 (t, J = 7.0 Hz, 3H)

ESI-MS m/z 312.1 ($M + H^+$).

*6.21 Synthesis of tridentate alcohol, (**24**)*

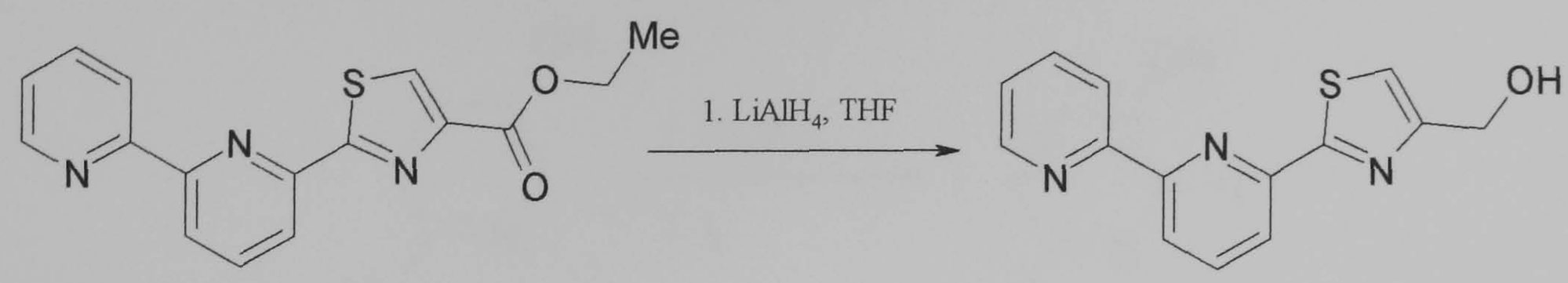

23 **24**

Under an atmosphere of nitrogen a dry 100 ml two neck round bottom flask was charged with the tridentate ester (**23**) (0.2 g g, 0.64 mmol). Anhydrous THF (30 ml) was added to the flask and the resulting solution stirred in an ice bath at 0°C for 15 minutes. Lithium aluminium hydride, (1.0 M solution in diethyl ether, 1.28 ml, 1.28 mmol) was slowly added over the course of 20 minutes. Stirring was continued for 2 hours at 0°C before removing the ice bath and allowing the reaction to gradually warm up to room temperature. Any remaining lithium aluminium hydride was quenched by slow addition of THF (2 ml), methanol (2 ml) and finally water (2 ml). The solvents were removed by rotary evaporation to leave a viscous yellow emulsion to which distilled water (20 ml) was added and extracted into DCM (4 × 50 ml). Evaporation of the organic solvent gave a yellow solid that was purified via column chromatography (3% MeOH in DCM, Al_2O_3) gave the tridentate alcohol (**24**) as a pale yellow solid (0.08 g, 0.29 mmol, 46%)

^{1}H NMR [500 MHz, $CDCl_3$]: δ (ppm) 8.71 (d, J = 5.0, 1H), 8.57 (d, J = 8.0, 1H), 8.48 (d, J = 8.0, 1H), 8.19 (d, J = 7.0, 1H), 7.95 (t, J = 8.0, 1H), 7.9 (dt, J = 7.5, 1.5, 1H), 7.37 (ddd, J = 7.5, 5.0, 1.0 Hz, 1H), 7.34 (s, 1H), 4.89 (s, 2H), 2.45 (brs, 1H, -OH).

ESI-MS *m/z* 292.0 (M + Na^+).

*6.22 Synthesis of 5-hydroxy-6-iodo-2-methylpyridine, (**26**)*

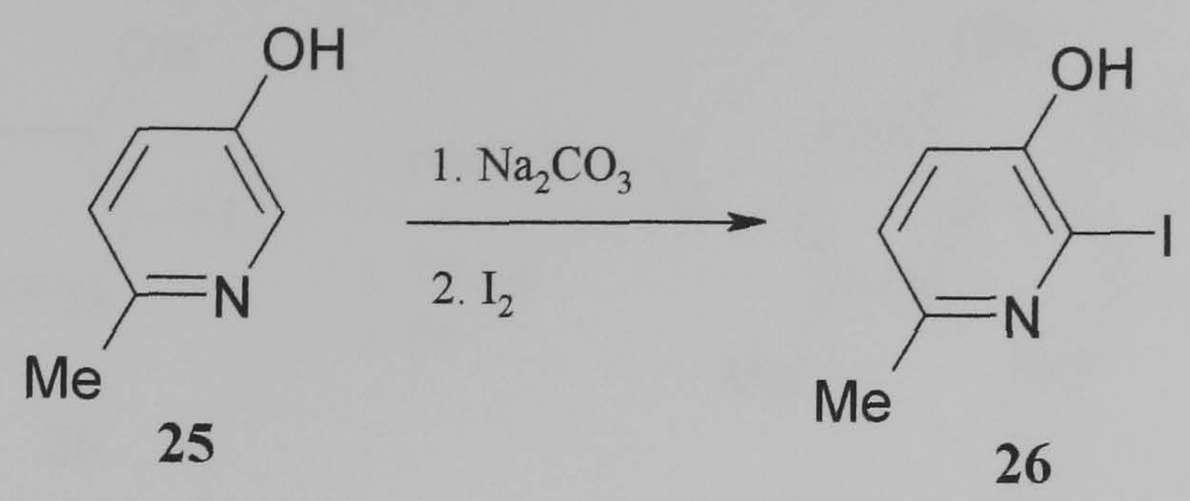

To a solution of 5-hydroxy-2-methylpyridine (**25**) (5.0 g, 0.046 mol) and sodium carbonate (9.7 g, 0.092 mol) in distilled water (200 ml), iodine bead (11.6 g, 0.046 mol) was added with vigorous stirring until complete dissolution (approximately two hours). Concentrated hydrochloric acid was slowly added with stirring until pH 3. Filtration and recrystallisation of the resulting solid form ethanol gave 5-hydroxy-6-iodo-2-methylpyridine (**26**) as a crystalline solid (4.6 g, 0.20 mol, 43%).

^{1}H NMR [400 MHz, $CDCl_3$]: δ (ppm) 6.91 (d, J = 8.0, 1H), 6.79 (d, J = 8.0 Hz, 1H), 5.10 (s, 1H), 2.27 (s, 3H)

6.23 Synthesis of 6,6'-dimethyl-2,2'-bipyridine-3,3'-diol, (27)

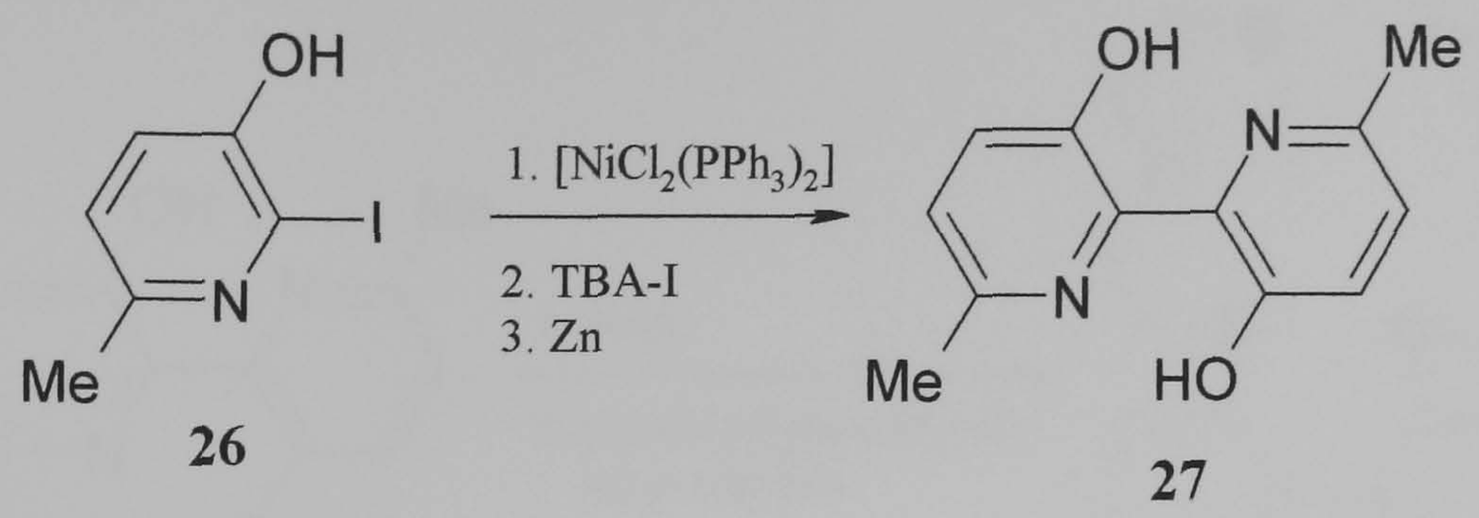

A mixture of $[NiCl_2(PPh_3)_2]$ (0.55 g, 1.40 mmol), tetra-N-butyl ammonium iodide (3.14 g, 8.50 mmol) and zinc dust (0.80 g, 0.012 mol) was added to a two neck round bottom flask equipped with a magnetic flea and placed under an atmosphere of nitrogen. Anhydrous DMF (30 ml) was added and the reaction mixture sonicated until red/brown in colour. To this 5-hydroxy-6-iodo-2-methylpyridine (**26**) (2.0 g, 8.51 mmol) was added and the reaction mixture heated to 80°C with stirring for 6 hours. Reduction of the solvent to half its volume by rotary evaporation, followed by the addition of concentrated ammonia (50 ml), the flask was then sealed for a period of 14 hours. Filtration of the reaction mixture to remove any solid followed by extraction of the aqueous filtrate with DCM (3 × 50 ml) gave (**27**) as a crude highly fluorescent yellow solid. Purification of the crude solid via column chromatography (1% MeOH in DCM, SiO_2) gave (**27**) as an analytically pure compound (0.9 g, 4.16 mmol, 78%). The synthesis of 6,6'-dimethyl-2,2'-bipyridine-3,3'-diol, (**27**) was carried out with reference to the procedure described by Rebek and co-workers.[94, 104]

^{1}H NMR [400 MHz, $CDCl_3$]: δ (ppm) 14.69 (s, 2H), 7.25 (d, J = 8.0, 2H), 7.04 (d, J = 8.0 Hz, 2H), 2.45 (s, 3H)

*6.24 Synthesis of 2,2'-bipyridine-crown ether, (**28**)*

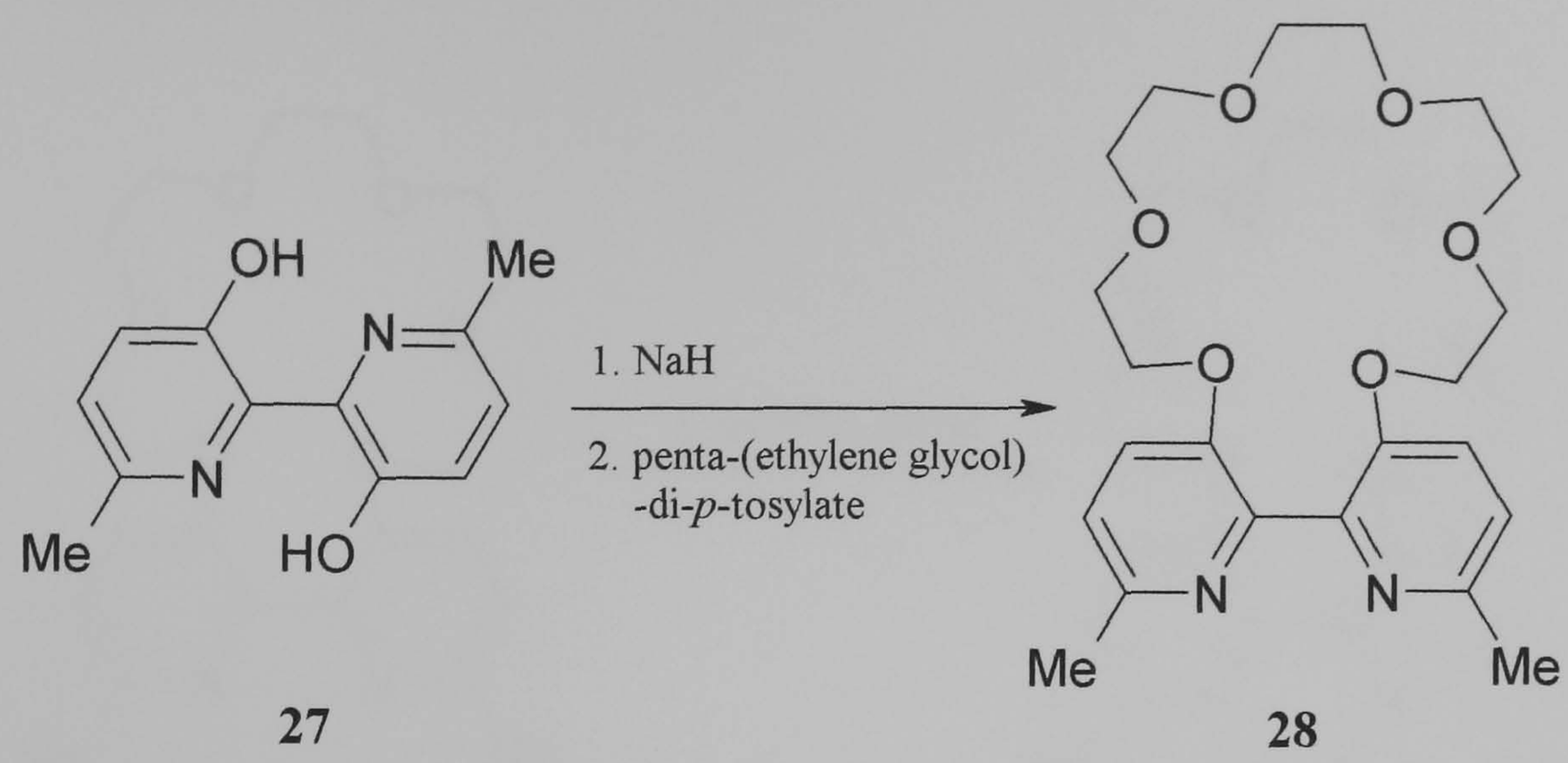

27 **28**

Under an atmosphere of nitrogen a 100 ml two neck round bottom flask was charged with 6,6'-dimethyl-2,2'-bipyridine-3,3'-diol (**27**) (1.0 g, 4.62 mmol) and sodium hydride (60% dispersion in oil, 0.74 g, 18.5 mmol). To this anhydrous DMF (50 ml) was added and the reaction heated to 60°C with stirring for 1 hour. After this time penta-(ethylene glycol)-di-*p*-tosylate (2.53 g, 4.62 mmol) was added to the reaction mixture and heating continued for a further 24 hours. The reaction was allowed to cool before any remaining sodium hydride was quenched by addition of methanol (5 ml). Removal of the solvents by rotary evaporation gave a brown oil to which $NaHCO_{3(aq)}$ (40 ml) was added and extracted into DCM (3 × 50 ml). Evaporation of the combined organic layers gave a brown oil that was purified via column chromatography (10% MeOH in DCM, SiO_2) gave (**28**) as a viscous amber oil. This solidifies on standing to give a pale brown waxy solid (1.44 g, 3.43 mmol, 74%).

^{1}H NMR [400 MHz, $CDCl_3$]: δ (ppm) 7.15 (d, J = 8.0, 2H), 7.04 (d, J = 8.0 Hz, 2H), 4.10-3.40 (m, 20H), 2.48 (s, 6H)

ESI-MS *m/z* 441.2 ($M + Na^+$).

*6.25 Synthesis of bis-N,N'-oxide, (**29**)*

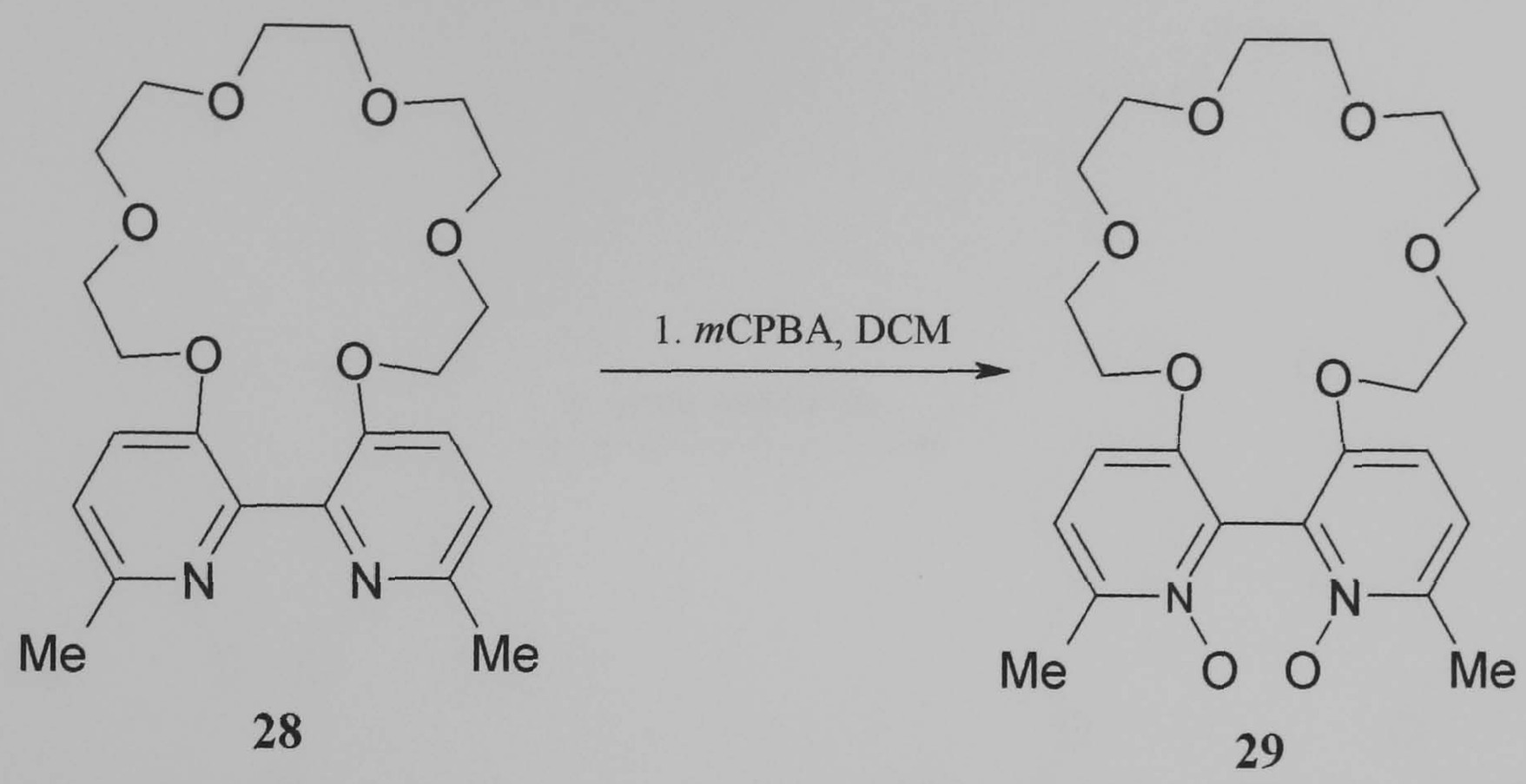

A solution of 2,2'-bipyridine-crown ether (**28**) (1.0 g, 2.39 mmol) and *m*CPBA 77% (1.18 g, 5.26 mmol) in DCM (40 ml) was stirred at room temperature for 6 hours. The reaction was followed by TLC and upon completion the solvent was reduced to half its volume by rotary evaporation. Purification of the crude product via column chromatography (1% MeOH in DCM, Al_2O_3) giving (**29**) as a white solid (0.95 g, 2.10 mmol, 88%).

^{1}H NMR [500 MHz, $CDCl_3$]: δ (ppm) 7.27 (d, J = 10.0, 2H), 6.95 (d, J = 10.0 Hz, 2H), 4.21-3.56 (m, 20H), 2.53 (s, 6H)

ESI-MS *m/z* 473.2 ($M + Na^+$).

*6.36 Synthesis of the acetylated 2,2'-bipyridine-crown ether, (**30**)*

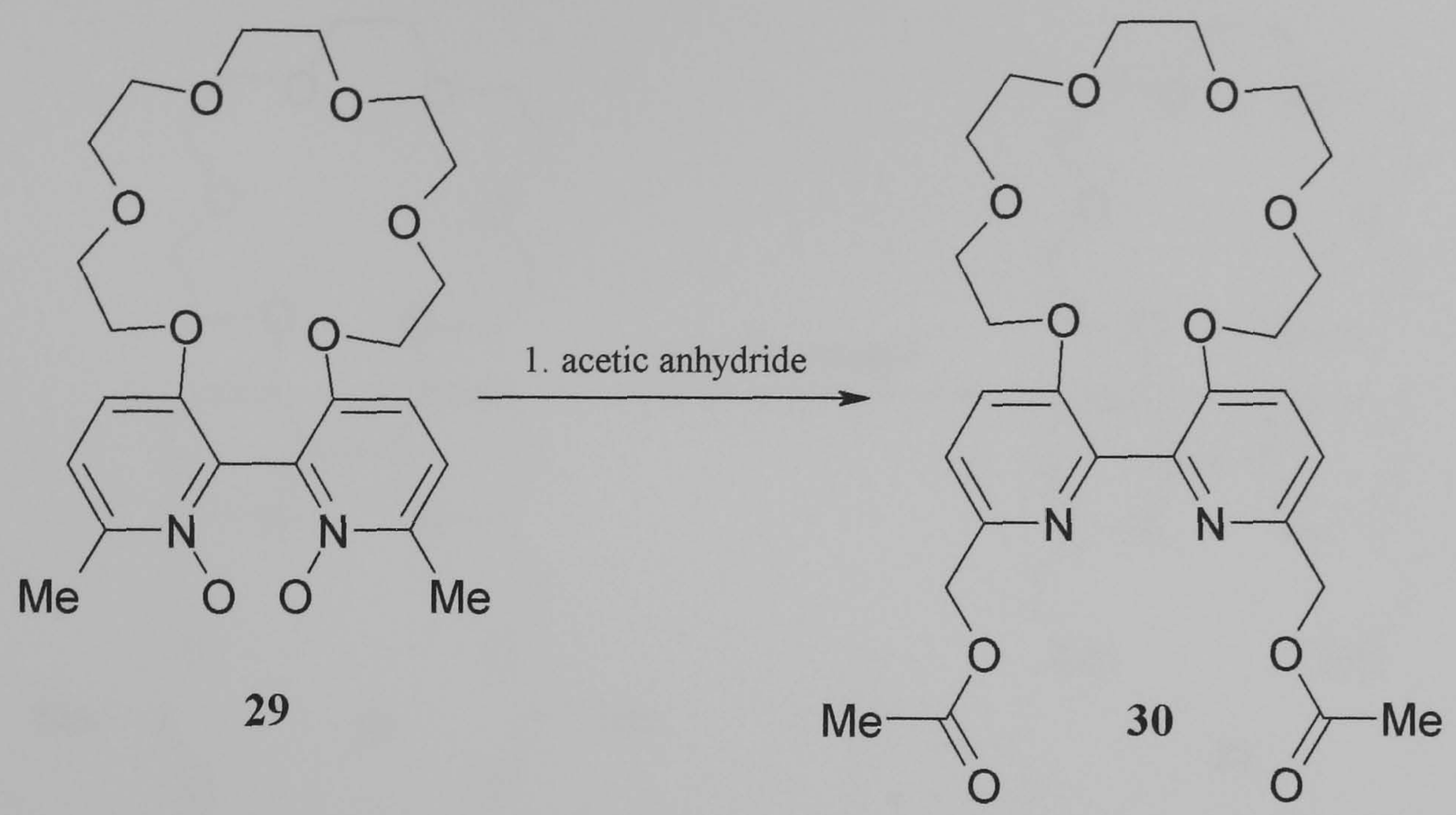

To a 50 ml round bottom flask the bis-N,N'-oxide (**29**) (0.4 g, 0.89 mmol) and acetic anhydride (10 ml) was added. The reaction vessel was then placed under an atmosphere of nitrogen and heated to 120°C for 4 hours with stirring. Upon completion toluene, (20 ml) was added to aid in the removal of the acetic anhydride by rotary evaporation. Following the removal of all the solvents the resulting brown oil was immediately purified via column chromatography (1% MeOH in DCM, Al_2O_3) gave (**30**) as a colourless oil (0.37 g, 0.69 mmol, 78%).

^{1}H NMR [400 MHz, $CDCl_3$]: δ (ppm) 7.29 (d, J = 8.0 , 2H), 7.23 (d, J = 8.0 Hz, 2H), 5.13 (s, 4H), 4.12-3.42 (m, 20H), 2.03 (s, 6H)

ESI-MS *m/z* 557.2 ($M + Na^+$).

*6.27 Synthesis of 2,2'-bipyridine-6,6'-dimethanol-crown ether, (**31**)*

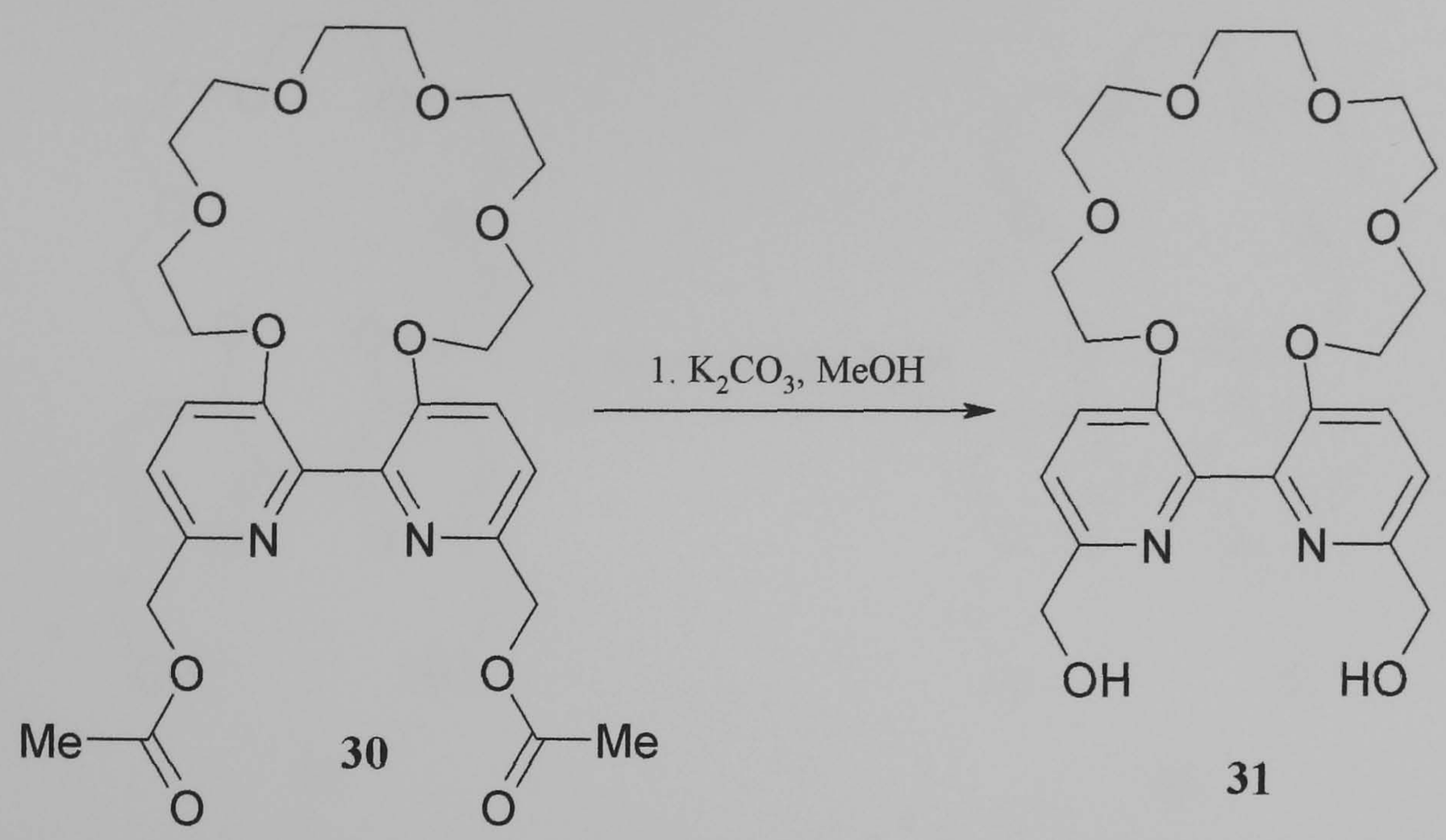

The acetylated 2,2'-bipyridine (**30**) (0.37 g, 0.69 mmol) was completely dissolved in anhydrous methanol (20 ml). To this an excess of potassium carbonate (0.38 g, 3.00 mmol) was added and stirred for 4 hours. Upon completion the solvent was removed by rotary evaporation to give a white emulsion to which distilled water (20 ml) was added and extracted into DCM (3 × 50 ml). Evaporation of the combined organic extracts gave (**31**) as an off white solid (0.29 g, 0.64 mmol, 93%).

^{1}H NMR [400 MHz, $CDCl_3$]: δ (ppm) 7.27 (d, J = 8.0, 2H), 7.24 (d, J = 8.0 Hz, 2H), 4.68 (s, 4H), 4.20-3.40 (m, 20H), 3.50 (overlap, 2H, -OH).

ESI-MS *m/z* 472.2 (M + Na^+).

*6.28 Synthesis of 2,2'-bipyridine-6,6'-dimethylchloride-crown ether, (**32**)*

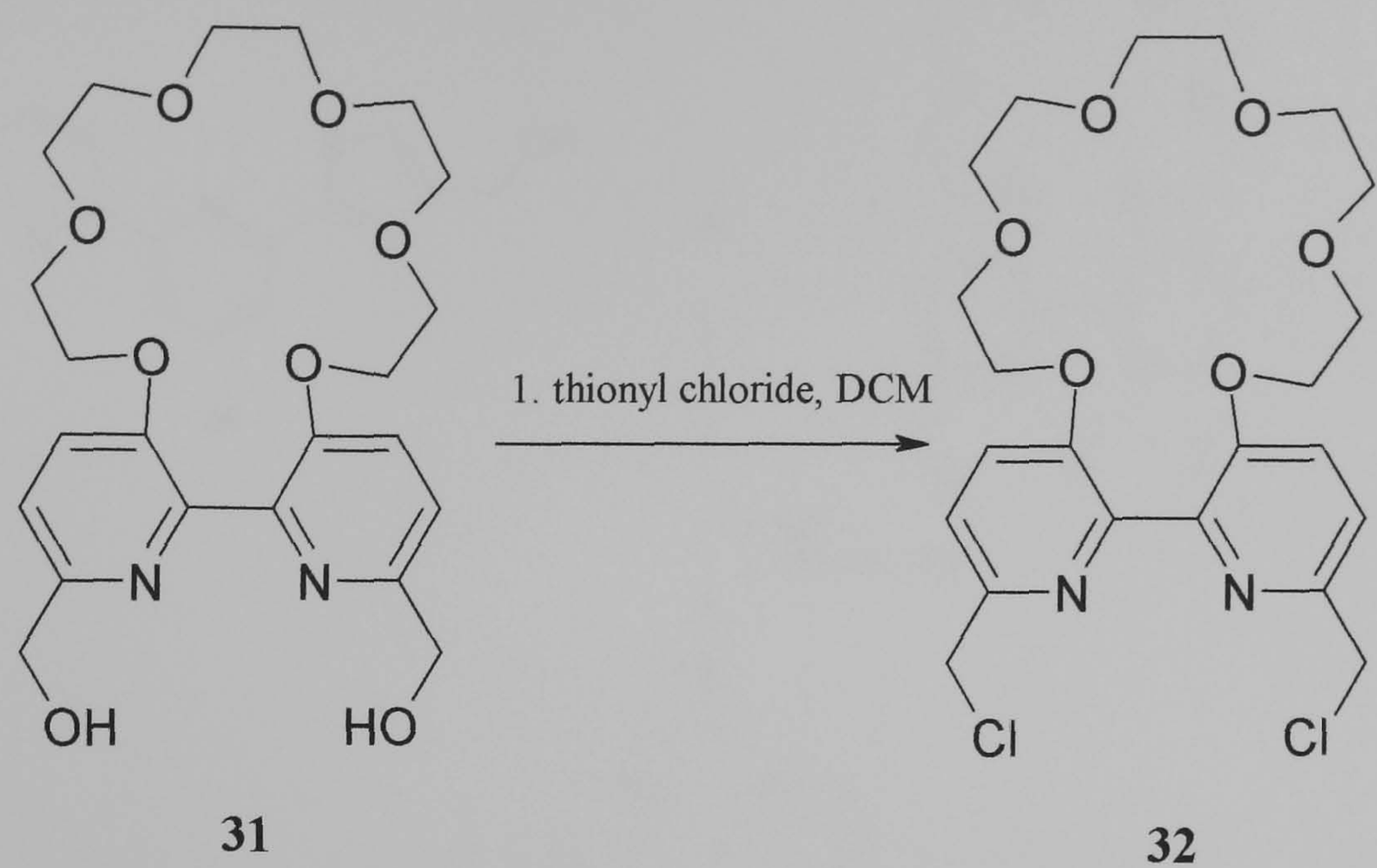

A solution of 2,2'-bipyridine dimethanol (**31**) (0.29 g, 0.64 mmol) and thionyl chloride (2 ml) in DCM (50 ml) was refluxed for 4 hours. Upon completion the solution was allowed to cool before slowly pouring into $NaHCO_{3(aq)}$ and extracted into DCM (3 × 20 ml). Removal of the solvent by rotary evaporation gave a brown oil which was immediately purified via column chromatography (1% MeOH in DCM, Al_2O_3) give (**32**) as a white solid (0.18 g, 0.37 mmol, 57%).

^{1}H NMR [400 MHz, $CDCl_3$]: δ (ppm) 7.53 (d, J = 8.0, 2H), 7.38 (d, J = 8.0 Hz, 2H), 4.72 (s, 4H), 4.24-3.57 (m, 20H)

ESI-MS *m/z* 487.1 (M^+).

*6.29 Synthesis of (**L**$_4$)*

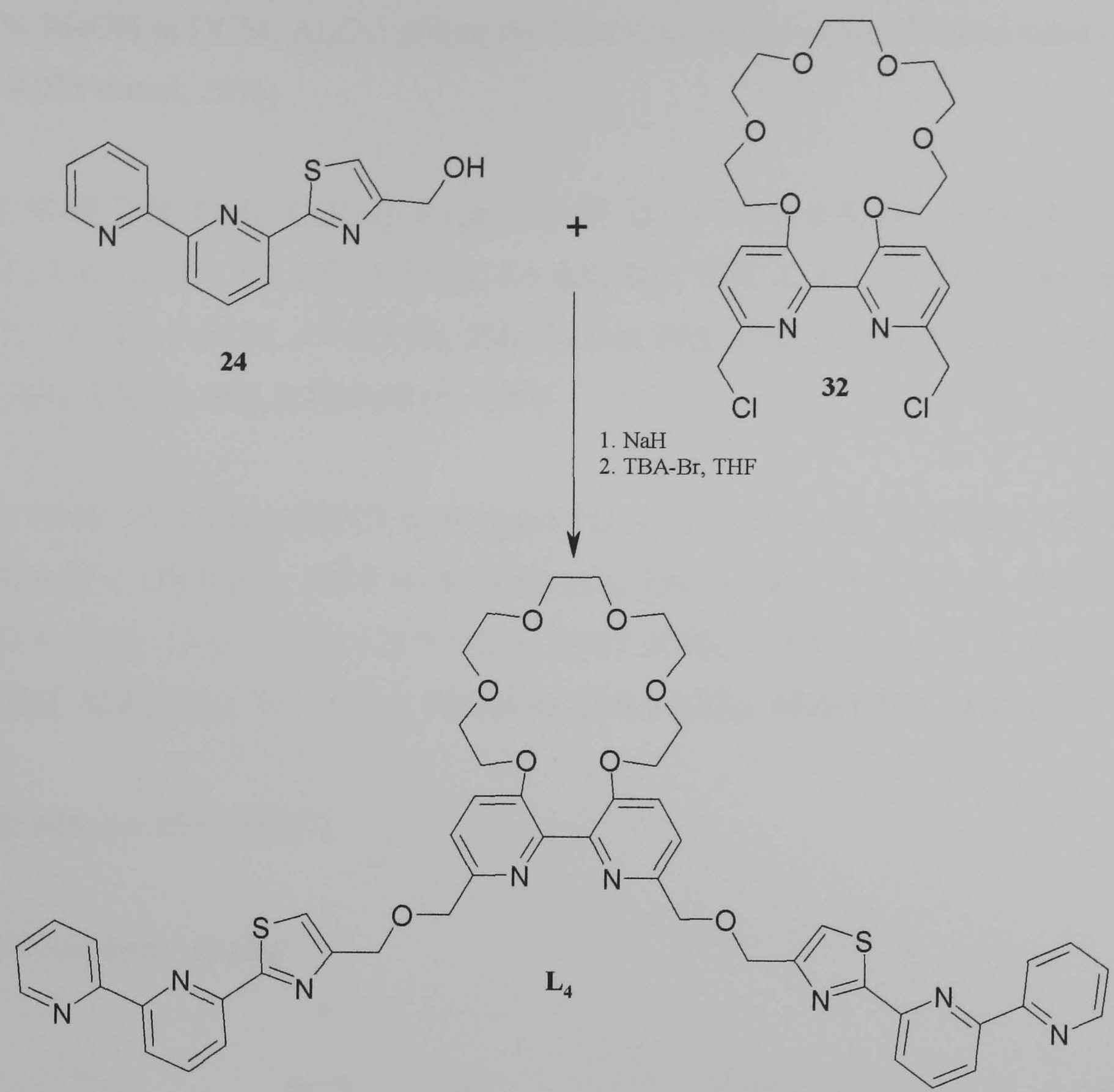

To a dry 100 ml two neck round bottom flask the tridentate unit (**24**) (0.050 g, 0.19 mmol), sodium hydride (60% dispersion in oil) (0.029 g, 0.74 mmol) and TBABr (5 mg, 0.015 mmol) were added. The flask was immediately fitted with a dry reflux condenser and placed under an atmosphere of nitrogen. To this anhydrous THF (40 ml) was added and the mixture heated under reflux for 1 hour. During this time the 2,2'-bipyridine-6,6'-dimethylchloride (**32**) (0.045 g, 0.093 mmol) was placed in a 25 ml round bottom flask fitted with a suba-seal and flushed with nitrogen for 1 hour. The 2,2'-bipyridine-6,6'-dimethylchloride (**32**) was then dissolved in anhydrous THF (5 ml) and transferred to the reaction vessel containing (**24**). The reaction was heated under reflux for a further 36 hours, monitoring the progress by TLC. Upon completion addition of methanol (5 ml) decomposed any un-reacted NaH. Removal of the solvents by rotary evaporation gave a yellow oil to which distilled water (10 ml) was added and extracted into DCM (3 × 50 ml). Evaporation of the combined

organic layers gave a crude product that was purified via column chromatography (1% MeOH in DCM, Al_2O_3) giving the final ligand (**L_4**) as an off white solid (0.024 g, 0.025 mmol, 28%).

^{1}H NMR [500 MHz, $CDCl_3$]: δ (ppm) 8.67 (dd, *J* = 4.0, 0.5, 2H), 8.54 (d, *J* = 7.5, 2H), 8.43 (d, *J* = 7.5, 2H), 8.18 (d, *J* = 8.0, 2H), 7.89 (t, *J* = 8.0, 2H), 7.84 (dt, *J* = 7.5, 3.0, 2H), 7.54 (d, *J* = 8.5 Hz, 2H), 7.41 (s, 2H), 7.34 (m,2H), 7.33 (m, 2H), 4.83 (s, 4H), 4.82 (s, 4H), 4.18-3.50 (m, 20H)

^{13}C NMR [500 MHz, ($CDCl_3$)]: δ (ppm) 155.4 (C), 155.3 (C), 155.1 (C), 152.9 (C), 150.4 (C), 149.5 (C), 148.8 (CH),145.5 (C), 138.1 (CH), 137.3 (CH), 124.1 (CH), 122.4 (CH), 121.6 (CH), 121.5 (CH), 120.7 (CH), 119.4 (CH), 119.0 (CH), 72.8 (CH_2), 70.8 (CH_2), 70.7 (CH_2), 70.6 (CH_2), 69.4 (CH_2), 68.6 (CH_2), 68.4 (CH_2).

ESI-MS *m/z* 953.30 (M^+).

6.30 Synthesis of, ***(L_5)***

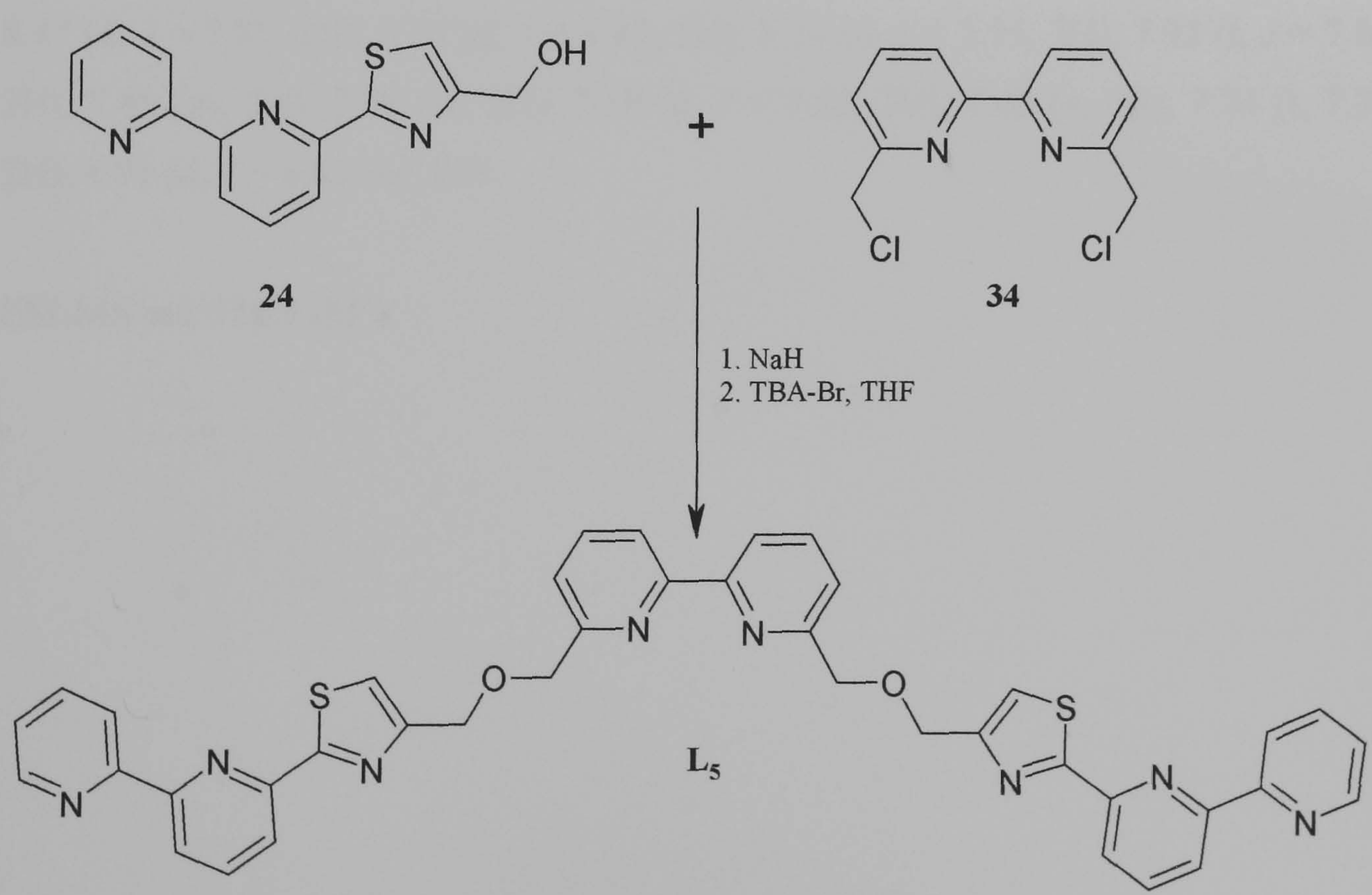

To a dry 100 ml two neck round bottom flask the tridentate unit (**24**) (0.050 g, 0.19 mmol), sodium hydride (60% dispersion in oil) (0.029 g, 0.74 mmol) and TBA-Br (5 mg, 0.015 mmol) were added. The flask was immediately fitted with a dry reflux condenser and placed under an atmosphere of nitrogen. To this anhydrous THF (40 ml) was added and the mixture heated under reflux for 1 hour. During this time the 2,2'-bipyridine-6,6'-dimethylchloride (**34**) (0.023 g, 0.093 mmol) was placed in a 25 ml round bottom flask fitted with a suba seal and flushed with nitrogen for 1 hour. The 2,2'-bipyridine-6,6'-dimethylchloride (**34**) was then dissolved in anhydrous THF (5 ml) and transferred to the reaction vessel containing (**24**). The reaction was heated under reflux for a further 36 hours, monitoring the progress by TLC. Upon completion addition of methanol (5 ml) decomposed any un-reacted NaH. Removal of the solvents by rotary evaporation gave a yellow oil to which distilled water (10 ml) was added and extracted into DCM (4 × 50 ml). Evaporation of the combined organic layers gave a crude product that was purified via column chromatography (1% MeOH in DCM, Al_2O_3) giving the final ligand (**L_5**) as an off white solid (0.015 g, 0.021 mmol, 23%).

^{1}H NMR [500 MHz, $CDCl_3$]: δ (ppm) 8.70 (d, J = 4.7, 2H), 8.57 (d, J = 8.0, 2H), 8.47 (d, J = 7.85, 2H), 8.32 (d, J = 7.85, 2H), 8.21 (d, J = 7.75, 2H), 7.92 (t, J = 7.8, 2H), 7.85 (m, 2H), 7.84 (m, 2H), 7.58 (d, J = 7.75, 2H), 7.45 (s, 2H), 7.34 (t, 7.3, 2H), 4.91 (d, J = 6.85 Hz, 8H)

ESI-MS *m/z* 718.9 (M^+).

*6.31 Synthesis of Compound (**36**)*

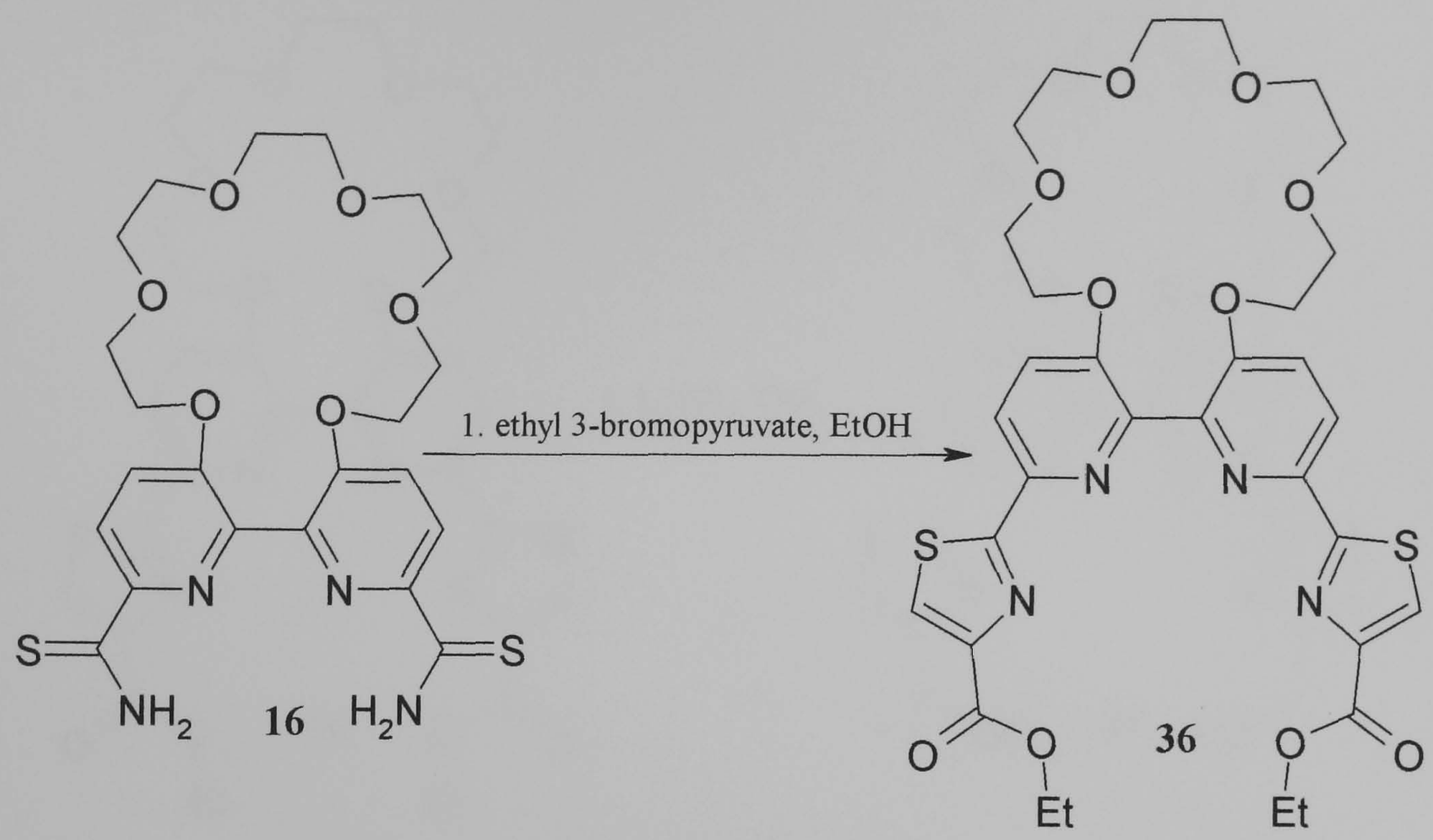

A solution of 2,2'-bipyridine-crown ether-6,6'-dithioamide (**16**) (0.6 g, 1.18 mmol) and ethyl 3-bromopyruvate (0.51 g, 2.60 mmol) in ethanol (50 ml) was refluxed for 6 hours. On cooling large brown crystals of (**36**) slowly formed which were filtered and washed with ethanol (2 ml) (0.57 g, 0.85 mmol, 72%).

^{1}H NMR [400 MHz, $CDCl_3$]: δ (ppm) 8.38 (d, J = 8.7, 2H), 8.19 (s, 2H), 7.45 (d, J = 8.7, 2H), 4.47 (q, J = 7.1, 4H), 4.26-3.58 (m, 20H), 1.45 (t, J = 7.1 Hz, 6H)

ESI-MS *m/z* 700.79 (M^+).

*6.32 Synthesis of Compound (**37**)*

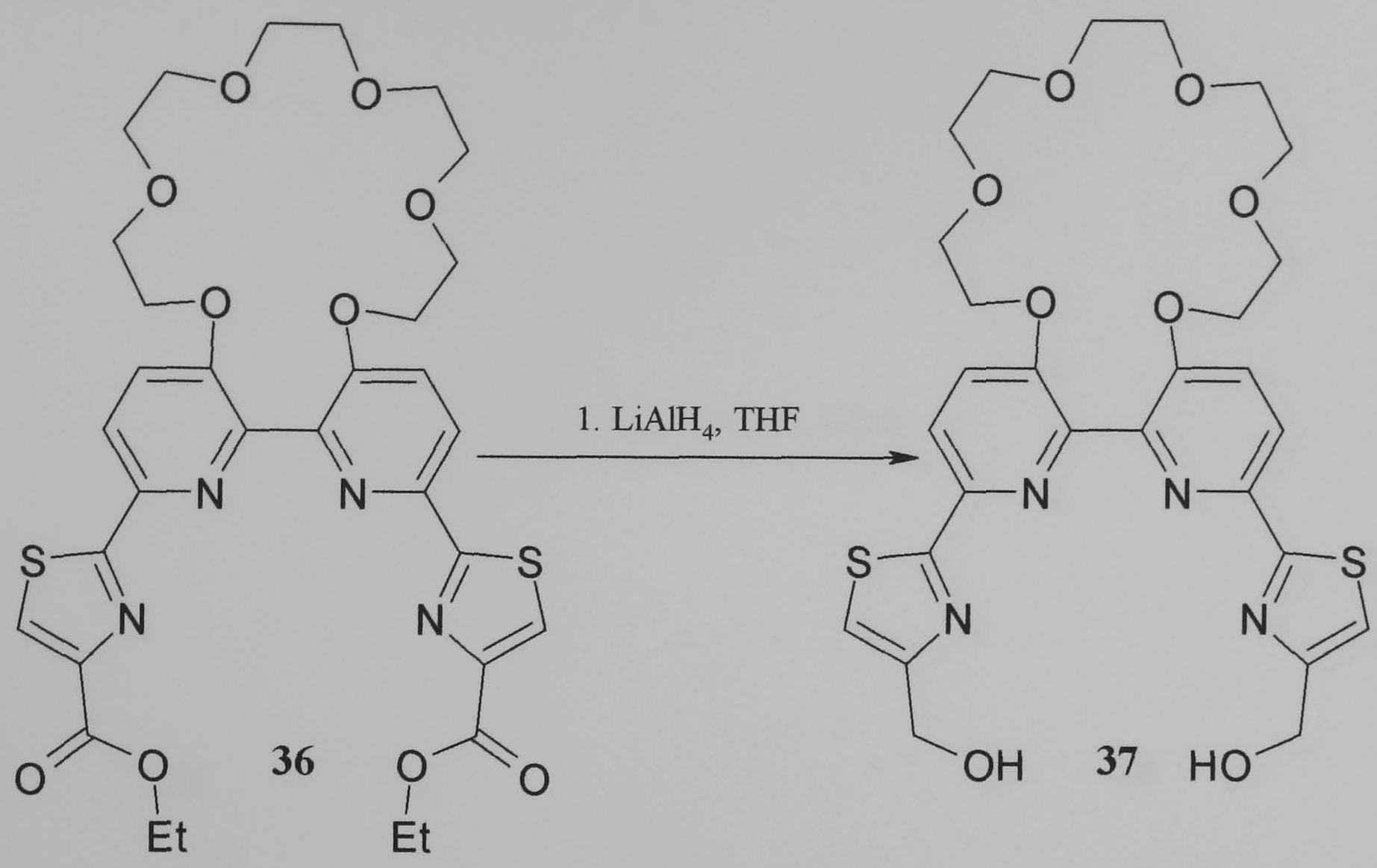

The diester (**36**) (0.2g g, 0.29 mmol) was added to a dry 100 ml two neck round bottom flask, under an atmosphere of nitrogen. Anhydrous THF (30 ml) was added to the flask and the resulting solution stirred in an ice bath at 0°C for 15 minutes. Lithium aluminium hydride, (1.0 M solution in diethyl ether, 1.14 ml, 1.14 mmol) was slowly added over the course of 20 minutes. Stirring was continued for 2 hours at 0°C before removing the ice bath and allowing the reaction to gradually warm up to room temperature. Any remaining lithium aluminium hydride was quenched by slow addition of THF (2 ml), methanol (2 ml) and finally water (2 ml). The solvents were removed by rotary evaporation to leave a viscous yellow emulsion to which distilled water was added and extracted into DCM (4 × 50 ml). Evaporation of the organic solvent gave a yellow solid that was purified via column chromatography (3% MeOH in DCM, Al_2O_3) gave the dimethyl alcohol (**37**) as a pale yellow solid (0.15 g, 0.24 mmol, 82%).

^{1}H NMR [400 MHz, $CDCl_3$]: δ (ppm) 8.20 (d, J = 8.7, 2H), 7.45 (d, J = 8.7, 2H), 7.22 (s, 2H), 4.84 (d, J = 4.6, 4H), 4.31-3.57 (m, 20H), 2.49 (t, J = 6.7 Hz, 2H, -OH).

ESI-MS *m/z* 639.1 (M + Na^+).

*6.33 Synthesis of Compound (**38**)*

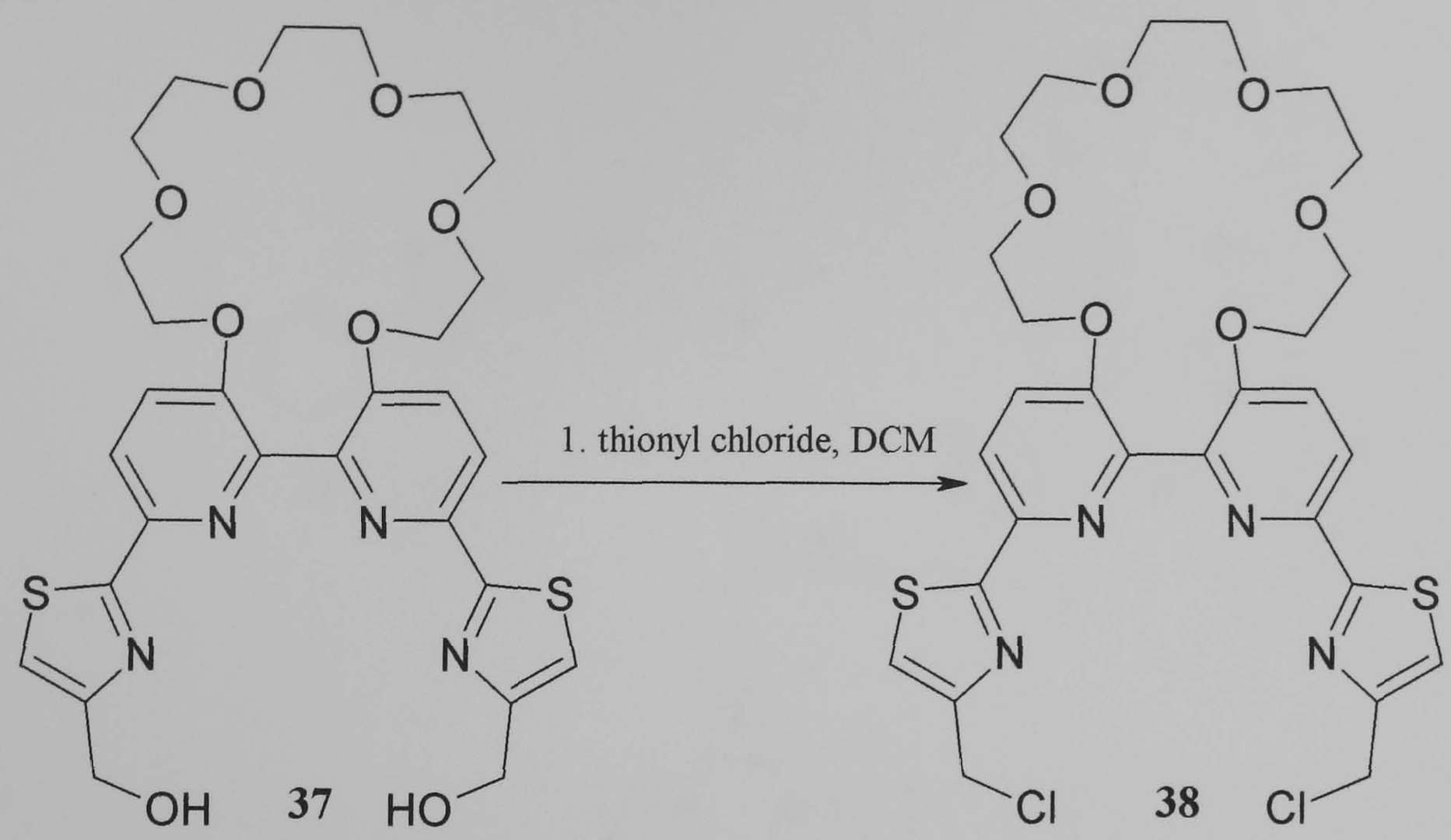

A solution of the dimethyl alcohol (**37**) (0.15 g, 0.24 mmol) and thionyl chloride (2 ml) in DCM (50 ml) was refluxed for 4 hours. Upon completion the solution was allowed to cool before slowly pouring into $NaHCO_{3(aq)}$ and extracted from DCM (3 × 20 ml). Removal of the solvent by rotary evaporation gave a brown oil which was immediately purified via column chromatography (1% MeOH in DCM, Al_2O_3) gave (**38**) as a white solid (0.11 g, 0.17 mmol, 69%).

^{1}H NMR [400 MHz, $CDCl_3$]: δ (ppm) 8.15 (d, J = 8.7, 2H), 7.35 (d, J = 8.7 Hz, 2H), 7.24 (s, 2H), 4.68 (s, 4H), 4.16-3.49 (m, 20H)

ESI-MS m/z 653.1 (M^+).

*6.34 Synthesis of (**L**$_6$)*

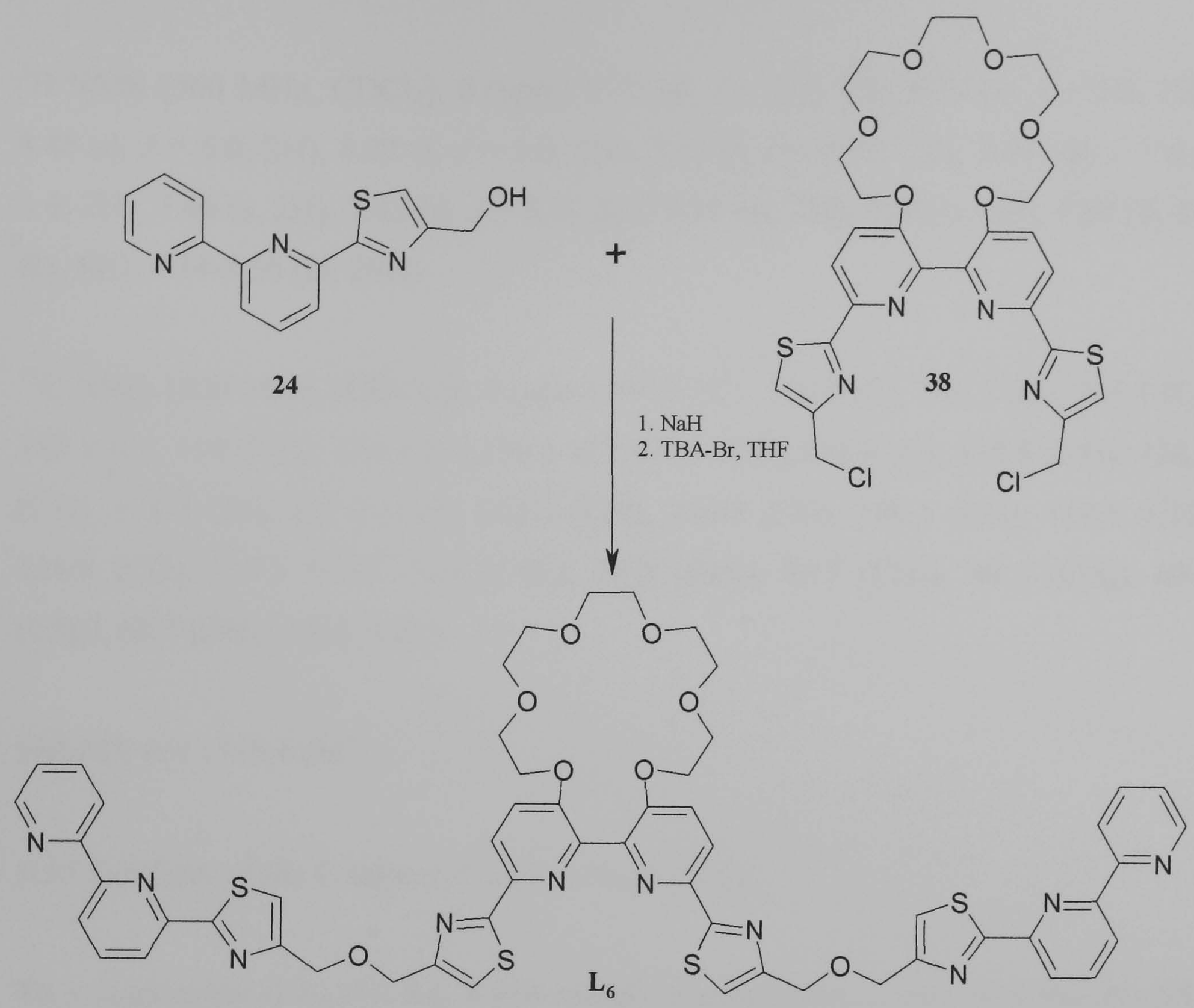

To a dry 100 ml two neck round bottom flask the tridentate unit (**24**) (0.050 g, 0.19 mmol), sodium hydride (60% dispersion in oil) (0.029 g, 0.74 mmol) and TBA-Br (5 mg, 0.015 mmol) were added. The flask was immediately fitted with a dry reflux condenser and placed under an atmosphere of nitrogen. To this anhydrous THF (40 ml) was added and the mixture heated under reflux for 1 hour. During this time the dimethylchloride (**38**) (0.060 g, 0.093 mmol) was placed in a 25 ml round bottom flask fitted with a suba-seal and flushed with nitrogen for 1 hour. The dichloride (**38**) was then dissolved in anhydrous THF (5 ml) and transferred to the reaction vessel containing (**24**). The reaction was heated under reflux for a further 36 hours, monitoring the progress by TLC. Upon completion addition of methanol (5 ml) decomposed any un-reacted NaH. Removal of the solvents by rotary evaporation gave a yellow oil to which distilled water (10 ml) was added and extracted into DCM (4 × 50 ml). Evaporation of the combined organic layers gave a crude product that

was purified via column chromatography (1% MeOH in DCM, Al_2O_3) gave the final ligand (**L_6**) as an off white solid (0.028 g, 0.025 mmol, 27%).

^{1}H NMR [500 MHz, $CDCl_3$]: δ (ppm) 8.70 (d, *J* = 5.0, 2H), 8.57 (d, *J* = 5.0, 2H), 8.46 (d, *J* = 5.0, 2H), 8.22 (t, *J* = 5.0, 4H), 7.93 (t, *J* = 7.85, 2H), 7.87 (dt, *J* = 6.3, 1.4, 2H), 7.46 (s, 2H), 7.43 (d, *J* = 8.7, 2H), 7.35 (m, 2H), 7.34 (s, 2H), 4.88 (d, 5.0 Hz, 8H), 4.34-3.56 (m, 20H)

^{13}C NMR [500 MHz, ($CDCl_3$)]: δ (ppm) 169.5 (C), 169.4 (C), 155.7 (C), 155.4 (C), 155.1 (C), 154.7 (C), 154.4 (C),150.6 (C),149.1 (CH),144.9 (C), 137.9 (CH), 136.9 (CH), 124.0 CH), 121.6 (CH), 121.2 (CH), 120.6 (CH), 120.1 (CH), 119.5 (CH), 118.6 (CH), 117.9 (CH), 70.9 (CH_2), 70.8 (CH_2), 70.7 (CH_2), 69.5 (CH_2), 68.9 (CH_2), 68.7 (CH_2), 68.6 (CH_2).

ESI-MS *m/z* 1119.4 (M^+).

6.35 Synthesis of the Complex $[Cu_2(\mathbf{L_1})_2Ba_2](ClO_4)_6$.

To a suspension of **L_1** (10 mg, 0.016 mmol) in acetonitrile (2 ml), $[Cu(MeCN)_4]PF_6$ (6.1 mg, 0.016 mmol) was added and the solution stirred until complete dissolution. To this excess $Ba(ClO_4)_2$ was added and the solution filtered followed by layering with diethyl ether (10 ml), afforded small orange crystals of $[Cu_2(\mathbf{L_1})_2Ba_2](ClO_4)_6$ which lost solvent rapidly (7.26 mg, 40% yield)

ESI-MS *m/z* 2124, $\{[Cu_2(\mathbf{L_1})_2Ba_2](ClO_4)_5\}^+$. Elemental Analysis found C: 32.1, H: 3.4, N: 5.6% $C_{60}H_{72}Ba_2Cl_6Cu_2N_8O_{36}S_4$ Requires: C: 32.8, H: 3.3, N: 5.6%.

*6.36 Synthesis of the Complex [Zn(**L**$_1$)Ba](ClO$_4$)$_4$*

Reaction of **L**$_1$ (10 mg, 0.016 mmol) with [Zn(H$_2$O)$_6$](ClO$_4$)$_2$ (6.1 mg, 0.016 mmol) in acetonitrile (2 ml) afforded a colourless solution upon complete dissolution . To this excess Ba(ClO$_4$)$_2$ was added and the solution filtered followed by layering with diethyl ether (10 ml), giving small pale yellow crystals of [Zn(**L**$_1$)Ba](ClO$_4$)$_4$ which rapidly lost solvent (9.0 mg, 45% yield).

ESI-MS *m/z* 1112, {[Zn(**L**$_1$)Ba](ClO$_4$)$_3$}$^+$. Elemental Analysis found C: 29.1, H: 3.4, N: 4.2% $C_{30}H_{38}BaCl_4N_4O_{23}S_2Zn$ Requires: C: 29.2, H: 3.1, N: 4.5%.

*6.37 Synthesis of the Complex [Cu$_2$(**L**$_2$)$_2$Ba$_2$](ClO$_4$)$_6$*

To a suspension of **L**$_2$ (10 mg, 0.017 mmol) in acetonitrile (2 ml), [Cu(MeCN)$_4$]PF$_6$ (6.4 mg, 0.017 mmol) was added and the resulting red solution stirred until complete dissolution. To this excess Ba(ClO$_4$)$_2$ was added and the solution filtered followed by layering with diethyl ether (10 ml), giving orange crystals of [Cu$_2$(**L**$_2$)$_2$Ba$_2$](ClO$_4$)$_6$ which were filtered and dried (7.25 mg, 41% yield).

ESI-MS *m/z* 2068, {[Cu$_2$(**L**$_2$)$_2$Ba$_2$](ClO$_4$)$_5$}$^+$. Elemental Analysis found C: 31.1, H: 3.4, N: 4.9% $C_{56}H_{64}Ba_2Cl_6Cu_2N_8O_{36}S_4$ Requires: C: 31.0, H: 3.0, N: 5.2%.

*6.38 Synthesis of the Complex [Zn$_2$(**L**$_3$)$_2$](ClO$_4$)$_4$*

To a suspension of **L**$_3$ (15 mg, 0.021 mmol) in acetonitrile, [Zn(H$_2$O)$_6$](ClO$_4$)$_2$ (7.8 mg, 0.021 mmol) was added, forming a colourless solution upon complete dissolution. Filtration followed by the slow diffusion of ethyl acetate vapour into the acetonitrile solution afforded small colourless crystals of [Zn$_2$(**L**$_3$)$_2$](ClO$_4$)$_4$ which were filtered and dried (9.88 mg, 48% yield).

ESI-MS *m/z* 1851, {[Zn$_2$(**L**$_3$)$_2$](ClO$_4$)$_3$}$^+$. Elemental Analysis found C: 43.8, H: 3.7, N: 8.1% $C_{72}H_{68}Cl_4Zn_2N_{12}O_{28}S_4$ Requires: C: 44.3, H: 3.5, N: 8.6%.

6.39 Synthesis of the Complex $[Zn_2(\mathbf{L_3})_2Ba_2](ClO_4)_8$

Reaction of $\mathbf{L_3}$ (15 mg, 0.021 mmol) with $[Zn(H_2O)_6](ClO_4)_2$ (7.8 mg, 0.021 mmol) in acetonitrile (2 ml) resulted in the formation of a clear colourless solution. To this excess $Ba(ClO_4)_2$ was added and the solution filtered followed by the slow diffusion of ethyl acetate vapour into the acetonitrile solution resulted in the formation of small colourless crystals of $[Zn_2(\mathbf{L_3})_2Ba_2](ClO_4)_8$ (10.2 mg, 37% yield).

ESI-MS *m/z* 1213, $\{[Zn_2(\mathbf{L_3})_2Ba_2](ClO_4)_6\}^{2+}$. Elemental Analysis found C: 29.2, H: 2.9, N: 6.1% $C_{72}H_{68}Ba_2Cl_8Zn_2N_{12}O_{44}S_4$ Requires: C: 33.0, H: 2.6, N: 6.4% (C 3.8% difference probably due to some sample contamination).

6.40 Synthesis of the Complex $[CuZn_2(\mathbf{L_4})_2](ClO_4)_5$.

Reaction of $\mathbf{L_4}$ (15 mg, 0.016 mmol), $[Zn(H_2O)_6](ClO_4)_2$ (5.9 mg, 0.016 mmol) and $[Cu(MeCN)_4]PF_6$ (2.9 mg, 0.008 mmol) in acetonitrile (2 ml) afforded an orange solution. To this a slight excess of $TBA(ClO_4)$ was added and the solution filtered followed by layering with diethyl ether (10 ml) giving small orange crystals of $[CuZn_2(\mathbf{L_4})_2](ClO_4)_5$ (7.2 mg, 35% yield).

ESI-MS *m/z* 1273, $\{[Zn_2Cu(\mathbf{L_4})_2](ClO_4)_3\}^{2+}$. Elemental Analysis found C: 46.5, H: 3.4, N: 8.7% $C_{100}H_{96}Cl_5Zn_2CuN_{16}O_{36}S_4$ Requires: C: 46.2, H: 3.7, N: 8.6%.

6.41 Synthesis of the Complex $[Cu_2Zn_2(\mathbf{L_6})_2](ClO_4)_6$.

To a suspension of $\mathbf{L_6}$ (15 mg, 0.013 mmol) in acetonitrile, $Zn(H_2O)_6](ClO_4)_2$ (5.0 mg, 0.013 mmol) and $[Cu(MeCN)_4]PF_6$ (5.0 mg, 0.013 mmol) was added and stirred until complete dissolution. To this a slight excess of $TBA(ClO_4)$ were added and the solution filtered followed by layering with diethyl ether (10 ml) afforded small orange crystals of $[Cu_2Zn_2(\mathbf{L_6})_2](ClO_4)_6$ (8.9 mg, 43% yield).

ESI-MS *m/z* 1542 $\{[Zn_2Cu_2(\mathbf{L_6})_2](ClO_4)_4\}^{2+}$. Elemental Analysis found C: 43.2, H: 3.3, N: 8.7% $C_{112}H_{100}Cl_6Zn_2Cu_2N_{20}O_{40}S_8$ Requires: C: 43.4, H: 3.2, N: 9.0%.

References

1 J.-M. Lehn, 'Supramolecular Chemistry: Concepts and Perspectives', VCH, Weinheim, 1995.

2 J. W. Steed and J. L. Atwood, 'Supramolecular Chemistry', John Wiley and Sons, 2000.

3 C. J. Pedersen, *J. Am. Chem. Soc*, 1967, **89**, 2495.

4 C. J. Pedersen, *J. Am. Chem. Soc*, 1967, **89**, 7017.

5 B. Dietrich, J.-M. Lehn, and J. P. Sauvage, *Tetrahedron Lett.*, 1969, 2885.

6 D. J. Cram, *Angew. Chem.*, 1986, **98**, 1041.

7 K. Brandt, R. Kruszynski, T. J. Bartczak, and Porwoli-Czomperlik, *Inorg. Chem. Acta.*, 2001, **322**, 138.

8 T. Gunnlaugsson, B. Bichell, and C. Nolan, *Tetrahedron.*, 2004, **60**, 5799.

9 T. Gunnlaugsson, M. Nieuwenhuyzen, L. Richard, and V. Thoss, *Tetrahedron Lett.*, 2001, **42**, 4725.

10 G. W. Gokel, W. M. Leevy, and M. E. Weber, *Chem. Rev.*, 2004, **104**, 2723.

11 S. Shinkai, T. Nakaji, Y. Nishida, T. Ogawa, and O. Manabe, *J. Am. Chem. Soc.*, 1980, **102**, 5860.

12 M. H. Hyun and S. C. Han, *J. Biochem. Biophys. Methods.*, 2002, **54**, 235.

13 S. A. McFarland and N. S. Finney, *Chem. Commun.*, 2003, 388.

14 T. Kaneda, K. Sugihara, H. Kamiya, and S. Misumi, *Tetrahedron Lett.*, 1981, **22**, 4407.

15 G. M. Whitesides and J. P. Mathias, *Science*, 1991, **254**, 1312.

16 S. Leininger, B. Olenyuk, and P. J. Stang, *Chem. Rev.*, 2000, **100**, 853.

17 M.-T. Youinou, N. Rahmouri, J. Fischer, and J. A. Osborn, *Angew. Chem. Int. Ed.*, 1992, **31**, 733.

18 W. Dong, Y. Ouyang, D.-Z. Liao, S.-P. Yan, P. Cheng, and Z.-H. Jiang, *Inorg. Chem. Acta.*, 2006, **359**, 3363.

19 J. S. Fleming, K. L. V. Mann, C.-A. Carrez, E. Psillakis, J. C. Jeffrey, J. A. McCleverty, and M. D. Ward, *Angew. Chem. Int. Ed.*, 1998, **37**, 1279.

20 A. Ray, M. Mijanuddin, R. Chatterjee, J. Marek, S. Mondal, and M. Ali, *Inorg. Chem. Commun.*, 2006, **9**, 167.

21 A. Credi, V. Balzani, S. Campagne, G. S. Hanan, C. R. Arana, and J.-M. Lehn, *Chem. Phys. Lett.*, 1995, **243**, 102.

22 M. Albrecht, *Chem. Rev.*, 2001, **101**, 3457.

23 C. Piguet, G. Bernardinelli, and G. Hopfgertner, *Chem. Rev.*, 1997, **97**, 2005.

24 S. T. Onions, A. M. Franklin, P. N. Horton, M. B. Hursthouse, and C. J. Matthews, *Chem. Commun.*, 2003, 2864.

25 L. Zhao, C. J. Matthews, L. K. Thompson, and S. L. Heath, *Chem. Commun.*, 2000, 265.

26 Z. Xu, L. K. Thompson, and D. O. Miller, *Polyhedron.*, 2002, **21**, 1715.

27 P. Tielmann, A. Marchal, and J.-M. Lehn, *Tetrahedron Lett.*, 2005, **46**, 6349.

28 G. S. Hanan, D. Volkmer, U. S. Schubert, J.-M. Lehn, G. Baum, and D. Fenske, *Angew. Chem. Int. Ed.*, 1997, **38**, 1842.

29 Z. R. Bell, L. P. Harding, and M. D. Ward, *Chem. Commun.*, 2003, 2432.

30 G. F. Swiegers and T. J. Malefetse, *Coord. Chem. Rev.*, 2002, **225**, 91.

31 O. V. Dolomanov, A. J. Blake, N. R. Champness, M. Schroder, and C. Wilson, *Chem. Commun.*, 2003, 682.

32 S. P. Argent, H. Adams, T. Riis-Johannessen, J. C. Jeffery, L. P. Harding, W. Clegg, R. W. Harrington, and M. D. Ward, *Dalton Trans.*, 2006, In Press.

33 Z. R. Bell, J. C. Jeffrey, J. A. McCleverty, and M. D. Ward, *Angew. Chem. Int. Ed.*, 2002, **41**, 2515.

34 K. Nakabayashi, M. Kawano, M. Yoshizawa, S. Ohkoshi, and M. Fujita, *J. Am. Chem. Soc.*, 2004, **126**, 16694.

35 M. Yoshizawa, K. Kumazawa, and M. Fujita, *J. Am. Chem. Soc.*, 2005, **127**, 13456.

36 M. Yoshizawa, T. Kusukawa, M. Kawano, T. Ohhara, I. Tanaka, K. Kurihara, N. Niimura, and M. Fujita, *J. Am. Chem. Soc.*, 2005, **127**, 2798.

37 M. Yoshizawa, K. Ono, K. Kumazawa, T. Kato, and M. Fujita, *J. Am. Chem. Soc.*, 2005, **127**, 10800.

38 B.-Y. Lou, D.-Q. Yuan, B.-L. Wu, L. Han, F.-L. Jiang, and M.-C. Hong, *Inorg. Chem. Commun.*, 2005, **8**, 539.

39 T. Sugimoto, K. Sada, Y. Tateishi, T. Suzuki, Y. Sei, K. Yamaguchi, and S. Shinkai, *Tetrahedron Lett.*, 2005, **46**, 5347.

40 P. N. W. Baxter, G. S. Hanan, and J.-M. Lehn, *Chem. Commun.*, 1996, 2019.

41 J. D. Woodward, R. V. Backov, K. A. Abboud, and D. R. Talham, *Polyhedron.*, 2006, **25**, 2605.

42 V. Patroniak, P. N. W. Baxter, J.-M. Lehn, Z. Hnatejko, and M. Kubicki, *Eur. J. Inorg. Chem.*, 2004, 2379.

43 V. Patroniak, P. N. W. Baxter, J.-M. Lehn, M. Kubicki, M. Nissinen, and K. Rissanen, *Eur. J. Inorg. Chem.*, 2003, 4001.

44 V. Patroniak, J.-M. Lehn, M. Kubicki, A. Ciesielski, and M. Walesa, *Polyhedron.*, 2006.

45 J.-M. Lehn, A. Rigault, J. Siegel, J. Harrowfield, B. Chevrier, and D. Moras, *Proc. Natl. Acad. Sci. USA.*, 1987, **84**, 2565.

46 C. Piguet, G. Bernardinelli, B. Bocquet, A. Quattropani, and A. F. Williams, *J. Am. Chem. Soc*, 1992, **114**, 7440.

47 E. C. Constable, *Tetrahedron.*, 1992, **48**, 10013.

48 B. Hasenknopf, J.-M. Lehn, G. Baum, and D. Fenske, *Proc. Natl. Acad. Sci. USA.*, 1995, **93**, 1397.

49 M. Greenwald, D. Wessely, E. Katz, I. Willner, and Y. Cohen, *J. Org. Chem.*, 2000, **65**, 1050.

50 D. M. L. Goodgame, S. P. W. Hill, and D. J. Williams, *J. Chem. Soc., Chem. Commun.*, 1993, 1019.

51 K. T. Potts, M. Keshavarz-K, F. S. Tham, H. D. Abruna, and C. R. Arana, *Inorg. Chem.*, 1993, **32**, 4422.

52 E. C. Constable, M. Neuburger, L. Whall, and M. Zehnder, *New J. Chem.*, 1998, **22**, 219.

53 R. L. Paul, S. M. Couchman, J. C. Jeffery, J. A. McCleverty, Z. A. Reeves, and M. D. Ward, *J. Chem. Soc., Dalton Trans.*, 2000, 845.

54 C. Piguet, G. Hopfgartner, A. F. Williams, and J.-C. G. Bunzli, *J. Chem. Soc., Chem. Commun.*, 1995, 491.

55 C. Piguet, E. Rivara-Minten, G. Hopfgartner, and J.-C. G. Bunzli, *Helv. Chim. Acta.*, 1995, **78**, 1541.

56 E. C. Constable, F. R. Heirtzler, M. Neuburger, and M. Zehnder, *Chem. Commun.*, 1996, 933-934.

57 E. C. Constable, A. J. Edwards, P. R. Raithby, D. R. Smith, J. V. Walker, and L. Whall, *Chem. Commun.*, 1996, 2551.

58 E. C. Constable, A. J. Edwards, P. R. Raithby, and J. V. Walker, *Angew. Chem.*, 1993, **105**, 1486.

59 E. C. Constable and J. V. Walker, *J. Chem. Soc. Chem. Commun.*, 1992, 884.

60 E. C. Constable, M. D. Ward, and D. A. Tocher, *J. Chem. Soc., Dalton Trans.*, 1991, 1675.

61 M. Barley, E. C. Constable, S. A. Corr, R. C. S. McQueen, J. C. Nutkins, and M. D. Ward, *J. Chem. Soc., Dalton Trans.*, 1988, 2655.

62 G. Baum, E. C. Constable, D. Fenske, C. E. Housecroft, and T. Kulke, *Chem. Commun.*, 1999, 195.

63 H. Murner, A. V. Zelewsky, and G. Hopfgarter, *Inorganica Chimica Acta.*, 1998, **271**, 36.

64 T. K. Ronson, H. Adams, T. Riis-Johannessen, J. C. Jeffery, and M. D. Ward, *New J. Chem.*, 2006, **30**, 26.

65 R. Kramer, J.-M. Lehn, and A. Marquis-Rigault, *Proc. Natl. Acad. Sci. USA.*, 1993, **90**, 5394.

66 R. Kramer, J.-M. Lehn, A. DeCian, and J. Fischer, *Angew. Chem. Int. Ed.*, 1993, **32**, 704.

67 R. Chotalia, E. C. Constable, M. Neuburger, D. R. Smith, and M. Zehnder, *J. Chem. Soc., Dalton Trans.*, 1996, 4207.

68 E. C. Constable and M. D. Ward, *J. Am. Chem. Soc*, 1990, **112**, 1256.

69 E. C. Constable, R. Chotalia, and D. A. Tocher, *J. Chem. Soc., Chem. Commun.*, 1992, 771.

70 C. R. Rice, S. Worl, J. C. Jeffery, R. L. Paul, and M. D. Ward, *Chem. Commun.*, 2000, 1529.

71 C. R. Rice, C. J. Baylies, L. P. Harding, J. C. Jeffrey, R. L. Paul, and M. D. Ward, *J. Chem. Soc., Dalton Trans.*, 2001, 3039.

72 C. R. Rice, C. J. Baylies, H. J. Clayton, J. C. Jeffrey, R. L. Paul, and M. D. Ward, *Inorganica Chimica Acta.*, 2003, **351**, 207.

73 E. C. Constable, S. M. Elder, J. Healy, and D. A. Tocher, *J. Chem. Soc., Dalton Trans.*, 1990, 1669.

74 E. C. Constable, S. M. Elder, M. J. Hannon, A. Martin, P. R. Raithby, and D. A. Tocher, *J. Chem. Soc., Dalton Trans.*, 1996, 2423.

75 C. R. Rice, S. Worl, J. C. Jeffery, R. L. Paul, and M. D. Ward, *J. Chem. Soc., Dalton. Trans.*, 2001, 550.

76 N. G. Berry, T. W. Shimell, and P. D. Beer, *Journal of Supramolecular Chemistry*, 2002, **2**, 89.

77 C. R. Rice, *Coord. Chem. Rev.*, 2006, In Press.

78 C. R. Rice, A. Guerrero, Z. R. Bell, R. L. Paul, G. R. Motson, J. C. Jeffrey, and M. D. Ward, *New J. Chem*, 2001, **25**, 185.

79 P. D. Beer and A. S. Rothin, *J. Chem. Soc., Chem. Commun.*, 1988, 52.

80 Y. Kubo, Y. Murai, J. Yamanaka, S. Tokita, and Y. Ishimaru, *Tetrahedron Lett.*, 1999, 6019.

81 J. M. Mahoney, K. A. Stucker, H. Jiang, I. Carmichael, N. R. Brinkmann, A. M. Beatty, B. C. Noll, and B. D. Smith, *J. Am. Chem. Soc*, 2004, **127**, 2922.

82 M. D. Lankshear, A. R. Cowley, and P. D. Beer, *Chem. Commun.*, 2006, 612.

83 J. M. Mahoney, A. M. Beatty, and B. D. Smith, *Inorg. Chem.*, 2004, **43**, 7617.

84 S. G. Telfer, G. Bernardinelli, and A. F. Williams, *Dalton Trans.*, 2003, 435.

85 S. G. Telfer, G. Bernardinelli, and A. F. Williams, *Chem. Commun.*, 2001, 1498.

86 W. Leslie, R. A. Poole, P. R. Murray, L. J. Yellowlees, A. Beedy, and J. A. G. Williams, *Polyhedron.*, 2004, **23**, 2769.

87 B. Wu, X.-J. Yang, C. Janiak, and P. G. Lassahn, *Chem. Commun.*, 2003, 902.

88 L. H. Uppadine, M. G. B. Drew, and P. D. Beer, *Chem. Commun.*, 2001, 291.

89 C. R. Bondy, P. A. Gale, and S. J. Loeb, *Chem. Commun.*, 2001, 729.

90 C. R. Bondy, P. A. Gale, and S. J. Loeb, *J. Am. Chem. Soc.*, 2004, **126**, 5030.

91 L. P. Harding, J. C. Jeffery, T. Riis-Johannessen, C. R. Rice, and Z. Zeng, *Chem. Commun.*, 2004, 654.

92 L. P. Harding, J. C. Jeffery, T. Riis-Johannessen, C. R. Rice, and Z. Zeng, *Dalton Trans.*, 2004, 2396.

93 L. Kovbasyuk and R. Kramer, *Chem. Rev.*, 2004, **104**, 3161.

94 J. Rebek and L. Marshall, *J. Am. Chem. Soc.*, 1983, **105**, 6668.

95 J. Rebek, J. E. Trend, R. V. Wattley, and S. Chakravorti, *J. Am. Chem. Soc.*, 1979, **101**, 4333.

96 J. Rebek and R. V. Wattley, *J. Am. Chem. Soc.*, 1980, **102**, 4853.

97 C. J. Baylies, L. P. Harding, J. C. Jeffrey, T. Riis-Johannessen, and C. R. Rice, *Angew. Chem. Int. Ed.*, 2004, **43**, 4515.

98 G. Bokolinis, T. Riis-Johannessen, L. P. Harding, J. C. Jeffery, N. McLay, and C. R. Rice, *Chem. Commun.*, 2006, 1980.

99 T. Riis-Johannessen, J. C. Jeffery, A. P. H. Robson, C. R. Rice, and L. P. Harding, *Inorganica Chimica Acta*, 2005, **358**, 2781.

100 C. J. Baylies, PhD Thesis, University of Huddersfield, 2003.

101 C. J. Baylies, J. C. Jeffery, T. A. Miller, R. Moon, C. R. Rice, and T. Riss-Johannessen, *Chem. Commun.*, 2005, 4158.

102 M. Greenwald, M. Eassa, E. Katz, I. Willner, and Y. Cohen, *Journal of Electroanalytical Chemistry.*, 1997, **434**, 77.

103 P. N. Baxter, J. A. Connor, W. B. Schweizer, and J. D. Wallis, *J. Chem. Soc., Dalton Trans.*, 1992, 3015.

104 J. J. Rebek and R. V. Wattley, *J. Heterocycl. Chem.*, 1980, **17**, 749.

105 C. J. Baylies, T. Riis-Johannessen, L. P. Harding, J. C. Jeffery, R. Moon, C. R. Rice, and M. Whitehead, *Angew. Chem., Int. Ed.*, 2005, **44**, 6909.

106 C. Naumann and H. Langhals, *Synthesis*, 1990, 279.

Appendix I

Crystal Data Tables

Table A1. Crystallographic data of the $\mathbf{L_1}$ complex $[Cu_2(\mathbf{L_1})_2Ba_2](ClO_4)_6$.[a]

Complex	$[Cu_2(\mathbf{L_1})_2Ba_2](ClO_4)_6$
Formula	$C_{66}H_{85}\ Ba_2Cl_6Cu_2N_{10}O_{37.5}S_4$
M/ /g	2361.14
System, space group	Triclinic, P-1
a /Å	13.54(5)
b /Å	18.91(7)
c /Å	21.35(8)
α /°	65.91(7)
β /°	72.42(7)
γ /°	85.18(7)
V /Å^3	4754(31)
Z	2
μ /mm^{-1}	1.602
Reflections collected:	54400, 21383, 0.0386
Total, independent, R_{int}	
Final R_1, wR_2 [I>2σ(I)]	0.0582, 0.1603
Final R_1, wR_2 [b,c]	0.0747, 0.1738

[a] Details in common: diffractometer, Bruker SMART using Mo-K_α radiation (0.71073 Å); temperature of data collection 100(2) K.

[b] Structure was refined on F_o^2 using all data; the value of R_1 is given for comparison with older refinements based on F_o with a typical threshold of $F \geq 4\sigma(F)$.

[c] $w^{-1} = \sigma^2(F_o^2) + (aP)^2 + (bP)$, where $P = [\max(F_o^2, 0) + 2F_c^2]/3$

Table A2. Crystallographic data of the $\mathbf{L_1}$ complex $[Zn(\mathbf{L_1})Ba](ClO_4)_4$.[a]

Complex	$[Zn(\mathbf{L_1})Ba](ClO_4)_4$
Formula	$C_{34}H_{49.25}BaCl_4N_5O_{25.25}S_2Zn$
M /g	1340.66
System, space group	Monoclinic, $P2_1/c$
a /Å	18.4309(12)
b /Å	17.9806(11)
c /Å	17.6143(11)
α /°	90.00
β /°	101.4330(10)
γ /°	90.00
V /Å^3	5721.5(6)
Z	4
μ /mm^{-1}	1.442
Reflections collected:	59644, 13134, 0.0858
Total, independent, R_{int}	
Final R_1, wR_2 [I>2σ(I)]	0.0702, 0.1888
Final R_1, wR_2 [b,c]	0.1233, 0.2109

[a] Details in common: diffractometer, Bruker SMART using Mo-K_α radiation (0.71073 Å); temperature of data collection 173(2) K.

[b] Structure was refined on F_o^2 using all data; the value of R_1 is given for comparison with older refinements based on F_o with a typical threshold of $F \geq 4\sigma(F)$.

[c] $w^{-1} = \sigma^2(F_o^2) + (aP)^2 + (bP)$, where $P = [\max(F_o^2, 0) + 2F_c^2]/3$

Table A3. Crystallographic data of the $\mathbf{L_2}$ complex $[Cu_2(\mathbf{L_2})_2Ba_2](ClO_4)_4(PF_6)_2$.[a]

Complex	$[Cu_2(\mathbf{L_2})_2Ba_2](ClO_4)_4(PF_6)_2$
Formula	$C_{60}H_{70}Ba_2Cl_4Cu_2\ F_{12}N_{10}O_{28}\ P_2S_4$
M /g	2341.00
System, space group	Monoclinic, C2/c
a /Å	24.3803(5)
b /Å	14.3839(4)
c /Å	28.4101(5)
α /°	90.00
β /°	111.0830(10)
γ /°	90.00
V /Å^3	9296.0(4)
Z	4
μ /mm^{-1}	10.120
Reflections collected:	34892, 8673, 0.0843
Total, independent, R_{int}	
Final R_1, wR_2 [I>2σ(I)]	0.0474, 0.1156
Final R_1, wR_2 [b,c]	0.0623, 0.1211

[a] Details in common: diffractometer, Bruker PROTEUM CCD using Cu-K_α radiation (1.54178 Å); temperature of data collection 100(2) K.

[b] Structure was refined on F_o^2 using all data; the value of R_1 is given for comparison with older refinements based on F_o with a typical threshold of $F \geq 4\sigma(F)$.

[c] $w^{-1} = \sigma^2(F_o^2) + (aP)^2 + (bP)$, where $P = [\max(F_o^2, 0) + 2F_c^2]/3$

Table A4. Crystallographic data of the $\mathbf{L_3}$ complex $[Zn_2(\mathbf{L_3})_2](ClO_4)_4$.[a]

Complex	$[Zn_2(\mathbf{L_3})_2](ClO_4)_4$
Formula	$C_{78}H_{78}Cl_4N_{15}O_{28.5}S_4Zn_2$
M /g	2082.33
System, space group	Triclinic, P-1
a /Å	13.641(3)
b /Å	17.738(4)
c /Å	18.898(4)
α /°	75.86(3)
β /°	82.89(3)
γ /°	84.78(3)
V /Å^3	4391.0(15)
Z	2
μ /mm^{-1}	0.853
Reflections collected:	49434, 20080, 0.0621
Total, independent, R_{int}	
Final R_1, wR_2 [I>2σ(I)]	0.0560, 0.1368
Final R_1, wR_2 [b,c]	0.1106, 0.1612

[a] Details in common: diffractometer, Bruker APEX CCD using Mo-K_α radiation (0.71073 Å); temperature of data collection 100(2) K.

[b] Structure was refined on F_o^2 using all data; the value of R_1 is given for comparison with older refinements based on F_o with a typical threshold of $F \geq 4\sigma(F)$.

[c] $w^{-1} = \sigma^2(F_o^2) + (aP)^2 + (bP)$, where $P = [\max(F_o^2, 0) + 2F_c^2]/3$

Table A5. Crystallographic data of the $\mathbf{L_3}$ complex $[Zn_2(\mathbf{L_3})_2Ba_2](ClO_4)_8$.[a]

Complex	$[Zn_2(\mathbf{L_3})_2Ba_2](ClO_4)_8$
Formula	$C_{79}H_{80.5}Ba_2Cl_8N_{15.5}O_{45}S_4Zn_2$
M /g	2784.35
System, space group	Triclinic, P-1
a /Å	16.9511(3)
b /Å	18.4571(3)
c /Å	20.1644(4)
α /°	108.4580(10)
β /°	103.3020(10)
γ /°	110.4970(10)
V /Å^3	5176.26(16)
Z	2
μ /mm^{-1}	9.887
Reflections collected:	41199, 17747, 0.0638]
Total, independent, R_{int}	
Final R_1, wR_2 [I>2σ(I)]	0.0525, 0.1281
Final R_1, wR_2 [b,c]	0.0771, 0.1419

[a] Details in common: diffractometer, Bruker PROTEUM CCD using Mo-K_α radiation (0.71073 Å); temperature of data collection 100(2) K.

[b] Structure was refined on F_o^2 using all data; the value of R_1 is given for comparison with older refinements based on F_o with a typical threshold of $F \geq 4\sigma(F)$.

[c] $w^{-1} = \sigma^2(F_o^2) + (aP)^2 + (bP)$, where $P = [\max(F_o^2, 0) + 2F_c^2]/3$

Table A6. Crystallographic data of the $\mathbf{L_4}$ complex $[CuZn_2(\mathbf{L_4})_2](ClO_4)_5$.[a]

Complex	$[CuZn_2(\mathbf{L_4})_2](ClO_4)_5$
Formula	$C_{116}H_{128}Cl_5CuN_{20}O_{38}S_4Zn_2$
M /g	2910.15
System, space group	Monoclinic, $P2_1/n$
a /Å	20.516(4)
b /Å	26.356(5)
c /Å	23.514(5)
α /°	90.00
β /°	93.22(3)
γ /°	90.00
V /Å^3	12694(4)
Z	4
μ /mm^{-1}	0.802
Reflections collected: Total, independent, R_{int}	46057, 16586, 0.0670
Final R_1, wR_2 [I>2σ(I)]	0.0714, 0.2023
Final R_1, wR_2 [b,c]	0.1233, 0.2596

[a] Details in common: diffractometer, Bruker APEX CCD using Mo-K_α radiation (0.71073 Å); temperature of data collection 100(2) K.

[b] Structure was refined on F_o^2 using all data; the value of R_1 is given for comparison with older refinements based on F_o with a typical threshold of $F \geq 4\sigma(F)$.

[c] $w^{-1} = \sigma^2(F_o^2) + (aP)^2 + (bP)$, where $P = [\max(F_o^2, 0) + 2F_c^2]/3$

Table A7. Crystallographic data of the $\mathbf{L_6}$ complex $[Cu_2Zn_2(\mathbf{L_6})_2](ClO_4)_6$.[a]

Complex	$[Cu_2Zn_2(\mathbf{L_6})_2](ClO_4)_6$
Formula	$C_{122}H_{119}Cl_{6.5}Cu_2N_{23}O_{43}S_8Zn_2$
M /g	3340.13
System, space group	Triclinic, P-1
a /Å	19.657(4)
b /Å	19.758(4)
c /Å	23.241(5)
α /°	94.39(3)
β /°	108.43(3)
γ /°	119.51(3)
V /Å^3	7152(2)
Z	2
μ /mm^{-1}	0.953
Reflections collected: Total, independent, R_{int}	67789, 25187, 0.0489
Final R_1, wR_2 [I>2σ(I)]	0.0877, 0.2458
Final R_1, wR_2 [b,c]	0.1252, 0.2704

[a] Details in common: diffractometer, Bruker APEX CCD using Mo-K_α radiation (0.71073 Å); temperature of data collection 100(2) K.

[b] Structure was refined on F_o^2 using all data; the value of R_1 is given for comparison with older refinements based on F_o with a typical threshold of $F \geq 4\sigma(F)$.

[c] $w^{-1} = \sigma^2(F_o^2) + (aP)^2 + (bP)$, where $P = [\max(F_o^2, 0) + 2F_c^2]/3$